

Tailored cloud point extraction studies for detection of ultratrace levels of uranium

By

**ABHIJIT SAHA
CHEM01201404012**

Bhabha Atomic Research Centre, Mumbai

*A thesis submitted to the
Board of Studies in Chemical Sciences*

*In partial fulfillment of requirements
for the Degree of*

DOCTOR OF PHILOSOPHY
of
HOMI BHABHA NATIONAL INSTITUTE



March, 2018

Tailored cloud point extraction studies for detection of ultratrace levels of uranium

By

**ABHIJIT SAHA
CHEM01201404012**

Bhabha Atomic Research Centre, Mumbai

*A thesis submitted to the
Board of Studies in Chemical Sciences*

*In partial fulfillment of requirements
for the Degree of*

DOCTOR OF PHILOSOPHY
of
HOMI BHABHA NATIONAL INSTITUTE


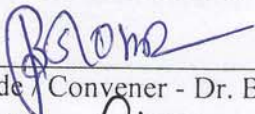
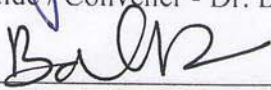

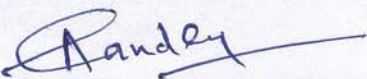


March, 2018

Homi Bhabha National Institute

Recommendations of the Viva Voce Committee

As members of the Viva Voce Committee, we certify that we have read the dissertation prepared by ABHIJIT SAHA entitled " **Tailored cloud point extraction studies for detection of ultratrace levels of uranium**" and recommend that it may be accepted as fulfilling the thesis requirement for the award of Degree of Doctor of Philosophy.

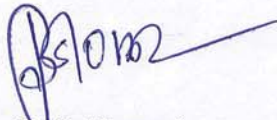
| | |
|---|----------------------------|
|  Chairman - Dr. R. M. Tripathi | <u>6/9/2018</u> Date: |
|  Guide / Convener - Dr. B. S. Tomar | <u>6.9.2018</u> Date: |
|  Examiner - Prof. M. S. Balakrishna | <u>06-09-2018</u> Date: |
| Member 1- Dr.(Mrs.) S.D. Kumar | Date: <u>06.09.2018</u> |
|  Member 2- Dr. P. K. Mohapatra | Date: <u>06.9.2018</u> |
| Member 3- Dr. A.K. Pandey | Date: <u>6.9.2018</u> |
|  | |

Final approval and acceptance of this thesis is contingent upon the candidate's submission of the final copies of the thesis to HBNI.

I/We hereby certify that I/we have read this thesis prepared under my/our direction and recommend that it may be accepted as fulfilling the thesis requirement.

Date: 6.9.2018


Place: Membari


(B. S. Tomar)

STATEMENT BY AUTHOR

This dissertation has been submitted in partial fulfillment of requirements for an advanced degree at Homi Bhabha National Institute (HBNI) and is deposited in the Library to be made available to borrowers under rules of the HBNI.

Brief quotations from this dissertation are allowable without special permission, provided that accurate acknowledgement of source is made. Requests for permission for extended quotation from or reproduction of this manuscript in whole or in part may be granted by the Competent Authority of HBNI when in his or her judgment the proposed use of the material is in the interests of scholarship. In all other instances, however, permission must be obtained from the author.


Abhijit Saha

DECLARATION

I, hereby declare that the investigation presented in the thesis has been carried out by me. The work is original and has not been submitted earlier as a whole or in part for a degree / diploma at this or any other Institution / University.



Abhijit Saha

List of Publications arising from the thesis

Journal

1. Simultaneous preconcentration of uranium and thorium in aqueous samples using cloud point extraction, **Abhijit Saha**, Sadhan Bijoy Deb, Arnab Sarkar, Manoj Kumar Saxena, B.S. Tomar, RSC Adv. **2016**, 6, 20109–20119.

2. Micellar extraction assisted fluorometric determination of ultratrace amount of uranium in aqueous samples by novel diglycolamide-capped quantum dot nanosensor, **Abhijit Saha**, Tushar Debnath, Suman Neogy, Hirendra N. Ghosh, Manoj Kumar Saxena, Bhupendra Singh Tomar, Sensors and Actuators: B Chemical **2017**, 253, 592-602.

3. Selective micellar extraction of ultratrace levels of uranium in aqueous samples by task specific ionic liquid followed by its detection employing total reflection X-ray fluorescence spectrometry, **Abhijit Saha**, Kaushik Sanyal, Neetika Rawat, Sadhan Bijoy Deb, Manoj Kumar Saxena, Bhupendra Singh Tomar, Anal. Chem. **2017**, 89, 10422-10430.

4. Spectrophotometric quantification and visual detection of ultratrace uranium in natural waters by novel amidoxime functionalized gold nanoparticles, **Abhijit Saha**, Suman Neogy, Dumpala Rama Mohana Rao, Sadhan Bijoy Deb, Manoj Kumar Saxena, Bhupendra Singh Tomar, Anal. Chem. (**Under review**).

Conferences

1. Synthesis of novel quantum dot nanosensor for fluorimetric determination of uranium in aqueous samples, Abhijit Saha, T. Debnath, M.K. Saxena, H.N. Ghosh and B.S. Tomar, 19thCRSI National Symposium in Chemistry (CRSI NSC-19) **2016**, 13.
2. Improvement in the enrichment factor of cloud point extraction of uranium in aqueous samples, Abhijit Saha, K. Sanyal, S.B. Deb, M.K. Saxena and B.S. Tomar, 13th National Symposium on Nuclear and Radioanalytical Chemistry (NUCAR) **2017**, E-73, 460-461.
3. Understanding the behaviour of cloud point extraction of uranium in terms of the zeta potential of colloidal dispersion, Abhijit Saha, S.B. Deb, Ajinkya Yadav, M.K. Saxena and B.S. Tomar, NUCAR **2017**, C-29, 222-223.


Abhijit Saha

To my parents

ACKNOWLEDGEMENTS

At the outset, I would like to express my most sincere gratitude to my supervisor, Dr. Bhupendra Singh Tomar for his guidance and constant support. His valuable suggestions, inspiration and constructive criticism inspired me to become an independent researcher and helped me to realize the power of critical analysis based on basic scientific knowledge.

I express my profound sense of gratitude to Shri Manoj Kumar Saxena, Head, Radioanalytical Chemistry Division, BARC for his constant support and scientific advice.

I would like to thank my co-workers Dr. S. B. Deb, Dr. T. Debnath, Dr. S. Neogi, Dr. N. Rawat, Dr. A. Sarkar and Mr. K. Sanyal from different divisions of BARC for their helpful assistance during the course of my research work.

I would like to thank my colleagues Smt. R. Halder, Mr. B. G. Vats, Dr. R. Chowdhury in BARC for always being there whenever I sought their help.

I am thankful to my lab mates Mr. B. K. Nagar, Mr. Ajinkya Yadav and Miss. Khushboo Kumari for their constant support and help.

I would like to express my heartfelt gratitude especially to my parents Mr. Pulak Saha and Smt. Jolly Saha for their selfless love and support throughout my life. I also thank my siblings Priyanka Saha, Kakali Saha, Anamika Saha, Sayan Saha and Subham Saha for always bringing happiness and joy in my life.

I would also like to acknowledge the inspiration, encouragement and whole-hearted cooperation received from my wife Dr. (Smt.) Amritaa Mitra (Saha).

I wish to thank all my colleagues from Radioanalytical Chemistry Division for their assistance and encouragement.

CONTENTS

| | Page No. |
|---|----------|
| SYNOPSIS | i |
| LIST OF FIGURES | xiii |
| LIST OF TABLES | xxi |
| ABBREVIATIONS | xxv |
| CHAPTER 1 Introduction | 1 |
| 1.1. Environmental impact of uranium | 4 |
| 1.2. Requirement of heavy metal ion detection | 6 |
| 1.3. Solution chemistry of uranium | 7 |
| 1.4. Liquid-liquid extraction and solid phase extraction | 8 |
| 1.5. Cloud point extraction | 8 |
| 1.5.1. Role of surfactant | 10 |
| 1.5.2. Role of metal coordinating ligands | 12 |
| 1.5.3. Role of phase modifiers | 13 |
| 1.5.4. Role of pH | 14 |
| 1.5.5. Role of electrolyte | 15 |
| 1.5.6. Role of temperature | 16 |
| 1.5.7. Basic equations of CPE | 16 |
| 1.6. Literature survey on CPE of uranium | 17 |
| 1.7. Motivation for the present work | 18 |
| CHAPTER 2 Experimental methods and instrumentation | 21 |
| 2.1. Preparation of buffer solutions | 23 |
| 2.2. Preparation of metal ion stock solution | 23 |
| 2.3. Synthesis procedures | 24 |
| 2.3.1. Synthesis of diglycolamide capped CdS/ZnS quantum dots (QDs) | 25 |
| 2.3.2. Synthesis of 3-mercaptopropionyl-amidoxime (3-MPD) capped gold nanoparticles (AuNPs) | 29 |

| | |
|--|----|
| 2.3.3 Synthesis of N-propyl-(diphenylphosphoramidate)trimethylammoniumbis-(trifluoromethane-sulfonyl)imide | 33 |
| 2.4. Instruments | 35 |
| 2.4.1. pH meter | 35 |
| 2.4.2. UV-visible spectrophotometry | 35 |
| 2.4.3. Fluorescence spectroscopy | 35 |
| 2.4.4. Transmission electron microscopy (TEM) | 36 |
| 2.4.5. X-ray photoelectron spectroscopy | 36 |
| 2.4.6. Infrared spectroscopy | 37 |
| 2.4.7. Nuclear magnetic resonance spectroscopy | 37 |
| 2.4.8. Elemental analysis | 38 |
| 2.4.9. Mass spectrometry | 38 |
| 2.4.10. X-ray fluorescence spectrometry | 39 |
| 2.4.11. Calorimetry | 39 |
| 2.4.12. Zeta potential analyzer | 40 |
| 2.4.13. Centrifuge | 40 |

| | | |
|---|--|----|
| CHAPTER 3 | Application of common organic ligands in cloud point extraction (CPE) of uranium (U) in aqueous samples | 41 |
| 3.1. Introduction | | 43 |
| 3.2. CPE procedure | | 44 |
| 3.3. UV-visible spectrophotometric detection procedure | | 45 |
| 3.4. Partial least square regression (PLSR) analysis of the absorption spectrum | | 45 |
| 3.5. Optimization of CPE procedure | | 47 |
| 3.5.1. Effect of pH | | 48 |
| 3.5.2. Selection of extractant(s) and their concentration effect | | 49 |
| 3.5.3. Effect of non-ionic surfactant | | 52 |
| 3.5.4. Effect of ionic surfactant concentration | | 53 |
| 3.5.5. Effect of electrolyte concentration | | 54 |

| | |
|--|----|
| 3.5.6. Effect of extraction and phase separation temperature | 55 |
| 3.6. Optimization of spectrophotometric procedure | 56 |
| 3.6.1. Basic principles of partial least square regression (PLSR) algorithm | 58 |
| 3.6.2. Factor optimization of PLSR analysis | 60 |
| 3.6.3. PLSR coefficient | 61 |
| 3.6.4. Accuracy and precision of PLSR analysis | 62 |
| 3.7. Effect of common interfering ions and their tolerance limit | 63 |
| 3.8. Analytical figures of merit and real sample analysis | 64 |
| 3.9. Conclusion | 66 |
| CHAPTER 4 Application of functionalized nanomaterials in cloud point extraction (CPE) of uranium (U) in aqueous samples | 67 |
| 4.1. Functionalized QDs in the CPE based fluorimetric detection of U | 69 |
| 4.1.1. Introduction | 69 |
| 4.1.2. Synthesis and characterization of the QD nanosensor | 70 |
| 4.1.2.1. Synthesis of CdS/ZnS QD | 72 |
| 4.1.2.2. Synthesis of OH-capped CdS/ZnS QD | 72 |
| 4.1.2.3. Synthesis of amino-silanized CdS/ZnS QD | 73 |
| 4.1.2.4. Synthesis of diglycolamide capped CdS/ZnS QD | 75 |
| 4.1.3. Procedure for fluorometric detection of UO_2^{2+} ion | 77 |
| 4.1.4. Cloud point extraction procedure | 79 |
| 4.1.5. Proposed interaction mechanism between UO_2^{2+} ion and QD nanosensor | 80 |
| 4.1.6. Validation of the proposed FRET mechanism and selectivity test | 84 |
| 4.1.7. Optimization of the CPE procedure | 87 |
| 4.1.8. Effect of common interfering ions on the U recovery | 93 |

| | |
|---|-----|
| 4.1.9. Analytical figures of merit | 94 |
| 4.1.10. Method validation and real sample analysis | |
| 4.1.11. Conclusion | 95 |
| | 96 |
| 4.2. Functionalized AuNPs in the CPE based spectrophotometric detection of U | 97 |
| 4.2.1. Introduction | 97 |
| 4.2.2. Synthesis and characterization of functionalized AuNPs | 98 |
| 4.2.2.1. Synthesis scheme | 98 |
| 4.2.2.2. IR and NMR spectroscopy | 99 |
| 4.2.2.3. Transmission electron microscopy (TEM) | 102 |
| 4.2.2.4. X-ray photoelectron spectroscopy (XPS) | 103 |
| 4.2.2.5. UV-visible spectrophotometry | 104 |
| 4.2.3. UV-visible spectrophotometric detection procedure of U(VI) ion | 105 |
| 4.2.4. Cloud point extraction (CPE) procedure | 105 |
| 4.2.5. Interaction of 3-MPD capped AuNPs with uranium | 106 |
| 4.2.6. Selectivity of 3-MPD capped AuNPs towards uranium | 111 |
| 4.2.7. Optimization of CPE of 3-MPD capped AuNPs with and without U(VI) | 113 |
| 4.2.8. Interference study and analytical figures of merit | 118 |
| 4.2.9. Validation of the proposed methodology | 119 |
| 4.2.10. Analysis of real water samples | 120 |
| 4.2.11. Proposed visual detection kit | 120 |
| 4.2.12. Conclusion | 122 |
| CHAPTER 5 Application of task specific ionic liquid (TSIL) in cloud point extraction (CPE) of uranium (U) in aqueous samples | 123 |
| 5.1. Introduction | 125 |
| 5.2. Synthesis and characterization of TSIL | 127 |
| 5.3. CPE procedure | 133 |
| 5.4. TXRF spectrometric analysis | 133 |
| 5.5. Complexation study between U(VI) and TSIL | 134 |

| | |
|---|-----|
| 5.6. Optimization of CPE conditions | 142 |
| 5.6.1. Effect of pH | 142 |
| 5.6.2. Effect of non-ionic surfactant concentration | 144 |
| 5.6.3. Effect of TSIL concentration | 145 |
| 5.6.4. Effect of ionic surfactant concentration | 146 |
| 5.6.5. Effect of electrolyte concentration | 148 |
| 5.6.6. Effect of temperature | 148 |
| 5.7. Optimization of TXRF spectrometric procedure | 149 |
| 5.8. Impact of common interfering ions on CPE | 150 |
| 5.9. Analytical figures of merit | 152 |
| 5.10. Analysis of certified reference material and real water samples | 155 |
| 5.11. Conclusion | 155 |
| CHAPTER 6 Summary and outlook | 157 |
| 6.1. Complete work at a glance | 159 |
| 6.2. Future outlook | 162 |
| REFERENCES | 163 |

Synopsis

The drastic increase in heavy metal contamination to the ambient environment over the last few decades has become a serious issue [1,2]. Although some of these elements like copper (Cu), iron (Fe) and zinc (Zn) are indispensable to the human body upto certain concentration but can lead to toxicity at higher concentrations. Other heavy metals like lead (Pb), mercury (Hg), cadmium (Cd), uranium (U) etc., are not essential to the human biological system and are harmful to organisms even at very low concentrations [1-3]. Uranium (U) is one of the most abundant naturally occurring long-lived actinides in the earth's crust. In nature U mainly occurs as its ore pitchblende, U_3O_8 . In addition to its naturally occurring isotopes viz., ^{234}U (0.005%), ^{235}U (0.720%) and ^{238}U (99.274%), some of its anthropogenic isotopes viz., ^{232}U , ^{233}U and ^{236}U are also being produced in man-made activities [4,5]. Both the natural and anthropogenic isotopes of U are considered to be chemically and radiologically toxic. Since all isotopes of U are alpha active, commonly inhalation and oral uptake of U compounds can affect living organisms. The chemical toxicity of all isotopes and isotopic mixtures of uranium are identical while the radiological toxicity is dependent upon specific activity of each isotope. U has appreciable solubility in water with the most stable chemical form being uranyl ion (UO_2^{2+}). Therefore bioavailable U poses greater risk to human health [3,5].

Apart from the natural occurrence of U in the environment, the other possible ways of its contamination are use of phosphate based fertilizers, leakage from mill tailing ponds, accidental release from nuclear facilities, nuclear explosive tests etc [3,5]. According to World Health Organization (WHO) and U.S. Environmental Protection Agency (EPA) the provisional guideline value for U in drinking water is 30 ng mL^{-1} and is solely based on its chemical toxicity aspect [6,7]. The Atomic Energy

Regulatory Board (AERB), India has established 60 ng mL^{-1} as the maximum permissible U concentration in drinking water [8]. WHO has also established 1 Bq L^{-1} as the guideline value for each isotope of U except ^{238}U (for which it is 10 Bq L^{-1}) [6]. On the other hand U.S. EPA has set 30 pCi L^{-1} for ^{234}U and ^{238}U as the protective measure in the groundwater of mill tailing sites [7].

Selective detection of these heavy metal ions can help in preventing their deleterious effects on environment and living organisms in the very early stage. This requires serious attention in order to precisely quantify ultratrace level of a heavy metal ion in presence of large number of common interfering ions. The above discussed provisional and radiological guideline values clearly indicate that this can be possible by on-line or off-line conjugation of pre-concentration procedures with simple and versatile spectroscopic techniques like UV-Visible spectrophotometry, fluorometry, atomic absorption spectroscopy (AAS), atomic emission spectroscopy (AES), X-ray fluorescence spectroscopy (XRF) etc. Hence development of simple and novel pre-concentration methodologies for improving the detection limit, cost effectiveness, on-site and real-time monitoring etc., are always desirable.

A number of pre-concentration procedures are reported in the literature and the most common being the liquid-liquid extraction (LLE). However the low pre-concentration factor and generation of significant to large volumes of organic waste are the major factors for its limited use in recent times [5]. Solid phase extraction (SPE) with surface modified graphene sheets, carbon nanotubes, carbon nanorods, carbon nanospheres, metaloxide nanoparticles etc., is one of the most emerging pre-concentration techniques in the recent times. However, the low retention capacity,

limited reusability, chances of cross contamination result in generation of significant amount of contaminated waste in SPE which makes the method disadvantageous [5].

During the last two decades, cloud point extraction (CPE) or micelle mediated extraction (MME) has come out as a simple and potential method for separation and pre-concentration of metal ions [5,9,10]. CPE or MME is basically based on the extraction of metal ion into the ligand dispersed micelle phase of non-ionic polyoxyethylene surfactants followed by temperature assisted phase separation and aggregation of micelles, referred as coacervation. This in turn enhances the metal-ligand interaction and hence no external forces are required as in LLE. Therefore CPE represents the modified and eco-friendly version of LLE. The temperature at which the surfactant solution separates into two immiscible phases i.e., (i) bulk aqueous phase containing surfactants at a concentration less than or equal to critical micelle concentration (CMC) and (ii) the surfactant rich phase (SRP), is called its cloud point temperature (CPT). The use of $\mu\text{mol L}^{-1}$ to mmol L^{-1} of reagents and generation of negligible amount of waste make the CPE process as one of the most eco-friendly pre-concentration procedures of all time. Selective pre-concentration of a particular metal ion by CPE requires optimization of various parameters like specific complexing agent and its concentration, pH of the medium, ionic strength of the solution, concentration of surfactant, concentration of co-surfactant (if required), temperature etc.

Application of CPE for pre-concentrating U in environmental aqueous samples can be beneficial for its detection as well as its remediation. This would require CPE methods with quantitative extraction efficiency (EE) so that almost negligible amount

of U is left in the supernatant. Further, CPE methods with quantitative EE and high pre-concentration factor (PF) could be successfully employed for the extraction of this metal from sources like sea water (average U concentration is 3 ng mL^{-1}) to be used as fuel in nuclear reactors. Almost all the literature reported CPE assisted detection of U uses common organic ligands as extractant and most of them lack in wide linear dynamic range, quantitative EE, cost effectiveness, low detection limit, tolerance to the presence of high concentration of various foreign ions etc [5,11-13]. These findings motivated us to explore a simple and novel CPE assisted detection of U in order to improve its linear dynamic range and detection limit; lower the analysis cost and time; tolerate high concentrations of various common interfering ions and enable on-site detection. To the best of our knowledge, till now there is no literature available on the use of functionalized nanomaterials and task specific ionic liquids (TSILs) in CPE of U. Hence we have synthesized and characterized some functionalized nanomaterials and TSIL. Using these materials in CPE of U, some new and versatile detection methodologies have been developed for U. The chapter wise brief description of the thesis is given below.

Chapter 1: Introduction

The first chapter of the thesis presents the brief outline on heavy metal contamination in environment and its impact on living organisms. The major sources of U contamination to the ambient environment in particular have been discussed in detail. Both chemical and radiological toxicity aspects of U along with its guideline values in drinking water have also been discussed. The low level detection of U in environmental aqueous samples is indispensable and requires serious attention. The knowledge of complexation chemistry of U in solution with different types of ligands

is required to develop a new pre-concentration procedure which is briefly outlined. The different pre-concentration methodologies that were developed over the years for detecting low level U have been reviewed. The genesis of CPE, its basic working mechanism, its advantages, its different applications and improvement over the years etc have been explained one by one [9,10]. The basic equations of extraction efficiency, recovery and pre-concentration factor of CPE procedure are mentioned. The available literature on the CPE of U has been discussed in detail. Thereafter the motivation for the work carried out to develop new CPE assisted detection methodologies for U and the scope of thesis are presented at the end of the chapter.

Chapter 2: Experimental methods and Instrumentation

In the beginning of this chapter preparation of all the stock solutions and buffers, standardization of the stock solutions and sample pretreatment procedure are presented. The complete synthesis procedure of functionalized nanomaterials and task specific ionic liquid (TSIL) have been discussed in detail. The details of all the analytical instruments used for characterizing the synthesized products are given here. A general outline of CPE procedure and its optimization process through cross-optimization of all the parameters have been elaborated. The analytical techniques used in U detection and those used to support the CPE mechanisms have also been mentioned.

Chapter 3: Application of common organic ligands in CPE of U in aqueous samples

This chapter deals with the most familiar CPE procedure of pre-concentrating heavy metal ions by common ligands and/or chromophores [5, 11-13]. The need to design a

new and simple CPE assisted detection procedure for U has been discussed in the beginning of this chapter. The selection of extractant and co-extractant pair along with the CPE optimization process has been discussed in detail. The selection of a chromophore and the process optimization for the UV-visible spectroscopic detection is then discussed.

A combination of trioctylphosphine oxide (TOPO) and N,N,N',N'-tetraoctyldiglycolamide (TODGA) is studied to be the most efficient pair for quantitative extraction of U(VI) along with Th(IV). Use of Arsenazo-III as the chromophoric agent in concentrated HNO₃ medium and application of partial least square regression (PLSR) analysis on the absorption spectrum allows precise analyte quantification. The interference study and analytical figures of merit of the developed technique compared to those reported in literature have been discussed. The chapter ends with the discussion on application of the developed analytical methodology to three natural water samples and the cross validation of the results by direct mass spectrometric analyses of those samples.

Chapter 4: Application of functionalized nanomaterials in CPE of U in aqueous samples

This chapter begins with the discussion of different types of nanomaterials and their applications. The scope of applying functionalized nanomaterials in CPE, the requirements and the advantages over conventional CPE techniques etc., have also been elaborated [14]. The chapter is divided into two parts. The first one deals with the use of a hydrophobic nanosensor in conjunction with CPE and the other uses a hydrophilic nanosensor for U detection. In the first part the characterization of the

synthesized novel diglycolamide-capped CdS/ZnS core-shell quantum dot (QD) by infrared (IR) and ^1H NMR spectroscopy, transmission electron microscopy (TEM) and X-ray photoelectron spectroscopy (XPS) have been discussed in the beginning. The fluorimetric U sensing mechanism by the nanosensor is explained in terms of direct Föster Resonance Energy Transfer (FRET) between the UO_2^{2+} ion and QD. The validation of the proposed sensing mechanism is also mentioned. The sensing mechanism is carried out in acetonitrile medium and hence in order to detect U in environmental aqueous samples, the nanosensor is dispersed in surfactant medium to carry out the CPE. The optimization of the CPE procedure with respect to the pH of the medium, electrolyte concentration, surfactant concentration, temperature and an added ionic liquid concentration has been explained. The tolerance of the developed procedure towards the presence of various concentrations of common interfering ions and its analytical figure of merit in comparison to the other competing procedures have been thoroughly discussed. At the end of this part the method validation by analyzing a certified reference material (CRM) and three real sample analysis have been presented.

The second part begins with a discussion of the scheme of preparing novel 3-mercaptopropionylamidoxime (3-MPD) functionalized gold nanoparticles (AuNPs). The characterization of the precursor of 3-mercaptopropionylamidoxime viz, 3,3'-dithiodipropionylamidoxime by IR and ^1H NMR spectroscopy is first discussed. Thereafter the characterization of synthesized 3-MPD capped AuNPs with respect to UV-spectroscopy, TEM, HRTEM and XPS measurements are elaborated. The direct U detection is described by optimizing the pH of the solution and adding poly vinyl alcohol (PVA). The sensing mechanism is described by analyte-triggered aggregation of 3-MPD capped AuNPs in presence of uranium which results in quenching as well

as red shift of its surface plasmon resonance (SPR) absorption spectrum. The proposed mechanism is also validated by TEM and selected area electron diffraction (SAED) measurements. The selectivity of the nanosensor is described by adding equimolar concentrations of U and other interfering elements individually. The modification in the experimental sensing procedure to tolerate high concentrations of some interfering elements is discussed later. The CPE of the functionalized AuNPs in absence and presence of U enables its much low level detection and visual sensing. The optimization of the CPE procedure is discussed in terms of surfactant and a co-surfactant concentration, electrolyte concentration and temperature. The validation of the developed procedure by analyzing a CRM and its application to real samples have been discussed at the end of this chapter.

Chapter 5: Application of task specific ionic liquid (TSIL) in CPE of U in aqueous samples

The chapter begins with a brief discussion on choosing TSIL as the extractant in pre-concentrating heavy metals in CPE [15]. The complete characterization of a novel synthesized TSIL employing IR, ^1H NMR, ^{13}C NMR and ^{31}P NMR spectroscopy, CHNS analysis and ESI-MS has been discussed. Using this TSIL a new CPE procedure for U has been designed and the optimization process with respect to various parameters is presented. In order to understand the mechanism of CPE extraction of U by the TSIL, complexation studies between the two at low acidic medium has been discussed. A brief discussion is made on selecting Total Reflection X-ray Fluorescence (TXRF) spectrometry as the off-line detection technique for U in the preconcentrated samples. The oxidative pyrolysis assisted TXRF spectrometric technique for quantification of U is then completely described.

The developed TSIL assisted CPE procedure in conjunction with TXRF spectrometry has been found to detect very low concentration of U in presence of high concentrations of interfering ions. The quantitative EE, selectivity towards U and resilience to high concentrations of interfering ions of the developed CPE procedure have been elaborated in terms of a newly studied U-TSIL complex. The analytical figures of merit of the developed analytical methodology are presented by comparing this with all reported pre-concentration methodologies. The method validation by analyzing a CRM and application to real samples are described at the end.

Chapter 6: Summary and outlook

The results of the studies carried out as a part of this thesis have been summarized in this chapter. The outcome of the works like (i) use of common organic ligands and chromophore results in a simple and cost effective detection technique for U with wide dynamic linear range, quantitative extraction efficiency, good pre-concentration factor, tolerance to various interfering ions including Zr(IV), Hf(IV), La(III), Eu(III) etc., (ii) development of new and novel UO_2^{2+} -specific nanosensors and their use in CPE of U reveals the possibility of cost effective, highly sensitive, selective and even visual detection of U by means of a single functionalized nanoparticle and (iii) first ever use of any task specific ionic liquid resulting highly selective micellar extraction of U have been discussed. The need for developing such sensitive and selective detection methodologies for other toxic elements and preparing on-site detection kits have been discussed at the end of this chapter for future research direction.

References

- [1] C.-S. Wu, M.K.K. Oo, X. Fan, ACS NANO 4 (2010) 5897-5904.
- [2] N. Verma, M. Singh, BioMetals 18 (2005) 121-129.
- [3] J. Liu, A.K. Brown, X. Meng, D.M. Cropek, J.D. Istok, J.D. Watson, Y. Lu, PNAS 104 (2007) 2056-2061.
- [4] C.T. Garten, E.A. Bondietti, R.L. Walker, J. Environ. Qual. 10 (1981) 207-210.
- [5] C. Labrecque, S. Potvin, L. Whitty-Léveillé, D. Larivière, Talanta 107 (2013) 284-291.
- [6] WHO: Guidelines for drinking-water quality, 4th ed., Geneva, Switzerland, (2011).
- [7] Common radionuclides found at superfund sites, EPA facts about uranium, Environmental Protection Agency, US, (2002).
- [8] AERB, Drinking water specifications in India, Department of Atomic Energy, Govt. of India, (2004).
- [9] C.D. Stalikas, Trends Anal. Chem. 21 (2002) 343-355.
- [10] C.B. Ojeda, F.S. Rojas, Microchim. Acta 177 (2012) 1-21.
- [11] H.S. Ferreira, M.D. Bezerra, S.L.C. Ferreira, Microchim. Acta 154 (2006) 163-167.
- [12] T. Madrakian, A. Afkhami, A. Mousavi, Talanta 71 (2007) 610-614.
- [13] S. Shariati, Y. Yamini, A.K. Zanjani, J. Hazard. Mater. 156 (2008) 583-590.
- [14] J.-f. Liu, R. Liu, Y.-g. Yin, G.-b. Jiang, Chem. Commun. (2009) 1514-1516.
- [15] S. Gao, T. Sun, Q. Chen, X. J. Shen, J. Hazard. Mater. 263 (2013) 562-568.

List of figures

| Chapter 1 | | Page no. |
|------------------|--|-----------------|
| Figure 1.1 | Pictorial representation of cloud point extraction (CPE) mechanism |13 |
| Chapter 3 | | |
| Figure 3.1 | Pictorial representation of the developed CPE procedure |46 |
| Figure 3.2 | Effect of pH on the recovery of 50 ng mL ⁻¹ of U and Th each. Other parameters were kept constant as presented in Table 3.2 |49 |
| Figure 3.3 | Effect of TOPO concentration on the recoveries of 50 ng mL ⁻¹ of U and Th each in absence and presence of equimolar La. TODGA had not been added during this exercise and the other parameters were kept constant as presented in Table 3.2. |51 |
| Figure 3.4 | Effect of TODGA concentration on the recoveries of 50 ng mL ⁻¹ of U and Th each in presence of 50 ng mL ⁻¹ La. Other parameters were kept constant as presented in Table 3.2. |51 |
| Figure 3.5 | Effect of TTX-114 concentration on the recoveries of 50 ng mL ⁻¹ of U and Th each. Other parameters were kept constant as presented in Table 3.2. |52 |
| Figure 3.6 | Effect of SDS concentration on the recoveries of 50 ng mL ⁻¹ of U and Th each. Other parameters were kept constant as presented in Table 3.2. |53 |
| Figure 3.7 | Effect of KNO ₃ concentration on the recoveries of 50 ng mL ⁻¹ of U and Th each. Other parameters were kept constant as presented in Table 3.2. |54 |
| Figure 3.8 | Effect of extraction and phase separation temperatures on the recovery of 50 ng mL ⁻¹ of U and Th each. Other parameters were kept constant as presented in Table 3.2. |56 |
| Figure 3.9 | (a) Structure of arsenazo-III and (b) visual colour change of Th-arsenazo-III complex (top) in HCl medium within 30 min; (middle) in HNO ₃ and sulfamic acid medium within 1 h and (bottom) in HClO ₄ medium within 5 min, where the Th concentration is 2.5 µg mL ⁻¹ . |58 |
| Figure 3.10 | Effect of mineral acids, 6 mol L ⁻¹ of HCl (a and d), HNO ₃ + 0.1 mol L ⁻¹ sulfamic acid (b and e) and HClO ₄ (c and f), and metal ion concentration, 1 µg mL ⁻¹ (a, b and c) and 5 µg mL ⁻¹ (d, e and f), on the absorption maximum of Th using arsenazo-III with time. Spectra were recorded after (1) 5 min, (2) 15 min, (3) 25 min, (4) 35 min and (5) 45 min of the addition of arsenazo-III. |59 |
| Figure 3.11 | Optimization of PLSR algorithm factor. |61 |
| Figure 3.12 | Absorption spectra of U and Th mixtures and the individual PLSRC's for U and Th. |62 |

| Chapter 4 | Page no. |
|--|----------|
| Figure 4.1 Complete reaction route of synthesizing diglycolamide-capped CdS/ZnS core-shell quantum dots (QDs) with respective IR spectra of all the products and also the NMR spectrum of the final product. |71 |
| Figure 4.2 Absorption spectrum of oleic acid-capped CdS/ZnS QDs |72 |
| Figure 4.3 TEM micrographs and the corresponding size distributions of (a,d) OH-capped, (b,e) amino-silanized and (c,f) diglycolamide-capped CdS/ZnS QDs. The emission spectra of (g) OH-capped, (h) amino-silanized and (i) diglycolamide-capped CdS/ZnS QDs were obtained with the excitation wavelength (λ_{ex}) of 355 nm. |74 |
| Figure 4.4 (a) High-resolution TEM (HRTEM) image of OH-capped CdS/ZnS QDs. (b) FFT image of HRTEM micrograph of OH-capped CdS/ZnS QDs. |75 |
| Figure 4.5 Normalized absorption spectra of the OH- and diglycolamide-capped CdS/ZnS QDs and emission spectra of UO_2^{2+} ($\lambda_{\text{ex}} = 355 \text{ nm}$) and Eu^{3+} ($\lambda_{\text{ex}} = 395 \text{ nm}$) ions in solution. |76 |
| Figure 4.6 (a) Survey scan XPS spectrum of OH-capped CdS/ZnS QDs along and its high-resolution XPS spectrum for 2p level of S. (b) Survey scan XPS spectrum of diglycolamide-capped CdS/ZnS QDs. |78 |
| Figure 4.7 Pictorial representation of CPE procedure |80 |
| Figure 4.8 Proposed FRET interaction between UO_2^{2+} ion and QD. |82 |
| Figure 4.9 Emission spectra of diglycolamide-capped CdS/ZnS QDs ($\lambda_{\text{ex}} = 355 \text{ nm}$) solution before and after addition of UO_2^{2+} and Eu^{3+} . |82 |
| Figure 4.10 Change of fluorescence intensity when UO_2^{2+} was added to OH-capped CdS/ZnS QDs solution. |83 |
| Figure 4.11 Emission spectra of amino-silanized CdS/ZnS QDs ($\lambda_{\text{ex}} = 355 \text{ nm}$) before and after addition of UO_2^{2+} . |83 |
| Figure 4.12 (a) Increase in fluorescence intensity of diglycolamide-capped CdS/ZnS QDs ($\lambda_{\text{ex}} = 355 \text{ nm}$) with gradual increase in added UO_2^{2+} concentration. (b) Increase in integrated emission intensity ($F-F_0$) was plotted as a function of UO_2^{2+} concentration. Inset: calibration plot of ($F-F_0$) vs, concentration of UO_2^{2+} . |85 |
| Figure 4.13 Time dependent fluorescence intensity (recorded at 495 nm) of diglycolamide-capped CdS/ZnS QDs ($\lambda_{\text{ex}} = 355 \text{ nm}$) in presence of different concentrations of UO_2^{2+} . |85 |

| | Page no. |
|--|-----------------|
| Figure 4.14 Time-resolved fluorescence measurements of the diglycolamide-capped CdS/ZnS QDs, recorded at 495 nm before and after adding UO_2^{2+} ions ($\lambda_{\text{ex}} = 355 \text{ nm}$). |87 |
| Figure 4.15 (a) Effect of pH; (b) effect of $\text{C}_4\text{mimNTf}_2$ concentration; (c) effect of different types of IL viz., $\text{C}_4\text{mimNTf}_2$ (1), $\text{C}_6\text{mimNTf}_2$ (2), $\text{C}_8\text{mimNTf}_2$ (3) and $\text{C}_{10}\text{mimNTf}_2$ (4) and (d) effect of non-ionic surfactant concentration on the percentage recovery of UO_2^{2+} when the CPE is carried out with keeping all other parameters constant as per Table 4.1. |89 |
| Figure 4.16 TEM micrographs and corresponding size distributions of (a,c) 2.5 mmol L^{-1} TTX-114 solution and (b,d) 2.5 mmol L^{-1} TTX-114 in presence of diglycolamide-capped CdS/ZnS QDs. |90 |
| Figure 4.17 Stepwise synthesis of 3-MPD functionalized AuNPs. |99 |
| Figure 4.18 IR spectra of (a) Methyl-3-mercaptopropionate; (b) 3,3'-dithiopropionamide; (c) 3,3'-dithiopropionitrile and (d) 3,3'-dithiopropionylamidoxime. |100 |
| Figure 4.19 ^1H NMR spectrum of 3,3'-dithiopropionylamidoxime. |101 |
| Figure 4.20 TEM micrographs and the corresponding size distribution of citrate stabilized AuNPs (a,b) and 3-MPD capped AuNPs (c,d) . |102 |
| Figure 4.21 HRTEM image of 3-MPD capped AuNPs |103 |
| Figure 4.22 (a) Survey scan XPS spectrum of 3-MPD capped AuNPs and (b) High resolution survey scan XPS spectrum of 3-MPD capped AuNPs. |104 |
| Figure 4.23 Absorption spectra of 20 nmol L^{-1} (a) citrate stabilized AuNPs and (b) 3-MPD capped AuNPs. |105 |
| Figure 4.24 (a) Absorption spectrum of 20 nmol L^{-1} 3-MPD capped AuNPs. Simultaneous quenching and red shift of absorption spectrum of 3-MPD capped AuNPs in presence of 100.0 ng mL^{-1} U at pH: (b) 5.0, (c) 5.5, (d) 6.0, (e) 6.5, (f) 7.0, (g) 7.5 and (h) 8.0. |108 |
| Figure 4.25 Aggregation of 3-MPD capped AuNPs via interaction with U(VI) ions. |109 |
| Figure 4.26 (a) TEM image of aggregated 3-MPD capped AuNPs in presence of U(VI) and (b) SAED image of the selected area in TEM image. |110 |
| Figure 4.27 Change in absorption spectrum of 3-MPD capped AuNPs with addition of (a) 0 (b) 5, (c) 10, (d) 20, (e) 30, (f) 40, (g) 50, (h) 60, (i) 70, (j) 80, (k) 90, (l) 100, (m) 110, (n) 120 and (o) 130 ng mL^{-1} U(VI) ion. |110 |
| Figure 4.28 (a) Calibration plot of A_0/A vs. concentration of U and (b) Calibration plot of $\lambda_0 - \lambda$ vs. concentration of U. |111 |

| | Page no. |
|--|-----------------|
| Figure 4.29 Change in absorption spectrum of 3-MPD capped AuNPs in presence of 100 ng mL ⁻¹ various metal ions. |112 |
| Figure 4.30 Bar diagram representing A_0/A values of 3-MPD capped AuNPs treated with respective interfering cations in the absence and presence of U(VI) ions. |113 |
| Figure 4.31 Effect of TTX-114 concentration on U recovery by CPE procedure when all other parameters in Table 4.6 remain constant. |115 |
| Figure 4.32 Effect of CTAB concentration on U recovery by CPE procedure when all other parameters in Table 4.6 remain constant. |116 |
| Figure 4.33 Effect of NaCl concentration on U recovery by CPE procedure when all other parameters in Table 4.6 remain constant. |116 |
| Figure 4.34 Effect of temperature on U recovery by CPE procedure when all other parameters in Table 4.6 remain constant. |117 |
| Figure 4.35 Change in colour of SRP as a function of various concentrations of U. |119 |
| Figure 4.36 Reference colour change in U detection kit at, below and above the WHO and USEPA guideline limit of 30 ng mL ⁻¹ U in drinking water. |121 |
| Chapter 5 | |
| Figure 5.1 Schematic representation of the complete synthesis route of TSIL. |127 |
| Figure 5.2 ¹ H NMR spectrum of synthesized TSIL. |129 |
| Figure 5.3 ¹³ C NMR spectrum of synthesized TSIL. |130 |
| Figure 5.4 ³¹ P NMR spectrum of synthesized TSIL. |131 |
| Figure 5.5 IR spectrum of synthesized TSIL. |131 |
| Figure 5.6 ESI-MS spectrum of synthesized TSIL. |132 |
| Figure 5.7 Log-log plot between the distribution ratio of U(VI) (D_U) and the concentration of the HNO ₃ in the aqueous phase when extracted by TSIL in [Me ₃ NBu][NTf ₂]. |135 |
| Figure 5.8 The peaks of power (micro watt) vs. time (s) graph for ICT experiment: (a) titration of U(VI) in 1:1 mixture of 4.0 mol L ⁻¹ HNO ₃ and acetonitrile and (b) titration of U(VI) in 1:1 mixture of 0.02 mol L ⁻¹ HNO ₃ and acetonitrile with TSIL in 1:1 water/ acetonitrile mixture. |137 |
| Figure 5.9 Plot of heat of reaction per mole of U(VI) ion (h_{vi}) vs. number of TSIL bound per U(VI) ion (n_{avg}) of the same reactions described in Figure 5.8. |137 |
| Figure 5.10 ³¹ P NMR spectrum of U(VI)-TSIL complex. |138 |

| | Page no. |
|--|-----------------|
| Figure 5.11 IR spectrum of U(VI)-TSIL complex. |139 |
| Figure 5.12 Proposed structure of the complex between U(VI) and TSIL. |140 |
| Figure 5.13 ESI-MS spectrum of UO_2^{2+} -TSIL complex in acetonitrile. |141 |
| Figure 5.14 Effect of pH on the recoveries of 10 ng mL^{-1} of U. Other parameters were kept constant as presented in Table 5.1. |143 |
| Figure 5.15 Effect of TTX-114 concentration on the recoveries of 10 ng mL^{-1} of U. Other parameters were kept constant as presented in Table 5.1. |144 |
| Figure 5.16 Effect of TSIL concentration on the recoveries of 10 ng mL^{-1} of U. Other parameters were kept constant as presented in Table 5.1. |145 |
| Figure 5.17 Proposed mechanism of selected CPE of UO_2^{2+} by TSIL. |146 |
| Figure 5.18 Effect of SDS concentration on the recoveries of 10 ng mL^{-1} of U. Other parameters were kept constant as presented in Table 5.1. |147 |
| Figure 5.19 Effect of KNO_3 concentration on the recoveries of 10 ng mL^{-1} of U. Other parameters were kept constant as presented in Table 5.1. |149 |
| Figure 5.20 TXRF spectra of $50 \text{ }\mu\text{L}$ SRP phase deposited on quartz sample support before the pyrolysis (black) and after the pyrolysis (red). |150 |

List of tables

| Chapter 1 | Page no. |
|--|-----------------|
| Table 1.1 List of commonly used nonionic and zwitterionic surfactants along with their CMC and CPT. |11 |
| Table 1.2 Comparison of reported CPE methodologies for uranium. |19 |
| Chapter 2 | |
| Table 2.1 Preparation of buffer solutions in 50 mL volumetric flask. |24 |
| Table 2.2 Categorization of newly synthesized materials. |25 |
| Chapter 3 | |
| Table 3.1 Concentration of the analytes in the calibration set (CS) and validation set (VS) used for the PLSR analysis of U and Th. |47 |
| Table 3.2 Optimized conditions for CPE system before coacervation (Total volume = 50 mL). |48 |
| Table 3.3 Concentrations of U and Th in VS solutions as predicted by PLSR and statistical parameters of the PLSR algorithm. |63 |
| Table 3.4 Tolerance limit of the developed method in the presence of selected cations and anions; Concentration of U and Th: 50 ng mL ⁻¹ each. |65 |
| Table 3.5. Analysis of real water samples by the developed analytical methodology (n = 5) and cross-validation of the results by direct analysis employing ICP-MS (n = 3). |66 |
| Chapter 4 | |
| Table 4.1. Optimized parameters for the developed CPE procedure before coacervation (Total volume = 50 mL). |88 |
| Table 4.2. Tolerance of the method to foreign metal ions (experiments carried out with 10 ng mL ⁻¹ of U). |94 |
| Table 4.3. Comparison of analytical performance of the developed method with the previously published other analytical methods for low level detection of U. |95 |
| Table 4.4. Determination of uranium in NIST SRM 1640a natural water standard (Sample volume = 5 mL; n = 3). |96 |
| Table 4.5. Analysis of real samples (n = 5). |96 |
| Table 4.6. Optimized conditions for CPE system before coacervation (Total volume = 10 mL). |114 |
| Table 4.7. Tolerance of the method to the presence of foreign metal ions (experiments carried out with 5.0 ng mL ⁻¹ of U). |118 |
| Table 4.8. Determination of U in NIST SRM 1640a natural water standard (Sample volume = 3 mL; n = 3). |120 |
| Table 4.9. Analysis of natural water samples (n = 5). |120 |
| Chapter 5 | |
| Table 5.1. Optimized conditions of CPE procedure for total 10 mL aqueous phase before coacervation. |142 |

| | Page no. |
|---|-----------------|
| Table 5.2. Tolerance of the method to common interfering metal ions (experiments carried out with 10 ng mL ⁻¹ of U). |152 |
| Table 5.3. Comparison of the important CPE characteristics of the developed method for U with reported methodologies. |154 |
| Table 5.4. Analysis of a CRM and real samples viz., sea water from Mumbai coast, India; well water from West Bengal, India and Spring water from Sikkim, India (n = 5). |155 |

Abbreviations

| | |
|--------------------|---|
| CPE | Cloud point extraction |
| MME | Micelle mediated extraction |
| CMC | Critical micelle concentration |
| CPT | Cloud point temperature |
| SRP | Surfactant rich phase |
| TTX-114 | Polyethylene glycol tert-octylphenyl ether (Triton X-114) |
| EE | Extraction efficiency |
| PF | Preconcentration factor |
| CTAB | Cetyl-trimethylammonium bromide |
| SDS | Sodium dodecylsulphate |
| LLE | Liquid-liquid extraction |
| SPE | Solid phase extraction |
| CS and VS | Calibration set and Validation set |
| PLSR | Partial least square regression |
| PLSRC | Partial least square regression coefficient |
| RMSE _{cv} | Root mean square error of cross validation |
| RMSEP | Root mean square of prediction |
| REP | Relative error of prediction |
| WHO | World Health Organization |
| USEPA | United States Environmental Protection Agency |
| AERB | Atomic Energy Regulatory Board |
| ICP-MS | Inductively coupled plasma mass spectrometry |
| ESI-MS | Electrospray ionization mass spectrometry |
| IR | Infrared |
| NMR | Nuclear magnetic resonance |
| TEM | Transmission electron microscopy |
| HRTEM | High resolution transmission electron microscopy |
| SAED | Small angle electron diffraction |
| XPS | X-ray photoelectron spectroscopy |
| TOPO | Tri-n-octyl phosphine oxide |
| TODGA | N,N,N',N'-tetraoctyldiglycolamide |
| NP | Nanoparticle |
| QD | Quantum dot |
| AuNP | Gold nanoparticle |
| 3-MPD | 3-mercaptopropionylamidoxime |
| FRET | Föster Resonance Energy Transfer |
| SPR | Surface plasmon resonance |
| IL | Ionic liquid |

| | |
|-------------------------------|-------------------------------------|
| RTIL | Room temperature ionic liquid |
| TSIL | Task specific ionic liquid |
| NTf ₂ ⁻ | bis(trifluoromethanesulfonyl) imide |
| DLR | Dynamic linear concentration range |
| DL | Detection limit |
| MDL | Method detection limit |
| LOQ | Limit of quantification |
| CRM | Certified reference material |
| TXRF | Total reflection X-ray fluorescence |
| ACN | Acetonitrile |

Chapter 1

Introduction



This page is kept blank intentionally

The accelerated pace of global industrialization has resulted in increased contamination of the biosphere with toxic heavy metals. This is a big issue in developing as well as in developed countries. Heavy metal contamination to the ambient environment is one of the most serious pollution problems of all time, as it poses great challenge to human health and ecological balance [1-5]. The environmental infectivity of non-biodegradable heavy metals has been significantly increased in the recent times [6,7]. Solid wastes and waste waters from different industrial branches, in particular metal plating, chemical fibre, dye and tanning factories etc., thermal and nuclear power plants, mining industries, vehicle emission etc., are the major contributors to heavy metal poisoning in the environment [1-11]. In addition to these, use of metal containing pesticides and therapeutic agents, use of phosphate based fertilizers, addition of tetra-ethyl lead to gasoline etc., are the additional sources of environmental hazard by heavy metals [1,11,12]. Contamination by heavy metals affects the biosphere e.g., air, soil and water with most common among them as, chromium (Cr) [13,14], iron (Fe) [15,16], copper (Cu) [17,18], zinc (Zn) [19,20], mercury (Hg) [21-23], cadmium (Cd) [24-26], lead (Pb) [27-29], uranium (U) [12,30-33] etc. Some of these heavy metals like Cu, Fe and Zn are essential to the human body upto certain concentration and toxic beyond these limits [15-17,19]. Others are not biologically essential to living organisms and toxic at even very low concentrations. Toxicity of these heavy metals is mostly chemical and in some cases it is radiological too. The chemical toxicity of an element is related to the interaction of its chemical species with the biochemical processes in the human body [34]. On the other hand radiological toxicity of an element is related to specific activity and biological half-life of its isotope(s) [34].

1.1. Environmental impact of uranium

Uranium, being one of the most abundant naturally occurring long-live actinides, is ubiquitously present in the environment [30-32,35]. In nature it mainly occurs as its ore pitchblende, U_3O_8 and is an important nuclear fuel material. In addition to its naturally occurring isotopes viz., ^{234}U (0.005%), ^{235}U (0.720%) and ^{238}U (99.274%), some of its anthropogenic isotopes viz., ^{232}U , ^{233}U and ^{236}U are also being produced in man-made activities [35-38]. Both the natural and anthropogenic isotopes of U are considered to be chemically and radiologically toxic [31-34,38]. Since all isotopes of U are alpha active, commonly inhalation and oral uptake of its compounds can affect living organisms [34]. The chemical toxicity of all isotopes and isotopic mixtures of uranium are identical while the radiological toxicity is dependent upon specific activity of each isotope. U has a considerable amount of solubility in water [39]. On a global basis, its concentration in soil varies from 1-5 $\mu\text{g g}^{-1}$ while in water it varies from 1-3 ng mL^{-1} [34]. Apart from its omnipresence in the environment, the possible ways of its environmental contamination are: (i) leakage from nuclear waste repository and mill tailing ponds, which can lead to the contamination of the surrounding soil and natural water systems via migration; (ii) accidental release from nuclear power plants and nuclear explosive tests, that can directly contaminate the surrounding air, soil and water and (iii) the use of phosphate based fertilizers which commonly contain uranium, can contaminate the agricultural land and after washing out can migrate to the ground water, lake water, river water etc [12,30-33]. These processes enhance the bioavailability of U and hence pose greater risk to living organisms [32,40-42]. The water solubility of U is mainly due to its well known stable chemical form viz., uranyl ion (UO_2^{2+}) in aerobic conditions and carbonate complexes prevalent in seawater viz., $(\text{UO}_2)_2(\text{CO}_3)_3^{2-}$ or $\text{UO}_2(\text{CO}_3)_2^{2-}$ [32,40-42]. Hence, due to

the high mobility and toxicity of uranium, worldwide several organizations have set guideline values for U in drinking water depending on its chemical and radiological toxicity.

The toxicity due to ingestion of U via drinking water into the human body is twofold – chemical as well as radiological. The ingested U can deposit in various body parts such as, liver, bone, kidney etc., and thereby causing several health problems such as renal dysfunction or failure and cancer [31,34,43-45]. Several epidemiology studies on human exposure to water soluble U had been carried out by many scientific groups as evidence of U to be a nephrotoxic metal, exerting its toxic effect by chemical action mostly in the renal proximal tubules of humans [45,46-49]. The increased levels of urinary glucose, β_2 -microglobulin, and alkaline phosphatase in humans with increasing uptake of U in drinking water is a clear evidence of U nephrotoxicity [46-49]. The chemical toxicity of U is due to the oxidizing power of UO_2^{2+} ions, as they induce oxidative stress on biomolecules through the generation of reactive oxygen species and resulting in disruption of metabolic processes [50]. There is no report available in literature linking oral exposure of U to human cancer. However, the oxidative and radiation affected DNA damage may cause long-term genotoxic effects in the form of carcinogenesis to humans [50]. The exact interaction mechanism is yet not clear. The World Health Organization (WHO) and United States Environmental Protection Agency (USEPA) have assessed the health risks caused by ingestion of U and thereby set guideline values for health-based exposure limits. Both WHO and USEPA have set 30 ng mL^{-1} as the provisional guideline value of U in drinking water and this value is solely based on its chemical toxicity aspect [34,51]. Monitoring the same chemical toxicological aspect, the Atomic Energy Regulatory Board (AERB) in

India, has established 60 ng mL^{-1} as the maximum permissible contamination level of U in drinking water [52]. Since the specific activity of natural U ($7.1 \times 10^{-7} \text{ Ci g}^{-1}$) is too low to exert any profound radiological toxicity, it is the chemical toxicological effect which is of concern to the scientists. However, enrichment of ^{235}U and generation of anthropogenic isotopes of U in various nuclear facilities have increased the possibilities of contamination several times by more radioactive U isotopes. In this regard, WHO has also established 1 Bq L^{-1} as the guideline value for each isotope of U except ^{238}U (for which it is 10 Bq L^{-1}) [34]. On the other hand USEPA has set 30 pCi L^{-1} for ^{234}U and ^{238}U as the protective measure in the groundwater of mill tailing sites [51].

1.2. Requirement of heavy metal ion detection

Detection of heavy metal(s) in environmental samples is indispensable in order to restrict the human exposure and take early measures for its remediation. However, detection and precise quantification of any heavy metal in such samples is always a challenging task to the scientists due to the complexity of these matrices. The major problem arises due to the presence of common interfering ions in higher concentration than that of the analyte(s) of interest. Similar ionic radius, charge and other chemical or physical properties of many metal ions makes it difficult to precisely quantify ultratrace level concentration of any metal ion in presence of high concentration of other ions using any analytical instrument. Therefore, the chemical and radiological guideline values of U in drinking water clearly indicate the need for developing selective extraction as well as preconcentration procedure for U. Hence, preconcentration of metal ions is a prerequisite to achieve better detection limits and reproducibility in results with simple and versatile spectroscopic instruments, like

UV-visible spectrophotometry [53-56], atomic absorption spectroscopy (AAS) [57-60] and X-ray fluorescence spectroscopy (XRF) [61,62] etc. Inductively coupled plasma mass spectrometry (ICP-MS) [63-65] and laser fluorimetry [66-68] were previously reported to directly quantify ultratrace levels of U in natural water samples, but their high cost and maintenance, sophisticated and complex instrumentation, requirement of trained personnel with well equipped laboratories and inability to do on-site and real-time monitoring make their use restricted. Hence, development of simple and novel preconcentration methodologies for heavy metals is always desirable.

1.3. Solution chemistry of uranium

In order to design the extraction methodology for any particular metal ion, knowledge about its aqueous chemistry and complexation mechanism with different ligands is essential. U can possess varying oxidation states like +4 and +6 in water, whereas the +6 oxidation state in the form of UO_2^{2+} ion is most stable [30,40,42]. UO_2^{2+} ion is an oxyanion of U(VI) and has a linear structure [69]. In water the UO_2^{2+} ion remains surrounded by five water molecules in the primary coordination sphere [70]. Due to the high charge density and vacant f-orbital of UO_2^{2+} ion, it acts as a hard acid and forms complexes particularly with O-donor ligands [71]. Maximum six monodentate ligands can be bound to the UO_2^{2+} ion in the equatorial plane by substituting the water molecules [71]. The stability of the UO_2^{2+} species in water is pH dependent [72,73]. In the pH range of 1 to 4, UO_2^{2+} ion is predominant [72,73]. As the pH increases, hydrolysis of UO_2^{2+} leads to increase in concentration of $\text{UO}_2(\text{OH})^+$, while that of UO_2^{2+} decreases. However, below pH 6.5, both UO_2^{2+} and $\text{UO}_2(\text{OH})^+$ ions co-exist in

solution [72,73]. Above pH 6.5 to the alkaline range, U mainly exists as $\text{UO}_2(\text{OH})_2$, UO_2CO_3 , $\text{UO}_2(\text{CO}_3)_2^{2-}$ etc., in aerobic condition [72,73].

1.4. Liquid-liquid extraction and solid phase extraction

Liquid-liquid extraction (LLE) is the most common preconcentration procedure known for a long time [58,74,75]. In this process, equilibration between the two immiscible phases results in extraction of metal ion from aqueous to the organic phase depending on its distribution ratio (K_D) value. Generation of large volumes of organic waste in LLE increases the environmental hazard risk by several times and thereby limits its use in recent times [32]. Solid phase extraction (SPE) is another widespread and effective preconcentration procedure to separate the analyte from common interfering ions [53,54,76-78]. The use of surface modified nanocomposites, like graphene sheets, carbon nanorods, carbon nanospheres, metaloxide nanoparticles etc., had upgraded the SPE process several times in the last two decades [53,54,76-78]. However, the low retention capacity of commercially available resins, limited reusability and chances of cross contamination result in generation of significant amount of contaminated solid waste in SPE, which makes the method disadvantageous [32,79,80]. Therefore, various research groups are working worldwide on developing more eco-friendly as well as selective preconcentration procedure for analyte(s) of interest.

1.5. Cloud point extraction (CPE)

In the last two decades, cloud point extraction (CPE) or micelle mediated extraction (MME) has emerged as a simple, cheap, potential and eco-friendly method for separation and preconcentration of metal ions from environmental matrices [81-85].

In the year 1976, Watanabe and co-workers first introduced CPE as separation and extraction technique for preconcentration of metal ions as their hydrophobic complexes [86]. Subsequently the method was also extensively used in purification of proteins [84]. CPE is based on the phenomenon of separation of two isotropic phases generated from micelle solution [81-85]. The clear and homogeneous aqueous solution of some surfactants becomes turbid at and above some particular temperature and separates into two immiscible phases, that is (i) bulk aqueous phase containing surfactants at a concentration less than or equal to critical micelle concentration (CMC) and (ii) the surfactant rich phase (SRP) of very small volume. This temperature is referred to the cloud point temperature (CPT) of that particular micellar system. However, the phase separation can also be achieved by change in pressure or adding any substance to the solution [81-85]. Hence any analyte, organic or inorganic, that gets trapped into the micellar core due to its hydrophobicity, can be separated and preconcentrated in the SRP from the bulk. Compared to a hydrated metal ion, selective metal-ligand complexation therefore can easily preconcentrate metal ion(s) in CPE method.

CPE has been turning out as one of the most eco-friendly preconcentration procedures for detection and remediation of heavy metal ions from environmental matrices due to its adherence to the principles of ‘Green Chemistry’ [81,85]. The analytical procedures, which are able to decrease or eliminate the use or generation of harmful and toxic substances come under this category [81,85]. The use of small amounts of less toxic surfactants in CPE compared to the toxic organic solvents in LLE results in generation of negligible laboratory residue [81,85]. In addition to that, surfactants are

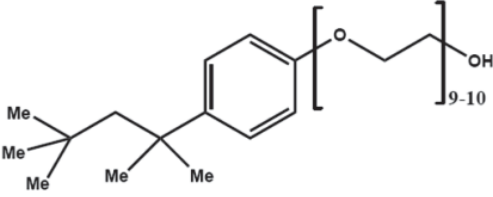
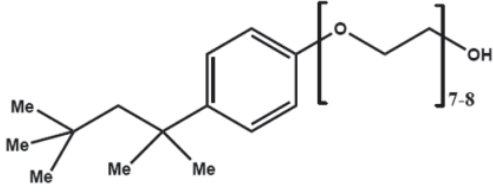
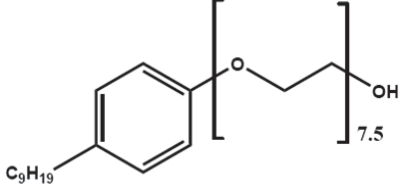
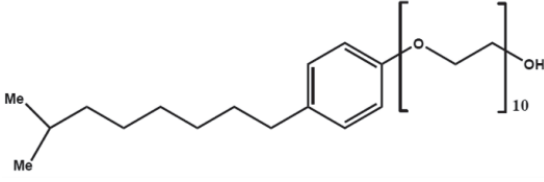
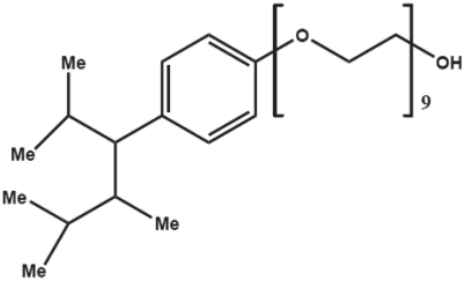
neither volatile nor easily flammable which minimizes the risk of creating explosive or hazardous conditions.

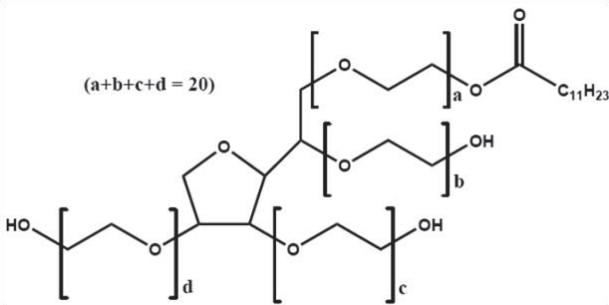
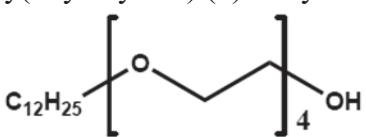
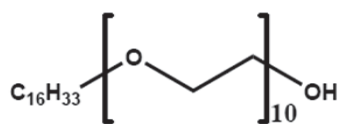
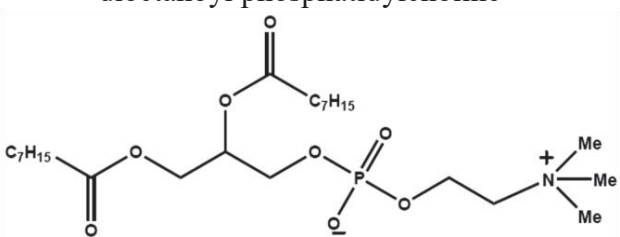
1.5.1. Role of surfactant

Surfactants are amphiphilic molecules containing a polar head-group and a non-polar tail and are of four types viz., non-ionic, cationic, anionic and zwitterionic [81-85,87]. The non-polar tail constitutes the hydrophobic part of the surfactant and generally consists of long chain hydrocarbons, branched hydrocarbons or carbon chain with aromatic rings. On the other, hand the hydrophilic head is either ionic or polar group. In aqueous medium, when these surfactants are added above their CMC, the hydrophobic tail of each monomer block gravitates to create aggregates called micelles [81-85,87]. The structure of micelles have two main parts i.e., core and corona. The micellar core being hydrophobic in nature can solubilize the metal-ligand complex and this phenomenon is utilized in CPE. At the corona, hydrophilic head-groups remain in direct contact with bulk water molecules via H-bonding, which results in solvation cage. At CPT the micelles get dehydrated through breaking of these H-bonds and separate out from the bulk aqueous phase to coacervate. In general non-ionic and zwitterionic surfactants are commonly used in CPE procedure [81-85]. The cationic and anionic surfactants are not suitable candidates for CPE, because the electrostatic repulsion among the similar head groups does not allow the micelles to get coacervated. A list of surfactants that have been employed in CPE by various research groups is given in **Table 1.1** along with the values of their individual CMC and CPT. This information is necessary to select an appropriate surfactant or sometimes mixture of surfactants for developing new CPE methodologies. Majority

of these surfactants used for CPE of metal ions are non-ionic, which contain hydrophilic polyoxyethylene chains and hydrophobic groups as mentioned earlier.

Table 1.1. List of commonly used nonionic and zwitterionic surfactants along with their CMC and CPT

| Surfactant | Commercial name | CMC ^a (mmol L ⁻¹) | CPT ^b (°C) |
|--|---------------------------|---|--------------------------|
| Polyethylene glycol tert-octylphenyl ether  | Triton X-100 (TTX-100) | 0.17-0.30 | 64-65 |
| Polyethylene glycol tert-octylphenyl ether  | Triton X-114 (TTX-114) | 0.20-0.35 | 23-25 |
| Polyoxyethylene (7.5)-nonylphenyl ether  | PONPE-7.5 | 0.085 | 5-20 |
| Polyoxyethylene (10)-p-isononylphenyl ether  | PONPE-10 | 0.07-0.085 | 62-65 |
| Polyoxyethylene (9)-nonylphenylether, branched  | IGEAL CO-630 | --- | 48-52 |

| Surfactant | Commercial name | CMC ^a (mmol L ⁻¹) | CPT ^b (°C) |
|--|-----------------|---|--------------------------|
| Polyoxyethylene (20) sorbitan monolaurate  | Tween 20 | 0.06 | 20-25 |
| Poly(oxyethylene) (4) lauryl ether  | Brij 30 | 0.02-0.06 | 2-7 |
| Polyoxyethylene (10) Cetyl Ether  | Brij 56 | 0.0006 | 64-69 |
| dioctanoyl phosphatidylcholine  | C8-lecithin | --- | 45 |

^{a,b}The CMC and CPT values are taken from reference [83].

1.5.2. Role of metal coordinating ligands

The CPE of metal ions invariably requires a chelating agent which can convert the hydrated metal ion into extractable metal chelates [81-85]. Therefore, hydrophobic chelating agents are more favorable compared to hydrophilic ones. The dispersion of a hydrophobic chelating agent into micellar medium enables it to enter the micelle core. As a result of this the coordinating head group of the ligand protrudes itself towards the micelle corona [88]. This in turn enhances the interaction between the metal and ligand and hence no external forces are required as in LLE. A pictorial representation of the arrangement of ligand molecules in micelle core is given in

Figure 1.1. Favre-Réguillon et al. [89] had shown that under the same acidic conditions the CPE of U by 8-hydroxyquinoline results in higher extraction efficiency (EE) compared to the LLE of U by the same ligand. The hydrophobic nature of the micellar core is most favorable for neutral metal chelates, whereas modifications of the micelles were reported to extract charged metal chelates as well [32,90,91]. The selection of ligand(s) for CPE of any metal ion is therefore a crucial factor as it can directly affect the selectivity of the method. A schematic representation of the cloud point phase separation procedure is also pictorially depicted in **Figure 1.1**.

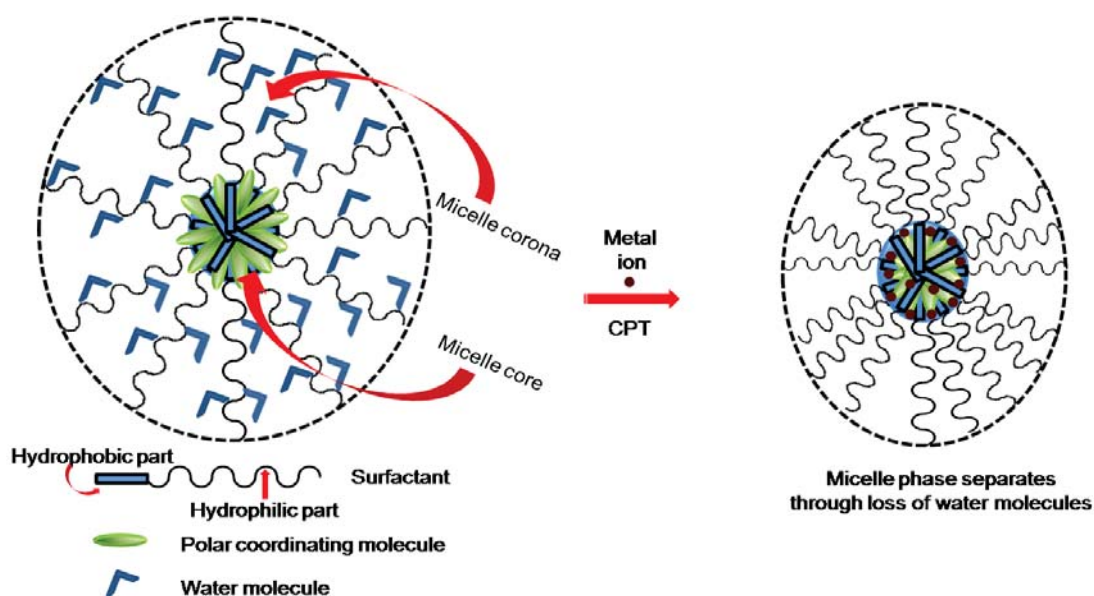


Figure 1.1. Pictorial representation of cloud point extraction (CPE) mechanism

1.5.3. Role of phase modifiers

Modification of the micellar system to extract charged metal chelates into the hydrophobic core can be done by addition of ionic co-surfactant or ionic liquid [32,90,91]. In addition, these modifiers also change the CMC and CPT of non-ionic and zwitterionic surfactants [92,93]. When an ionic co-surfactant is added to any

micelle medium below its CMC, the surface active ions can either remain as monomers or as mixed micelles with the major surfactant. The most commonly used co-surfactants are cetyl-trimethylammonium bromide (CTAB) and sodium dodecylsulphate (SDS) [32,90,91]. In the mixed micelle state these modifiers facilitate the metal chelation by imposing electrostatic attraction to oppositely charged complexes or sometimes by taking part in complexation [32,90,91]. The charge neutralization of the metal chelates in presence of oppositely charged hydrophilic head group of the co-surfactant increases the hydrophobicity of the metal chelate and facilitates the extraction process. Labrecque et al. [32] and Madrakian et al. [95] had reported quantitative extraction of U(VI) by P,P-di(2-ethylhexyl) methanediphosphonic acid and pyrocatechol violet respectively in presence of CTAB. On the other hand ionic liquids (IL) are not vastly explored for the CPE of metal ions. Only one report from Gao et al. [91] is available in the literature showing the effect of IL addition on CPE of metal ion viz., U(VI). Addition of hydrophobic ionic liquid containing bis(trifluoromethanesulfonyl) imide (NTf_2^-) as an anionic part, was reported to neutralize the charged U(VI)-trioctylphosphine complex by complexation process and consequently enhances the U extraction by its incorporation in the micelle [91]. Hence the selection of modifier in CPE process is case specific and requires knowledge of the extraction mechanism.

1.5.4. Role of pH

CPE is generally carried out in the pH range of 1 to 10, as high acid concentration hampers the coacervation of micelles due to the stripping potential of acids which causes disruption of the micelle systems. Since the solubility and speciation of many metal ions is pH dependent, optimization of pH is required to have maximum

extraction efficiency (EE) [81-85]. In addition metal ligand complexation is greatly dependent on pH due to many factors like effect of competing ions, requirement of preferred metal ion species for complexation and sometimes pK_a value of the chelating agent [81-85] etc. Hence, maintenance of solution pH before and after the phase separation process is important for reproducible result and is usually done by adding buffer solution. However, recently Labrecque et al. [93] had demonstrated the CPE of plutonium (Pu) in $3 \text{ mol L}^{-1} \text{ HNO}_3$ medium by providing a protecting shield of bromine around micelles.

1.5.5. Role of electrolyte

Addition of electrolyte helps in maintaining ionic strength of the solution which has a direct impact on CPT of the micelle system and extraction process. Metal salts of chloride (Cl^-), bromide (Br^-), iodide (I^-), nitrate (NO_3^-) and thiocyanate (SCN^-) etc., are known to influence the micellar environment and decrease the CPT [81-85,94]. The polarizability of the anion influences the CPT of micellar system. Higher polarizable anion results in greater interaction between the micelles and the ion in the aqueous phase, thereby achieving lower CPT. The influence of electrolyte on CPT of micellar system depends on concentration of the former and can be optimized to tune the CPT accordingly. In addition, electrolyte acts as salting out agent forcing the metal-ligand complex to form inside the micelles [81-85]. The selection of an electrolyte for developing new CPE methods for metal ions should be made carefully. Anions like NO_3^- , SCN^- and acetate (CH_3COO^-) have significant complexing ability with metal ions and hence can affect the selectivity of the method [93]. At $\text{pH} < 2.5$, iodide gets converted into elemental iodine which can enter the micelle and affect the

metal ion EE [32]. The addition of electrolyte, which is essential, should be made carefully.

1.5.6. Role of temperature

The determination of CPT of the micelle system with all optimized parameters can be done by visual inspection or measurements like dynamic light scattering (DLS), viscosity measurement etc [81-85]. The incubation time and equilibration temperature are important parameters to obtain efficient phase separation. The incubation time should be sufficient to ensure maximum metal-ligand complexation [81-85]. CPT around the room temperature is generally preferred, since heating can affect the EE due to (i) inherent volatility of some elements like mercury and (ii) exothermicity of some metal-ligand complexation process [81-85]. TTX-114 is thus the most common non-ionic surfactant used in CPE methods due to its theoretical CPT at 23-25 °C above its CMC (**Table 1.1**).

1.5.7. Basic equations of CPE

The development of a new CPE methodology for a particular metal ion is assessed by calculating the percentage EE, percentage recovery and preconcentration factor (PF) employing the following equations [32]:

$$EE = \frac{C_{\text{initial}}V_{\text{initial}} - C_{\text{supernatant}}V_{\text{supernatant}}}{C_{\text{initial}}V_{\text{initial}}} \times 100 \quad (1)$$

$$\text{Recovery} = \frac{C_{\text{SRP}}V_{\text{SRP}}}{C_{\text{initial}}V_{\text{initial}}} \times 100 \quad (2)$$

$$PF = \frac{C_{\text{initial}}V_{\text{initial}} - C_{\text{supernatant}}V_{\text{supernatant}}}{C_{\text{supernatant}}V_{\text{supernatant}}} \quad (3)$$

where C_{initial} , C_{SRP} and $C_{\text{supernatant}}$ are the concentrations of respective analyte initially taken, in the SRP and in the supernatant after phase separation respectively. Similarly, V_{initial} , $V_{\text{supernatant}}$ and V_{SRP} are the initial volume of the solution, volume of the supernatant phase after phase separation and volume of the redispersed SRP respectively. The aim of any CPE procedure is to have quantitative EE and recovery values and maximum PF value.

1.6. Literature survey on CPE of uranium

The literature reported CPE studies of U in environmental matrices are listed in **Table 1.2**. Laespada et al. [95] was the first to report the CPE of U by 1-(2-Pyridylazo)-2-Naphthol. No literature on CPE of U was published in the next ten to twelve years after the first report. In the year 2005, Shemirani et al. [96] published their work on CPE of U by dibenzoylmethane. Subsequently various research groups had published new CPE methods for preconcentrating U by various common organic ligands, as tabulated in **Table 1.2**. In these reports the detection of U in preconcentrated samples were carried out by instruments like UV-visible spectrophotometry [56,90,95-97], liquid scintillation counting (LSC) [98], ICP-MS [32] or ICP-optical emission spectroscopy (ICP-OES)[99]. Most of the literature reported CPE techniques for U lack in providing quantitative EE value [56,90,95-100] which is an important parameter in dictating the quantitative extraction of U by the corresponding CPE method. The maximum and minimum reported PF values for CPE of U are 122 and 14.3 respectively [89,90]. The higher PF of any typical CPE procedure would result in better detection limit (DL) of the analyte of interest. The lowest reported DL value of 0.003 ng mL^{-1} was reported by Labrecque et al. [32] where costly, sophisticated and high maintenance intensive ICP-MS was used in offline conjugation with CPE.

Although Madrakian et al. [90] had reported a DL value of 0.06 ng mL^{-1} by using simple and versatile UV-visible spectrophotometry in conjugation with CPE, but their methodology lacks in dynamic linear concentration range (DLR). Wide DLRs of 2.5-1240 and $0.01\text{-}1000 \text{ ng mL}^{-1}$ respectively were only achieved previously by Labrecque et al. [32] and Shariati et al. [99] by CPE/ICP-MS and CPE/ICP-OES respectively. In addition none of the reports on CPE methods for U (**Table 1.2**) had studied the tolerance of their methods to the presence of interfering lanthanides. Since the ore of U viz., pitchblend contains 0.01 to 0.15% of lanthanides and nuclear waste contains lanthanides as fission product, the co-occurrence of U and lanthanides in environmental matrices is quite possible.

1.7. Motivation for the present work

Development of simple and cost effective CPE based detection methodologies for U is always desirable to achieve quantitative EE, high PF value, wide DLR, better DL value and tolerance to the interfering ions. This will allow on-site and real-time monitoring of the analyte in contaminated areas. The increased production and use of short lived U isotopes viz., ^{233}U , ^{235}U etc. in enrichment plants and nuclear power reactors, calls for the improvement in the detection limits of simple and easily accessible CPE based detection methodologies due to their very low radiological guideline values. Use of versatile spectroscopic techniques in conjugation with CPE to achieve wide DLR and better DL values requires development of new and efficient CPE procedures. On the other hand, dilution of the SRP for analysis of the analyte diminishes the effective PF at the time of analysis and hence affects the DL value. Hence, offline coupling of the CPE procedure with a detection technique needs to be

Table 1.2. Comparison of reported CPE methodologies for uranium

| Ion(s) | Extractants | Instruments | DLR (ng mL ⁻¹) | EE (%) | Recovery (%) | PF | DL (ng mL ⁻¹) | RSD (%) | Reference |
|--------------------------------|--|-------------|-------------------------------|----------|-----------------|------|------------------------------|------------|-----------|
| U(VI)-Th(IV)- Zr(IV)-Hf(IV) | Dibenzoylmethane | ICP-OES | 2.5-1240 | N.P. | N.P. | 37 | 1.0 | 6.1 | [99] |
| U(VI) | P,P'-di(2-ethylhexyl)- methanediphosphonic acid | ICP-MS | 0.01-1000 | 99.5±0.5 | 99 | 92 | 0.003 | 4 | [32] |
| U(VI) | 1-(2-Pyridylazo)-2-Naphthol | UV-Visible | N.P. | N.P. | 98 | 100 | 1.1 | 5.1 | [95] |
| U(VI) | Dibenzoylmethane | UV-Visible | 15-300 | N.P. | 98 | 62 | 11 | <3.7 | [96] |
| U(VI) | 2-(5-Bromo-2-Pyridylazo)- 5-(Diethylamino) Phenol | UV-Visible | N.P. | N.P. | 98-105 | 50.4 | N.P. | N.P. | [56] |
| U(VI) | 8-Hydroxyquinoline | ICP-OES | N.P. | 99 | > 98 | 122 | N.P. | N.P. | [89] |
| U(VI) | Pyrocatechol Violet | UV-Visible | 0.18-10 | N.P. | N.P. | 14.3 | 0.06 | 3 | [90] |
| U(VI) | Red arsenazo S | UV-Visible | 6-10 | N.P. | 105 | N.P. | 2 | 9 | [97] |
| U(VI) | Tributyl Phosphate | LSC | N.P. | N.P. | 50 | N.P. | 1.42 x 10 ⁵ | 10 | [98] |
| U(VI) | Tetracycline | UV-Visible | 80-1600 | N.P. | N.P. | 14.3 | 74.6 | 3.6 | [100] |

N.P. = Not present

modified to achieve better DL values by using cost effective analytical instruments. To the best of our knowledge, functionalized nanomaterials have never been explored for CPE of U. The use of functionalized nanomaterials, having high quantum yield or high optical density, for CPE of U could result in better DL values employing simple UV-visible spectrophotometer or fluorometer. The reported CPE methodologies for U so far have not shown selectivity in presence of higher concentration of lanthanides which are known to decrease the selectivity for many ligands towards U(VI) at low acidic medium [91]. Since CPE is generally carried out in the pH range, the interference from lanthanides needs to be overcome. In the present study we have developed some new and simple CPE methods for preconcentration of U in environmental water samples by some existing and newly synthesized functional materials followed by its detection using simple and versatile spectroscopic techniques. The developed CPE methodologies have been categorized under three broad headings (as described in **Chapter 3, 4 and 5**) as they represent the applicability of three different types of materials viz., common organic ligands, functional nanoparticles (NPs) and task specific ionic liquids (TSILs) in the extraction procedure. The synthesis and complete characterization of novel functional NPs and TSIL were carried out as a part of the present work program. The developed analytical techniques were successfully applied to determine U in real water samples.

Chapter 2

Experimental methods and instrumentation



This page is kept blank intentionally

2.1. Preparation of buffer solutions

Buffers are aqueous solutions containing mixtures of a weak acid and its conjugated base or weak base and its conjugated acid. The pH of buffer solutions is resistant to the addition of small amount of strong acid or base. Buffer solutions are used as a means of keeping pH at a nearly constant value in a wide variety of chemical applications. Since pH is one of the major factors that decide the extraction efficiency (EE) of metal ions in cloud point extraction (CPE) procedures, maintenance of solution pH in our experiments, presented in **chapter 3, 4 and 5** was done by adding buffer solutions of desired pH. Buffers ranging from pH 1 to 10 were prepared by mixing different portions of reagent solutions [101] as listed in **Table 2.1**.

2.2. Preparation of metal ion stock solution

High purity uranyl nitrate hexahydrate, $\text{UO}_2(\text{NO}_3)_2 \cdot 6\text{H}_2\text{O}$ and thorium nitrate pentahydrate, $\text{Th}(\text{NO}_3)_4 \cdot 5\text{H}_2\text{O}$ were dissolved in 1.0 mol L^{-1} nitric acid (HNO_3) medium to prepare individual $\sim 10 \text{ mg L}^{-1}$ stock solution. The U(VI) ion stock solution was standardized by the well-known biamperometric titration as reported by Nair et al. [102]. On the other hand, the Th(IV) ion stock solution was standardized by gravimetry. Firstly, Th was precipitated as iodate and then filtered. The residue was dissolved by adding concentrated hydrochloric acid (HCl), followed by precipitation with ammonia addition in presence of hydrogen peroxide and finally ignited and weighed as thorium oxide (ThO_2) [103]. These stock solutions were diluted accordingly and used in the experiments as described in **chapter 3, 4 and 5**.

Table 2.1. Preparation of buffer solutions in 50 mL volumetric flask

| pH | Volume (mL) of 0.2 mol L ⁻¹ potassium chloride (KCl) | Volume (mL) of 0.2 mol L ⁻¹ hydrogen chloride (HCl) | Volume of Milli-Q water |
|------|--|--|-------------------------|
| 1.0 | 12.5 | 33.5 | 4.0 |
| 1.5 | 12.5 | 10.35 | 27.15 |
| 2 | 12.5 | 3.25 | 34.25 |
| pH | Volume (mL) of 0.1 mol L ⁻¹ potassium hydrogen plthalate | Volume (mL) of 0.1 mol L ⁻¹ hydrogen chloride (HCl) | Volume of Milli-Q water |
| 2.5 | 25 | 19.4 | 5.6 |
| 3.0 | 25 | 11.15 | 13.85 |
| 3.5 | 25 | 4.1 | 20.9 |
| 4.0 | 25 | 0.05 | 24.95 |
| pH | Volume (mL) of 0.1 mol L ⁻¹ potassium hydrogen plthalate | Volume (mL) of 0.1 mol L ⁻¹ sodium hydroxide (NaOH) | Volume of Milli-Q water |
| 4.5 | 25 | 4.35 | 20.65 |
| 5.0 | 25 | 11.3 | 13.7 |
| 5.5 | 25 | 18.3 | 6.7 |
| pH | Volume (mL) of 0.1 mol L ⁻¹ potassium dihydrogen phosphate (KH ₂ PO ₄) | Volume (mL) of 0.1 mol L ⁻¹ sodium hydroxide (NaOH) | Volume of Milli-Q water |
| 6.0 | 25 | 2.8 | 22.2 |
| 6.5 | 25 | 6.95 | 18.05 |
| 7.0 | 25 | 14.55 | 10.45 |
| 7.5 | 25 | 20.55 | 4.45 |
| pH | Volume (mL) of 0.025 mol L ⁻¹ sodium tetraborate or borax (Na ₂ B ₄ O ₇ ·10H ₂ O) | Volume (mL) of 0.1 mol L ⁻¹ hydrogen chloride (HCl) | Volume of Milli-Q water |
| 8.0 | 25 | 10.25 | 14.75 |
| 8.5 | 25 | 7.6 | 17.4 |
| 9.0 | 25 | 2.3 | 22.7 |
| pH | Volume (mL) of 0.025 mol L ⁻¹ sodium tetraborate or borax (Na ₂ B ₄ O ₇ ·10H ₂ O) | Volume (mL) of 0.1 mol L ⁻¹ sodium hydroxide (NaOH) | Volume of Milli-Q water |
| 9.5 | 25 | 4.4 | 20.6 |
| 10.0 | 25 | 9.15 | 15.85 |

2.3. Synthesis procedures

Two new functionalized nanomaterials (NPs) and one new task specific ionic liquid (TSIL), as listed in **Table 2.2**, were synthesized in our laboratory as a part of this study.

Table 2.2. Categorization of newly synthesized materials

| Name of the material | Category | Source |
|--|--------------------|-----------|
| Diglycolamide capped CdS/ZnS quantum dots (QDs) | Functionalized NPs | Chapter 4 |
| 3-mercaptopropionylamidoxime (3-MPD) capped gold nanoparticles (AuNPs) | Functionalized NPs | Chapter 4 |
| N-propyl-(diphenylphosphoramidate)-trimethylammonium bis-(trifluoromethanesulfonyl)imide | TSIL | Chapter 5 |

2.3.1. Synthesis of diglycolamide capped cadmium sulfide/zinc sulfide (CdS/ZnS) core-shell quantum dots (QDs)

A mixture of oleic acid (3.4 mL, 10.6 mmol), cadmium oxide (0.51 g, 4.0 mmol), and 1-octadecene (11.6 mL) was heated in a three-neck round-bottom flask to 180 °C in an inert gas (Ar) atmosphere until a clear and gold-brown solution of cadmium oleate was obtained. The reaction temperature was then allowed to increase up to 260–270 °C to obtain a colorless solution. In order to prepare the stock sulfur (S) injection solution, sulfur shot (64 mg, 2 mmol) was reacted with trioctyl phosphine (TOP) (1.1 mL, 2.5 mmol) in 1-octadecene (4.4 mL). This TOPS solution was swiftly injected through a syringe to the reaction mixture at 260–270 °C. The solution temperature was allowed to fall below 100 °C followed by dissolving in chloroform (CHCl₃) and finally re-precipitated thrice with methanol (CH₃OH) to get the CdS QD.

For preparing CdS/ZnS core-shell, the above CdS QD solution in chloroform was directly used as core. ZnS shell was made by using zinc oleate as zinc precursor with S powder as sulfur precursor. Zinc oleate was prepared by taking Zn-acetate (0.109 g, 0.5 mmol) and oleic acid (0.425 mL, 1.3 mmol) in 1-octadecene (1.5 mL) under reflux condition (at 180 °C) into a three-neck round bottom flask in inert atmosphere.

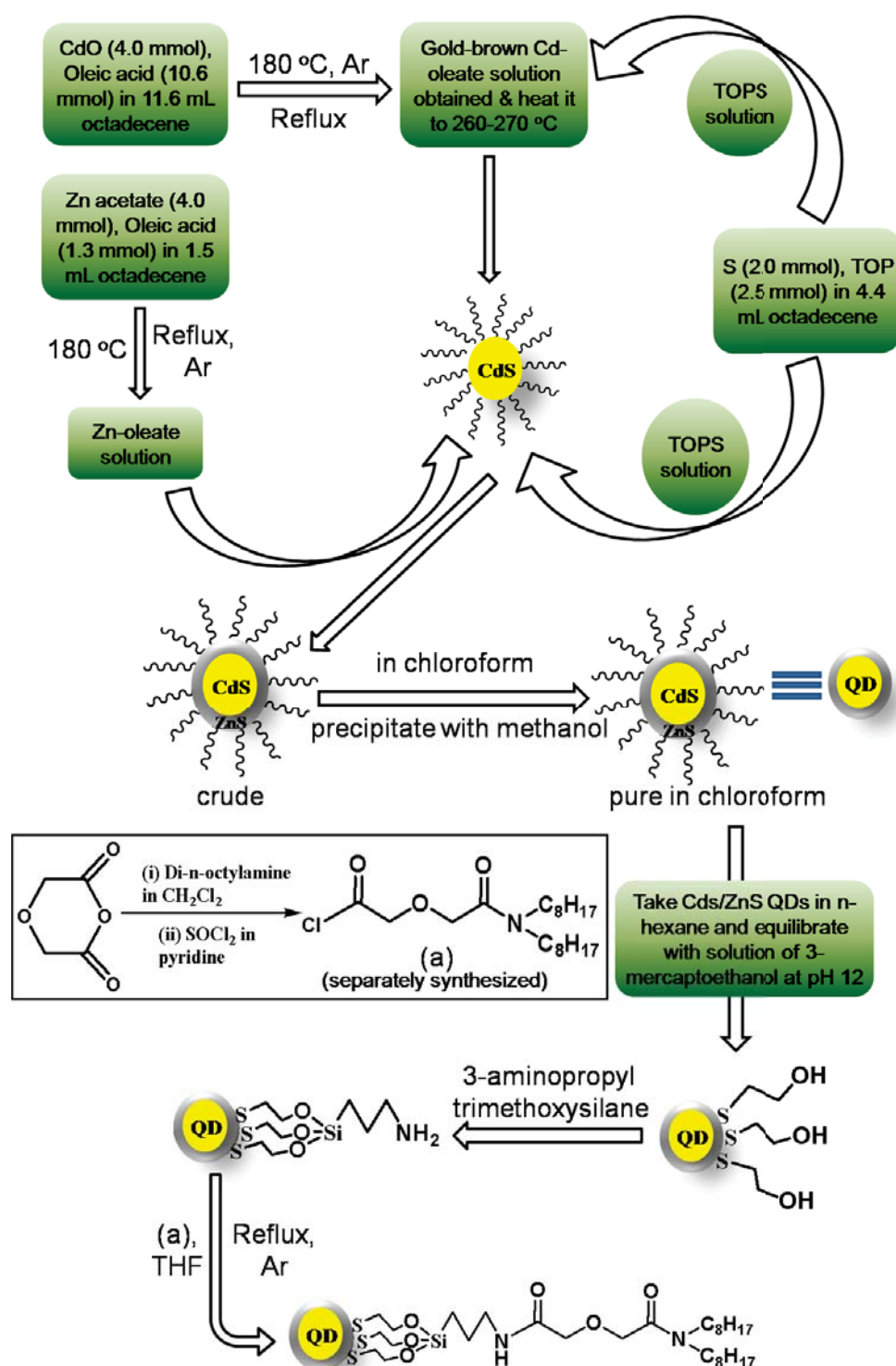
Thereafter, Zn-oleate was added to a solution (5 mmol CdS) kept in a 250 mL round bottom flask. The preparation of stock S injection solution is same as discussed in the case of CdS QD. This so formed TOPS was then added drop wise to the solution of Zn-oleate in CdS through a syringe at 180 °C. The solution temperature was allowed to fall below 100 °C and dissolved with CHCl_3 and finally re-precipitated thrice with CH_3OH to obtain CdS/ZnS core-shell QD.

In order to obtain OH-capped CdS/ZnS QDs, oleic acid-capped CdS/ZnS QDs were dried by evaporation and then 100 mg of the QDs were taken in 10 mL of n-hexane. 1 mL of 2-mercaptoethanol and 0.5 mL of methanol was taken in 3 mL of water and the pH was adjusted to 12 with 0.1 M NaOH. This solution was added dropwise to the QD solution in n-hexane under vigorous stirring which was continued overnight at room temperature 26 ± 1 °C. The resulting water soluble OH-capped QDs were precipitated by adding 10 mL of acetone. The suspension was then centrifuged at 6000 rpm for 10 min. The supernatant solvent was then removed, and the QDs were dissolved in 1 mL of water to get a clear solution. The silanization of the OH-capped QDs was done by following the steps as described by Wu et al. [104]. 0.5 mL of 3-aminopropyltrimethoxysilane (3-APS) diluted with 2 mL of methanol was added to 1 mL of OH-capped CdS/ZnS QDs (15 μmol) slowly at 0 °C with vigorous mixing. After 10 min of stirring, the solution was heated to ~ 60 °C for 30 min and then cooled to ~ 30 °C. A mixture of 15 mL of methanol and 1.5 mL of chlorotrimethylsilane basified with 2.3 g of solid tetramethylammonium hydroxide pentahydrate was added at room temperature afterwards to quench the silanization reaction. After 2 h of stirring, the solution was heated to ~ 60 °C for 30 min and then stirred slowly under Ar at room temperature for 24 h. Methanol was removed in

vacuo and the solution was filtered through a 0.45 μm syringe filter. Free silane in the reaction mixture was removed via size-exclusion chromatography using a NAP-25 column with deionized H_2O . Then the solution was concentrated twice with a centrifuge (8000 rpm). Finally, the amino-silanized CdS/ZnS QD solution was reduced to 1 mL and stored in a 4-5 $^\circ\text{C}$ dark room. The amino-silanized QD solution was precipitated using anhydrous CHCl_3 . The wet precipitate (~ 100 mg) was then suspended in 10 mL tetrahydrofuran (THF) for further steps.

In a round bottom flask diglycolic anhydride was suspended in dichloromethane (CH_2Cl_2). Equimolar amount of di-n-octylamine was dissolved in CH_2Cl_2 and mixed with the above mentioned suspension at room temperature under constant stirring. The stirring was continued until the suspension became completely clear forming diglycolamic acid amide. The solution was then passed through anhydrous sodium sulfate (Na_2SO_4) to remove traces of water. Removal of the solvent under reduced pressure yielded the pale yellow diglycolamic acid amide (yield 96%). About 32 mg (~ 0.1 mmol L^{-1}) of that solid was then dissolved in 5 mL of dry tetrahydrofuran (THF) in presence of pyridine in a three neck round bottom flask. An excess of thionyl chloride (SOCl_2) was added to it and the mixture was refluxed for 1 h. The mixture was then heated at 80 $^\circ\text{C}$ to remove the excess SOCl_2 . To this solution the amino-silanized QD suspension in THF was added and the resulting mixture was refluxed for 4 h under inert (argon) atmosphere. After cooling, the precipitate was filtered and washed with 15 mL of CH_2Cl_2 . The raffinate was first equilibrated with 10% HCl in a separating funnel and then the same with water. The organic portion was then passed through anhydrous Na_2SO_4 to remove water and the solvent was evaporated to dryness. The residue was dissolved in acetonitrile (ACN) and filtered

through 0.2 μm syringe filter to a final volume of 10 mL. The complete synthesis procedure is pictorially depicted in **Scheme 1**.



Scheme 1. Synthesis procedure of diglycolamide capped CdS/ZnS quantum dots (QDs).

2.3.2. Synthesis of 3-mercaptopropionylamidoxime (3-MPD) capped gold nanoparticles (AuNPs)

The synthesis of 3-mercaptopropionylamidoxime capped AuNPs was carried out in seven steps which are described below.

(a) Synthesis of methyl-3-mercaptopropionate: A solution of 3-mercaptopropionic acid (20.0 g, 0.19 mol) in dry methanol (54 mL) was placed in a round bottom flask. To this solution, 5.2 mL of concentrated sulfuric acid (~ 0.1 mol) was added slowly and the mixture was then refluxed for 36 h with a soxhlet extractor followed by a condenser fitted to the round bottle flask. The reaction mixture was then cooled to the room temperature and transferred to a separating funnel. The unreacted reagents were extracted into aqueous medium by two successive contacts. The organic layer was then passed through anhydrous Na_2SO_4 and quantitatively transferred by dry CH_3OH wash. Evaporation of the solvent in a rotating vaporizer yielded 16.8 g of methyl-3-mercaptopropionate (0.14 mol, $\sim 74\%$).

(b) Synthesis of 3,3'-dithiopropionamide: An excess of concentrated ammonia solution (NH_4OH) was added dropwise to 16.8 g of methyl-3-mercaptopropionate (0.14 mol) at $4-5^\circ\text{C}$ with vigorous stirring. After continuous stirring at this temperature for another 2 h, the mixture was slowly brought to room temperature and the stirring further continued for another 24 h resulting the formation of white precipitate of 3,3'-dithiopropionamide. The precipitate was filtered, washed 5 to 6 times with 10 mL diluted HCl (2.0 mol L^{-1}) and then dried. The yield of the product was 19.8 g (0.095 mol, $\sim 68\%$).

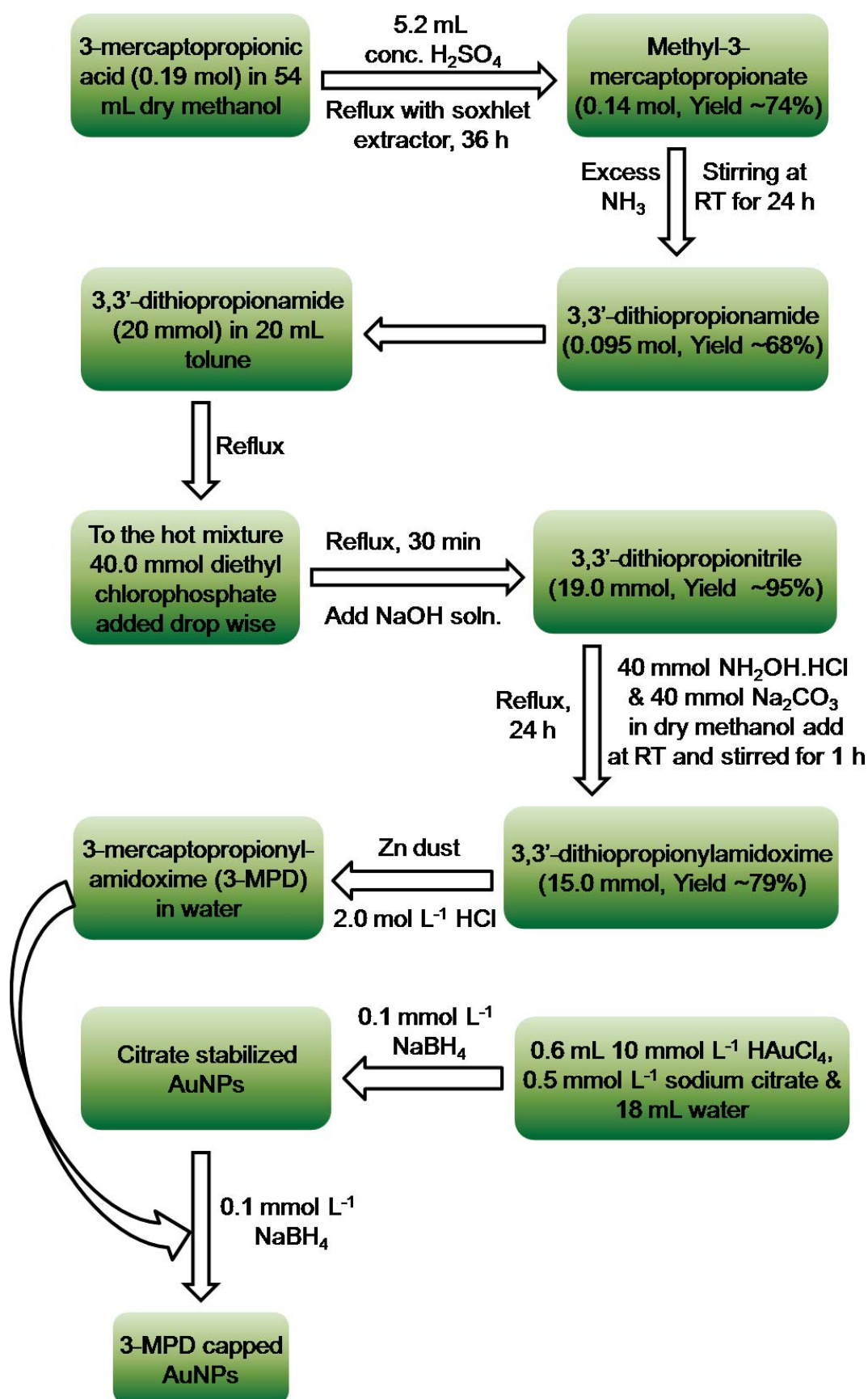
(c) *Synthesis of 3,3'-dithiopropionitrile*: In a three neck round bottom flask 4.2 g of 3,3'-dithiopropionamide (20 mmol) was taken along with 20 mL of toluene. The mixture was then refluxed and diethyl chlorophosphate (7.0 g, 40 mmol) was added dropwise to the hot mixture with a syringe. The solution was again refluxed for another 30 min and then cooled to room temperature. The mixture was then neutralized with 50 mL of 20% (w/v) sodium hydroxide (NaOH) solution. The crude product was extracted into ethyl acetate (EA) phase by contacting 20 mL of EA, twice in a separating funnel. The EA phase containing the product was then equilibrated with distilled water for 3 to 4 times and then the organic phase was passed through anhydrous Na₂SO₄. Evaporation of the solvent in a rotating vaporizer yielded 3.2 g of 3,3'-dithiopropionitrile (19 mmol, ~95%).

(d) *Synthesis of 3,3'-dithiopropionylamidoxime*: To a solution of hydroxylamine hydrochloride (NH₂OH.HCl, 2.9 g, 40 mmol) in dry CH₃OH, 3.4 g of sodium bicarbonate (40 mmol) was added and resulting mixture was then stirred for 20 min at room temperature. This mixture was then added to 3.2 g of 3,3'-dithiopropionitrile (19 mmol) in a round bottom flask. This solution was first stirred at room temperature for 1 h and then refluxed for 24 h. The mixture was then cooled to room temperature and the solvent was evaporated to dryness in a rotating vaporizer. Addition of EA (20 mL) to the residue resulted in the separation of 3,3'-dithiopropionylamidoxime at the bottom. The upper crude EA layer was pipette out and the bottom layer of 3,3'-dithiopropionylamidoxime was dried in rotating vaporizer. The yield of the product was 3.6 g (15 mmol, ~79%).

(e) *Synthesis of 3-mercaptopropionylamidoxime (3-MPD)*: In order to prepare 0.1 mol L⁻¹ 3-MPD solution, 0.31 g of 3,3'-dithiopropionylamidoxime (1.3 mmol) was taken in 5 mL of 2 mol L⁻¹ HCl. The mixture was heated to about 40 °C and 0.17 g of Zn dust was gradually added to it in multiple portions with vigorous stirring. Stirring was continued at the same temperature for another 30 min and then cooled to room temperature. The mixture was then filtered through WhatmanTM filter paper 542 and the filtrate was collected in a 50 mL volumetric flask and the volume was then make up to the mark with distilled water.

(f) *Synthesis of AuNPs*: In a 50 mL conical flask 0.6 mL of 10 mmol L⁻¹ tetrachloroauric(III) acid (HAuCl₄), 0.5 mmol L⁻¹ of sodium citrate and 18 mL of distilled water were taken and stirred for 10 min. To this mixture 0.5 mL of freshly prepared 0.1 mol L⁻¹ sodium borohydride (NaBH₄) was added when the solution turned red immediately. The solution was then allowed to settle for 2 h to complete the reduction of HAuCl₄ by NaBH₄ to form AuNPs.

(g) *Surface modification of AuNPs*: To prepare a 0.01 mol L⁻¹ 3-MPD solution initially, a 0.1 mol L⁻¹ 3-MPD solution (1 mL) was diluted to 10 mL by adding distilled water. 40 µL of 0.01 mol L⁻¹ 3-MPD solution was then added to the above prepared AuNP solution with continuous stirring. After stirring continuously for 2 h, 1.2 mL of freshly prepared NaBH₄ (0.1 mol L⁻¹) was added, and the solution was stored in refrigerator (4-5 °C) overnight. The overall synthesis procedure has been pictorially depicted as block diagram in **Scheme 2**.

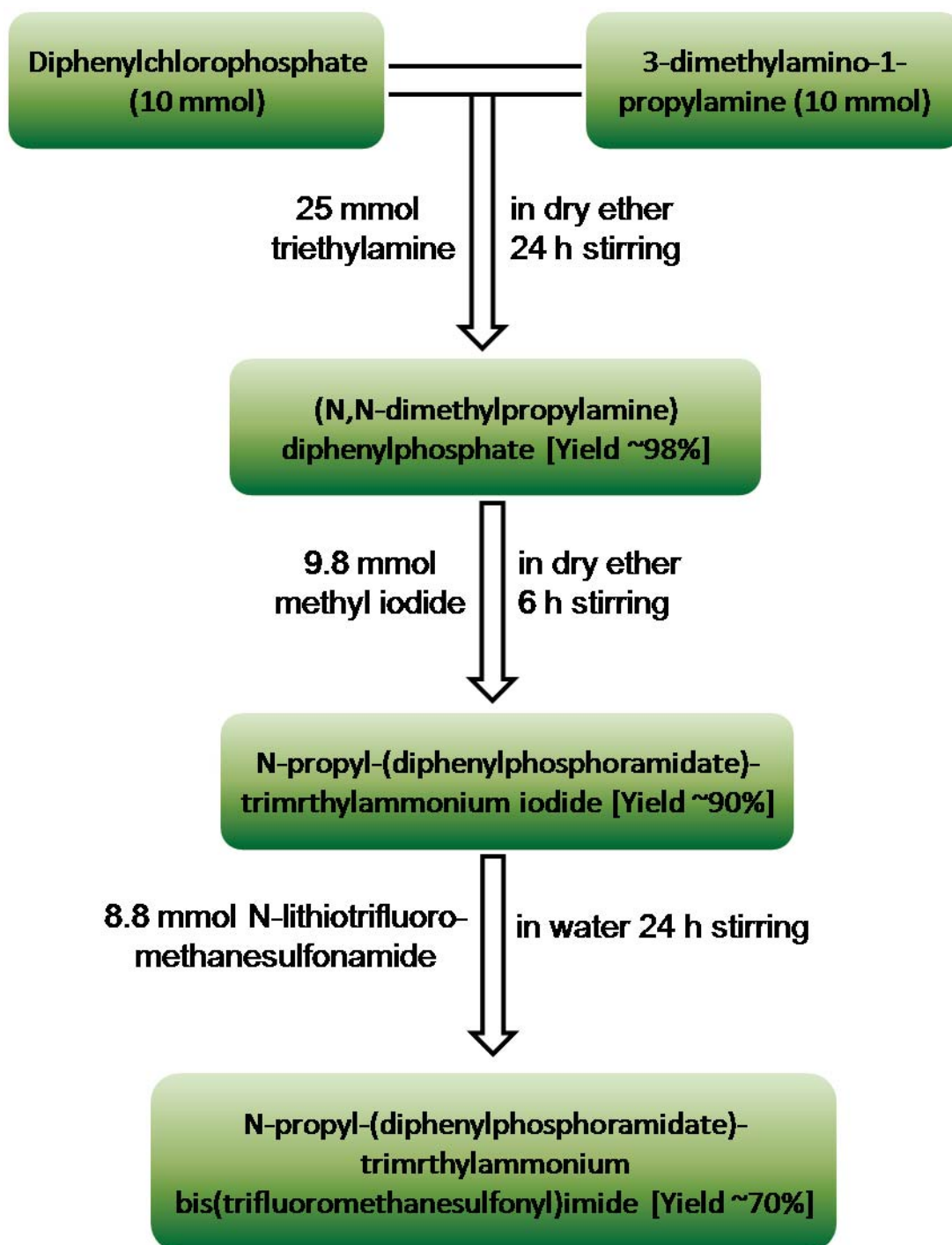


Scheme 2. Block diagram of synthesizing 3-MPD capped AuNPs.

2.3.3. Synthesis of task specific ionic liquid (TSIL) viz., N-propyl-(diphenylphosphoramidate)trimethylammonium bis(trifluoromethanesulfonyl)-imide

In a solution of diphenylchlorophosphate (2 mL, 10 mM) in dry diethyl ether (Et_2O , 10 mL), a mixture of 3-dimethylamino-1-propylamine (1.26 mL, 10 mM) and triethylamine (3.3 mL, 25 mM) in dry diethyl ether (Et_2O , 25 mL) was added dropwise at 3-5 °C under inert N_2 atmosphere with vigorous stirring, which was continued for 24 h at room temperature under the inert atmosphere. The white precipitate of triethylamine chloride was filtered and the residue was washed 3 times with 10 mL of Et_2O . Evaporation of the solvent in the raffinate yielded 98% of the (N,N-dimethylpropylamine)diphenylphosphate as colourless oil. This colourless oil was again dissolved in 30 mL of dry Et_2O , to which a solution of methyl iodide (CH_3I , 1.4 g, 9.8 mM) in 10 mL of dry Et_2O was added at 3-5 °C under vigorous stirring. The stirring was continued for 6 h at room temperature. The precipitate was filtered and washed 3 times with 10 mL of Et_2O . The supernatant was then dried under reduced pressure which yielded the product viz. N-propyl-(diphenylphosphoramidate)trimethylammonium iodide, $[\text{phamdNMe}_3][\text{I}]$, as pale yellow oil (yield 90%). The oil was then suspended in 20 mL of deionized water followed by the drop wise addition of a solution of N-lithiotrifluoromethanesulfonimide (LiNTf_2 , 2.53 g, 8.8 mM) in deionized water (20 mL) at room temperature under vigorous stirring. The stirring was continued for another 24 h at room temperature. The viscous wine-red TSIL settles at the bottom and the top aqueous layer was removed. The viscous oil was washed with 10 mL of deionized water for 5 times and then dried at 70 °C in vacuo. The yield of the TSIL viz., N-propyl(diphenylphosphoramidate)trimethylammonium bis(trifluoromethane-

sulfonyl)imide or $[\text{phamdNMe}_3][\text{NTf}_2]$, was 70%. A block diagram of the complete synthesis procedure is given in **Scheme 3**.



Scheme 3. Block diagram of synthesizing *N*-propyl-(diphenylphosphoramidate)trimethylammonium bis(trifluoromethanesulfonyl)imide.

2.4. Instruments

2.4.1. pH meter

The pH of the solutions was measured throughout the present study by LABINDIA, India, make PICO+ pH meter. For carrying out pH measurements throughout a day, the pH meter was always calibrated in the beginning. Every time calibration was done by measuring the pH of commercially available buffer solutions of pH 4.01, 7.00 and 9.00 from MERCK.

2.4.2. UV-visible spectrophotometry

A JASCO make, model V-670, UV-visible-NIR double beam spectrophotometer at Radioanalytical Chemistry Division, BARC was used for measuring the absorbance spectra. The V-670 measures the spectrum of a sample over a wavelength range of 190 to 3200 nm. A PMT detector is provided for the UV/VIS region and a Peltier-cooled PbS detector is employed for the NIR region. A pair of 1 cm or 0.5 cm quartz cuvette, containing the sample and blank solution of similar solvent composition was used for spectra measurement. Background correction was made each time before recording the absorption spectra of solutions of similar composition.

2.4.3. Fluorescence spectroscopy

The emission spectra were recorded using a Hitachi make, model 4010, spectrofluorometer at Radiation and Photochemistry Division, BARC. The fluorometer was also used to record time dependent emission intensity at a particular wavelength and hence to measure the reaction rate involving two fluorophors. A 1 cm quartz cuvette with all sides polished was used to record the sample spectrum. A time-correlated single photon counting spectrophotometer from Horiba Jobin Yvon at

Radiation and Photochemistry Division, BARC was used for time resolved fluorescence measurements of fluorophores. LED light source with a definite wavelength was used for sample excitation and MCP-PMT was used for fluorescence detection.

2.4.4. Transmission electron microscopy (TEM)

TEM analyses were carried out using a LIBRA 200FE instrument, available at Material Science Division, BARC. The instrument was operated at an acceleration voltage of 200 kV. 200 mesh size carbon-coated Cu grid was used to support the sample for examination in TEM. About 10 μ L of low concentrated nanoparticle solution in water or any other solvent was drop cast on the Cu grid and dried. The high resolution TEM (HRTEM) and small area electron diffraction (SAED) images were also recorded by the same instrument.

2.4.5. X-ray photoelectron spectroscopy

X-ray photoelectron spectroscopic (XPS) analysis was carried out in SPECS instrument with PHOBIOS hemispherical chamber analyzer at Material Science Division, BARC. We have used Mg K α (1253.6 eV) source at pass energy of 11 eV. The flood gun correction was carried out during analysis to compensate for charging of the material. The survey scan was carried out in the range of 0 to 1100 eV with step of 0.1 eV energy. High-resolution XPS spectrum was recorded at a resolution of 1.2 eV. C (1s) peak (284.6 eV) was used as the internal standard.

2.4.6. Infrared spectroscopy

The IR spectra were recorded on a Bruker ALPHA Platinum-ATR spectrophotometer at Fuel Chemistry Division, BARC. The Platinum-ATR is a single reflection diamond ATR spectrophotometer whose one-finger clamp mechanism allows the direct infrared analysis of all solid and liquid samples during the present work. The instrument can record the sample spectrum in the range of 7500 cm^{-1} - 375 cm^{-1} . The instrument uses a diode laser as the light source and thermal detector of deuterated triglycine sulfate (DTGS). The spectral resolution is of better than 2 cm^{-1} .

2.4.7. Nuclear magnetic resonance (NMR) spectroscopy

The ^1H and ^{13}C NMR spectroscopic data were recorded with Varian make 500 MHz (^1H NMR: 500 MHz, ^{13}C NMR: 125 MHz) spectrometers at Bio-organic Division, BARC. The ^{31}P NMR spectroscopic data was recorded with Bruker make 400 MHz spectrometer at Chemistry Division, BARC.

The ^1H NMR spectrum of diglycolamide capped CdS/ZnS QDs was taken in deuterated chloroform (CDCl_3) solvent and the chemical shifts in ppm (δ scale) were measured relative to CHCl_3 (7.27 ppm) as internal standard.

The aqueous solubility and synthesis of 3-mercaptopropionylamidoxime (3-MPD) restricts its proton NMR characterization. Hence ^1H NMR measurement of its dimer viz., 3,3'-dithiopropionylamidoxime was carried out as the characterization step in the synthesis procedure. Deuterated dimethyl sulfoxide (CD_3SOCD_3) was used as the solvent and the chemical shifts were measured relative to CH_3SOCH_3 (2.49 ppm) as internal standard.

The ^1H and ^{13}C NMR spectroscopic data of $[\text{phamdNMe}_3][\text{NTf}_2]$ were recorded in deuterated acetone (CD_3COCD_3) solvent. The ^1H and ^{13}C chemical shifts were measured relative to CH_3COCH_3 (3.22 ppm) and CD_3COCD_3 (205.75 ppm) respectively, as internal standard. The ^{31}P NMR spectroscopic data was recorded in CD_3SOCD_3 and the chemical shift was measured relative to external standard 85% orthophosphoric acid (H_3PO_4).

2.4.8. Elemental analysis

Elemental analysis (CHNS) was carried out by Eurovector – EA 3000 using combustion followed by thermal conductivity detection (TCD) method at Analytical Chemistry Division, BARC.

2.4.9. Mass spectrometry

A VG Plasma Quad inductively coupled plasma quadrupole mass spectrometer (ICP-QMS) of model no. PQ2 Turbo Plus at Radioanalytical Chemistry Division, BARC was used for (i) determination of analyte concentration in the supernatant after CPE procedure in order to calculate the extraction efficiency (EE) and preconcentration factor (PF) by using equations 1 and 3 in **chapter 1** and (ii) sometimes for direct sample analysis to cross validate the proposed methodology. The sample introduction into the plasma was carried out by a Meinhard pneumatic nebulizer and a water cooled Scott type double pass spray chamber. Ions transmitted by the quadrupole mass filter are detected by continuous dynode channel electron multipliers (channeltron) detector. The detector is operated in a dual (pulse counting/analog counting) mode.

On the other hand the mass spectra of synthesized organic molecules were recorded in Bruker Daltonics make microTOF MS with the help of soft electrospray ionization. The microTOF MS can detect masses from 50 to 3000 amu with a resolution of > 10000 FWHM.

2.4.10. X-ray fluorescence spectrometry

A TX-2000 ITAL structures total reflection X-ray fluorescence (TXRF) spectrometer, having Mo $K\alpha$ (17.44 keV) as excitation source at Fuel Chemistry Division, BARC was used to determine analyte concentration in preconcentrated samples whenever required. The tube voltage and tube current applied during the TXRF measurement were 40 kV and 30 mA respectively. A Roentec Si (Li) detector of 30 mm² area and having resolution of 139 eV (at 5.9 keV) was used to detect and measure X-rays. The sample support for TXRF measurements was quartz on which a few microlitre of the sample was deposited and dried. TXRF measurements were done in live time mode for acquisition time of 1000s. U was detected by using U $L\alpha$ X-ray line at 13.61 keV.

2.4.11. Calorimetry

The calorimetric experiments were carried out at constant temperature (25 °C) with an isothermal titration calorimeter TAM-III from Thermometric AB, available at Radioanalytical Chemistry Division, BARC. It is a twin thermopile heat conduction type calorimeter and the measured differential power signal is dynamically corrected for the thermal inertia of the system. The titration assembly consists of 4 mL reaction vessel and a reference vessel. The heat capacity of reaction vessel and reference vessel was balanced by keeping the same volume of solutions in both sides in order to minimize the short-term noise. The isothermal calorimetric titration (ICT) was carried

out by taking titre solution in the titration vessel while the titrant solution was added with the help of a precision syringe connected to a stainless steel cannula. The base line (power vs. time) drift was < 500 nW/h and short term noise of the instrument was $< \pm 50$ nW. Before each experiment the instrument was calibrated electrically and the performance of the instrument was tested by measuring stability constant ($\log K$) and enthalpy change (ΔH) for the reaction between BaCl_2 and 18 Crown 6 in water. The equations related to ICT experiments can be found in the report by Rawat et al. [105].

2.4.12. Zeta potential analyzer

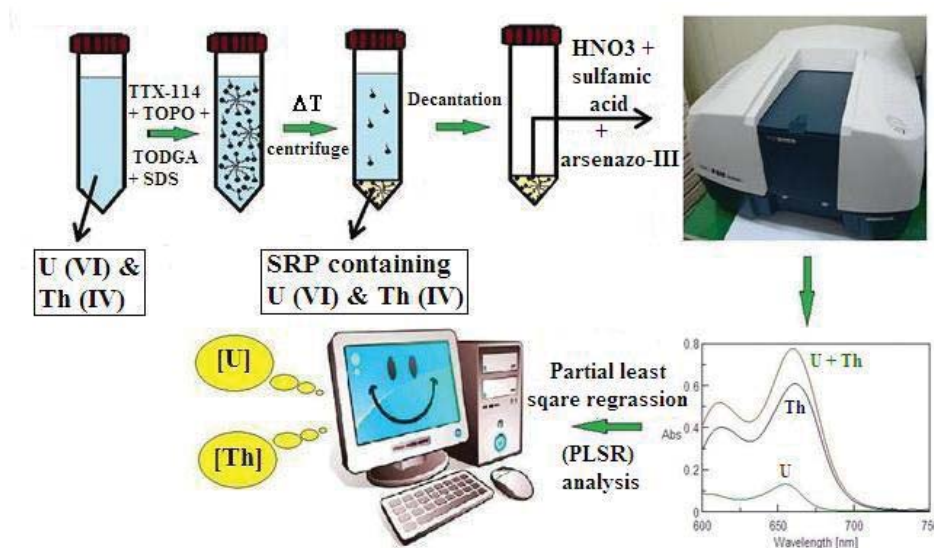
The zeta potential (ζ) of nanoparticles (NPs) and micelles with and without NPs and ionic liquids (ILs) were determined by Zetasizer Nano Z zeta potential analyzer from Malvern Panalytical, available at Chemistry Division, BARC. It is a high performance two angle particle and molecular size analyzer which uses dynamic light scattering (DLS) with Non-Invasive Backscatter optics (NIBS). The instrument uses He-Ne laser (633 nm) as light source and the laser beam scattered at 90° angle is detected. The determined ζ values provide valuable information about aggregation of NPs and insertion of NPs and ILs inside the micelles.

2.4.13. Centrifuge

A high speed centrifuge (Sigma make, model no. 3K30) at Radioanalytical Chemistry Division, BARC was used for complete phase separation after CPE by centrifugation. The ultracentrifuge can be operated at maximum speed of 30000 rpm and RCF up to 70000 g. It uses fixed angle rotors for different size and shape centrifuge tubes.

Chapter 3

Application of common organic ligands in cloud point extraction (CPE) of uranium (U) in aqueous samples



This page is kept blank intentionally

3.1. Introduction

Over the years the cloud point extraction (CPE) of various metal ions has been carried out by using common organic ligands. Their easy availability and known complexation chemistry with various metal ions in different solution conditions make it easier to choose a particular ligand for selective CPE of the analyte of interest. Since CPE is considered to be a more eco-friendly alternative to LLE, extractants employed for LLE of U [106] viz., tri-n-butyl phosphate (TBP), tri-n-octyl phosphine oxide (TOPO), cyanex-923, tris (2-ethylhexyl) phosphate (TEHP), di-(2-ethylhexyl) phosphoric acid (D2EHPA), 2-ethylhexyl hydrogen 2-ethylhexyl phosphonate (KSM-17) etc., can also cater the CPE of the same. However, the CPE behavior of all these extractants towards U has not been completely explored yet.

A limited number of literature reports are available on the CPE of U employing some of the above mentioned extractants [32,89,95,96,98-100] and some chromophoric agents like red arsenazo S [97], pyrocatechol violet [90] and 2-(5-bromo-2-pyridylazo)-5-(diethylamino) phenol [56] etc. A detailed discussion on all these available literature reports is presented in **section 1.6 of chapter 1**, where we have demonstrated the need of developing common organic ligand assisted simple, versatile and cost-effective CPE based spectroscopic detection methodology for U. Hence, the present study was aimed at developing a new and simple CPE based UV-visible detection methodology for U in order to obtain quantitative extraction efficiency (EE), higher preconcentration factor (PF), wide dynamic linear concentration range (DLR), better detection limit (DL) etc., compared to the previous works [56,90,95-98,100]. With the availability of portable UV-visible spectrophotometers, on-site and real-time monitoring of U could be made feasible by such development.

Thorium (Th) is another most abundant naturally occurring long-lived actinide found in the earth's crust. In addition, its anthropogenic isotope viz., ^{229}Th is also being produced in man-made nuclear activities. The United States Environmental Protection Agency (USEPA) had specified the maximum contaminant level (MCL) of 15 nCi mL^{-1} for alpha activity, excluding radon (Rn) and uranium (U) in drinking water [107]. Th being an alpha emitting radionuclide, its approximate maximum permissible concentration limit in drinking water should be less than 68 ng mL^{-1} and this value has been arrived at by considering only the specific activity of natural Th. Like U, Th is also both chemically and radiologically toxic [108]. However, due to the low solubility of Th compounds in water, its bioavailability is less than U. Nevertheless, the presence of both U and Th in environmental samples can exert adverse health effects on living organisms and hence need to be detected precisely. Thus the present work has been extended for simultaneous preconcentration and UV-visible spectrophotometric detection of U and Th in real water samples.

3.2. CPE procedure

The water sample was first filtered through WhatmanTM filter paper 541 and then passed through a $0.2 \text{ }\mu\text{m}$ syringe filter to get clear solution. 40 mL aliquot of the sample was taken in a 50 mL graduated glass centrifuge tube and 1 mL of $5 \text{ mol L}^{-1} \text{ KNO}_3$ was added into it to maintain the proper ionic strength. The pH of the solution was adjusted to pH 6 by adding dilute HNO_3 and NaOH and then 2.5 mL solution of pH 6 phosphate buffer was added to maintain the pH. Afterwards, $100 \text{ }\mu\text{L}$ of $0.25 \text{ mol L}^{-1} \text{ SDS}$, 2.5 mL of both $1 \times 10^{-2} \text{ mol L}^{-1} \text{ TOPO}$ and $2 \times 10^{-3} \text{ mol L}^{-1} \text{ N,N,N',N'-tetraoctyldiglycolamide (TODGA)}$ in TTX-114 ($4 \times 10^{-2} \text{ mol L}^{-1}$) were added to it. Finally the solution was diluted to 50 mL using water. The solution was then continuously stirred for 1 h in an ice bath to attain

equilibrium. The tube was then kept in a thermostatic water bath at 50 °C for 1 h. In this step the solution becomes cloudy and the SRP gets separated by the gravity. The complete phase separation was achieved by centrifugation at 4000 rpm for 10 min at room temperature. The tube was then placed in an ice bath for 5 min to make the SRP phase more viscous and hence facilitate separation of the aqueous phase by decantation. A pictorial representation of the above demonstrated CPE procedure is given in **Figure 3.1**.

3.3. UV-visible spectrophotometric detection procedure

In order to carry out colorimetric detection of the analytes in the SRP, it was made less viscous by adding 2 mL of a solution containing 20:80 (v/v) methanol/conc. HNO₃ and transferred quantitatively into a 5 mL beaker. The solution was then evaporated near to dryness and allowed to cool down at room temperature. Then the volume of the solution was made upto 1 mL by adding oxalic acid (0.1 mol L⁻¹), HNO₃ (6 mol L⁻¹), sulfamic acid (0.1 mol L⁻¹), arsenazo-III (0.07% w/v) and MilliQ water (18.2 MΩ.cm at 25 °C). Higher dilution factors were sometimes required depending upon the maximum peak absorbance. The solution was mixed well for 1 min and subsequently transferred into a 0.5 cm quartz cell and the absorbance was measured in the 600-750 nm range.

3.4. Partial least square regression (PLSR) analysis of the absorption spectrum

The maximum absorbance of U-arsenazo III and Th-arsenazo III complexes takes place at 656 and 662 nm respectively. Therefore, simultaneous determination of U and Th is difficult due to the closeness of their absorbance maxima resulting in high degree of spectral overlapping. In order to overcome this difficulty it is necessary to

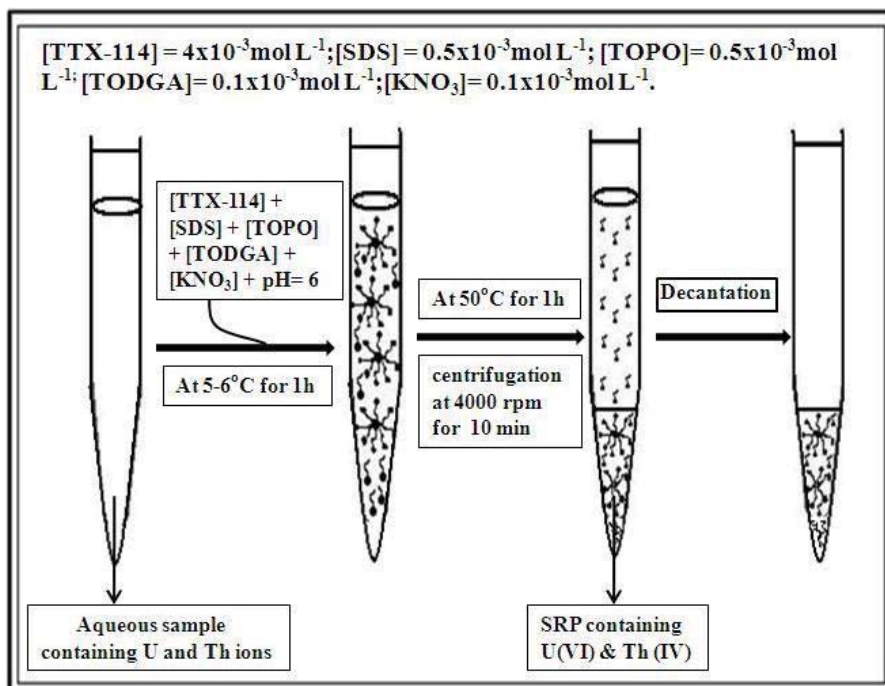


Figure 3.1. Pictorial representation of the developed CPE procedure

resolve their spectra by the application of PLSR algorithm. The complete absorption spectra (600-750 nm) of the samples were used for PLSR analysis, which is a purely empirical approach. Two sets of standard samples were prepared for PLSR i.e., calibration set (CS) consisting of 15 standards, which was used for constructing the calibration curves and the validation set (VS) consisting 5 samples to validate the calibration models generated by PLSR algorithm. The concentrations of U and Th in these standard sample sets are given in **Table 3.1**. In order to maintain the peak absorbance below 2, the concentration of U and Th in CS and VS solutions was maintained accordingly and preconcentrated samples were diluted suitably. A discussion on basic principles of PLSR algorithm is given in the later part of this chapter. The predictive capability of the PLSR method was validated by determining the root mean square error of prediction (RMSEP) and percentage relative error of prediction (REP) of VS sample analysis.

Table 3.1. Concentration of the analytes in the calibration set (CS) and validation set (VS) used for the PLSR analysis of U and Th

| Sample code | Uranium ($\mu\text{g mL}^{-1}$) | Thorium ($\mu\text{g mL}^{-1}$) | Sample code | Uranium ($\mu\text{g mL}^{-1}$) | Thorium ($\mu\text{g mL}^{-1}$) |
|-------------|--------------------------------------|--------------------------------------|-------------|--------------------------------------|--------------------------------------|
| CS1 | 0.5 | 0.25 | CS11 | 3 | 1 |
| CS2 | 0.75 | 0.5 | CS12 | 5 | 2 |
| CS3 | 1 | 1 | CS13 | 7.5 | 2.5 |
| CS4 | 1 | 2.75 | CS14 | 10 | 1 |
| CS5 | 1 | 6 | CS15 | 15 | 1 |
| CS6 | 1.5 | 4 | VS1 | 1 | 4 |
| CS7 | 1.5 | 5 | VS2 | 1.5 | 2.5 |
| CS8 | 2 | 1.5 | VS3 | 3 | 3 |
| CS9 | 2 | 3.5 | VS4 | 6.5 | 1.5 |
| CS10 | 2.5 | 2.5 | VS5 | 8 | 2 |

3.5. Optimization of CPE procedure

In the beginning of the experiment, tentative concentrations of surfactant, co-surfactant, extractant and salting out agent were selected on the basis of their literature reported values [32,56,89,90,95-100] at various pH to first confirm the pH which would result in partial maximum recovery of analytes (i.e., local maxima). Once the pH was fixed, one parameter was then varied at a time keeping others same as the first step to get local maxima for that parameter. The extraction temperature was kept at 5-6 °C and the phase separation temperature was kept at 70 °C during these experiments. Complete phase separation was achieved by centrifuging the biphasic mixture at 4000 rpm. The rigorous approach followed in the beginning of the process is based on several trial and error steps of all parameters and presented here in the form of cross-optimization process for better understanding to the reader. The CPE conditions were varied near their optimal value in a cross-optimization process to provide a deeper understanding of the impact of each parameter on the simultaneous CPE of U and Th. This cross-optimization method would result in actual maxima rather than local maxima for a particular parameter. Over the years this is the most common procedure followed by several research groups for

representing CPE optimization procedure [32,56,89,90,95-100]. The optimized CPE conditions are given in **Table 3.2**.

Table 3.2. *Optimized conditions for CPE system before coacervation (Total volume = 50 mL)*

| Parameters | Optimized conditions of total aqueous phase before coacervation | Units |
|-------------------------------|---|---------------------|
| Sample volume | 40 | mL |
| pH | 6 | --- |
| [TTX-114] | 4×10^{-3} | mol L ⁻¹ |
| [SDS] | 0.5×10^{-3} | mol L ⁻¹ |
| [TOPO] | 0.5×10^{-3} | mol L ⁻¹ |
| [TODGA] | 0.1×10^{-3} | mol L ⁻¹ |
| [KNO ₃] | 0.1 | mol L ⁻¹ |
| T _{extraction} | 5-6 | (°C) |
| t _{extraction} | 1 | (h) |
| T _{phase separation} | 50 | (°C) |
| t _{phase separation} | 1 | (h) |

3.5.1. Effect of pH

Trioctylphosphine oxide (TOPO) and N,N,N',N'-tetraoctyldiglycolamide (TODGA) are known to have the highest distribution ratios for both U and Th in concentrated HNO₃ medium [109-111]. But such high acid concentration hampers the coacervation of micelles and is not recommended for CPE. Hence the recoveries for both U and Th were determined for the pH range from 1 to 10, typical for CPE procedure. The effect of pH on the recoveries is shown in **Figure 3.2**. The increase in percentage recovery of both U and Th from pH 1 to 5 is expected to be due to the decrease in competition between H⁺ and UO₂²⁺ or Th⁴⁺ to get extracted by the extractants as their nitrate adduct. The optimal recoveries were obtained for pH values ranging from 5.5 to 7 for U and 5 to 8 for Th. The decrease in recoveries at higher pH is due to the formation of hydroxide, carbonate and/or bicarbonate complexes of U and Th in environmental samples. Therefore a pH value of 6 was selected as the optimum one.

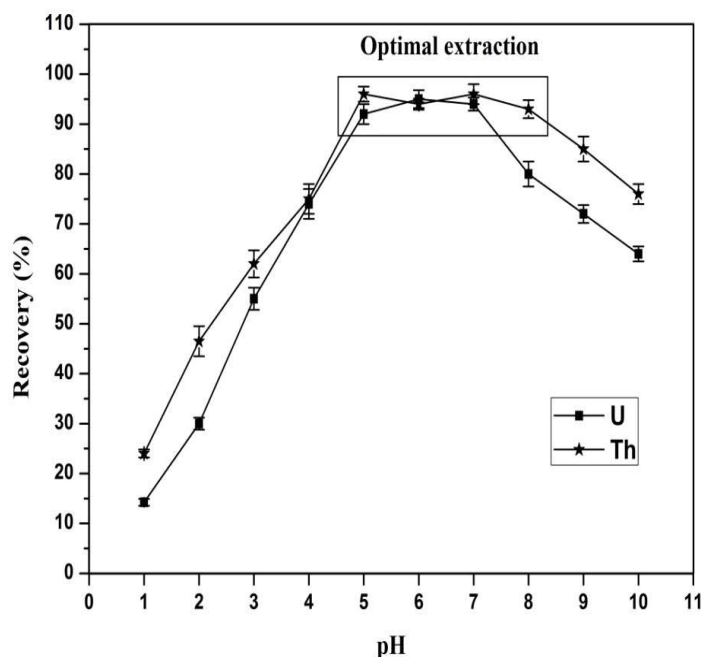


Figure 3.2. Effect of pH on the recovery of 50 ng mL^{-1} of U and Th each. Other parameters were kept constant as presented in Table 3.2.

3.5.2. Selection of extractant(s) and their concentration effect

TOPO is known to have high selectivity for tri-, tetra- and hexa-valent actinides and hence is widely used for the extraction of U and Th from various matrices [112]. Since TOPO can extract the analytes of interest at higher acidity as well as in the pH region [122,113], it should be applicable at pH values typical for use in CPE systems. The effects of varying TOPO concentrations on the recoveries of U and Th were studied in the range of 0 to $0.5 \times 10^{-3} \text{ mol L}^{-1}$ and are shown in **Figure 3.3**. The maximum recoveries for both U and Th were found to be 85% and 99% respectively when the concentration of TOPO was in the range of $(0.1-0.5) \times 10^{-3} \text{ mol L}^{-1}$. Since TOPO can extract tri-valent lanthanides at acidity less than 2 mol L^{-1} [91], the co-occurrence of lanthanides with the analytes of interest can affect their recoveries. Consequently, recovery studies were also carried out by taking equimolar quantity of lanthanum (as a representative of lanthanides) along with U and Th, for the same TOPO concentration range and the results are

represented in **Figure 3.3**. A decrease in recoveries was observed for both U and Th in the entire TOPO concentration range. Recoveries were found to increase with increase in TOPO concentration from 0.025×10^{-3} to 0.2×10^{-3} mol L⁻¹ and later remain the same. Hence the TOPO concentration was fixed at 0.5×10^{-3} mol L⁻¹ to prevent the large reduction in the recoveries of analytes in presence of lanthanides. Previously Gao et al. [91] had shown improvement in the CPE of U by TOPO in presence of La through the addition of bis[(trifluoromethyl)sulphonyl]imide (NTf₂⁻) based ionic liquid. The improvement was due to the formation of smaller $[\text{UO}_2(\text{NO}_3)(\text{H}_2\text{O})_2(\text{TOPO})_2][\text{NTf}_2]$ complex than La^{3+} which has higher coordination number. However, this method cannot be applied to the simultaneous extraction of U and Th, as by the same analogy Th would not be extracted into the SRP. Hence, we introduced a co-extractant along with TOPO in our micelle system which would preferentially complex trivalent lanthanides and thereby minimizing the competition between lanthanides and U or Th for complexation with TOPO. TODGA was explored as co-extractant, as it is known to have very high selectivity towards lanthanides and tri-valent actinides and also have good selectivity for tetra- and hexa-valent ions [114]. The concentration of TODGA was varied in the range of $(0.025 - 0.2) \times 10^{-3}$ mol L⁻¹, in presence of 0.5×10^{-3} mol L⁻¹ of TOPO, to observe the recoveries of both U and Th in presence of equimolar lanthanide. The results are shown in **Figure 3.4** which show that addition of 0.1 mmol L⁻¹ of TODGA in presence of 0.5×10^{-3} mol L⁻¹ of TOPO not only helps in diminishing the lanthanide interference but also results in quantitative extraction of both U and Th.

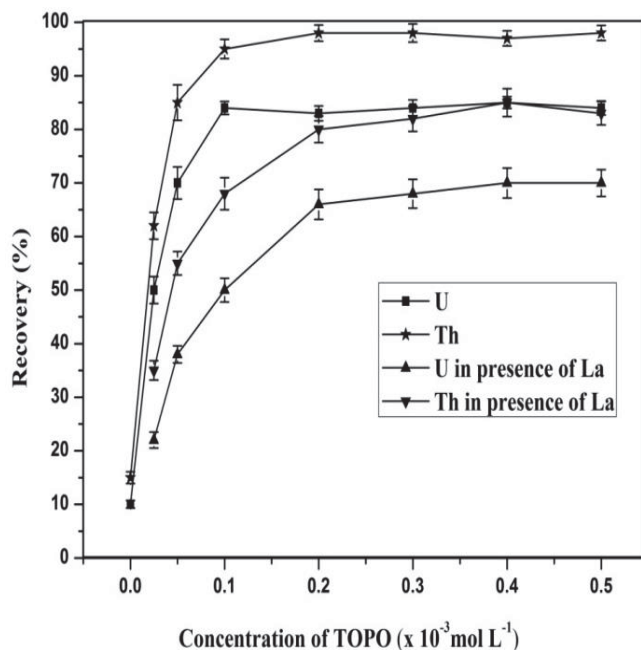


Figure 3.3. Effect of TOPO concentration on the recoveries of 50 ng mL^{-1} of U and Th each in absence and presence of equimolar La. TODGA had not been added during this exercise and the other parameters were kept constant as presented in Table 3.2.

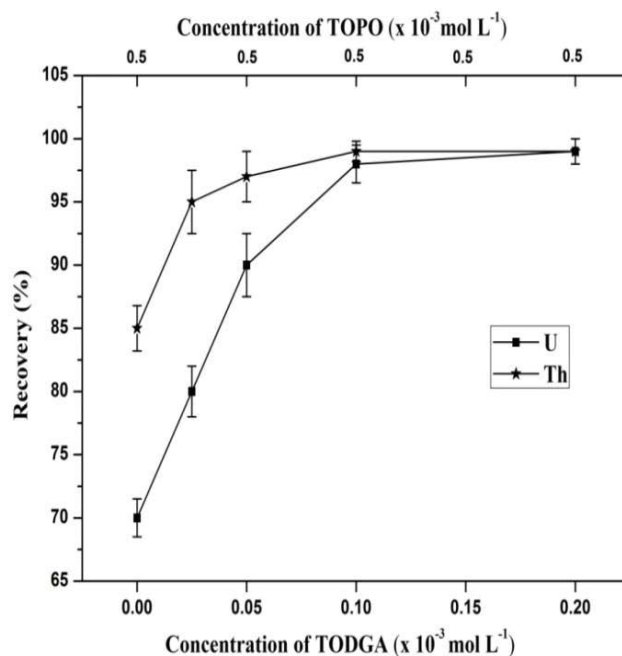


Figure 3.4. Effect of TODGA concentration on the recoveries of 50 ng mL^{-1} of U and Th each in presence of equimolar La ($\sim 30 \text{ ng mL}^{-1}$). Other parameters were kept constant as presented in Table 3.2.

3.5.3. Effect of non-ionic surfactant

Triton X-114 (TTX-114) was chosen as the surfactant because of its low theoretical CPT (23-25 °C) above its CMC of $0.2 \times 10^{-3} \text{ mol L}^{-1}$ which would not have significant toxicological impact on the environment [115]. The higher density of the TTX-114 SRP compared to water facilitates the phase separation process which was further improved by centrifugation. The goal of a successful CPE is to achieve highest EE and minimum volume of the surfactant to improve PF. The effect of TTX-114 concentration on the recovery of U and Th was studied in range of $(1-6) \times 10^{-3} \text{ mol L}^{-1}$. The variations in the analyte recoveries with TTX-114 concentration are represented in **Figure 3.5**. The analyte recoveries were found to increase with surfactant concentration upto $4 \times 10^{-3} \text{ mol L}^{-1}$ and later remain constant. Hence $4 \times 10^{-3} \text{ mol L}^{-1}$ of TTX-114 concentration was selected to minimize the SRP volume for further experiments.

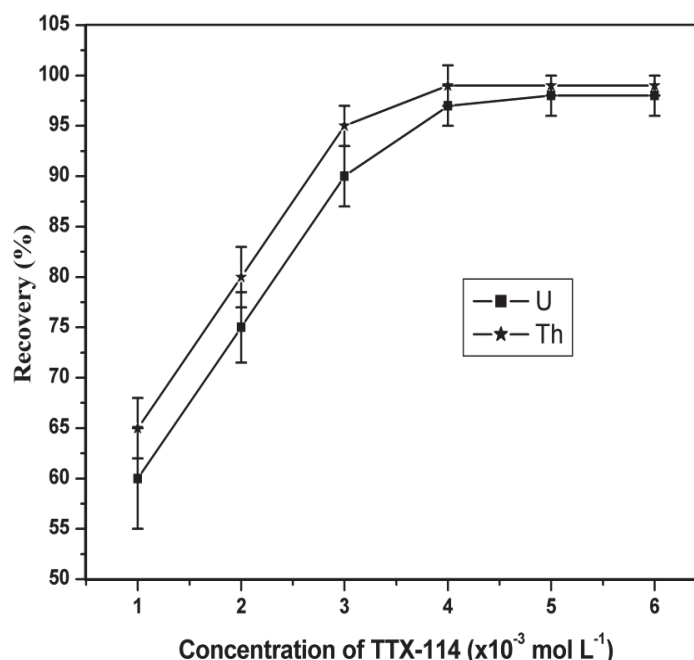


Figure 3.5. Effect of TTX-114 concentration on the recoveries of 50 ng mL^{-1} of U and Th each.

Other parameters were kept constant as presented in Table 3.2.

3.5.4. Effect of ionic surfactant concentration

Both TOPO and TODGA are individually known to extract $\text{UO}_2(\text{NO}_3)_2$ and $\text{Th}(\text{NO}_3)_4$ as their neutral adduct from concentrated HNO_3 media to the organic phase [112,114]. But in the typical pH range for CPE analysis, the extraction is dominated by the positively charged complexes of U(VI) and Th(IV), which is due to the lack of nitrate concentration. This resulted in low analyte recoveries as evident from **Figure 3.6**. As soon as SDS was added to the micellar medium, a sharp increase in analyte recoveries was observed with increase in SDS concentration from 0 to $0.2 \times 10^{-3} \text{ mol L}^{-1}$ followed by a slow increase at higher concentrations. SDS was chosen as the anionic co-surfactant to increase the analyte recoveries by stabilizing the positively charged complexes through its negatively charged hydrophilic head group at the expense of its hydrophilic counter cation. The highest reproducible recoveries were obtained at $0.5 \times 10^{-3} \text{ mol L}^{-1}$ of SDS concentration. The recoveries of U and Th were found to drop sharply above SDS concentration of $0.6 \times 10^{-3} \text{ mol L}^{-1}$ and resulted in less than 40% of recoveries.

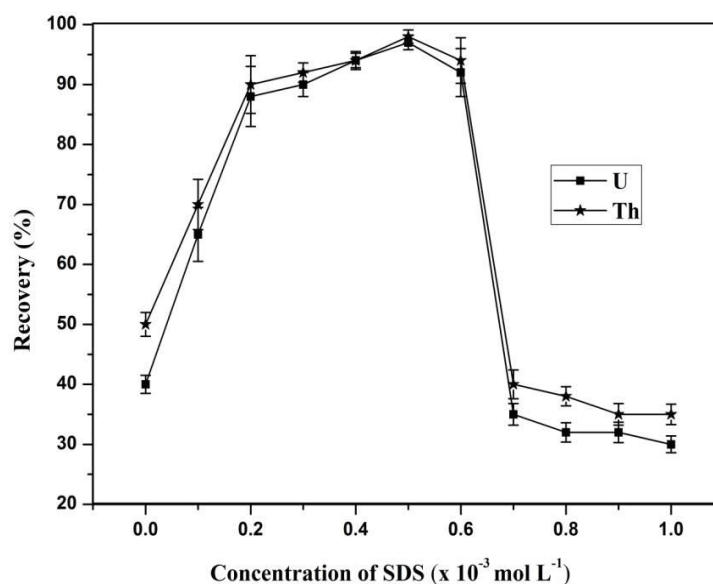


Figure 3.6. Effect of SDS concentration on the recoveries of 50 ng mL^{-1} of U and Th each. Other parameters were kept constant as presented in Table 3.2.

At high SDS concentrations the CPT of the CPE system becomes high which results in lower recoveries as demonstrated by Gu et al. [94]. Hence, the concentration of SDS was kept at $0.5 \times 10^{-3} \text{ mol L}^{-1}$.

3.5.5. Effect of electrolyte concentration

The role of electrolyte on the CPE has been previously discussed in **section 1.5.5.** of **chapter 1.** Owing to the requirement of NO_3^- ion for complexation of U and Th with TOPO and TODGA, the ionic strength of the medium was maintained with KNO_3 addition. The effect of KNO_3 concentration on the analyte recoveries were studied in the range of 0 to 0.2 mol L^{-1} as shown in **Figure 3.7.**

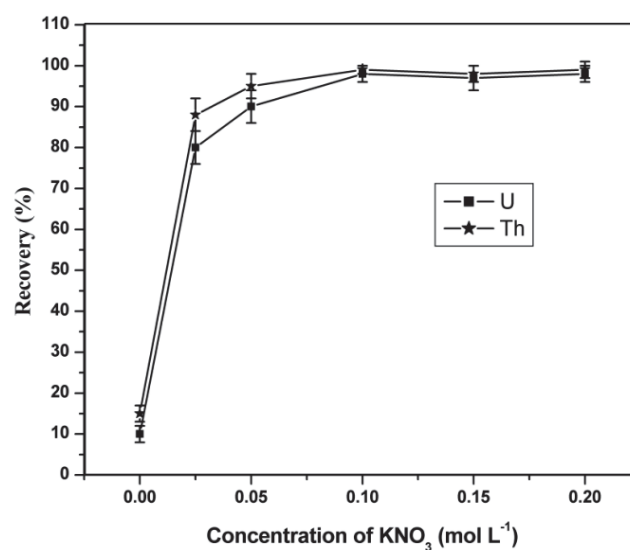


Figure 3.7. Effect of KNO_3 concentration on the recoveries of 50 ng mL^{-1} of U and Th each. Other parameters were kept constant as presented in Table 3.2.

The very low analyte recoveries in absence of KNO_3 was attributed to various factors like insufficient NO_3^- ion concentration, increase in CPT of the micelle system in presence of extractants and SDS resulting in resolubilization of the SRP at room temperature and

absence of salting-out effect. A 0.1 mol L^{-1} concentration of KNO_3 was found to be optimal, as further increase in ionic strength had no appreciable effect on the analyte recoveries.

3.5.6. Effect of extraction and phase separation temperature

The efficiency of any CPE procedure is largely dependent on its incubation temperature. The CPT of our micellar system was found to be $30 \pm 1 \text{ }^\circ\text{C}$ which was obtained by visually observing the clear surfactant solution to get opaque above a particular temperature once heating the solution started from $20 \text{ }^\circ\text{C}$ in step of $1 \text{ }^\circ\text{C}$. Decrease in temperature in the same manner resulted in a clear solution just below that particular temperature. The analyte recoveries were examined at different extraction temperatures in conjugation with different phase separation temperatures. In the first case, the solutions were allowed to stand for 1 h in an ice bath ($5\text{-}6 \text{ }^\circ\text{C}$) with constant stirring and then phase separation was carried out at different temperatures ranging from $30\text{-}70 \text{ }^\circ\text{C}$ with constant incubation time of 1 h. In the second case, the extraction was carried out at room temperature ($24 \pm 2 \text{ }^\circ\text{C}$) and rest of the conditions was maintained same as in the previous case. In the third case the extraction and phase separation was carried out at temperatures ranging from $30\text{-}70 \text{ }^\circ\text{C}$ for 2 h. After the incubation period the complete phase separation was done by centrifugation at 4000 rpm for 10 min at room temperature. The analyte recoveries found in all three cases are represented in **Figure 3.8**. The highest recoveries were obtained with the extraction temperature of $5\text{-}6 \text{ }^\circ\text{C}$ and phase separation temperature of $50\text{-}70 \text{ }^\circ\text{C}$. When the extraction was carried out near or above the CPT of the micellar system, the coacervation of micelles causes lesser metal-ligand interaction and results in lower analyte recoveries. It was reported by Safavi et al. [116] that the highest PFs were obtained when phase separation temperature is above the CPT of the system. This

happens due to higher degree of dehydration of the micelles at temperatures above its CPT which results in minimum SRP volume. Since no change in SRP volume was obtained above 50 °C, it was fixed as the phase separation temperature.

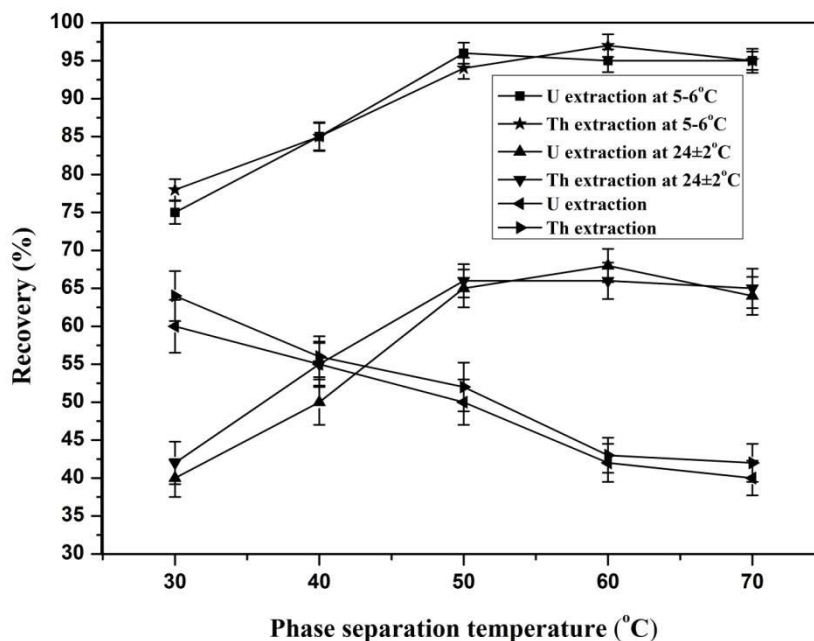


Figure 3.8. Effect of extraction and phase separation temperatures on the recovery of 50 ng mL⁻¹ of U and Th each. Other parameters were kept constant as presented in Table 3.2.

3.6. Optimization of spectrophotometric procedure

The simultaneous spectrophotometric detection of U and Th in the preconcentrated samples requires the use of a chromophoric agent which can form stable complexes with U and Th. Among many organic dyes used for the spectrophotometric determination of actinides [117], arsenazo-III (**Figures 3.9a**) was selected as the chromophoric agent in this work. It has the advantage of forming stable metal complexes in strongly acidic media eliminating the possibilities of hydrolysis, formation of polynuclear species and complexes of arsenazo-III with other elements which may interfere with the spectrophotometric determination of the analytes [177]. The type of the mineral acid

medium i.e. HCl, HNO₃ (with small quantity of sulfamic acid) or HClO₄ and their molar concentrations play an important role in the determination of U and Th as reported in the literature [117-120]. Both U and Th form complexes with arsenazo-III instantaneously and the U-arsenazo-III complex were found to be stable upto 3 to 4 weeks in all three mineral acids. On the other hand, the stability of Th-arsenazo-III complex was found to be dependent on Th concentration as well as the acid medium [118]. The visual and spectrophotometric observations for Th-arsenazo-III complex are depicted in **Figures 3.9b and 3.10 respectively**. As evident from **Figure 3.10**, in HCl medium the decrease in absorbance of Th-arsenazo-III complex was observed for Th concentration above 1.5 $\mu\text{g mL}^{-1}$ and below that the absorbance was found to be quite stable for 1 h period. But in HClO₄ medium the decrease was observed even at 1.0 $\mu\text{g mL}^{-1}$ of Th (**Figure 3.10**). The rate of decrease in absorbance in HClO₄ medium was found to be much faster than that in HCl medium, which can be visually observed from **Figure 3.9b**. Only in HNO₃ medium containing sulfamic acid (NH₂SO₃H) no appreciable decrease in absorbance of Th complex was observed for a period of 1 h and Beer's Law was found to be followed in the concentration range of 0.25-6.0 $\mu\text{g mL}^{-1}$. In case of U, the Beer's law was found to be followed in the concentration range of 0.5-15.0 $\mu\text{g mL}^{-1}$. The molar absorptivities for U and Th at 656 nm and 662 nm were found to be 2.2×10^4 and $6.4 \times 10^4 \text{ mol}^{-1} \text{ L cm}^{-1}$ respectively at room temperature. NH₂SO₃H was added during the spectrometric determination of U and Th by arsenazo-III in HNO₃ medium to destroy any nitrous acid and oxides of nitrogen which are invariably present in equilibrium with nitric acid [120]. The deconvolution of overlapped absorption spectra of U-arsenazo-III and Th-arsenazo-III coloured complexes was carried out by applying PLSR algorithm as follows.

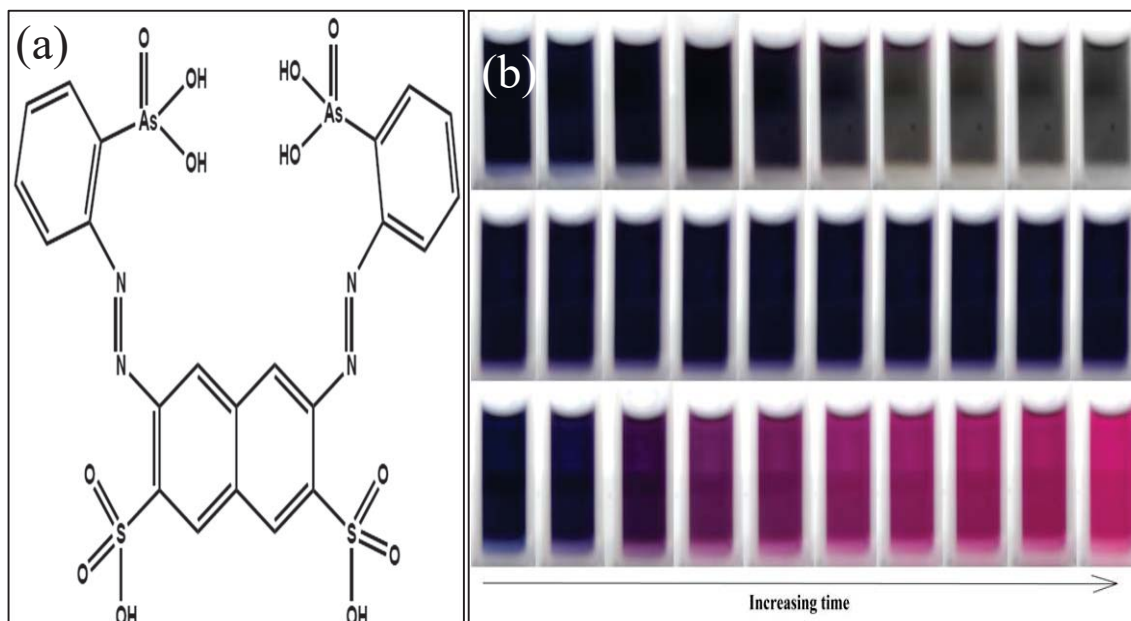


Figure 3.9. (a) Structure of arsenazo-III and (b) visual colour change of Th-arsenazo-III complex in HCl medium within 30 min (top); in HNO₃ and sulfamic acid medium within 1 h (middle) and in HClO₄ medium within 5 min (bottom), where the Th conc. is 2.5 $\mu\text{g mL}^{-1}$.

3.6.1. Basic principles of partial least square regression (PLSR) algorithm

Modern spectrophotometers generate spectrum consisting of 1k to 8k pixel. Every pixel is a signature of a particular wavelength depending on the resolution and calibration of the system. It is often the case with spectrum or data involving large numbers of independent variables, i.e., pixel in the spectrum case, that there exists extensive colinearity or correlation between these variables. Colinearity adds redundancy to the regression model, since more variables may be included in the model than is necessary for adequate predictive performance. Of the methods available to the analytical chemist for regression analysis with protection against the problems induced by correlation between variables, principal components regression (PCR) is the most commonly employed [121,122]. The calibration model, referred to a partial least squares regression (PLSR) is a relatively modern technique, developed and popularized in analytical science [121,122]. The

method differs from PCR by including the dependent variable in the data compression and decomposition operations. Simultaneous use of dependent and independent variable information makes the method more complex than PCR.

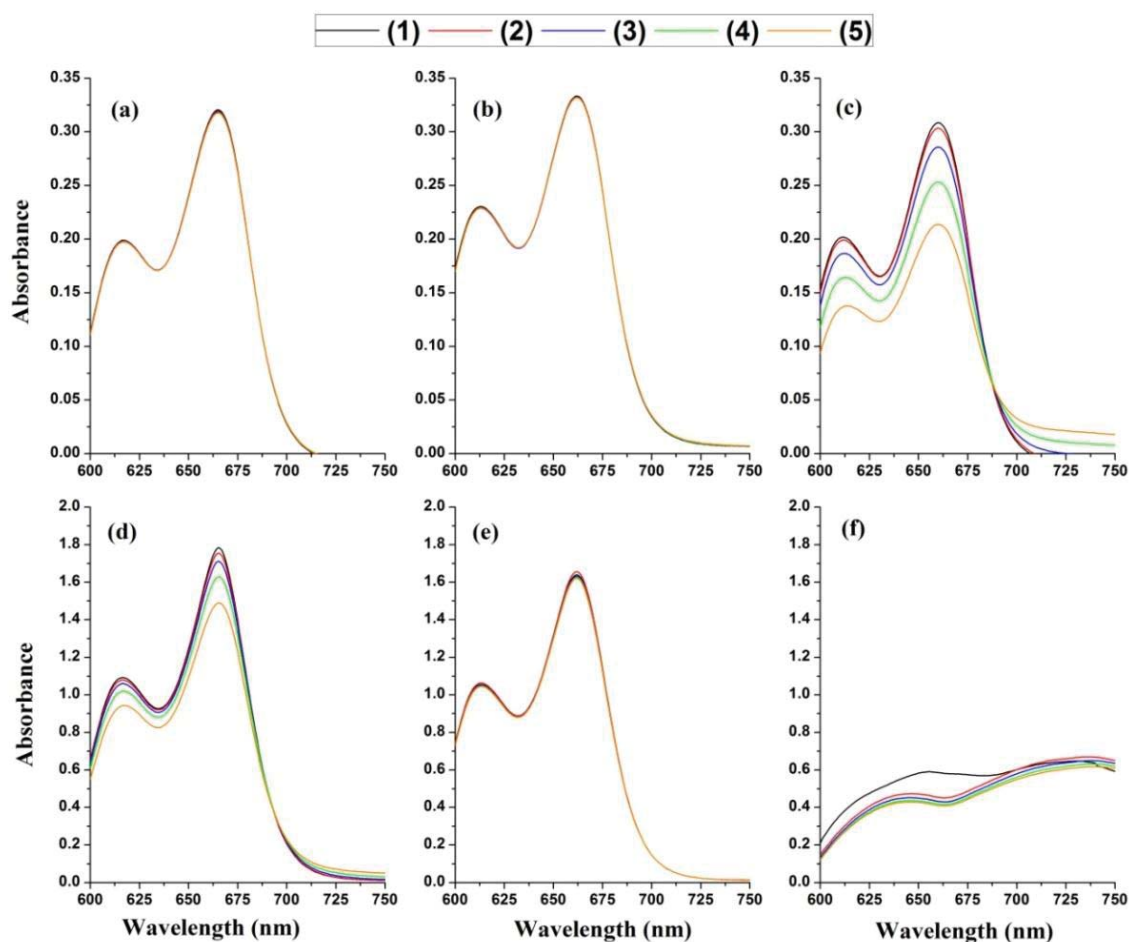


Figure 3.10. Effect of mineral acids, 6 mol L⁻¹ of HCl (a and d), HNO₃ + 0.1 mol L⁻¹ sulfamic acid (b and e) and HClO₄ (c and f), and metal ion concentration, 1 μg mL⁻¹ (a, b and c) and 5 μg mL⁻¹ (d, e and f), on the absorption maximum of Th using arsenazo-III with time. Spectra were recorded after (1) 5 min, (2) 15 min, (3) 25 min, (4) 35 min and (5) 45 min of the addition of arsenazo-III.

Briefly, a library of reference spectra from standard samples was compiled. The matrix of the independent variables is the mean-centered spectral intensities (**X**). Each row of the

data matrix \mathbf{X} gives the spectral intensities of one of the standard samples. The dependent variables are the mean-centered elemental concentrations (\mathbf{Y}) of the corresponding element. The PLSR approach reduces the number of variables to a few principal components (PC) by redistributing the total variance of \mathbf{X} . \mathbf{X} is then expressed as product of score (\mathbf{T}) and loading vectors (\mathbf{P}) by the formula, $\mathbf{X} = \mathbf{TP} + \mathbf{E1}$, where $\mathbf{E1}$ is an error matrix. The concentrations, \mathbf{Y} are then regressed on the new data matrix \mathbf{T} using $\mathbf{Y} = \mathbf{TB} + \mathbf{E2}$, where \mathbf{B} is a matrix relating the variables or PLSR coefficient (PLSRC) by minimizing $\mathbf{E2}$. This action serves to minimize the potential effects of intensities having large variances but which are irrelevant to the calibration model.

When the PLSRC i.e., \mathbf{B} is calculated individually for each element, i.e., \mathbf{Y} only have one element's concentration in each run, the method is called PLSR-1. This approach is also known as PLSR-1 approach. PLSRC is a 1-D matrix with same number of elements as the number of variables, i.e., pixel in the present case. The positive PLSRC values indicate positive correlation between the intensity at the pixel and the elemental concentration used in \mathbf{Y} . The negative coefficient values indicate the reverse, i.e., decrease of intensity with increasing concentration. The PLSRC values can be used to select relevant variables according to the magnitude of their absolute values. Once \mathbf{B} has been finalized for unknown sample, the concentration is simply calculated by matrix multiplication of \mathbf{B} with unknown spectrum.

3.6.2. Factor optimization of PLSR analysis

In PLSR analysis, the number of factors to be included in the algorithm for calibration purpose was determined by comparing root mean square error of cross validation (RMSEcv). Since these factors are the re-distributed version of the total variance,

introduction of more than necessary factors will increase the noise in the regression. In this work the number of factors was optimized by determining the RMSEcv of calibration set (CS) of samples for U and Th. The change in RMSEcv values for both U and Th with the change in number of factors in the PLSR model is shown in **Figure 3.11**. It can be seen that minimum 6 factors are required for both U and Th to obtain the minimum RMSEcv values of the elements.

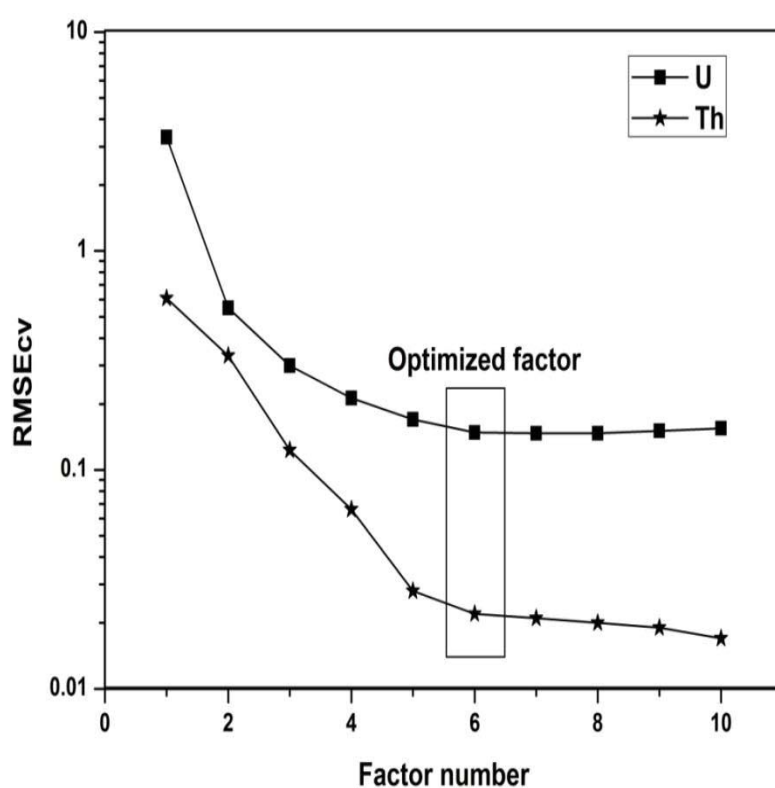


Figure 3.11. Optimization of PLSR algorithm factor.

3.6.3. PLSR coefficient

The acquired UV-visible spectra for corresponding U and Th concentrations were correlated with each other mathematically and a column matrix or vector, also known as PLSR coefficient (PLSRC) for individual element was constructed. A graphical representation of the PLSRC, obtained by using 6 factors, is represented in **Figure 3.12**.

The generated PLSRC indicate correlation between the intensity at the pixels and the elemental concentration used in unknown sample. It can be seen from **Figure 3.12** that both U and Th have two positive correlation peaks at different places indicating high sensitivity of those areas to the corresponding element.

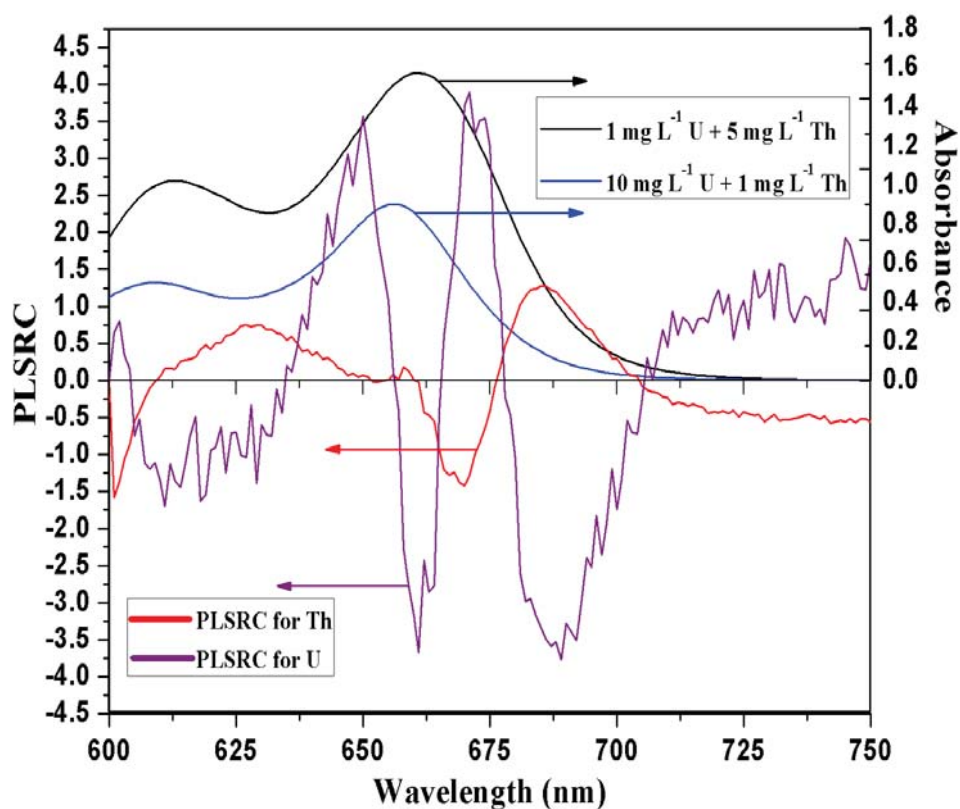


Figure 3.12. Absorption spectra of U and Th mixtures and the individual PLSRC's.

3.6.4. Accuracy and precision of PLSR analysis

The accuracy and precision of the PLSR model was obtained by analyzing the validation set (VS) samples. Five replicate spectra of each sample were treated to calculate these parameters. The accuracy was examined by checking the elemental percentage recovery and the precision was expressed in terms of root mean square of prediction (RMSEP) and

percentage relative error of prediction (REP). All the calculated values are given in **Table 3.3**.

Table 3.3. Concentrations of U and Th in VS solutions as predicted by PLSR and statistical parameters of the PLSR algorithm

| Sample code | Spiked amount ($\mu\text{g mL}^{-1}$) | | PLSR predicted amount ($\mu\text{g mL}^{-1}$) | | Recovery (%) | |
|-------------------|---|-----|---|-----------------|--------------|-------|
| | U | Th | U | Th | U | Th |
| VS1 | 1 | 4 | 1.01 \pm 0.01 | 3.96 \pm 0.02 | 101 | 99 |
| VS2 | 1.5 | 2.5 | 1.53 \pm 0.03 | 2.47 \pm 0.01 | 102 | 99 |
| VS3 | 3 | 3 | 2.98 \pm 0.01 | 3.03 \pm 0.02 | 99 | 101 |
| VS4 | 6.5 | 1.5 | 6.52 \pm 0.06 | 1.46 \pm 0.01 | 100 | 97 |
| VS5 | 8 | 2 | 8.0 \pm 0.1 | 2.00 \pm 0.01 | 99 | 100 |
| Mean recovery (%) | | | | | 100 | 99 |
| RMSEP | | | | | 0.029 | 0.032 |
| REP (%) | | | | | 0.734 | 1.224 |

3.7. Effect of common interfering ions and their tolerance limit

The various cations and anions are distributed asymmetrically in soil, water and air. Hence, detection of particular metal ion(s) in environmental matrices faces interference from other ions which are present in higher concentrations. Solutions containing 50 ng mL⁻¹ of U and Th individually were analyzed in presence of maximum concentrations of individual interfering ions as listed in **Table 3.4**. These interfering ion concentrations were found not to diminish the analyte recoveries less than 95% to their actual value in absence of interfering ion. The most abundant alkali metals were found to be tolerated upto 10000 $\mu\text{g mL}^{-1}$, owing to their low oxidation state and hence negligible extraction. Alkaline earth metals are also significantly abundant in environment and their +2 oxidation state can also affect the extraction by competing in the complexation process. The proposed CPE based analytical procedure was found to be resilient to 1500 $\mu\text{g mL}^{-1}$ of Mg²⁺ and 500 $\mu\text{g mL}^{-1}$ of Ca²⁺, Sr²⁺ and Ba²⁺. The higher oxidation states and vacant

d- or f-orbitals in transition metal and lanthanide ions increase their affinity towards O-donor ligands and hence can exert negative impact on U and Th recoveries. Their maximum tolerance limits are given in **Table 3.4**. The low tolerance limits for Cr^{3+} and Fe^{3+} is consistent with the previously reported simultaneous CPE of U and Th by Shariati et al. [99]. Mercury is a highly toxic element and as per WHO recommendations its concentration should be less than $0.002 \mu\text{g mL}^{-1}$ in drinking water. Hence, a 100-fold higher concentration of Hg^{2+} was examined and found to have no interference on the CPE of U. As discussed earlier the addition of TODGA in presence of TOPO in the micelle system was found to tolerate lanthanide concentration equivalent to double of the total target metal ion concentrations. The CPE as well as spectrophotometric interference of Zr^{4+} and Hf^{4+} restrict their tolerance limits to concentrations equivalent to double of the total target ion concentrations. Some common anions like carbonate (CO_3^{2-}), phosphate (PO_4^{3-}), sulfate (SO_4^{2-}), chloride (Cl^-) and bromide (Br^-) were found to exert no negative effect on analyte recoveries up to concentrations mentioned in **Table 3.4**.

3.8. Analytical figures of merit and real sample analysis

The proposed CPE based simultaneous spectrophotometric detection of U and Th is a simple and cost effective analytical procedure with (i) wide DLR of 15-1000 and 10-1000 ng mL^{-1} ; (ii) quantitative EEs of $98 \pm 0.5\%$ and $99.5 \pm 0.5\%$; (iii) PF values of 94 and 100 and (iv) DL values of 4.0 and 2.0 ng mL^{-1} for U and Th respectively. These values are better than the literature reported CPE based simple, versatile and cost effective detection methodologies for U and/or Th [56,89,90,95-98,100,108,123]. Since the PLSR analysis does not provide any straight line fit between absorbance and analyte concentration, individual analyte was preconcentrated and analyzed by spectrophotometry to evaluate

their DL values ($3\sigma_{\text{blank}}/\text{sensitivity}$). The RSDs (1σ) were found to be between 1-3% and 2-5% respectively in absence and presence of interfering ions.

Table 3.4. Tolerance limit of the developed method in the presence of selected cations and anions; Concentration of U and Th: 50 ng mL⁻¹ each

| Interfering ions | Tolerance limit ($\mu\text{g mL}^{-1}$) |
|--|---|
| Na ⁺ , K ⁺ | 10000 |
| Mg ²⁺ | 1500 |
| Ca ²⁺ , Sr ²⁺ , Ba ²⁺ | 500 |
| Zr ⁴⁺ Hf ⁴⁺ La ³⁺ , Ce ⁴⁺ , Eu ³⁺ | Double the total target ions concentration |
| Co ²⁺ , Zn ²⁺ , Cd ²⁺ | 250 |
| Cr ³⁺ , Fe ³⁺ | 10 |
| Mn ²⁺ , Ni ²⁺ , Cu ²⁺ , Pb ²⁺ | 200 |
| Hg ²⁺ | 0.2 |
| Cl ⁻ , Br ⁻ | 10000 |
| CO ₃ ²⁻ , PO ₄ ³⁻ , SO ₄ ²⁻ | 1500 |

Cations were prepared using their chloride or nitrate salts. Anions were prepared using their sodium or potassium salts.

This comparison shows versatility of the proposed analytical methodology over the literature reports. Three different water samples viz., ground water from Punjab (India), sea water from Mumbai coast (India) and lake water from West Bengal (India) were analyzed by the proposed method. All these three samples were also analyzed directly by inductively coupled plasma mass spectrometry (ICP-MS) to validate the proposed analytical methodology. The results are listed in **Table 3.5**. The results obtained by the proposed method are found to be in good agreement with the values obtained by ICP-MS within 95% confidence interval.

Table 3.5. Analysis of real water samples by the developed analytical methodology ($n=5$) and cross-validation of the results by direct analysis employing ICP-MS ($n=3$).

| Sample | Added (ng mL ⁻¹) | | Found by CPE-UV- Visible (ng mL ⁻¹) | | Found by ICP-MS (ng mL ⁻¹) | |
|--------------|---------------------------------|----|--|----------|---|------|
| | U | Th | U | Th | U | Th |
| Ground water | 0 | 0 | 110±3 ^a | ND | 110±5 | ND |
| | 15 | 15 | 124±4 | 14.3±0.5 | 124±4 | 15±1 |
| | 25 | 25 | 135±5 | 24.2±0.7 | 136±4 | 25±1 |
| Lake water | 0 | 0 | ND | ND | ND | ND |
| | 15 | 15 | 14.5±0.4 | 14.8±0.4 | 15±1 | 15±1 |
| | 25 | 25 | 24.0±0.6 | 25.1±0.7 | 25±2 | 24±2 |
| Sea water | 0 | 0 | ND | ND | 2.8±0.3 | ND |
| | 15 | 15 | 17.6±0.5 | 14.6±0.5 | 18±2 | 15±1 |
| | 25 | 25 | 28 ±1 | 25.0±0.9 | 28±2 | 25±2 |

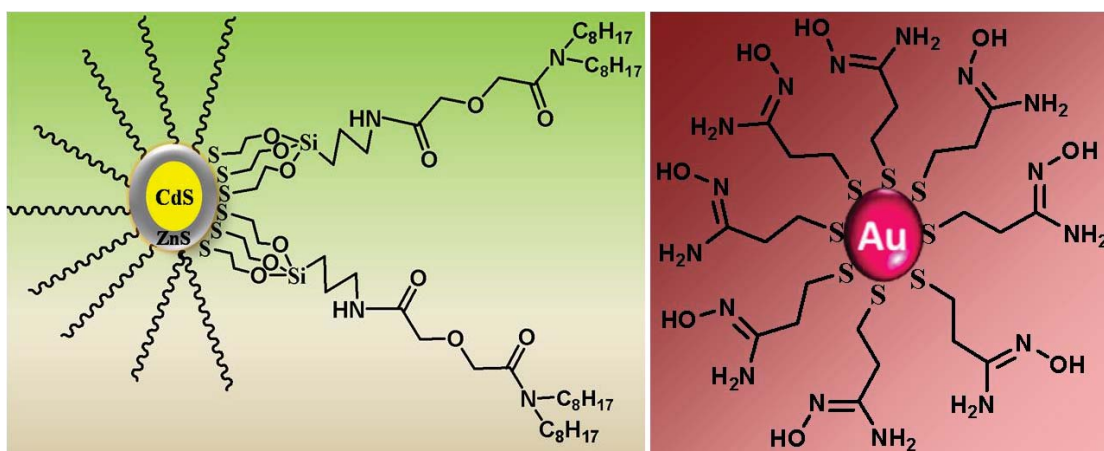
ND = Not detected; ^aConcentration of U above its WHO, USEPA and AERB guideline values are reported in literature by Bajwa et al. [124].

3.9. Conclusion

The guideline values of U in drinking water, established by WHO, USEPA and AERB based on its chemical toxicity, easily fall in the DLR of the developed analytical procedure. Hence according to these guideline values, this methodology can easily distinguish between drinkable and non-drinkable water. The limit of quantification (LOQ) value of U reported in this method is 15.0 ng mL⁻¹ and any value less than that is not always safer to ingest because of still lower radiological guideline values of its isotopes. The increased production and use of short lived U isotopes has enhanced the probability of their environmental contamination. Therefore, the chances of both chemical and radiological adverse health effects of U have increased manifold. The improvement in the DL and LOQ values of simple and cost effective CPE based detection procedure is thus important for the benefit of the society. Subsequently works were carried out to further improve the DL value of U by simple and inexpensive CPE based detection procedures.

Chapter 4

Application of functionalized nanomaterials in cloud point extraction (CPE) of uranium (U) in aqueous samples



This page is kept blank intentionally

Traditional dye chemosensors are less efficient in highly sensitive metal ion detection compared to chemical nanosensor materials. The lower quantum yield or molar absorptivity of metal complexes of dye sensors compared to nanosensors is the major reason of such discrimination. Surface modification of nanoparticles (NPs) for their selective interaction with metal ions can bring changes in the parameters of NP's optoelectronic properties. A correlation between varying optoelectronic property and added metal ion concentration is the basis of spectroscopic metal ion detection by nanosensor materials. The literature reports on application of NPs in the cloud point extraction (CPE) of metal ions are limited [125-129]. Most of these reports used functionalized NPs as the thermoreversible extracting agents to cater the CPE of metal ions as suggested by Liu et al. [130]. The study by Tan et al. [129] is the only report revealing variation in optical property of functionalized gold NPs (AuNPs) on CPE of Hg(II) ions. Hence, there is a lot of scope of applying NPs in the simultaneous CPE and spectrophotometric or fluorometric detection of U to achieve its better detection limit (DL) values. In this chapter we have separately discussed the metal ion detection mechanisms of two newly synthesized functional NPs viz., quantum dots (QDs) and gold nanoparticles (AuNPs).

4.1. Functionalized QDs in the CPE based fluorometric detection of uranium

4.1.1. Introduction

In recent times semiconductor QDs have emerged as the highly sensitive fluorophore sensors for heavy metal detection compared to traditional dye, as they are photochemically stable and have high quantum yield [104,131,132]. Moreover, QDs of different fluorescence wavelengths can easily be prepared by simply varying the QD size and all wavelengths of QDs can be excited by a single excitation source. This

makes them much easier to excite than traditional fluorescent dyes which have relatively narrow absorption bands [133-135]. QD labeled with uranyl ion (UO_2^{2+})-specific DNAzyme and modified with quencher, was previously reported for detection of U in aqueous samples [131]. DNAzymes for a particular metal ion are not commonly available in the market and their handling requires sophisticated laboratories. Therefore, functionalization of QDs with common organic molecules instead of DNAzymes would make the method easy, cost effective and feasible for common laboratories. Very recently Dutta et al. [40] have reported ultratrace level detection of UO_2^{2+} ions by strongly photoluminescent responsive amine-modified mercaptoacetic acid capped cadmium sulfide (CdS) QDs. In their report the specified tolerance limits of different commonly available cations are very low [40]. This is expected due to the fact that thiourea is well known to form stable complexes with many transition metal ions [136-138]. Hence, the synthesis of a common ligand labeled UO_2^{2+} -specific QD nanosensor needs serious efforts. In this regard, novel diglycolamide-capped CdS/zinc sulfide (ZnS) core-shell QDs were synthesized and characterized by us for the first time. The fluorometric determination of ultratrace levels of U in environmental aqueous samples by the synthesized QD nanosensor was made possible through its micellar dispersion, leading to cloud point extraction (CPE).

4.1.2. Synthesis and characterization of the QD nanosensor

The complete synthesis route of the diglycolamide-capped CdS/ZnS core-shell QDs is represented in **Figure 4.1**. Being insoluble in water the synthesized QD nanosensor was always kept in acetonitrile (ACN) medium. The complete experimental synthesis procedure is given in **section 2.3.1** of **chapter 2**.

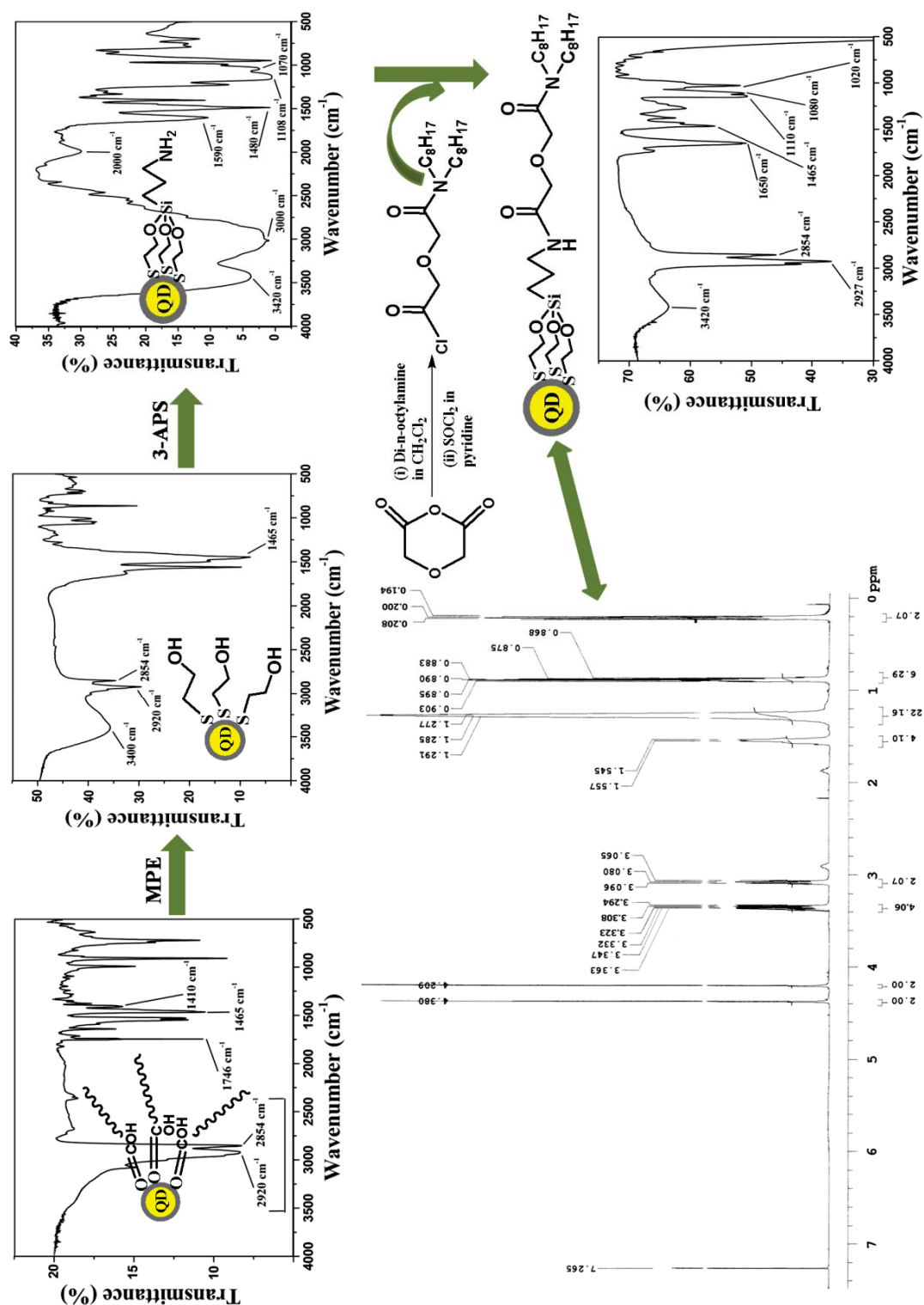


Figure 4.1. Complete reaction route of synthesizing diglycolamide-capped CdS/ZnS core-shell quantum dots (QDs) with respective IR spectra of all the products and also the NMR spectrum of the final product.

4.1.2.1. Synthesis of CdS/ZnS QD

In the beginning CdS/ZnS QD was synthesized in chloroform medium from its precursors and was stabilized by oleic acid capping. The absorption spectrum of oleic acid-capped CdS/ZnS QD, as shown in **Figure 4.2**, shows the first, second and third excitons at 448, 395 and 355 nm respectively.

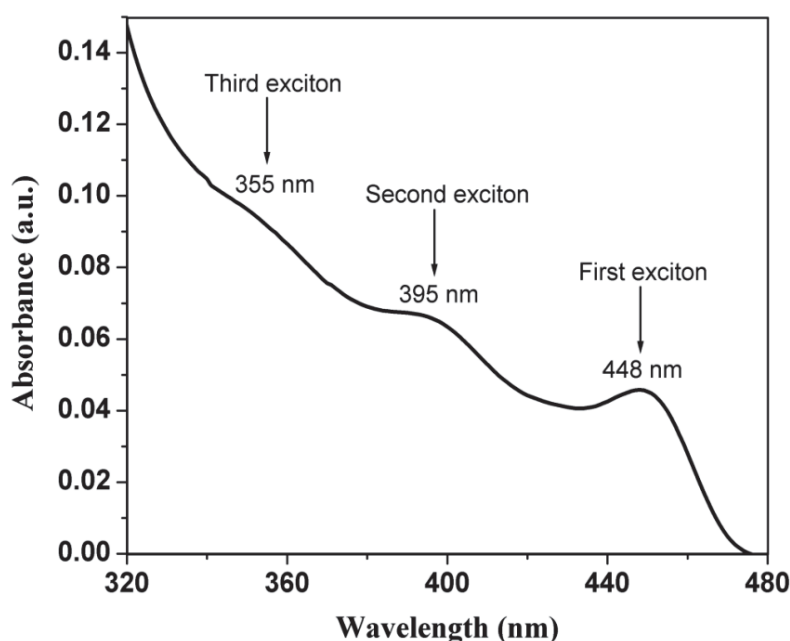


Figure 4.2. Absorption spectrum of oleic acid capped CdS/ZnS QDs

4.1.2.2. Synthesis of OH-capped CdS/ZnS QD

The oleic acid-capped CdS/ZnS QD was transferred from chloroform to aqueous phase via formation of OH-capped CdS/ZnS QDs employing 2-mercaptoethanol (2-MPE). The appearance of broad O-H stretching frequency at 3400 cm^{-1} and disappearance of O-H and C=O stretching frequencies of carboxylic acid group at $3000\text{--}2500$ (various peaks) and 1726 cm^{-1} in their IR spectra (**Figure 4.1**) confirms the generation of OH-capped QDs. The additional CH_3 and CH_2 stretching and bending vibrations at 2920 , 2854 and 1465 cm^{-1} remained unchanged in both. The

transmission electron microscopy (TEM) image and fluorescence intensity measurement of OH-capped QD revealed its size of 4.2 ± 0.2 nm and emission peak at 462 nm when excited at 355 nm (λ_{ex}), as shown in **Figure 4.3**. Additionally high-resolution TEM (HRTEM) image and its FFT version of OH-capped CdS/ZnS QDs were recorded and are given in **Figure 4.4**. The HRTEM image reveals signatures of lattice fringes with an interplanar distance of 0.34 ± 0.01 nm. In addition, the FFT of the HRTEM image confirms the face centered cubic (fcc) structure of the CdS/ZnS core-shell QD NPs. The value of 0.34 ± 0.01 nm agrees well with the reported interplanar spacing of (111) plane in fcc CdS crystals (JCPDS 89-0440).

4.1.2.3. Synthesis of amino-silanized CdS/ZnS QD

Upon addition of 3-aminopropylsilane (3-APS) to OH-capped QDs, the O-H peaks disappeared and as a result of silanization (**Figure 4.1**) i.e., O-Si bond formation, several broad peaks at 3400, 3000 and 2000 cm^{-1} and strong peaks at 1590 and 1480 cm^{-1} appeared corresponding to the hydrolyzed $-\text{NH}_2$ group of $(\text{RO})_3\text{Si}-\text{CH}_2\text{CH}_2\text{CH}_2\text{NH}_2$. A strong doublet at 1108 and 1070 cm^{-1} corresponding to Si-OCH₂CH₂ group also confirmed the silanization process. The TEM image of amino-silanized QDs (**Figure 4.3**) showed ~ 4 nm size increase due to silanization and the resulting size was found to be 8.2 ± 0.2 nm. This resulted in red shift of fluorescence peaks from 462 nm in OH-capped QD to 466 nm in amino-silanized QD (**Figure 4.3**).

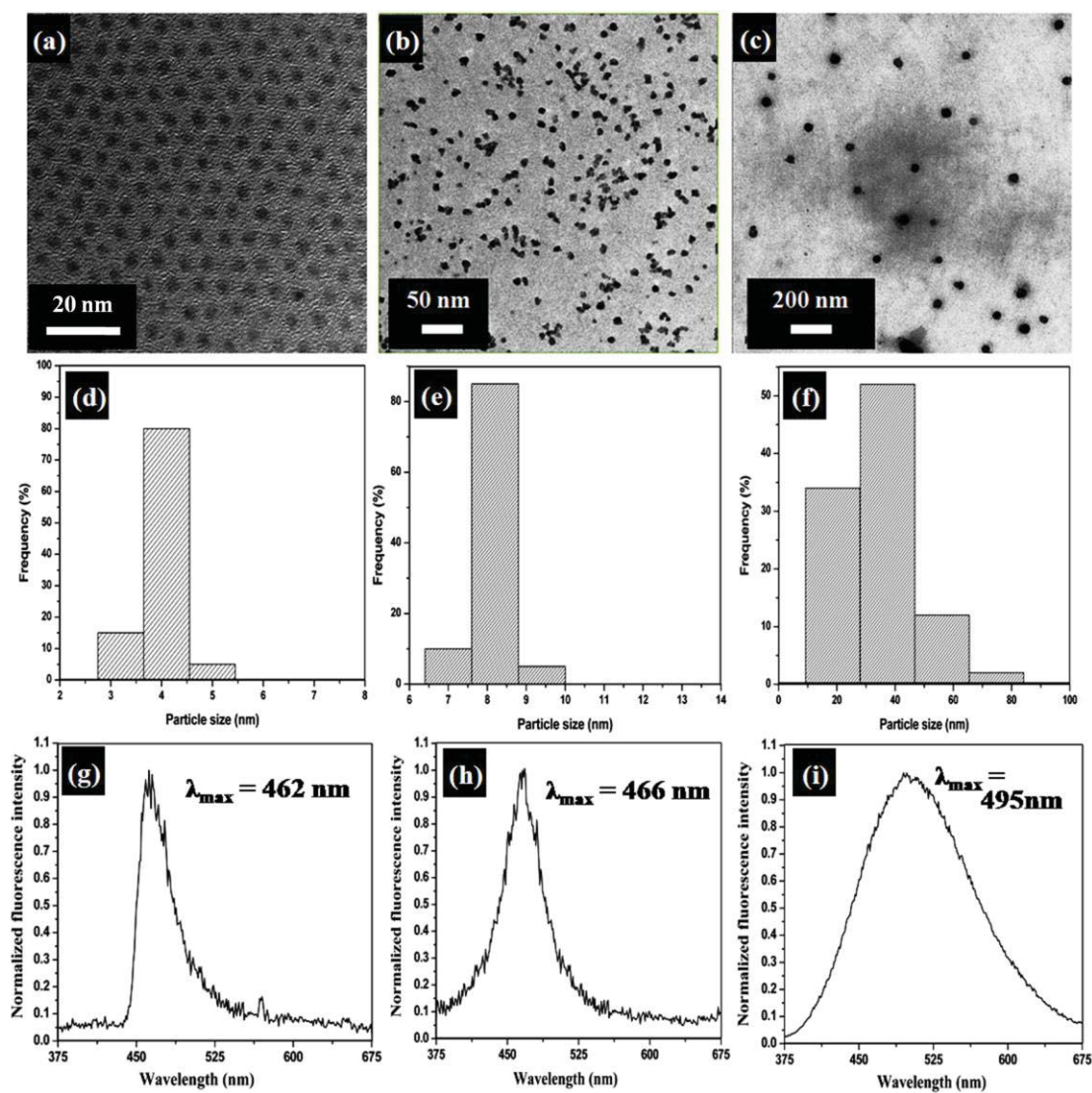


Figure 4.3. TEM micrographs and the corresponding size distributions of (a,d) OH-capped, (b,e) amino-silanized and (c,f) diglycolamide-capped CdS/ZnS QDs. The emission spectra of (g) OH-capped, (h) amino-silanized and (i) diglycolamide-capped CdS/ZnS QDs were obtained with the excitation wavelength (λ_{ex}) of 355 nm.

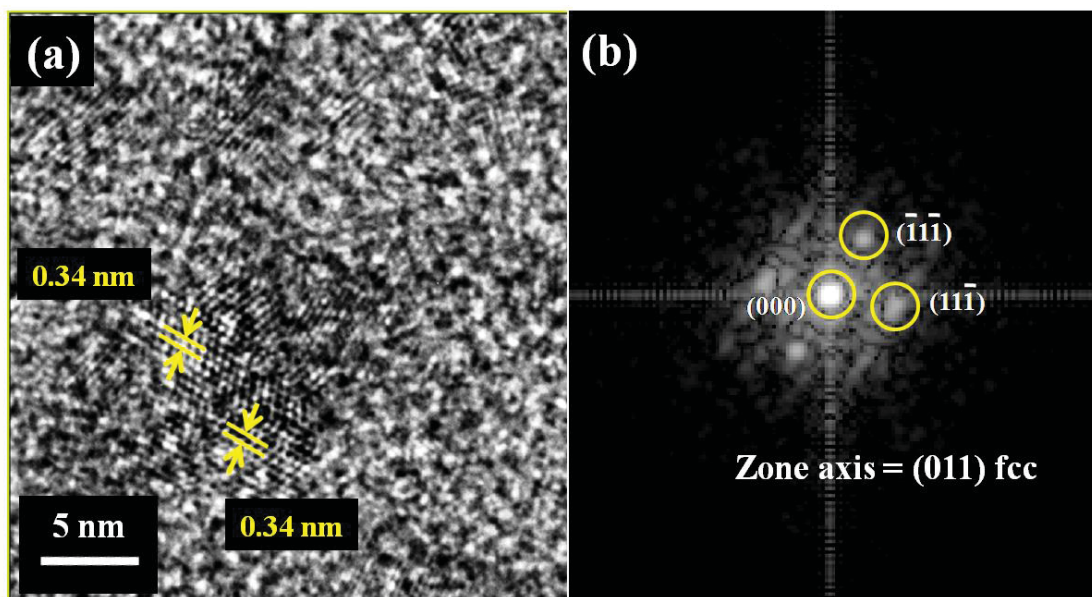


Figure 4.4. (a) High-resolution TEM (HRTEM) image of OH-capped CdS/ZnS QDs. (b) FFT image of HRTEM micrograph of OH-capped CdS/ZnS QDs.

4.1.2.4. Synthesis of diglycolamide capped CdS/ZnS QD

In the final step acid chloride of dioctyldiglycolamic acid amide was reacted with the amino-silanized QDs via amination reaction to form diglycolamide-capped QDs. A weak broad peak at 3420 cm^{-1} corresponding to the secondary amide group, a sharp peak at 1650 cm^{-1} corresponding to C=O group of amide and a strong doublet at 1110 and 1080 cm^{-1} confirmed the formation of diglycolamide-capped QDs (**Figure 4.1**). Diglycolamide-capped QD was also characterized by its ^1H NMR spectrum, taken in deuterated chloroform (CDCl_3) solvent and the chemical shifts in ppm (δ scale) were measured relative to CHCl_3 (7.27 ppm) as internal standard: 0.2 (t, 2H, SiCH_2), 0.89 (m, 6H, $\text{NCH}_2(\text{CH}_2)_6\text{CH}_3$), 1.28 (m, 20H, $\text{NCH}_2\text{CH}_2(\text{CH}_2)_5\text{CH}_3$), 1.28 (m, 2H, $\text{NHCH}_2\text{CH}_2\text{CH}_2\text{Si}$), 1.54 (m, 4H, $\text{NCH}_2\text{CH}_2(\text{CH}_2)_5\text{CH}_3$), 3.08 (t, 2H, $\text{NHCH}_2\text{CH}_2\text{CH}_2\text{Si}$), 3.32 (m, 4H, $\text{NCH}_2(\text{CH}_2)_6\text{CH}_3$), 4.21 (s, 2H, OCH_2CO) and 4.38 (s, 2H, OCH_2CO). The average size of the final diglycolamide-capped CdS/ZnS QDs as found to be $\sim 37.4\text{ nm}$ with the range being $\sim 18.6\text{ nm}$ to $\sim 75\text{ nm}$, as shown in

Figure 4.3. The aggregation of the QD nanoparticles during the diglycolamide capping resulted in the overall size increase and size variation of the QDs. It has been reported earlier that when nanocomposites aggregate in presence of organic molecules, the exciton size is dictated instead of electron-hole interactions by the physical dimension and organization of the nanoscale system [139]. Hence, in these aggregates the exciton shifts to the site of smaller band gap resulting in large red shift in the absorption and emission spectra. Accordingly a red shift in the absorption and fluorescence peaks was observed as we moved from OH-capped QDs to diglycolamide-capped QDs, as shown in **Figure 4.3 and 4.5**. The first absorption peaks of OH-capped QDs and diglycolamide-capped QDs appeared at 448 and 475 nm respectively (**Figure 4.5**). The fluorescence peaks of the same appeared at 462 and 495 nm respectively on excitation at 355 nm (**Figure 4.3**). The quantum yield (Q.Y.) of the synthesized diglycolamide capped CdS/ZnS core-shell QDs was determined to be $\sim 5\%$ using coumarin 343 in acetonitrile as standard.

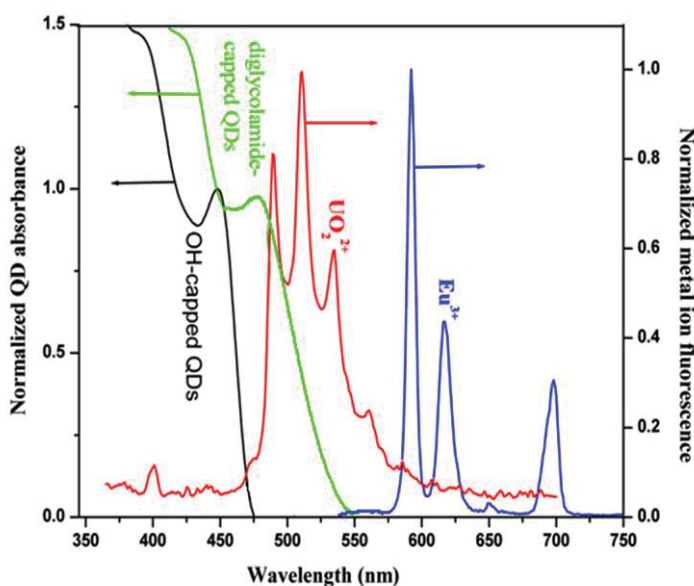


Figure 4.5. Normalized absorption spectra of the OH- and diglycolamide-capped CdS/ZnS QDs and emission spectra of UO_2^{2+} ($\lambda_{\text{ex}} = 355 \text{ nm}$) and Eu^{3+} ($\lambda_{\text{ex}} = 395 \text{ nm}$) ions in solution.

The X-ray photoelectron spectroscopic (XPS) measurements of OH-capped and diglycolamide-capped CdS/ZnS QDs were carried out by depositing them on carbon tape, mounted on a 1 cm x 1 cm glass plate. These measurements were carried out to obtain the elemental composition and nature of capping the QDs. The XPS spectra of both QD systems are given in **Figure 4.6**. In **Figure 4.6a** the two strong peaks at 410.9 eV (Cd 3d_{3/2}) and 404.2 eV (Cd 3d_{5/2}), separated by a binding energy interval of 6.7 eV, correspond to the Cd (3d) transitions in CdS [140]. Similarly the two peaks at 1043.9 eV (Zn 2p_{1/2}) and 1020.8 eV (Zn 2p_{3/2}), separated by a binding energy interval of 23.1 eV, correspond to the Zn (2p) transitions in ZnS [140]. The S 2p peaks (**Figure 4.6a**) found at 163.4 eV and 162.2 eV are due to the inner sulfide (S²⁻) of CdS/ZnS and surface S²⁻ of Zn-S_{thiol} bond respectively [140]. This confirms the thiol capping of the QDs via Zn-S_{thiol} bonding. The O (1s) peak at 530.2 eV is of the capping agent (MPE) on the QD surface. The XPS spectrum of diglycolamide-capped CdS/ZnS QDs (**Figure 4.6b**) shows the Si 2p peak at 102.5 eV in addition to the O (1s) and N (1s) peaks [140]. The silanization and aggregation of the nanoparticles restricts the complete elemental mapping in diglycolamide-capped CdS/ZnS QDs.

4.1.3. Procedure for fluorometric detection of UO₂²⁺ ion

The insolubility of the QD nanosensor in water restricts its direct application in environmental water samples. But in order to generate calibration curve for U detection through QD nanosensor assisted CPE, very small volumes of aqueous concentrated UO₂²⁺ solution were added to the synthesized QD nanosensor solution in acetonitrile (CAN). 2 mL diglycolamide-capped QD solution in ACN was taken in a quartz cuvette in which 10 µL of different UO₂²⁺ ion stock solutions in 1 mol L⁻¹ HNO₃ having varying U concentrations were added at room temperature. The

concentrations of UO_2^{2+} in stock solutions were maintained in such a way that its concentration varies from 1 to 150 ng mL^{-1} in the total volume of the cuvette. A 355 nm excitation wavelength (λ_{ex}) was used to excite the QDs and the fluorescence spectra were recorded after 10 min of addition.

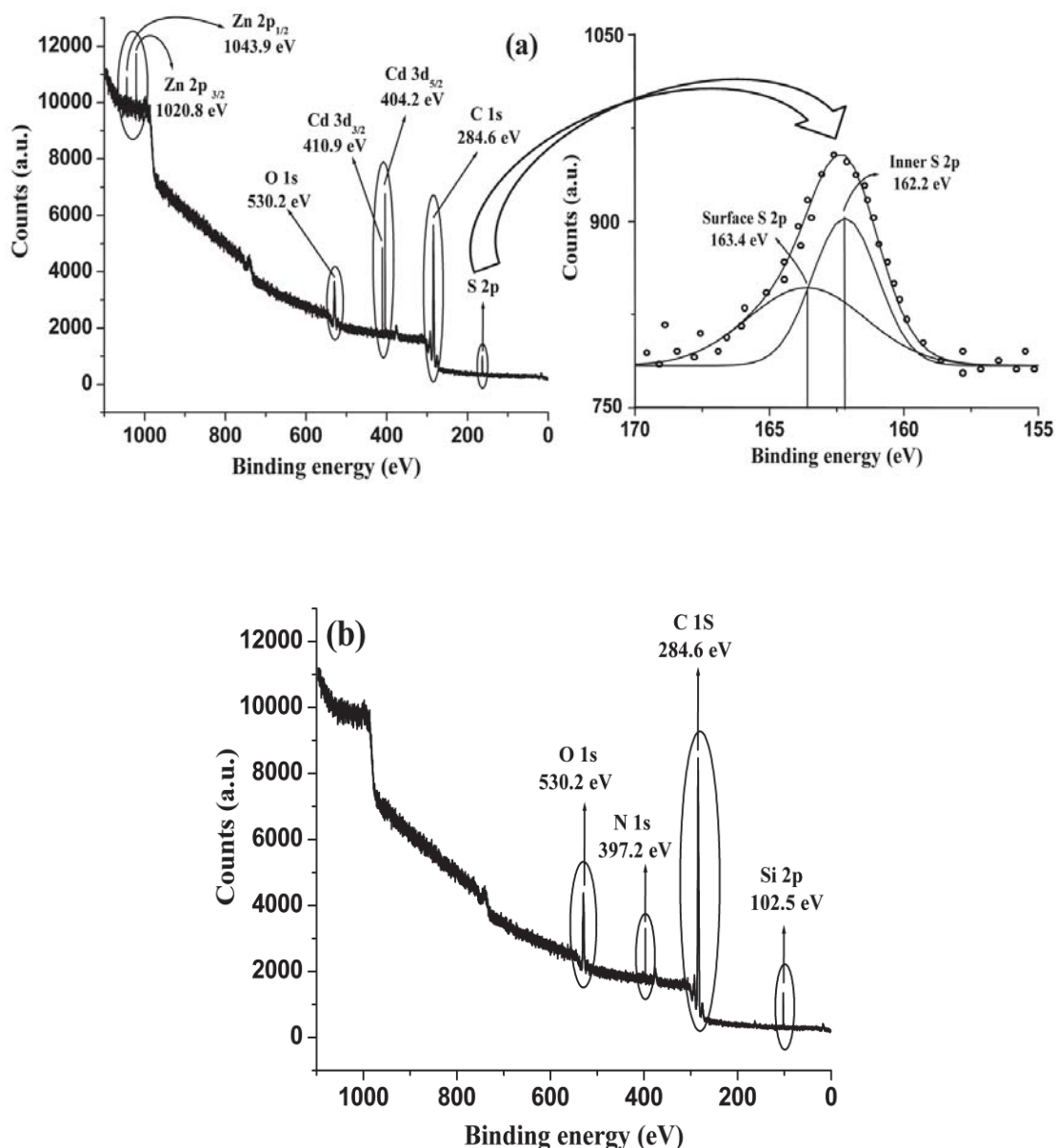


Figure 4.6. (a) Survey scan XPS spectrum of OH-capped CdS/ZnS QDs along and its high-resolution XPS spectrum for 2p level of S. (b) Survey scan XPS spectrum of diglycolamide-capped CdS/ZnS QDs.

4.1.4. Cloud point extraction procedure

The aqueous sample was first filtered through WhatmanTM filter paper 541 to get a clear solution. To carry out the CPE, 40 mL of this solution was filtered through 0.2 μm PTFE membrane fitted syringe filter and quantitatively transferred to a 50 mL graduated glass centrifuge tube. Then the pH of the solution was adjusted at 6 by adding dilute HNO_3 or NaOH . 2.5 mL of phosphate buffer of pH 6 and 0.25 g of KNO_3 (0.1mol L^{-1}) were added into it. Afterwards 2 mL of QD solution in ACN was dried under reduced pressure and the residue along with 0.21 g of 1-butyl-3-methylimidazolium bis(trifluoromethylsulfonyl)imide ($\text{C}_4\text{mimNTf}_2$, 10 mmol L^{-1}) was dispersed in 2.5 mL of 60 mmol L^{-1} TTX-114 solution. The mixture was then added to the sample solution. The volume was made up to 50 mL and the mixture was kept in an ice bath at $5\text{--}6\text{ }^\circ\text{C}$ for 30 min with constant stirring. The solution was then brought into room temperature of $26\pm 1\text{ }^\circ\text{C}$ and kept for 30 min. The phase separation occurs and due to high viscosity the surfactant rich phase settles down at the bottom. The same 2.5 mL mixture of QD nanosensor and $\text{C}_4\text{mimNTf}_2$ in 60 mmol L^{-1} TTX-114 solution was again added to the sample and the above process was repeated. Complete phase separation was achieved by centrifuging the biphasic system at 4000 rpm for 5 min. The upper aqueous layer was pipetted out and the surfactant rich phase (SRP) was diluted with ACN to 4 mL for fluorescence measurement. A pictorial representation of the complete CPE procedure is given in **Figure 4.7**.

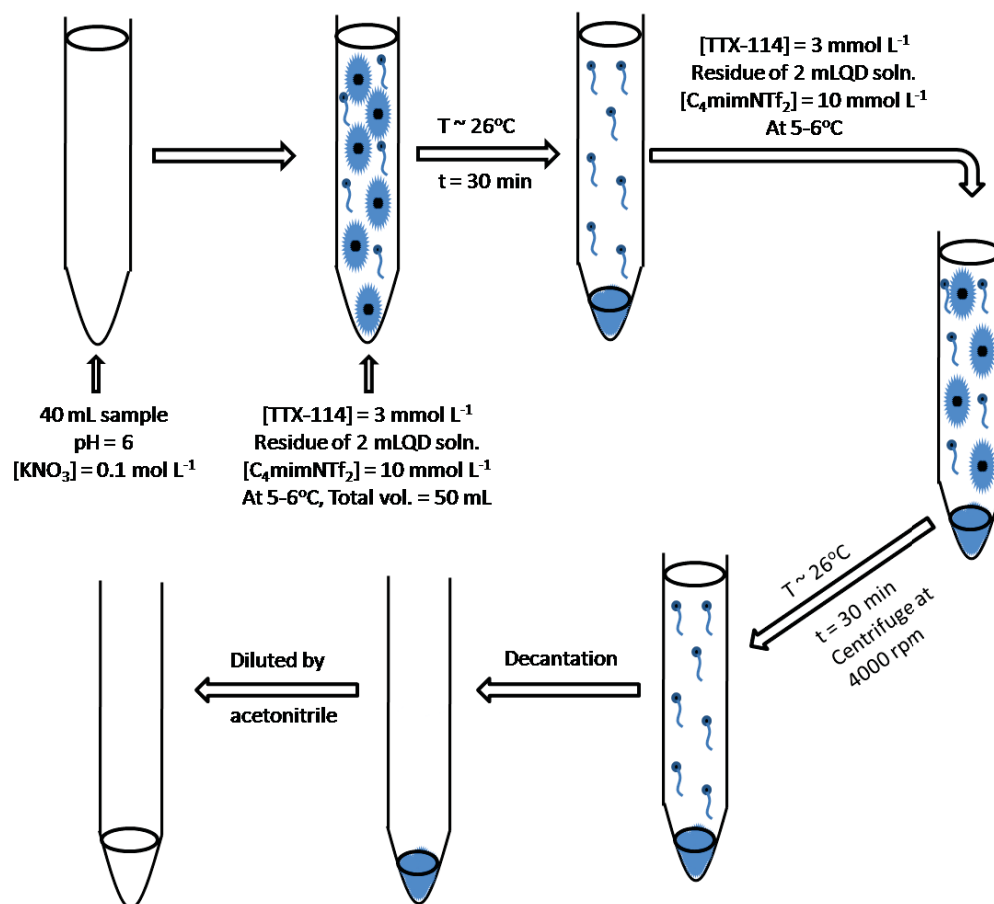


Figure 4.7. Pictorial representation of CPE procedure

4.1.5. Proposed interaction mechanism between UO₂²⁺ ion and QD nanosensor

It is well reported in the literature that diglycolamides extract UO₂²⁺ ions as 1:1 metal/ligand complex from high acidic medium and as 1:2 metal/ligand complex from low acidic medium into the organic phase [114,141-144], as shown in **Figure 4.8**. Hence, this moiety was attached to the QDs to synthesize the UO₂²⁺-specific nanosensor. Equilibration of UO₂²⁺ ions with diglycolamide-capped CdS/ZnS QDs for 30 min was found to increase the QD emission intensity and the increased emission was found to be constant for a long period. This observation is represented in **Figure 4.9**. The increase in QD emission intensity in presence of UO₂²⁺ ions could be explained in terms of direct Föster Resonance Energy Transfer (FRET) interaction between the QD and UO₂²⁺ ion, as shown in **Figure 4.8**. The FRET mechanism

(**Figure 4.8**) will be operative only between UO_2^{2+} (donor) and the QD (acceptor) when the fluorescence emission spectrum of UO_2^{2+} overlaps with the first exciton of the QD's absorption spectrum, as shown in **Figure 4.5**. Thus the selection of QD was made in such a way that its first exciton absorption band overlaps only with the emission spectra of UO_2^{2+} and does not overlap with the same of other metal ions which can easily bind to the diglycolamide group. The calculated length of dioctyldiglycolamic acid amide (obtained by using Gauss View 3.09 software, Gaussian, Inc., Pittsburg) was found to be ~ 1.6 nm which ensures efficient energy transfer between UO_2^{2+} ions (donor) and CdS/ZnS QDs (acceptor). This finding was also in favor of the FRET mechanism which can be operative only over short distances between the donor and acceptor, typically 1-10 nm. Thus the purpose of the diglycolamide group is just to hold the metal ion near to the QD so that energy transfer can take place. It can be seen from **Figure 4.5** that the attachment of diglycolamide group over the CdS/ZnS core-shell QD surface modified its absorption spectrum appropriate to our application. The ZnS shell growth onto CdS core was done to decrease the hole trapping by negatively charged thiolate groups bound on the surface of the QDs which otherwise would lead to complete quenching of the fluorescence intensity of the CdS QD [104]. The silanization of the QDs was done to restrict non-specific binding of UO_2^{2+} ion onto QD surface [104]. When OH-capped and amino-silanized CdS/ZnS QD solutions were separately exposed to UO_2^{2+} ion, an increase in emission intensity of both QD solutions was observed. After 5 min the resulting emission intensity of OH-capped CdS/ZnS QDs dropped to $\sim 70\%$ of its value whereas the emission intensity of amino-silanized QDs remained constant even after 1 hr. These observations are shown in **Figure 4.10 and 4.11** respectively. The small overlap between the absorption spectrum of OH-capped QD and the

fluorescence spectrum of UO_2^{2+} (Figure 4.3), resulted in its initial emission intensity enhancement but the nonradiative electron/hole recombination between them brought it down. Therefore, the silica shell became necessary to avoid any measurement complications.

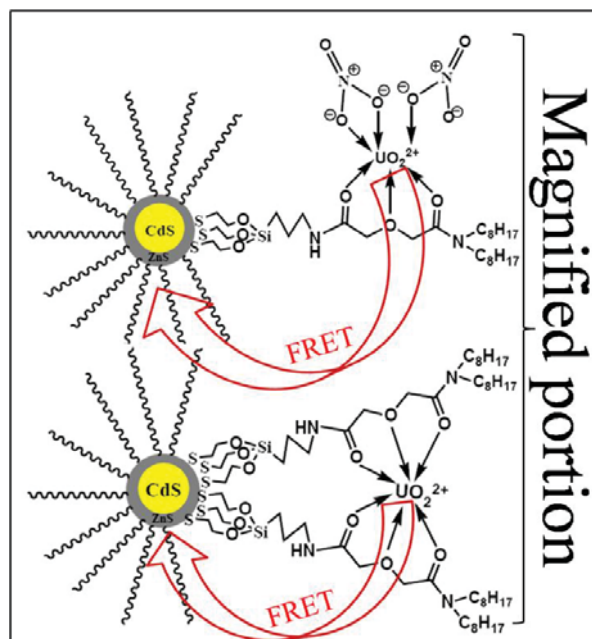


Figure 4.8. Proposed FRET interaction between UO_2^{2+} ion and QD.

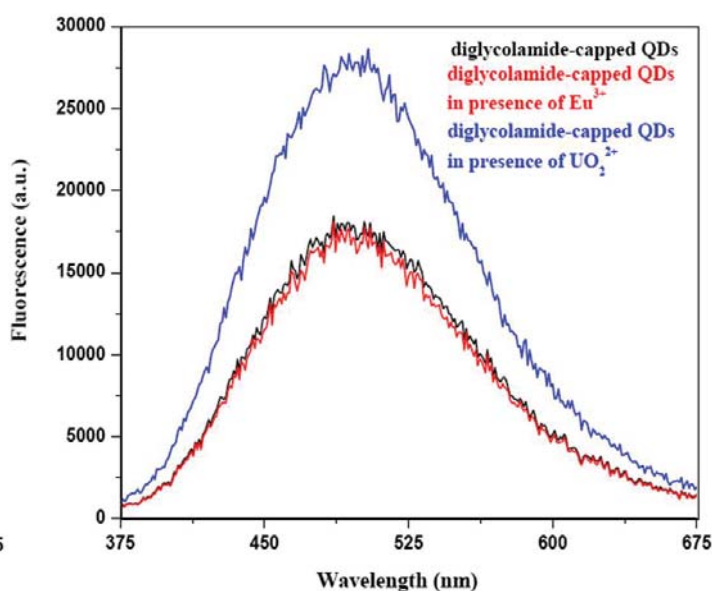


Figure 4.9. Emission spectra of diglycolamide-capped CdS/ZnS QDs ($\lambda_{ex} = 355 \text{ nm}$) solution before and after addition of UO_2^{2+} and Eu^{3+} .

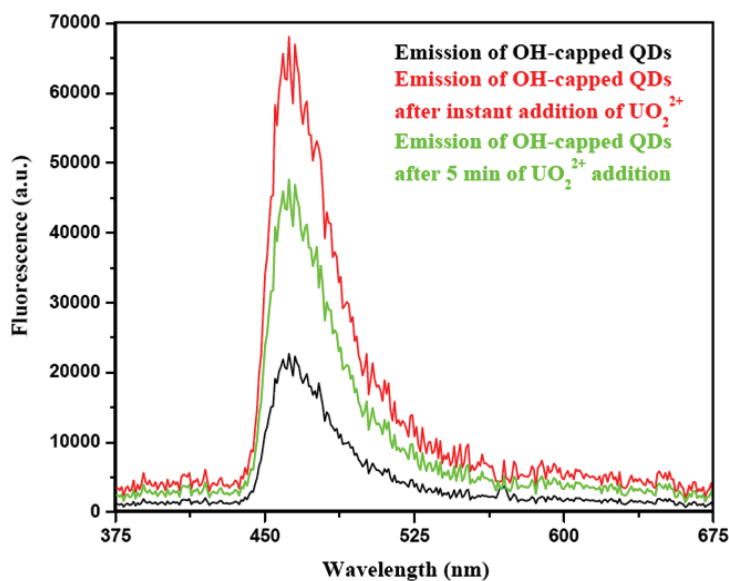


Figure 4.10. Change of fluorescence intensity when UO_2^{2+} was added to OH-capped CdS/ZnS QDs solution.

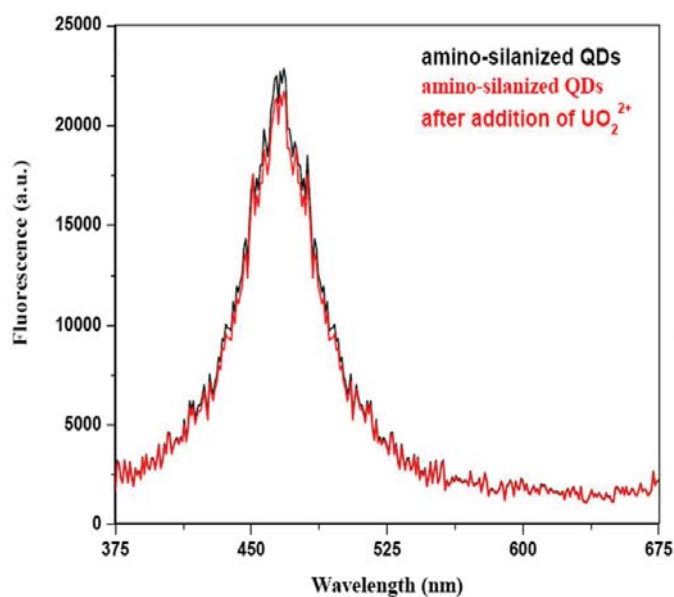


Figure 4.11. Emission spectra of amino-silanized CdS/ZnS QDs ($\lambda_{\text{ex}} = 355 \text{ nm}$) before and after addition of UO_2^{2+} .

The gradual addition of more and more UO_2^{2+} ions to diglycolamide-capped CdS/ZnS QDs for 30 min equilibration was found to gradually increase the QD fluorescence intensity. The observations are presented in **Figure 4.12a**. The increase in integrated emission intensity ($F-F_0$) [where F_0 and F are the integrated emission intensities of

diglycolamide-capped CdS/ZnS QDs without and with the addition of UO_2^{2+} respectively] was plotted against UO_2^{2+} ion concentration in **Figure 4.12b**. The intensity was found to increase linearly in the concentration range of 10 to 100 ng mL^{-1} (**Figure 4.12b inset**). The time dependent fluorescence intensity of the QD in presence of varying concentrations of metal ions is represented in **Figure 4.13**. The higher reaction rate was found to be associated with higher ion concentration (**Figure 4.13**). Even for the maximum added concentration of UO_2^{2+} saturation was reached in ~ 8.5 min and no further decrease in fluorescence intensity was observed. Therefore, 10 min equilibration time was fixed for all the fluorescence intensity measurements. A detectable change in QD fluorescence intensity was found for minimum UO_2^{2+} concentration of 0.3 ng mL^{-1} . The 3σ of the blank value (i.e., integrated emission intensity of the nanosensor without uranium) was used to determine this detection limit (DL) value using the slope of the straight line equation ($\text{DL} = 3\sigma/\text{slope}$, **Figure 4.12b inset**).

4.1.6. Validation of the proposed FRET mechanism and selectivity test

The increase in QD emission intensity in presence of UO_2^{2+} ions is expected due to direct FRET between the two fluorophores. However the fluorescence enhancement can also occur due to the disaggregation of aggregated diglycolamide-capped CdS/ZnS QDs, which is evident from its TEM image (**Figure 4.3**) and broad emission spectrum. Attachment of metal ions with ligands on the QD surface may increase the overall hydrophilic nature of the QD and this can lead its disaggregation-based fluorescence enhancement. Two independent methods were opted to investigate

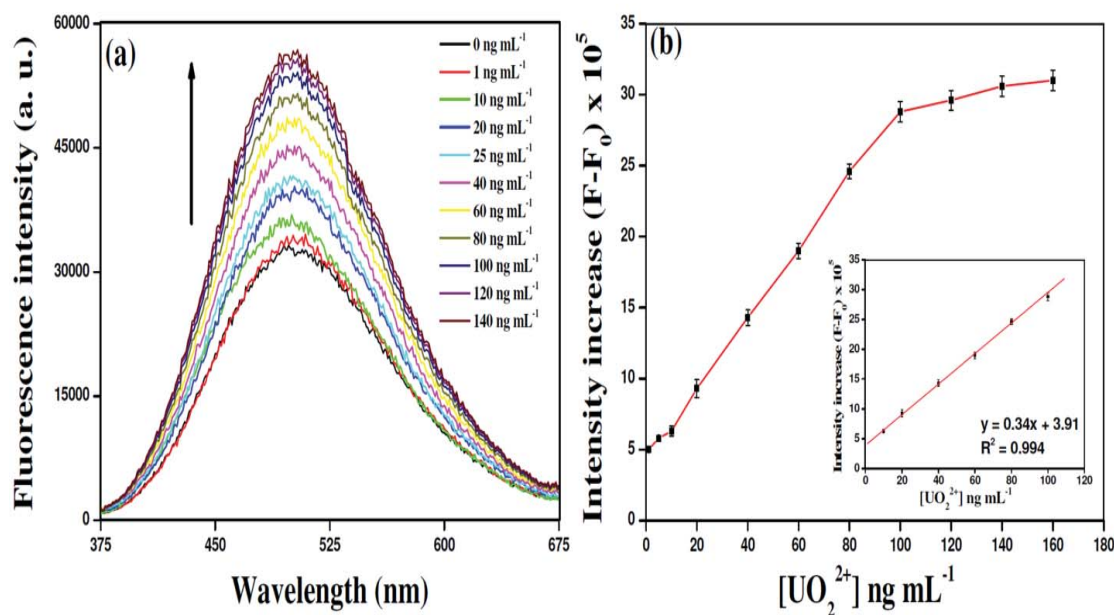


Figure 4.12. (a) Increase in fluorescence intensity of diglycolamide-capped CdS/ZnS QDs ($\lambda_{\text{ex}} = 355 \text{ nm}$) with gradual increase in added UO_2^{2+} concentration. (b) Increase in integrated emission intensity $(F-F_0)$ was plotted as a function of UO_2^{2+} concentration. Inset: calibration plot of $(F-F_0)$ vs, concentration of UO_2^{2+} .

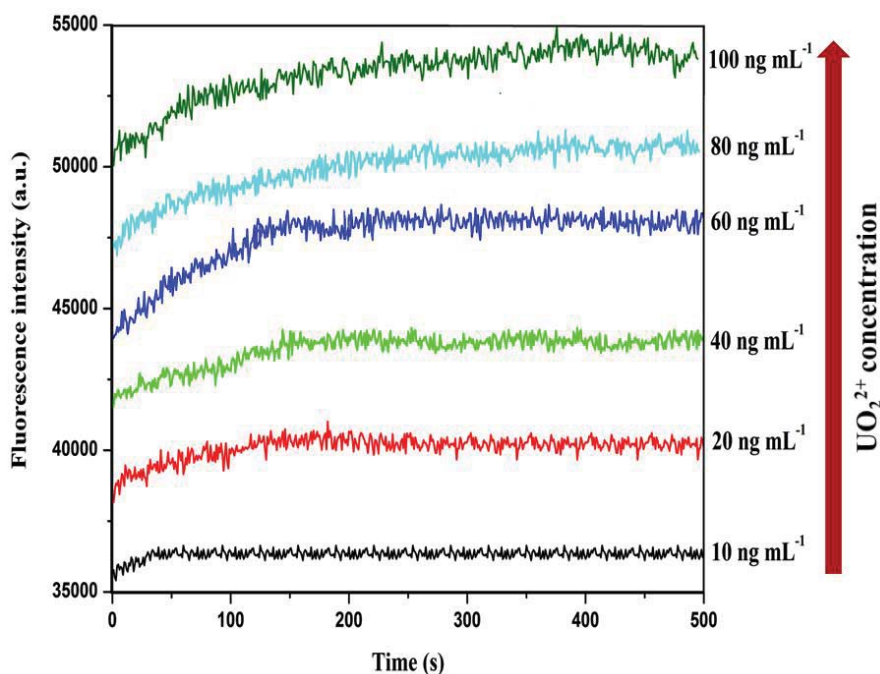


Figure 4.13. Time dependent fluorescence intensity (recorded at 495 nm) of diglycolamide-capped CdS/ZnS QDs ($\lambda_{\text{ex}} = 355 \text{ nm}$) in presence of different concentrations of UO_2^{2+} .

the actual fluorescence enhancement mechanism. Firstly, we had equilibrated the diglycolamide-capped CdS/ZnS QDs with Eu^{3+} ions in solution under the same conditions as maintained in case of UO_2^{2+} ions in solution. Since diglycolamides are known to form stronger complexes with trivalent lanthanides [114,142,143], it is expected that the QD nanosensor will show emission intensity enhancement in presence of Eu^{3+} ions as well only if disaggregation-based fluorescence enhancement mechanism prevails. No change was observed in the emission intensity of the QD nanosensor even after 30 min equilibration with Eu^{3+} ions as shown in **Figure 4.10**. This experiment indirectly corroborates the FRET mechanism between UO_2^{2+} ions and QDs. Since the emission spectrum of Eu^{3+} ions in solution does not have any overlap with the absorption spectrum of diglycolamide-capped CdS/ZnS QDs (**Figure 4.5**), there will not be any energy transfer between Eu^{3+} and QD even though they are within the Förster distance. Time-resolved fluorescence measurements of the diglycolamide-capped CdS/ZnS QDs before and after addition of UO_2^{2+} ions was also carried out to provide a direct evidence of energy transfer mechanism. The time-resolved fluorescence spectra were recorded at 495 nm ($\lambda_{\text{ex}} = 355$ nm) and results are shown in **Figure 4.14**. Typical average fluorescence lifetime (τ) of the diglycolamide-capped QDs was determined to be 1.25 ns. The τ values were found to increase to 1.49 and 2.16 ns upon addition of 20 and 100 ng mL⁻¹ of UO_2^{2+} ions respectively. The increase in fluorescence lifetime of the QD is a direct confirmation of the proposed FRET mechanism.

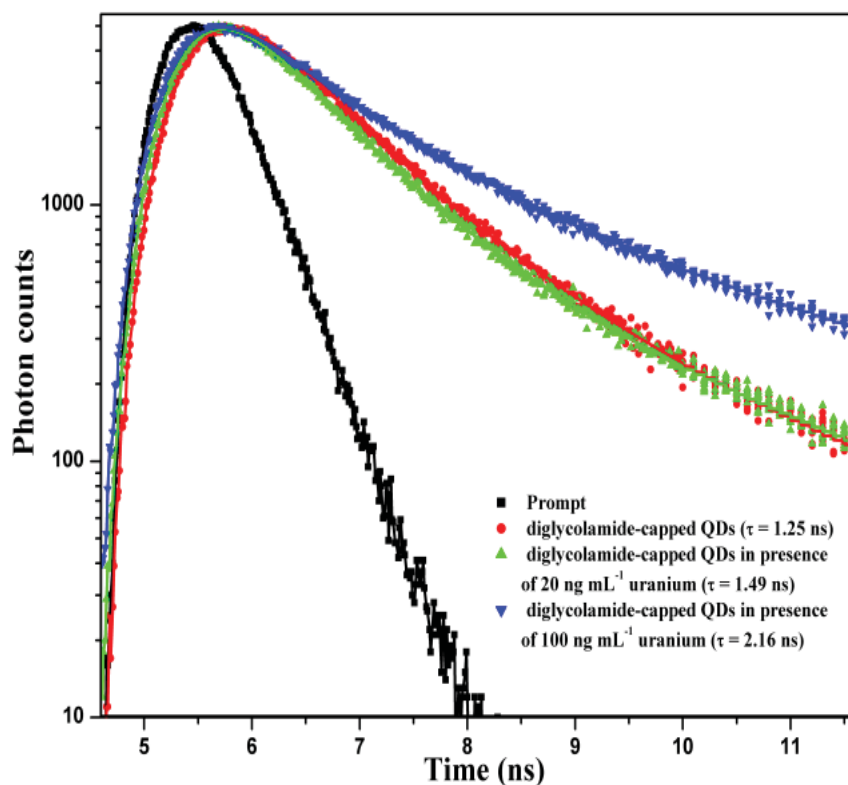


Figure 4.14. Time-resolved fluorescence measurements of the diglycolamide-capped CdS/ZnS QDs, recorded at 495 nm before and after adding UO_2^{2+} ions ($\lambda_{\text{ex}} = 355 \text{ nm}$).

4.1.7. Optimization of the CPE procedure

Fluorometric detection of ultratrace levels of U in environmental aqueous samples was carried out by dispersing the QD nanosensors into the sample solution with the help of TTX-114 micelles. This allowed the interaction between QD and UO_2^{2+} ions at the micellar corona and resulted in extraction of U in the surfactant rich phase (SRP) via CPE procedure. The optimized CPE conditions for quantitative extraction efficiency (EE) and recovery of U were obtained through cross-optimization of all the parameters and are presented in **Table 4.1**.

Table 4.1. *Optimized parameters for the developed CPE procedure before coacervation*
(Total volume = 50 mL)

| Parameters | Conditions | Units |
|---------------------------------------|------------|----------------------|
| Sample volume | 40 | mL |
| pH | 6.0 | --- |
| [TTX-114] | 2.5 | mmol L ⁻¹ |
| [C ₄ mimNTf ₂] | 0.5 | mmol L ⁻¹ |
| [KNO ₃] | 0.1 | mol L ⁻¹ |
| T _{extraction} | 5-6 | (°C) |
| t _{extraction} | 30 | (min) |
| T _{phase separation} | 26 | (°C) |
| t _{phase separation} | 30 | (min) |
| Centrifugation | 4000 | rpm |

Note: Concentrations presented are for total
50 mL volume (aqueous phase prior to
surfactant rich phase separation)

The recovery studies of U by the CPE process were carried out in the pH range of 1-10 and the observations are presented in **Figure 4.15a**. The recovery of U was found to be very low in acidic pH region (pH 1-3) which then increased upto pH 6 and subsequently decreased in the alkaline region. Optimum recovery of $\geq 98\%$ was obtained at pH 6. The higher critical micelle concentration (CMC) and hydrated volume of micelles and competition between H^+ and UO_2^{2+} to get extracted are the main reason for low U recovery at lower pH values [145]. The higher CMC requires more surfactant to accommodate maximum metal complex and higher hydrated volume diminishes the total number of potential coordinating groups via H-bonding. With increase in pH all these three factors get suppressed more and more, resulting higher U recovery. The decrease in recoveries above pH 6 is due to the dominance of non-extractable hydroxide, carbonate and/or bicarbonate complexes of U at these pH values. Therefore, a pH value of 6 was selected as the optimum one.

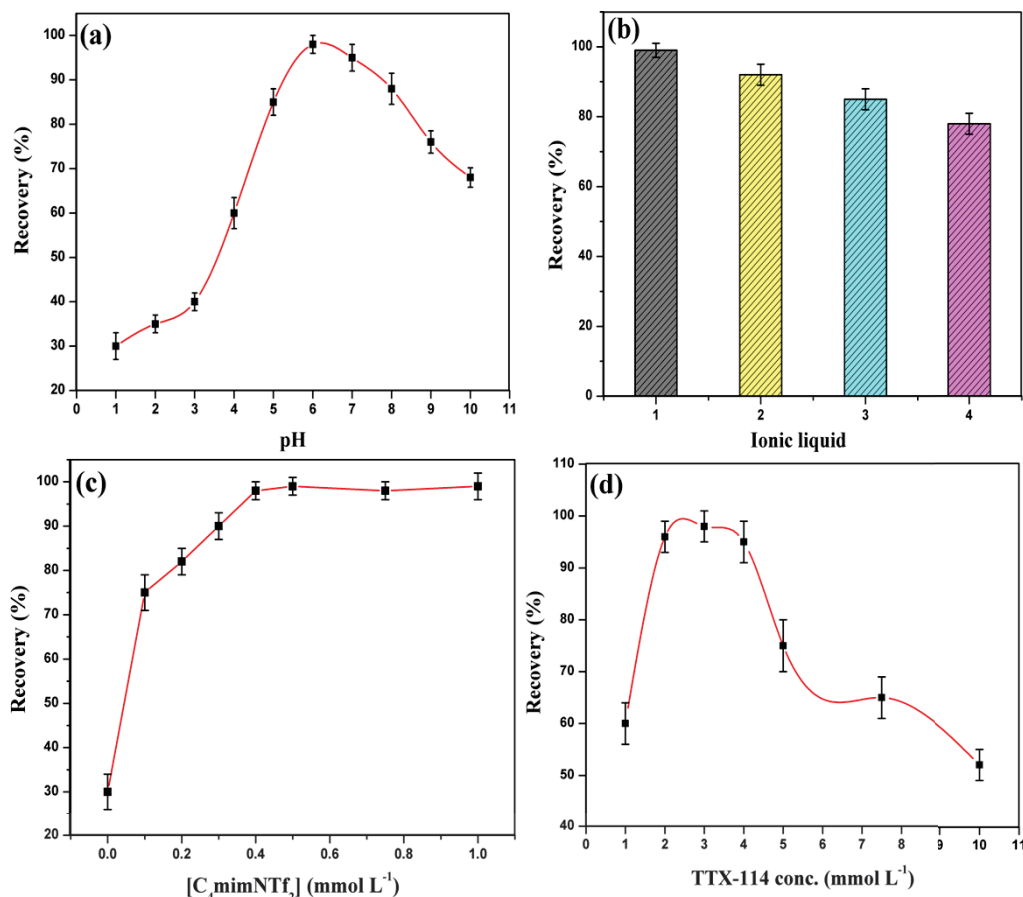


Figure 4.15. (a) Effect of pH; (b) effect of $\text{C}_4\text{mimNTf}_2$ concentration; (c) effect of different types of IL viz., $\text{C}_4\text{mimNTf}_2$ (1), $\text{C}_6\text{mimNTf}_2$ (2), $\text{C}_8\text{mimNTf}_2$ (3) and $\text{C}_{10}\text{mimNTf}_2$ (4) and (d) effect of non-ionic surfactant concentration on the percentage recovery of UO_2^{2+} when the CPE is carried out with keeping all other parameters constant as per Table 4.1.

The QD nanosensor was used as both extract and fluorophore in the CPE based fluorometric detection of U. Since 2 mL of the synthesized QD nanosensor solution was used to obtain the calibration plot, the same 2 mL volume of the nanosensor was dried under reduced pressure and dispersed in the micelle to carry out the CPE procedure. The TEM micrographs of the 2.5 mmol L^{-1} TTX-114 solution with and without the QD nanosensors are shown in **Figure 4.16**. The increase in average micelle size from $\sim 30 \text{ nm}$ to $\sim 100 \text{ nm}$ revealed the inclusion of these QDs into the hydrophobic core. The complete preconcentration procedure involves a dual CPE

mode and each time the 2 mL QD solution was treated and used as described above. Finally, the surfactant rich phase (SRP) phase was diluted to 4 mL in order to maintain the QD concentration same as in its synthesized solution.

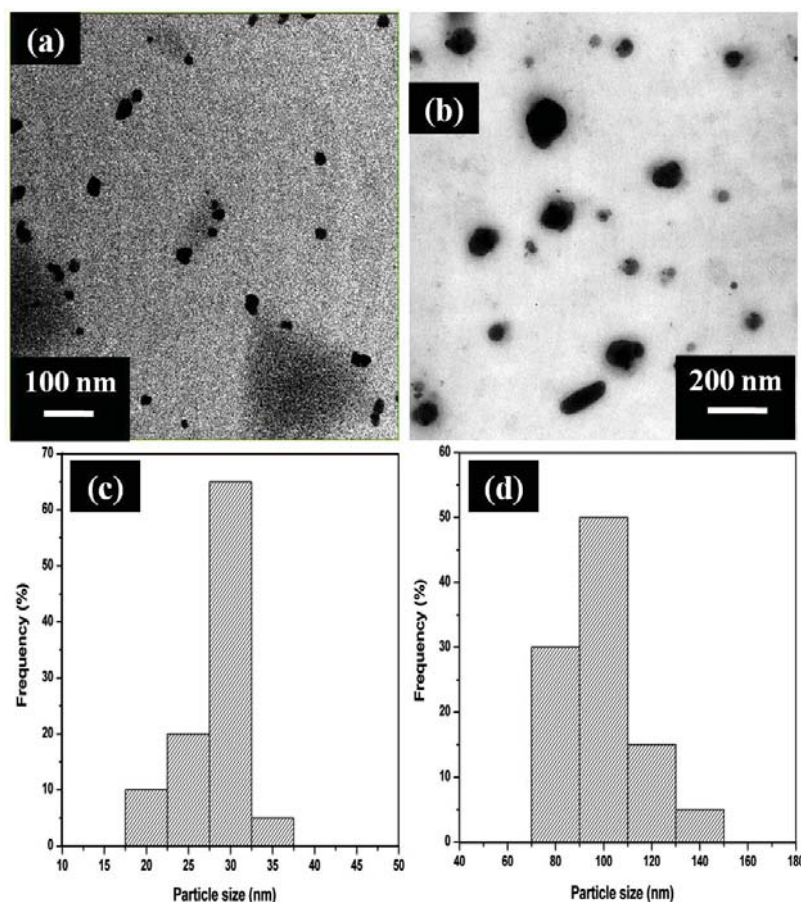


Figure 4.16. TEM micrographs and corresponding size distributions of (a,c) 2.5 mmol L^{-1} TTX-114 solution and (b,d) 2.5 mmol L^{-1} TTX-114 in presence of diglycolamide-capped CdS/ZnS QDs.

The addition of a hydrophobic IL in the micelle system is expected to increase the recovery values, because diglycolamides are known to extract UO_2^{2+} ion from low nitric acid medium into the ionic liquid (IL) phase by cation exchange mechanism [143,144]. The extracted species being $\text{UO}_2(\text{L})_2^{2+}$, as shown in **Fig. 4.8**. Such an extraction mechanism does not depend upon the availability of nitrate ions in the

aqueous phase and is best suitable in procedures like CPE which operates typically in the pH region. To act as an efficient modifier in the CPE process, the IL should possess sufficient alkyl or aryl group in its cationic part which can cause its maximum penetration in the micelle and at the same time it should be sufficient to allow the cation exchange mechanism by solubilizing in water [91]. 1-alkyl-3-methylimidazolium ($C_n\text{mim}$) ILs with various chain lengths ($n = 4, 6, 8$ and 10) but same counter anion viz., bis(trifluoromethanesulfonyl)imide(NTf_2^-): $C_4\text{mimNTf}_2$, $C_6\text{mimNTf}_2$, $C_8\text{mimNTf}_2$ and $C_{10}\text{mimNTf}_2$ were examined individually to obtain the maximum recovery of uranium (**Figure 4.14b**). Among the various ILs examined $C_4\text{mimNTf}_2$ was observed to provide the maximum recovery of uranium (**Figure 4.14b**). Therefore, we had added different concentrations of $C_4\text{mimNTf}_2$ to our CPE system in order to get maximum recovery (%) of uranium (**Figure 4.14c**). The recovery studies of U in absence and presence of a hydrophobic ionic liquid (IL) is shown in **Figure 4.15c**. The low recovery (%) of U in the CPE by diglycolamide-capped CdS/ZnS QDs in absence of a hydrophobic IL is expected to be due to low concentration of the extractable neutral $\text{UO}_2(\text{NO}_3)_2(\text{L})$ ($\text{L} = \text{diglycolamide}$) species (**Figure 4.8**). Optimum percentage recoveries were found to be obtained in the range of 0.4 to 1.0 mmol L^{-1} concentrations of the IL. Accordingly 0.5 mmol L^{-1} of $C_4\text{mimNTf}_2$ was added to the CPE system. The inclusion of the IL into the TTX-114 micelles was confirmed by measuring the zeta potential (ζ) of the aggregates formed by TTX-114 and QD nanosensor in absence and presence of $C_4\text{mimNTf}_2$. The ζ values of the micelles in absence and presence of IL were found to be -26 ± 3 and $-48 \pm 5 \text{ mV}$ respectively. The more negative ζ value in presence of IL confirmed its penetration ions inside the micelles.

In our previous work (section 3.5.5 of chapter 3) we had experienced that the presence of an electrolyte in the micelle medium is indispensable to control the system CPT. Though here the UO_2^{2+} extraction mechanism does not depend upon NO_3^- ion concentration, but the salting-out effect of the electrolyte is very important to achieve maximum recovery of analytes. Hence we employed 0.1 mol L^{-1} of KNO_3 in each of our experiment and the same concentration was found to be sufficient for maximum analyte recovery.

The concentration of the surfactant viz., TTX-114 was also optimized for the highest possible recovery of U. The variation of recovery for the concentration range of 0.5 to 5 mmol L^{-1} of TTX-114 is shown in **Figure 4.15d**. Optimal recoveries were obtained for $2\text{-}4 \text{ mmol L}^{-1}$ TTX-114. The decrease in recovery on further increase in TTX-114 concentration is due to the higher density of the surfactant which affects the emission intensity. The cloud point temperature of the system $25 \pm 1 \text{ }^\circ\text{C}$ was determined by increasing and decreasing the temperature by $1 \text{ }^\circ\text{C}$ after every 10 min . Since the complexation of diglycolamide with metal ions is known to be an exothermic reaction [114,142-145], the extraction was carried out at $5\text{-}6 \text{ }^\circ\text{C}$ and the phase separation at $26 \pm 1 \text{ }^\circ\text{C}$. The reported recovery of uranium at any particular condition was determined by using the integrated emission intensity ($F - F_0$) value i.e., fluorescent intensity of QD in presence (F) and in absence (F_0) of uranium at that particular point. The Q.Y. of the QD at every experimental condition was determined from the F_0 value and measuring the absorbance value of the corresponding exciton peak (355 nm). The Q.Y. of the QD at every point was found to be $\sim 5\%$ which is similar to the Q.Y. of the synthesized pure QD. This clearly confirms the photostability of QD under different experimental conditions. Hence, the variation in the recovery of U at

various CPE conditions is purely due to the different extent of uranium extraction. With the help of the calibration plot in **Figure 4.11b** (inset) the preconcentration procedure can quantify uranium from 1.0 to 100 ng mL⁻¹ in aqueous samples. The DL value of the methodology is 0.03 ng mL⁻¹.

4.1.8. Effect of common interfering ions on the U recovery

A list of the interfering ions and their maximum tolerance limits towards the recovery of 10 ng mL⁻¹ of U by $\geq 95\%$ is tabulated in **Table 4.2**. The various reasons behind choosing all these foreign ions have been previously discussed in **section 3.8** of **chapter 3**. This developed methodology was found to tolerate high concentrations of alkali, alkaline earth and transition metal ions without affecting the recovery of U. Since some metal ions like Ca²⁺, Sr²⁺, Ba²⁺, Cr³⁺ and Pb²⁺ can complex with diglycolamides and these metals ions were in higher concentration compared to U, the CPE of U got hampered in their presence. So in order to mask these ions 1.0 mmol L⁻¹ ethylenediaminetetraacetic acid (EDTA) was used. It had been investigated that the presence of EDTA did not affect the CPE of U whereas can preferentially mask these foreign metal ions. This is because EDTA is known to form very stable complexes with these interfering metal ions but not with uranium [146]. The UO₂²⁺-specificity of the QD nanosensor because of the energy transfer mechanism and the dual CPE mode, results in increased tolerance ratio for lanthanides ($\text{Ln}^{n+}/\text{UO}_2^{2+} = 1000/10 = 100$) compared to our previous work in **chapter 3** ($\text{Ln}^{n+}/\text{UO}_2^{2+} = 2$). Due to the low concentrations of Zr⁴⁺, Hf⁴⁺ and Th⁴⁺ in natural water, their effect was studied upto 100 ng mL⁻¹. The results showed no effect of these elements on the analyte recovery.

Table 4.2. Tolerance of the method to foreign metal ions (experiments carried out with 10 ng mL⁻¹ of U)

| Foreign metal ion (M ⁿ⁺) | Tolerance limit (µg mL ⁻¹) |
|---|---|
| Li ⁺ , Na ⁺ , K ⁺ | 10000 |
| Mg ²⁺ | 1500 |
| Ca ²⁺ , Sr ²⁺ , Ba ²⁺ | 500 ^a |
| Cu ²⁺ , Ni ²⁺ , Zn ²⁺ | 200 |
| Co ²⁺ , Mn ²⁺ | 200 |
| Al ³⁺ | 100 |
| Fe ³⁺ | 50 |
| Cr ³⁺ | 50 ^a |
| Cd ²⁺ | 200 ^a |
| Pb ²⁺ | 50 ^a |
| Hg ²⁺ | 0.2 |
| La ³⁺ , Ce ⁴⁺ , Eu ³⁺ | 1.0 |
| Zr ⁴⁺ , Hf ⁴⁺ , Th ⁴⁺ | 0.1 |
| PO ₄ ³⁻ , SO ₄ ²⁻ , CO ₃ ²⁻ | 2000 |
| Cl ⁻ , Br ⁻ | 10000 |

Note: Cations were prepared using their chloride or nitrate salts. Anions were prepared using their sodium or potassium salts. ^aSolution spiked with 1.0 mmol L⁻¹ EDTA

4.1.9. Analytical figures of merit

The wide dynamic linear concentration range (DLR) of 1.0-100 ng mL⁻¹, low DL of 0.03 ng mL⁻¹, fluorometric detection specificity towards UO₂²⁺ and selectivity of the overall methodology, make this technique a simple alternative to the costly instrumental analysis. A comparison of the previously reported cost effective analytical techniques on ultratrace level detection of U with our developed technique is represented in **Table 4.3**. It was found that the present work provides much better DLR and DL values of U than all other reported ones [40,54,76,77,90,95-97,147,148]. The EE and preconcentration factor (PF) values of the method were determined to be 99.0±1.0% and 100 respectively.

Table 4.3. Comparison of analytical performance of the developed method with the previously published other analytical methods for low level detection of U

| Brief description of the method | Instrument | DLR (ng mL ⁻¹) | DL (ng mL ⁻¹) | Ref. |
|-------------------------------------|-------------|-------------------------------|------------------------------|-------|
| Present work | Fluorometer | 1.0-100 | 0.03 | --- |
| PAN assisted CPE | UV-Vis | N.P. | 1.1 | [95] |
| DBM assisted CPE | UV-Vis | 15-300 | 11 | [96] |
| PCV assisted CPE | UV-Vis | 0.18-10 | 0.06 | [90] |
| ARS assisted CPE | UV-Vis | 6-10 | 2 | [97] |
| SPE with malonamide grafted polymer | UV-Vis | N.P. | 20 | [147] |
| SPE with CACP | UV-Vis | 100-15000 | 6.14 | [76] |
| SPE with modified activated carbon | UV-Vis | 5-200 | 5 | [54] |
| Modified ODS disk | UV-Vis | N.P. | 0.1 | [77] |
| Amine-modified CdS QDs | Fluorometer | 0.231-10 | 0.07 | [30] |
| APA-modified gold nanoparticle | SERS | 200-2000 | 200 | [148] |

Note: SPE = Solid phase extraction; PAN = 1-(2-Pyridylazo)-2-Naphthol; DBM = Dibenzoylmethane; PCV = Pyrocatechol Violet; ARS = Red arsenazo S; CACP = Calix[4]arene anchored chloromethylated polystyrene; APA = (Aminomethyl)phosphonic acid; SERS = Surface Enhanced Raman Spectroscopy.

4.1.10. Method validation and real sample analysis

The method was validated by analyzing a certified reference material (CRM) viz., NIST SRM 1640a natural water which shows a good agreement between the certified and determined uranium values at 95% confidence level, as shown in **Table 4.4**. The developed analytical technique was employed in the determination of U concentration in three real water samples viz., sea water, ground water and river water. The robustness of the technique was further investigated by recovery study employing standard addition to these real samples. The results are shown in **Table 4.5**. The quantitative recovery ($\geq 94\%$) of the spiked amount of U gives confidence on our detection methodology.

Table 4.4. Determination of uranium in NIST SRM 1640a natural water standard (Sample volume = 5 mL; $n = 3$)

| Certified value (ng mL ⁻¹) | Analyzed value (ng mL ⁻¹) | Recovery (%) |
|---|--|-----------------|
| 25.35±0.27 | 25.1±0.6 | 99.0±2.4 |

Table 4.5. Analysis of real samples ($n=5$)

| Sample | Source | Added U conc. (ng mL ⁻¹) | Found U conc. (ng mL ⁻¹) | Recovery (%) |
|--------------|----------------------------------|---|---|-----------------|
| Sea water | Mumbai coast, India | 0 | 2.9±0.1 | - |
| | | 1.0 | 3.9±0.1 | 100±14 |
| | | 5.0 | 8.0±0.2 | 102±4 |
| Ground water | West Bengal, India | 0 | BDL | - |
| | | 1.0 | 0.95±0.05 | 95±5 |
| | | 5.0 | 4.8±0.2 | 96±4 |
| River water | Teesta canal, West Bengal, India | 0 | BDL | - |
| | | 1.0 | 0.94±0.04 | 94±4 |
| | | 5.0 | 4.9±0.2 | 98±4 |

BDL = Below detection limit

4.1.11. Conclusion

To the best of our knowledge, direct FRET interaction mechanism between QD and UO_2^{2+} ion for ultratrace level detection of U has been demonstrated for the first time. This detection technique provides a new and novel approach for simple and cost effective low level metal ion detection. With the availability of portable fluorometers, on-site and real-time environmental monitoring of U could be made feasible by the developed method.

4.2. Functionalized AuNPs in the CPE based spectrophotometric detection of U

4.2.1. Introduction

Gold NPs (AuNPs) are one of the most widely used chemical nanosensors owing to their optoelectronic properties like surface plasmon resonance (SPR) absorption, surface enhanced Raman scattering (SERS), conductivity or redox behavior which can be used for sensitive signal generation occurring at the monolayer surface [149-151]. Typically alkylthiols are used to form organic monolayer onto gold nanocore via stable Au-S bond [149-151]. AuNPs containing metal binding sites in the monolayer have emerged as a potential tool for visual or colorimetric detection of metal ions through the analyte-triggered aggregation of AuNPs. The red colour of small sized AuNPs ($d = 1-25$ nm) arising from SPR absorption, changes to blue upon size increase via analyte-triggered aggregation. In recent years, DNAzyme functionalized AuNPs were mostly used for sensitive detection of UO_2^{2+} ions in natural water systems [152,153]. The advantage of using simple organic molecules, containing metal coordinating sites, instead of DNAzymes to modify the NP surface has been discussed earlier in **section 4.1.1** of this chapter. Though our recent work on fluorometric detection of U by QD nanosensor assisted CPE is able to detect concentrations as low as 0.03 ng mL^{-1} , it cannot be applied for on-site visual detection of U in water samples. Very recently Xiao et al. [154] had reported real-time monitoring and removal of UO_2^{2+} ions from water samples employing a new photonic crystal hydrogel (PCH) material. However, the coloration pattern of PCH they presented in absence and presence of UO_2^{2+} does not show a prominent colour change in the vicinity of World Health Organization (WHO) and United States Environmental Protection Agency (USEPA) recommended guideline values of U (30 ng mL^{-1} or $0.13 \times 10^{-6} \text{ } \mu\text{mol L}^{-1}$) [34,51]. Hence with the aim of preparing a visual

detection kit for sensing ultratrace U in natural water samples around its guideline values, we had synthesized 3-mercaptopropionylamidoxime (3-MPD) functionalized AuNPs for the first time and applied it for detection of U in real water samples.

4.2.2. Synthesis and characterization of functionalized AuNPs

4.2.2.1. Synthesis scheme

A stepwise synthesis procedure of 3-MPD functionalized AuNPs is presented in **Figure 4.17**. The citrate stabilized AuNPs and 3-mercaptopropionylamidoxime (3-MPD) were first synthesized separately and then the surface modification of citrate stabilized AuNPs was done by 3-MPD to prepare 3-MPD capped AuNPs. Reduction of chloroauric acid (HAuCl_4) by sodium borohydride (NaBH_4) produces the AuNPs of required size. A five step synthesis procedure starting from 3-mercaptopropionic acid (3-MPA) was adopted to synthesize 3-MPD. In the first step 3-MPA was converted into its methyl ester. Methyl-3-mercaptopropionate was then treated with concentrated ammonia where it was converted into 3,3'-dithiopropionamide. Dehydration of 3,3'-dithiopropionamide by diethyl chlorophosphate resulted in formation of 3,3'-dithiopropionitrile. The nitrile was then reacted with hydroxylamine to generate 3,3'-dithiopropionylamidoxime which is the dimeric form of our desired compound viz., 3-MPD. The S-S bond breaking of this dimer by Zn in hydrochloric acid (HCl) medium finally gives us the desired product 3-MPD. Equilibration between the aqueous solution of 3-MPD and citrate stabilized AuNPs resulted in formation of 3-MPD capped AuNPs through Au-S bond formation.

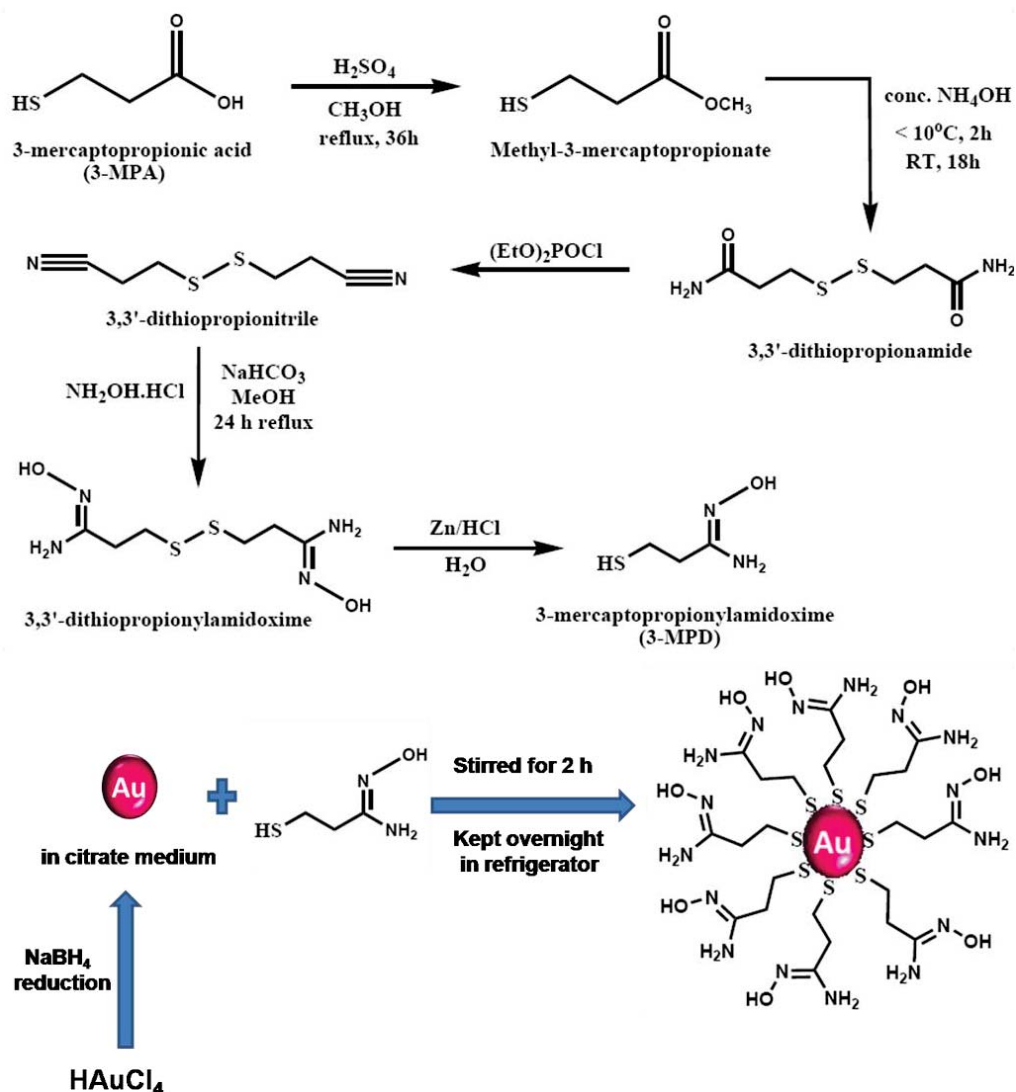


Figure 4.17. Stepwise synthesis of 3-MPD functionalized AuNPs.

4.2.2.2. IR and NMR spectroscopy

The preparation of 3-MPD in aqueous medium made its separation difficult in the pure form. Hence chemical characterization of 3,3'-dithiopropionylamidoxime is considered to be the confirmation of amidoxime synthesis. The IR spectrum of each synthesized product and ^1H NMR spectrum of 3,3'-dithiopropionylamidoxime, as shown in **Figure 4.18** and **4.19** respectively, confirmed the stepwise synthesis of the latter one. Methyl-3-mercaptopropionate was characterized by its S-H stretching

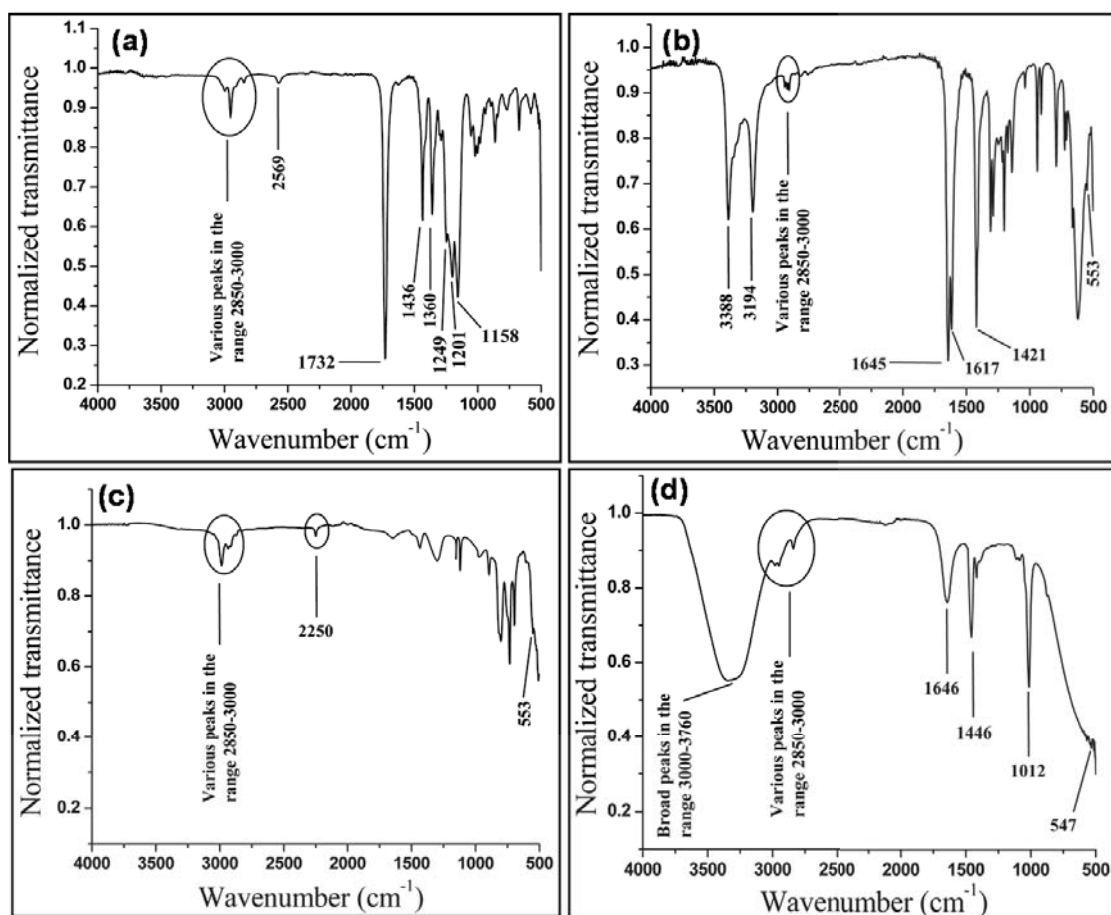


Figure 4.18. IR spectra of (a) Methyl-3-mercaptopropionate; (b) 3,3'-dithiopropionamide; (c) 3,3'-dithiopropionitrile and (d) 3,3'-dithiopropionylamidoxime.

frequency at 2569 cm^{-1} , C=O stretch at 1732 cm^{-1} , CO-O stretch at 1249, 1201 and 1158 cm^{-1} , CH₃ and CH₂ groups stretching vibrations at $3000\text{--}2850\text{ cm}^{-1}$ and their bending vibrations at 1460 and 1436 cm^{-1} (**Figure 4.18a**). In **Figure 4.18b** the strong doublets of N-H stretch at 3388 and 3194 cm^{-1} and C=O stretch at 1645 and 1617 cm^{-1} are the typical vibrational frequencies of primary amide. In addition to these, weak S-S stretching frequency at 553 cm^{-1} in **Figure 4.18b** confirms the formation of 3,3'-dithiopropionamide. On going from the dithioamide to dithionitrile the IR spectrum becomes much simpler with characteristic C≡N vibrational frequency at 2250 cm^{-1} and S-S, CH₃ and CH₂ stretching vibrations as described above (**Figure 4.18c**). A

broad peak in the range of $3760\text{--}3000\text{ cm}^{-1}$ corresponding to O-H and N-H stretching vibrations, a sharp peak at 1646 cm^{-1} corresponding to C=N group, another sharp peak at 1012 cm^{-1} corresponding to N-O group, various stretching and bending vibrational peaks of CH₃ and CH₂ groups and weak signal of S-S group at 547 cm^{-1} (**Figure 4.18d**) clearly indicate the synthesis of 3,3'-dithiopropionylamidoxime. The 3,3'-dithiopropionylamidoxime was also characterized by its ¹H NMR spectrum (**Figure 4.18**) taken in CD₃SOCD₃ solvent and the chemical shifts in ppm (δ scale) were measured relative to CH₃SOCH₃ (2.49 ppm) as internal standard: 1.040 (t, 4H, CH₂SSCH₂), 3.379 (s, 6H, 2[C(=NOH)(NH₂))] and 3.432 (t, 4H, CH₂CH₂SSCH₂CH₂).

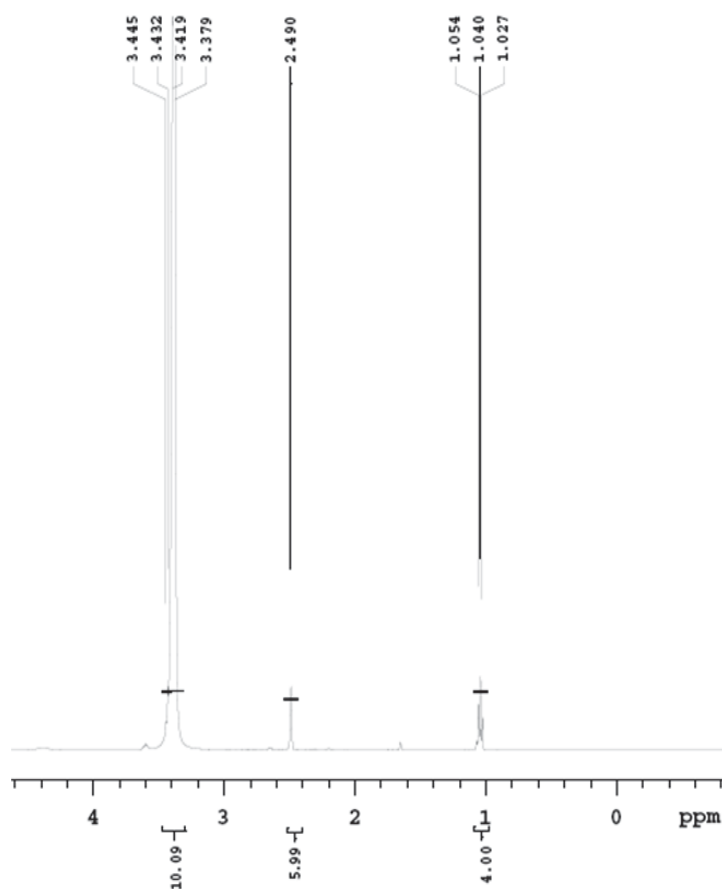


Figure 4.19. ¹H NMR spectrum of 3,3'-dithiopropionylamidoxime.

4.2.2.3. Transmission electron microscopy (TEM)

The TEM image of citrate stabilized and 3-MPD functionalized AuNPs, as shown in **Figure 4.20**, revealed their size of 4.9 ± 0.2 and 5.0 ± 0.2 nm respectively. Practically no size change on surface modification of AuNPs suggested their monolayer coating by 3-MPD. In addition to that HRTEM of 3-MPD capped AuNPs was also recorded and presented in **Figure 4.21**. The HRTEM image showed signatures of lattice fringes with an interplanar distances of 0.23 ± 0.01 nm and 0.20 ± 0.01 nm which agreed well with the literature reported interplanar spacing of (111) and (200) planes respectively in fcc AuNPs [155].

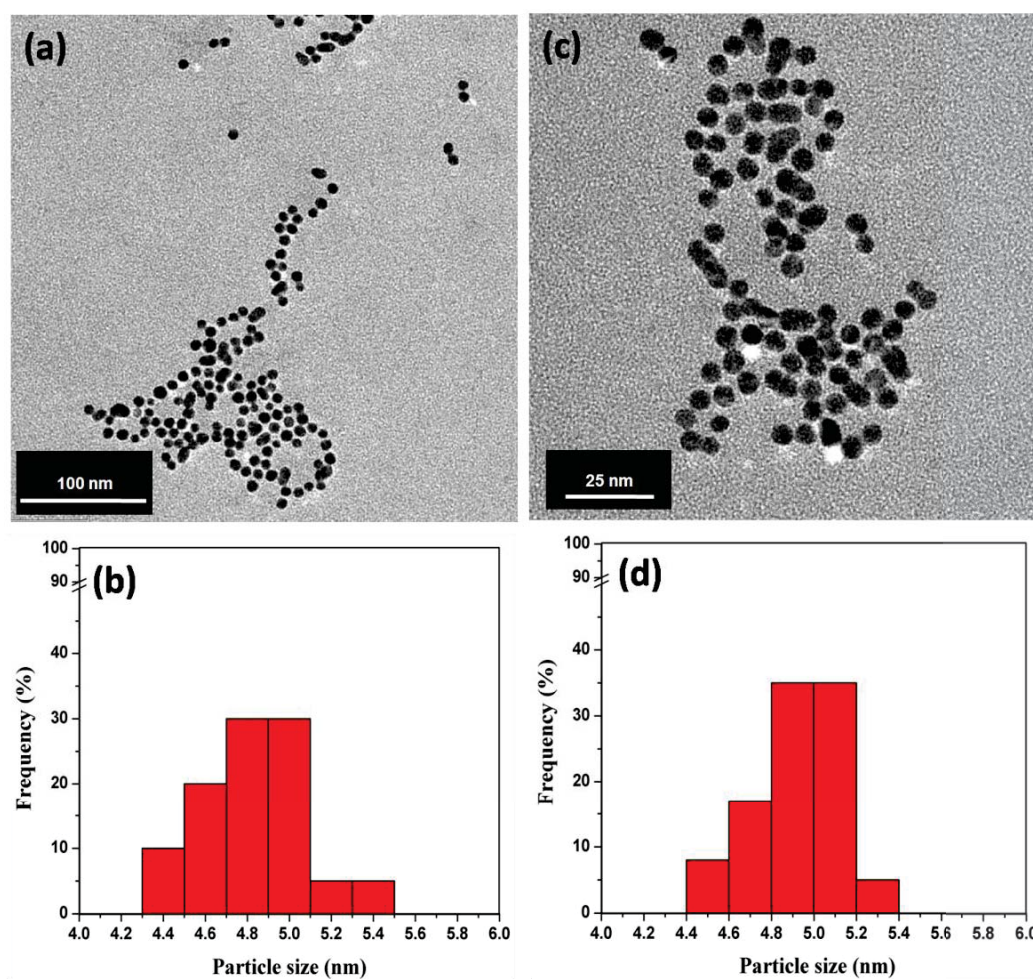


Figure 4.20. TEM micrographs and the corresponding size distribution of citrate stabilized AuNPs(a,b) and 3-MPD capped AuNPs (c,d).

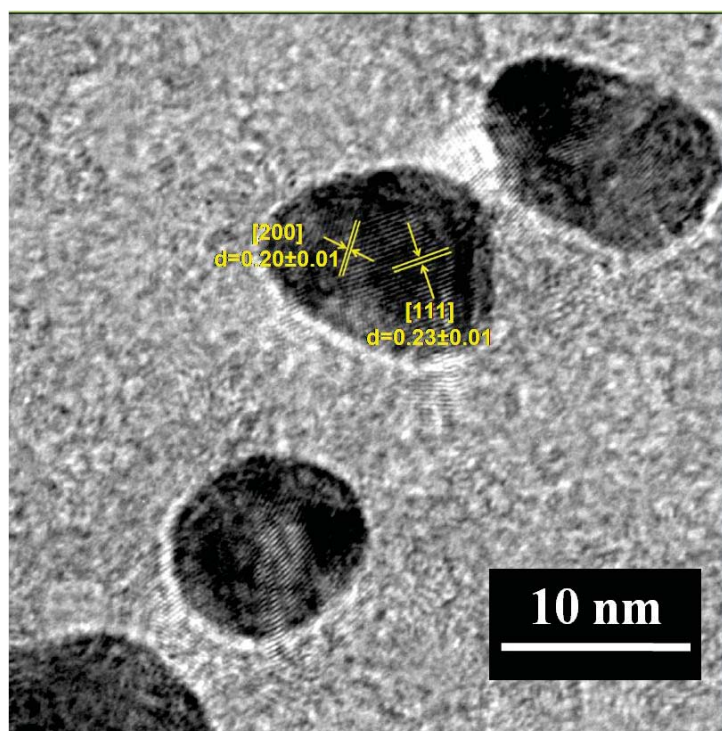


Figure 4.21. HRTEM image of 3-MPD capped AuNPs

4.2.2.4. X-ray photoelectron spectroscopy (XPS)

The XPS measurement of 3-MPD capped AuNPs was carried out to ascertain qualitative elemental composition which would confirm surface modification of AuNPs by 3-MPD. The measurement was carried out by depositing the NPs on a 1 cm x 1 cm glass plate. The XPS spectra of the NPs obtained from survey scan and high resolution measurement are given in **Figure 4.22**. In the **Figure 4.22a** with increasing binding energy, firstly a doublet appears near the 80-90 eV range. When the XPS spectrum was recorded at 1.2 eV resolution (**Figure 4.22b**), those two peaks were found exactly at 87.2 eV (Au 4f_{5/2}) and 83.5 eV (Au 4f_{7/2}) [140]. They are separated by binding energy interval of 3.7 eV and correspond to the Au (4f) transitions [140]. The presence of S 2p peak at 164.1 eV confirms the surface capping of AuNPs by 3-MPD [140]. In addition the strong peaks at 284.6 eV (C 1s), 397.9 eV (N 1s) and 531.6 eV (O 1s) are attributed to the C, N and O-atoms of 3-MPD [140]. The Si 2p

peak at 103.4 eV is from Si in glass plate on which the NPs were deposited for measurement.

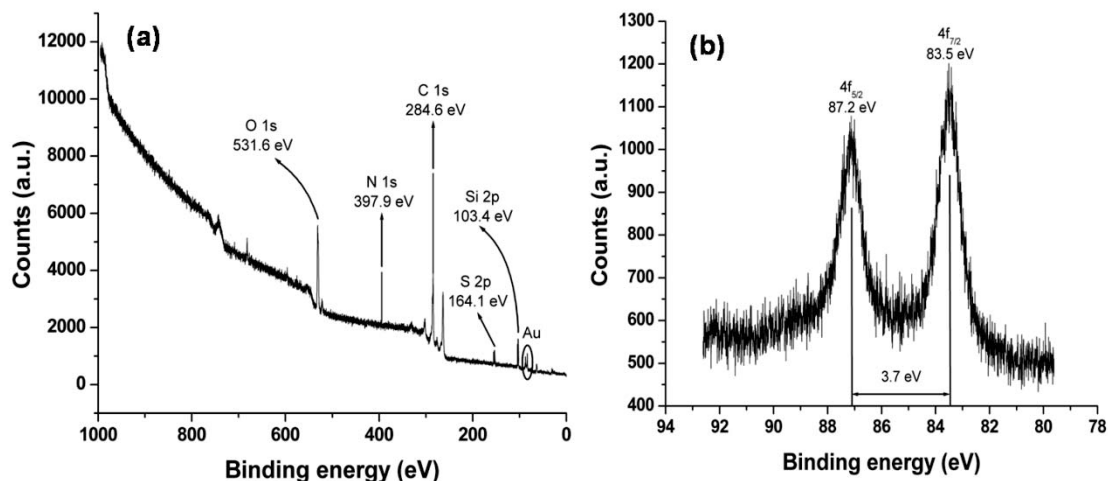


Figure 4.22. (a) Survey scan XPS spectrum of 3-MPD capped AuNPs and (b) High resolution survey scan XPS spectrum of 3-MPD capped AuNPs.

4.2.2.5. UV-visible spectrophotometry

The primarily synthesized 4.9 ± 0.2 nm citrate stabilized AuNPs showed SPR absorption peak at 520 nm, as shown in **Figure 4.23**. The particle concentration of AuNPs, obtained by Beer's law using an extinction coefficient of $8.6 \times 10^6 \text{ L mol}^{-1} \text{ cm}^{-1}$ at 520 nm [156], was approximately 20 nmol L^{-1} . On surface modification by 3-MPD the surface plasmon resonance (SPR) absorption peak did not get shifted but it experienced quenching in absorbance intensity, as shown in **Figure 4.23**. This observation indicates monolayer of 3-MPD on the surface of AuNPs.

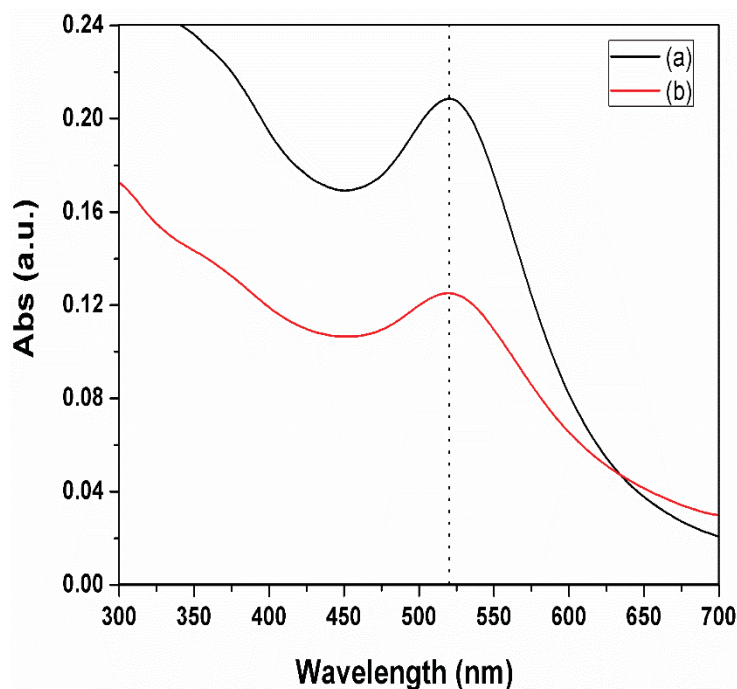


Figure 4.23. Absorption spectra of 20 nmol L^{-1} (a) citrate stabilized AuNPs and (b) 3-MPD capped AuNPs.

4.2.3. UV-visible spectrophotometric detection procedure of U(VI) ion

1 mL of $\sim 20 \text{ nmol L}^{-1}$ 3-MPD capped AuNPs and 1 mL of pH 6 phosphate buffer was mixed in a quartz cuvette in which $10 \mu\text{L}$ of different U(VI) ion stock solutions in $0.01 \text{ mol L}^{-1} \text{ HNO}_3$ having varying U concentrations were added at room temperature. The concentration of U(VI) in stock solutions was maintained in such a way that its concentration varies from 1 to 130 ng mL^{-1} in the total volume of the cuvette.

4.2.4. Cloud point extraction (CPE) procedure

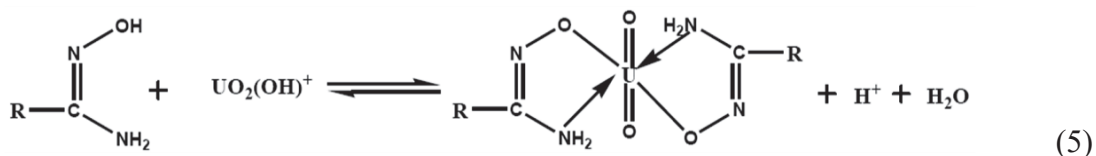
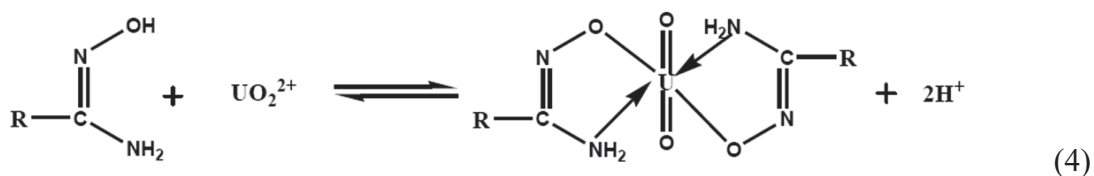
Maximum 6 mL aliquot of the sample was first filtered through a WhatmanTM filter paper 541 and then through a $0.2 \mu\text{m}$ membrane fitted syringe filter in a graduated glass centrifuge tube. 0.1 mL solution of $1.5 \text{ mol L}^{-1} \text{ NaCl}$ was then added to it. The pH of the solution was maintained at 6 by adding dilute HNO_3 and/or NaOH followed by adding 1.0 mL of pH 6 phosphate buffer. Separately 1 mL of 20 nmol L^{-1} 3-MPD

capped AuNPs was mixed with 1 mL 10% (w/v) polyvinyl alcohol (PVA) and then this mixture was added to the sample solution. The solution was then stirred at room temperature for 5 min. subsequently 0.25 mL of 0.1 mol L⁻¹ TTX-114 solution and 15 µL of 10.0 mmol L⁻¹ of CTAB solution were added to the sample solution. The volume was then made up to 10 mL and the solution mixture was kept in a water bath at 50 °C for 30 min. The phase separation occurs due to high viscosity of the SRP which settles down at the bottom. Complete phase separation was achieved by centrifuging the biphasic mixture at 4000 rpm for 10 min. The surfactant rich phase was isolated by pipetting out the supernatant. The surfactant rich phase was then diluted with 20:80 (v/v) methanol/pH 6 phosphate buffer to a total volume of 1 mL and was transferred quantitatively in a 0.5 cm quartz cell by to record the absorption spectrum.

4.2.5. Interaction of 3-MPD capped AuNPs with uranium

Amidoxime functional group containing polymeric adsorbents were previously studied by many groups around the world for the extraction of U mainly from seawater [157-160]. All these adsorbents were reported to extract maximum U in the pH range of 5-8.5 [157-160]. The amidoxime group is known to remain protonated in the lower pH region and hence is not able to undergo complexation. With increase in pH deprotonation takes place and it goes towards its neutral form. It is the neutral amidoxime group which is responsible for complexation with various U species [157-160]. According to the Henderson equation, the pH at which both protonated and deprotonated species are in equal concentration, is the first dissociation constant (pK_{a1}) of the molecule. Hence solution pH values above the pK_{a1} of the amidoxime group containing molecules are certainly the prime requirement of these extraction

processes. However these molecules also have a second dissociation constant (pK_{a2}) owing to the loss of second proton from $=N-OH$ group and these values are still higher. In literature the pK_{a1} and pK_{a2} values of simple acetamidoxime molecule are reported to be 5.78 and 13.21 respectively [161]. Hence the amidoxime group remains in its neutral form for an appreciable pH range. The neutral amidoxime group is known to show two possible isomerization equilibria as shown below [158]. These were reported to result in 1:1, 1:2, 1:3 and 1:4 type of complexes between U(VI) and amidoxime chelating group. However, the formation of 1:2 complex by the following mechanisms is the most common [157]:



Owing to these properties 3-mercaptopropionylamidoxime was selected as the AuNP surface modifier which facilitated preparation of water soluble NPs. The complexation pH range of amidoxime group supports the fact that the 3-MPD capped AuNPs will certainly be applicable at pH values typical for use in CPE systems. The structure of 3-MPD suggested that this compound will possess three pK_a values. The additional pK_a is expected to be due to the deprotonation of thiol group whose value generally varies in between 9-11 in non-conjugated aliphatic thiols [162]. Considering all these information, 3-MPD capped AuNPs were equilibrated with 100 ng mL^{-1} U(VI) in aqueous solutions of pH 5-8. The results are presented in **Figure 4.24**. It was

found that in the pH range of 5.5-6.5, the initial intensity of 3-MPD functionalized AuNPs at 520 nm get maximum quenched as well as red shifted. Hence pH 6 was fixed for all the later experiments. The simultaneous intensity reduc-

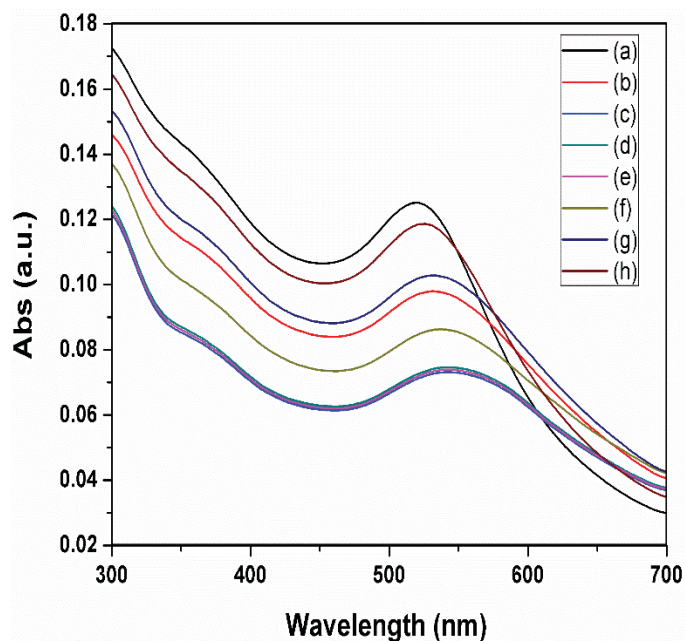


Figure 4.24. (a) Absorption spectrum of 20 nmol L^{-1} 3-MPD capped AuNPs. Simultaneous quenching and red shift of absorption spectrum of 3-MPD capped AuNPs in presence of 100.0 ng mL^{-1} U at pH: (b) 5.0, (c) 5.5, (d) 6.0, (e) 6.5, (f) 7.0, (g) 7.5 and (h) 8.0.

tion and red shift in the absorption spectrum of AuNPs, indicates an analyte-triggered aggregation mechanism of functionalized AuNPs in presence of U(VI), as shown in **Figure 4.25**. TEM image and small angle electron diffraction (SAED) measurement of U(VI) treated functionalized AuNPs, as presented in **Figure 4.26**, clearly proved the aggregation of these NPs in presence of U. When the concentration of U(VI) in solution was varied over a range of $1\text{-}130 \text{ ng mL}^{-1}$, a gradual decrease in intensity in addition to gradual shift in absorption peak was observed. The findings are presented in **Figure 4.27**. The ratio of maximum absorbance of AuNPs in absence and presence

of U (A_0/A , where A_0 and A are peak intensities in absence and presence of U(VI) respectively) and the shift in λ_{\max} in terms of wavelength difference ($\lambda_0 - \lambda$, where λ_0 and λ are the maxima in absorbance in absence and presence of U(VI) respectively) were plotted individually against the U(VI) concentration and shown in **Figure 4.28**. Linear relationship was observed in both cases for the U(VI) concentration range of 10-100 ng mL⁻¹. Due to the broad nature of UV-visible spectrum, the peak absorbance is not very sharp and only a 2 nm variation could clearly be observed from previous spectrum on every 10 ng mL⁻¹ change in U concentration (spectra were recorded at 0.2 nm band width). On the other hand, the slope of A_0/A vs. concentration of U(VI) curve showed a better sensitivity towards U determination and hence it was considered for analysis purpose. The DL ($3\sigma_{\text{blank}}/\text{slope}$) of the procedure was calculated to be 1.2 ng mL⁻¹.

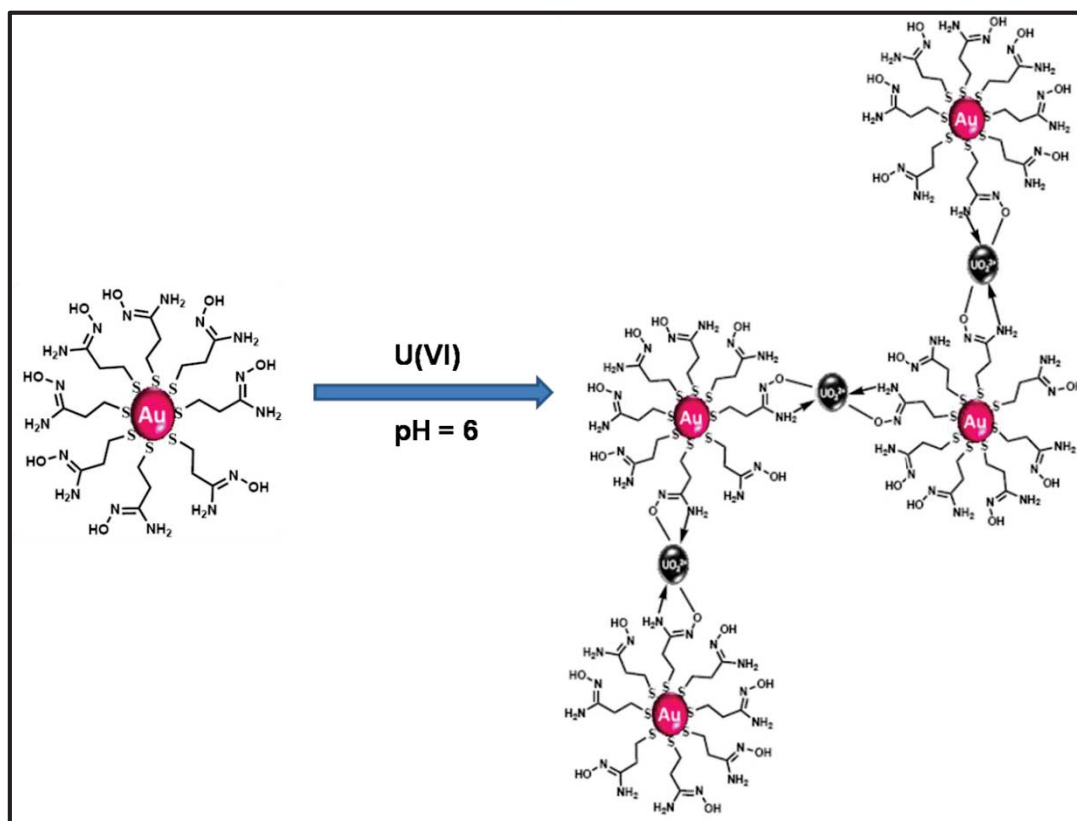


Figure 4.25. Aggregation of 3-MPD capped AuNPs via interaction with U(VI) ions.

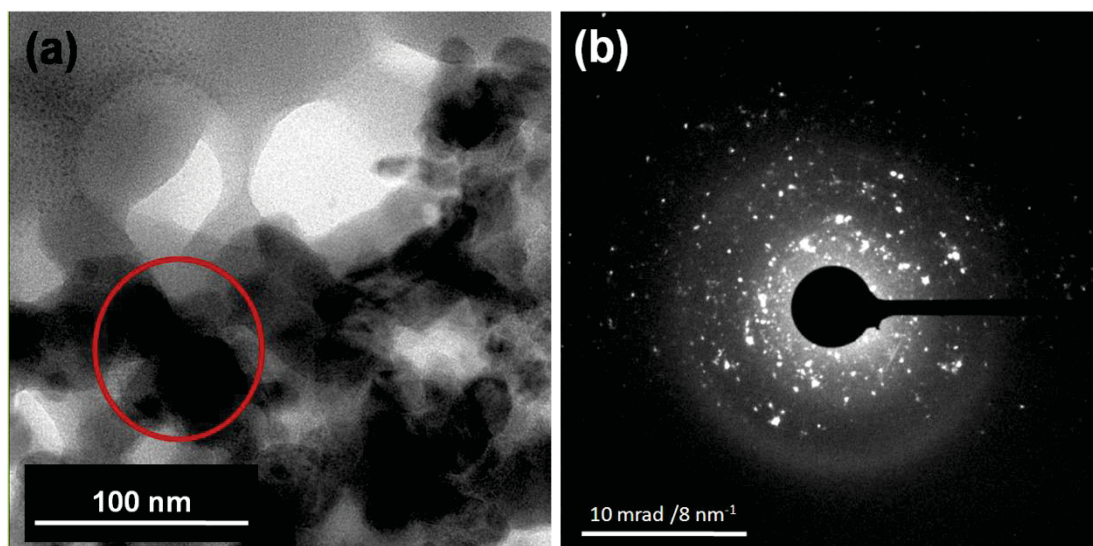


Figure 4.26. (a) TEM image of aggregated 3-MPD capped AuNPs in presence of U(VI) and (b) SAED image of the selected area in TEM image.

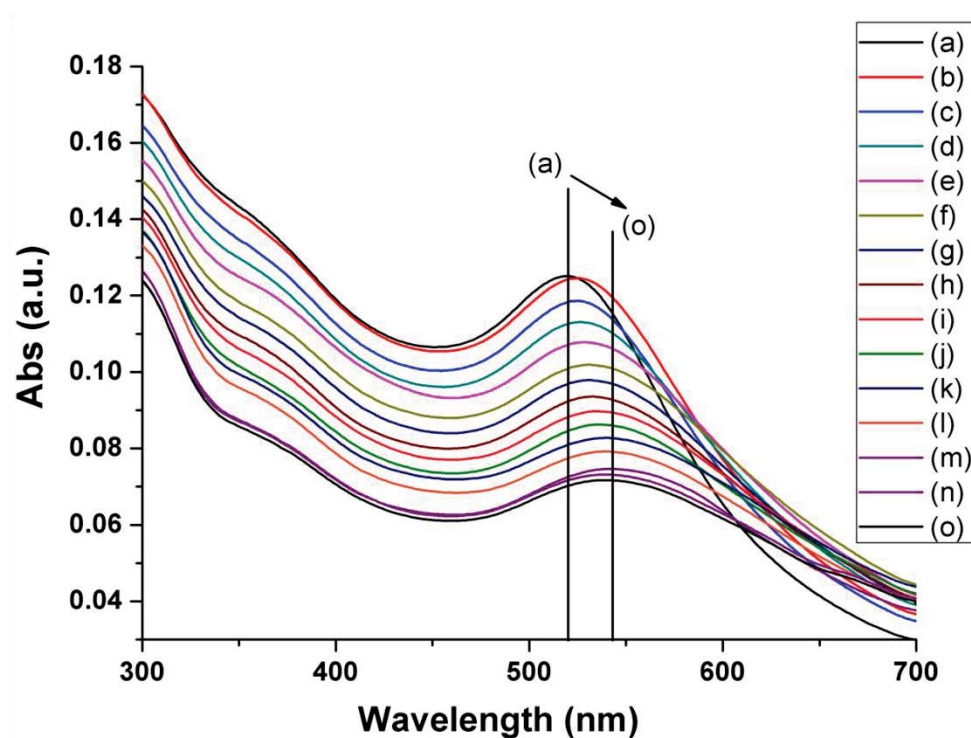


Figure 4.27. Change in absorption spectrum of 3-MPD capped AuNPs with addition of (a) 0 (b) 5, (c) 10, (d) 20, (e) 30, (f) 40, (g) 50, (h) 60, (i) 70, (j) 80, (k) 90, (l) 100, (m) 110, (n) 120 and (o) 130 ng mL⁻¹ U(VI) ion.

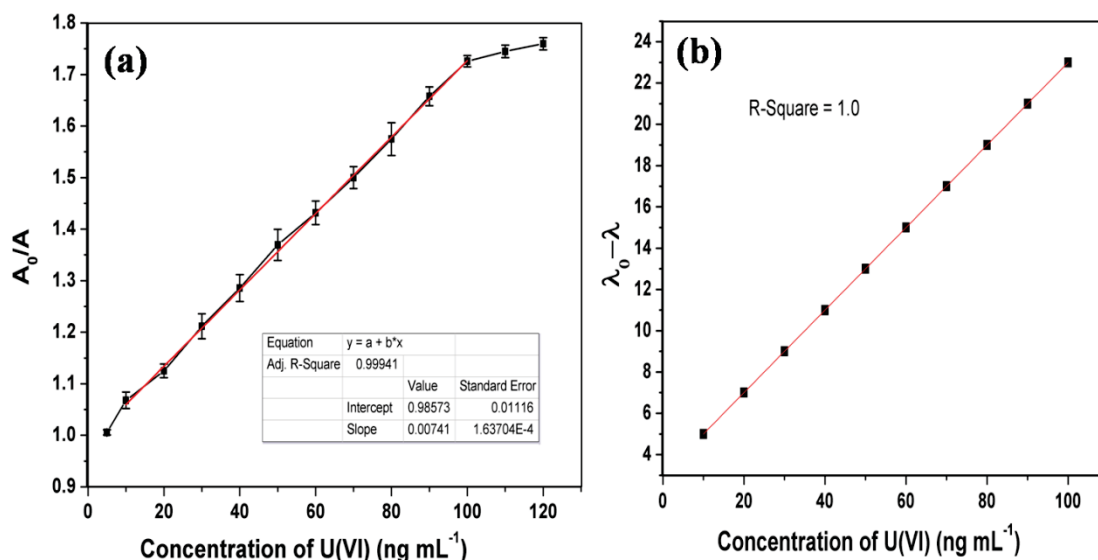


Figure 4.28. (a) Calibration plot of A_0/A vs. concentration of U and (b) Calibration plot of $\lambda_0 - \lambda$ vs. concentration of U.

4.2.6. Selectivity of 3-MPD capped AuNPs towards uranium

The metal ion sensing mechanism of the nanosensor indicates that its selectivity will be entirely guided by the interaction of amidoxime group with various metal ions under the experimental conditions. According to the literature reports, amidoxime group was reported to be highly selective towards U(VI) compared to alkali, alkaline earth and many transition metal ions [157-160]. However some transition metals were also reported to get extracted in significant amount with U and the selectivity order was reported to follow this order: $\text{U(VI)} > \text{V(V)} \gg \text{Co(II)}, \text{Cu(II)} \gg \text{Ni(II)}$ [159]. Hence, in order to check the selectivity of the nanosensor, 100 ng mL^{-1} of various metal ions were individually equilibrated with it and the observations are shown in **Figure 4.29**. U(VI) was found to result in maximum quenching of the surface plasmon resonance (SPR) absorption intensity of AuNPs among all the ions tested. Alkali and alkaline earth metal ions were found not to affect the absorption spectrum. Transition metal ions, except V(V), Co(II) and Cu(II), and lanthanides were also

found to quench the SPR absorption intensity marginally. The quenching of SPR absorption intensity by V(V), Co(II) and Cu(II) ions followed a trend supported by their reported selectivity order towards amidoxime group [159]. Later 100 ng mL^{-1} or $4.2 \text{ } \mu\text{mol L}^{-1}$ of U(VI) and equimolar mixtures of U(VI) and any of the above studied metal ion ($4.2 \text{ } \mu\text{mol L}^{-1}$ of each) were equilibrated separately with the nanosensor and the intensity quenching ratio (A_0/A) was measured in each case. These A_0/A values are represented as bar graph in **Figure 4.30** which shows no significant changes in results when different metal ions are present along with U. These studies confirm the U(VI) specificity of the nanosensor over other metal ions.

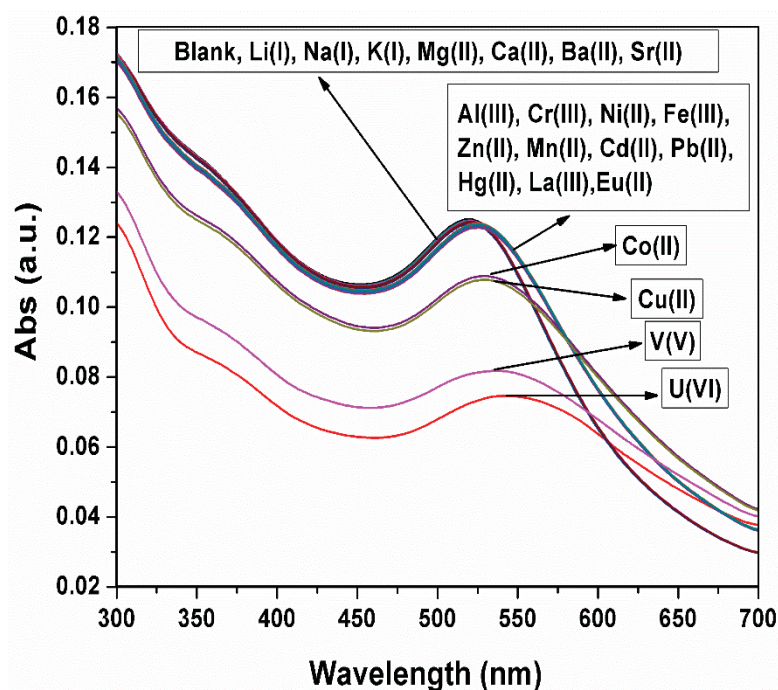


Figure 4.29. Change in absorption spectrum of 3-MPD capped AuNPs in presence of 100 ng mL^{-1} various metal ions.

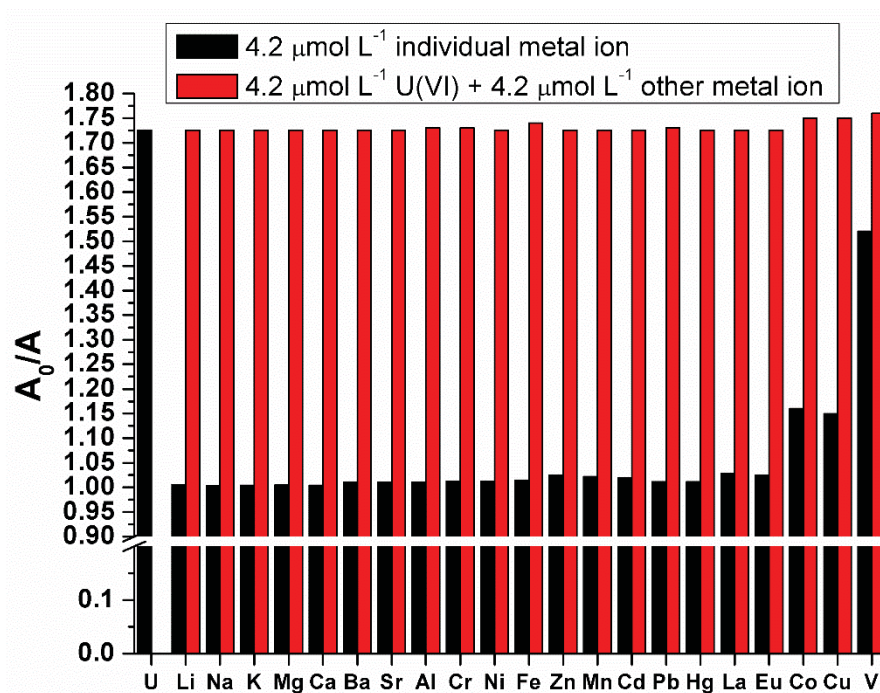


Figure 4.30. Bar diagram representing A_0/A values of 3-MPD capped AuNPs treated with respective interfering cations in the absence and presence of U(VI) ions

4.2.7. Optimization of CPE of 3-MPD capped AuNPs with and without U(VI)

According to Liu et al. [130] thermoreversible CPE of NPs preserve their shape and size in the micelles of non-ionic surfactants during the phase transfer and storage. The maximum extraction of NPs in CPE procedure was reported to be obtained at around zero point charge of the NPs [129,130]. The aggregation of water soluble NPs results in change of their protecting layer from hydrophilic to hydrophobic and hence facilitates the transfer of aggregated NPs from the bulk aqueous phase to the micellar core of surfactants. The zeta potential (ζ) of 3-MPD capped AuNPs in solution of pH 6, before and after the addition of U(VI) ions was found to be -14.2 ± 0.5 eV and -1.5 ± 0.3 eV respectively. Such reduction in ζ value encouraged us to couple the proposed U(VI) sensing procedure with CPE. The optimized CPE conditions obtained through cross-optimization of different parameters are given in **Table 4.6**.

Table 4.6. *Optimized conditions for CPE system before coacervation (Total volume = 10 mL)*

| Parameters | Conditions | Units |
|----------------|------------|----------------------|
| Sample volume | 6 | mL |
| pH | 6.0 | --- |
| [TTX-114] | 2.5 | mmol L ⁻¹ |
| [CTAB] | 15 | μmol L ⁻¹ |
| [NaCl] | 15 | mmol L ⁻¹ |
| Temperature | 50 | (°C) |
| time | 30 | (min) |
| Centrifugation | 4000 | rpm |

A 6 mL aliquot of 5.0 ng mL⁻¹ U solution was used as the sample for optimization purposes. The pH of the CPE procedure was kept at 6 for reasons discussed above. Similar to the calibration step 1 mL of ~ 20 mmol L⁻¹ 3-MPD capped AuNPs was used as the reagent in CPE. TTX-114 was used as the surfactant and its concentration was optimized with a view to accommodate the maximum possible NPs in it. Hence the concentration of TTX-114 was studied from just above its theoretical CMC (0.2-0.35 mmol L⁻¹) to 5 mmol L⁻¹ and the results are represented in **Figure 4.31**. The A₀/A value corresponding to 30 ng mL⁻¹ of U(VI) was observed at and above TTX-114 concentration of 2.0 mmol L⁻¹. Hence 2.5 mmol L⁻¹ of TTX-114 was fixed as its optimized concentration.

Since the ratio of surface plasmon resonance (SPR) absorption intensity in absence and presence of U(VI) is considered as the measurement value of the analyte, hence the concentration of functionalized AuNPs in the SRP should always be the same to generate reproducible A₀/A values. The free 3-MPD capped AuNPs were found to get partially solubilized in the hydrophobic micelle phase due to their low negative ζ value. This was found to result in A₀/A values less than 1 as shown in **Figure 4.32** where the CTAB concentration was varied from 0 to 50.0 μmol L⁻¹. CTAB was reported to undergo ion-pair formation with negatively charged NPs and induce the

phase transfer of very small sized NPs to the hydrophobic micelle phase [129,130]. The addition of minimum $12.5 \mu\text{mol L}^{-1}$ of CTAB was found to result in A_0/A value corresponding to 30 ng mL^{-1} of U(VI). $15.0 \mu\text{mol L}^{-1}$ of CTAB was considered as the optimized concentration.

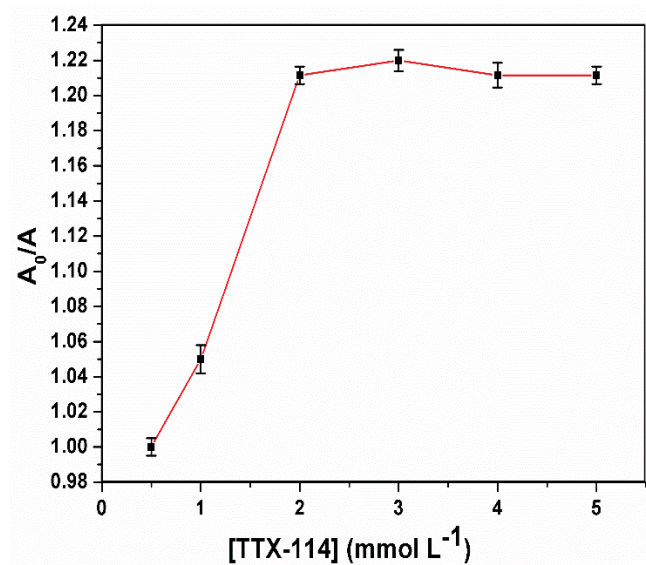


Figure 4.31. *Effect of TTX-114 concentration on U recovery by CPE procedure when all other parameters in Table 4.6 remain constant.*

Sodium chloride (NaCl) was used as the electrolyte in this case to maintain the solution ionic strength. The concentration of NaCl was varied from 0 to 25.0 mmol L^{-1} and the results are given in **Figure 4.33**. U recovery was not affected significantly in absence of electrolyte due to the interaction between U(VI) and the functionalized AuNPs in the bulk aqueous medium. The small improvement in the A_0/A value with the addition of NaCl is expected to be due to salting out mechanism. Hence 15.0 mmol L^{-1} of NaCl was used in all experiments.

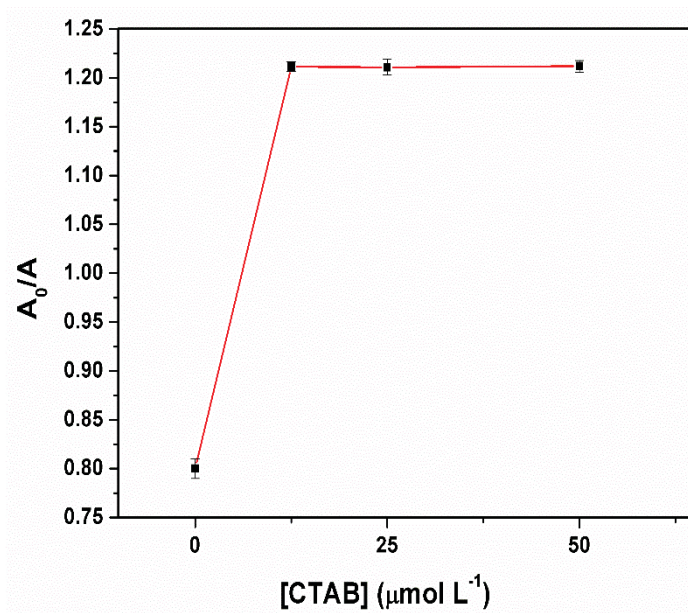


Figure 4.32. Effect of CTAB concentration on U recovery by CPE procedure when all other parameters in Table 4.6 remain constant.

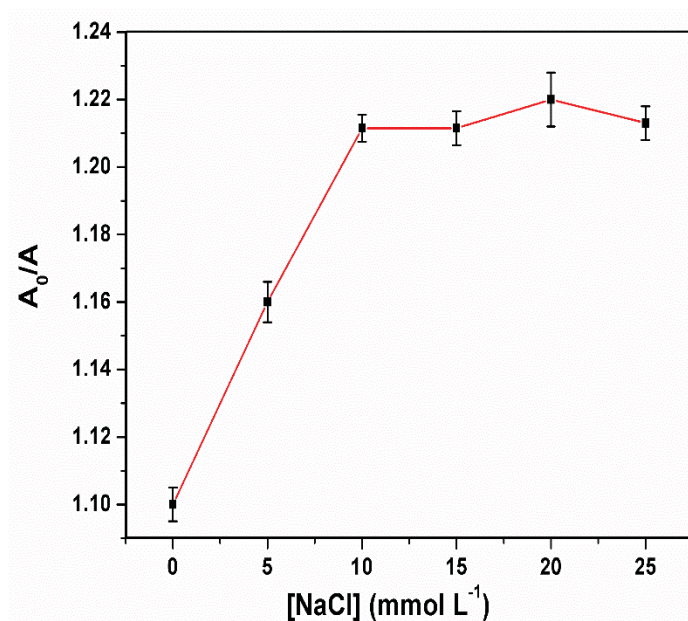


Figure 4.33. Effect of NaCl concentration on U recovery by CPE procedure when all other parameters in Table 4.6 remain constant.

High electrolyte concentrations are previously reported to result in agglomeration of functionalized AuNPs by the screening of the electrostatic repulsion between them

[163]. In environmental sample analysis the 3-MPD capped AuNPs will be exposed to higher concentration of various cations and anions. In order to avoid any such possibilities of NP aggregation in absence of analyte of interest, 1% (w/v) polyvinyl alcohol (PVA) was used in the CPE procedure as a stabilizer to these functionalized AuNPs [163-166]. The SRP absorption intensity of functionalized AuNPs in absence and presence of U(VI) was found to remain unaffected by the addition of PVA.

The CPT of the system was measured to be 23 ± 1 °C. The temperature was varied from room temperature (~ 25 °C) to 60 °C with 30 min incubation time to see the temperature effect on extraction study. As reported earlier by Liu et al. [130] the increase in temperature was found to provide slight improvement on extraction efficiency, as shown in **Figure 4.34**. At and above 50 °C, maximum A_0/A value corresponding to 30 ng mL^{-1} of U was obtained and hence it was fixed as the optimized temperature with 30 min incubation time.

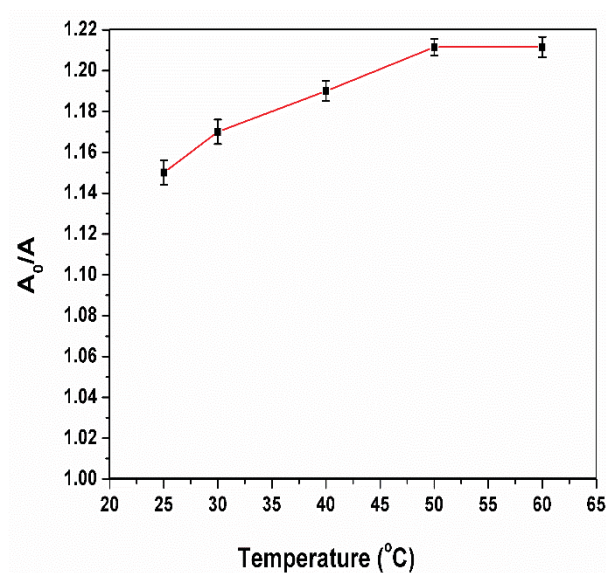


Figure 4.34. Effect of temperature on U recovery by CPE procedure when all other parameters in Table 4.6 remain constant.

4.2.8. Interference study and analytical figures of merit

As discussed previously, depending on their natural abundance in various streams of water a large number of cations and anions were tested at different concentrations to investigate their effect on the recovery of U. A list of the maximum tolerable interference ion concentrations is given in **Table 4.7**. This table is in accordance with the observations made earlier during the selectivity test of the nanosensor. 1.0 mmol L⁻¹ of EDTA was required to avoid the interference from Co(II) and Cu(II). Some common anions like Cl⁻, Br⁻, PO₄³⁻, SO₄²⁻, CO₃²⁻ etc., were also tested according to their maximum tolerance limit in **Table 4.7** and were found to exert no adverse effect on U detection.

Table 4.7. Tolerance of the method to the presence of foreign metal ions (experiments carried out with 5.0 ng mL⁻¹ of U)

| Foreign metal ion (M ⁿ⁺) | Tolerance limit(μg mL ⁻¹) |
|---|--|
| Li ⁺ , Na ⁺ , K ⁺ | 10000 |
| Mg ²⁺ | 1500 |
| Ca ²⁺ , Sr ²⁺ , Ba ²⁺ | 500 |
| Al ³⁺ | 200 |
| Mn ²⁺ , Ni ²⁺ , | 200 |
| Zn ²⁺ Fe ³⁺ , Cr ³⁺ , | 200 |
| Cd ²⁺ | |
| Co ²⁺ , Cu ²⁺ | 200 ^a |
| Pb ²⁺ | 50 |
| Hg ²⁺ | 0.2 |
| La ³⁺ , Eu ³⁺ | 10 |
| PO ₄ ³⁻ , SO ₄ ²⁻ , CO ₃ ²⁻ | 2000 |
| Cl ⁻ , Br ⁻ | 10000 |

Note: Cations were prepared using their chloride or nitrate salts. Anions were prepared using their sodium or potassium salts.^aSolution spiked with 1.0 mmol L⁻¹ EDTA.

The maximum 6 mL sample volume resulted in LOQ value of the method to be 2 ng mL⁻¹, resulting in the DLR and DL of the methodology as 2-100 ng mL⁻¹ and 0.3 ng

mL^{-1} respectively. Although the proposed methodology is comparable to the previously reported cost effective analytical techniques with respect to LOQ, DLR and DL etc., [40,54,76,77,90,95-97,147,148] but is superior to them in terms of naked-eye visual detection of ultratrace levels of U. The surfactant rich phase colour after CPE of 6 mL sample aliquot with 0, 5, 10 and 15 ng mL^{-1} of U is shown in **Figure 4.35**. The bright red colour of the 3-MPD capped AuNP containing SRP was found to turn blue in presence of minimum 10 ng mL^{-1} ($0.042 \times 10^{-6} \text{ mol L}^{-1}$) of U. To the best of our knowledge it is the first ever report on such low level U detection by clearly visible bright colour change. The EE and PF values of the methodology were calculated to be $98.0 \pm 2.0\%$ and 99 respectively.

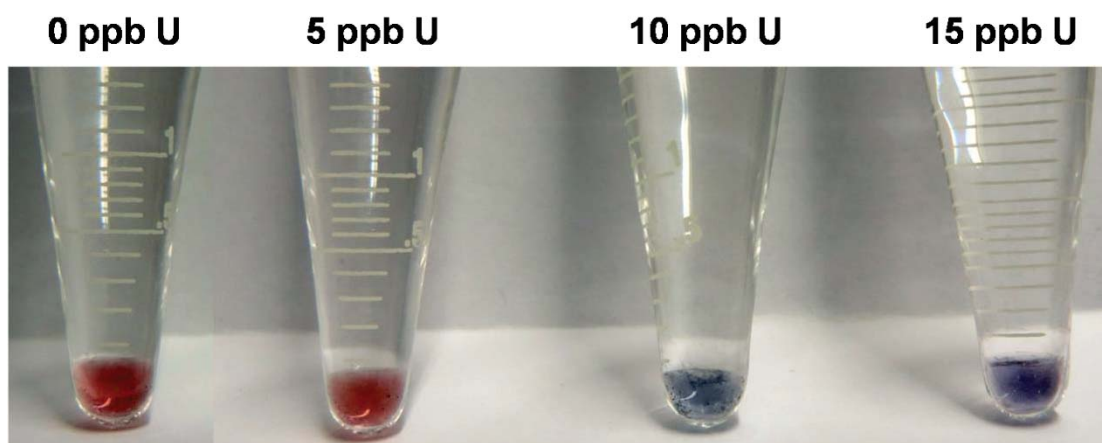


Figure 4.35. Change in colour of SRP as a function of various concentrations of U.

4.2.9. Validation of the proposed methodology

Validation of any proposed analytical technique was done by analyzing the NIST SRM 1640a, natural water. The result is given in **Table 4.8** where the determined U concentration was found to be in good agreement, at 95% confidence level, with its certified value.

Table 4.8. Determination of U in NIST SRM 1640a natural water standard (Sample volume = 3 mL; n = 3)

| Certified value (ng mL ⁻¹) | Analyzed value (ng mL ⁻¹) | Recovery (%) |
|---|--|-----------------|
| 25.35±0.27 | 25.2±0.4 | 99.4±1.6 |

4.2.10. Analysis of real water samples

The same water samples as described in **section 4.1.10** of this chapter were tested by this developed methodology by standard addition technique. The results are given in **Table 4.9**. The quantitative recovery ($\geq 95\%$) of the spiked amount of U cross-validates our detection methodology.

Table 4.9. Analysis of natural water samples (n=5)

| Sample | Source | Added U conc. (ng mL ⁻¹) | Found U conc. (ng mL ⁻¹) | Recovery (%) |
|--------------|--|---|---|-----------------|
| Sea water | Mumbai coast, India | 0 | 2.8±0.1 | - |
| | | 5.0 | 7.7±0.2 | 98±4 |
| | | 10.0 | | |
| Ground water | West Bengal, India | 0 | ND | - |
| | | 5.0 | 5.1±0.2 | 102±4 |
| | | 10.0 | 9.9±0.3 | 99±3 |
| River water | Teesta canal, West Bengal, India | 0 | ND | - |
| | | 5.0 | 4.9±0.1 | 98±2 |
| | | 10.0 | 9.8±0.2 | 98±2 |

ND = Not detected

4.2.11. Proposed visual detection kit

A visual colorimetric change of the probe at and above the WHO and USEPA recommended guideline limit of 30 ng mL⁻¹ U, will be beneficial in easy and simple on-site testing of drinking water samples. The test kit consists of a 10 mL conical bottom glass test tube with cap (test kit **A**) and another is 5 mL micro centrifuge tube (test kit **B**). Test kit **A** contains 7.35 mL reagent solution which consists of 1 mL 20

nmol L⁻¹ 3-MPD capped AuNPs, 1 mL 10% (w/v) PVA solution, 100 µL of 1.5 mol L⁻¹ NaCl, 250 µL of 0.1 mol L⁻¹ TTX-114 solution and rest 5.0 mL of pH 6 phosphate buffer. Test kit **B** contains only 150 µL of 1.0 mmol L⁻¹ CTAB. The test kit **A** was found to maintain the same SPR absorption intensity after 6 months when kept at room temperature. The testing process consists of these steps: (i) incubation of the test kit **A** in an ice bath for 10 min; (ii) addition of 2.5 mL of clear water sample in test kit **B**; (iii) addition of final test kit **B** solution to test kit **A** in cold condition with proper mixing; (iv) finally keeping the test kit **A** at room temperature (25 °C or above) for 1 hr. The colour of the surfactant rich phase that will appear on application of the test kit are represented in **Figure 4.36**. The colours appearing at (30 ng mL⁻¹), below and above the guideline value can easily be differentiated. However a minimum 10 ng mL⁻¹ difference in U concentration above or below its guideline value gives clear colour indication.

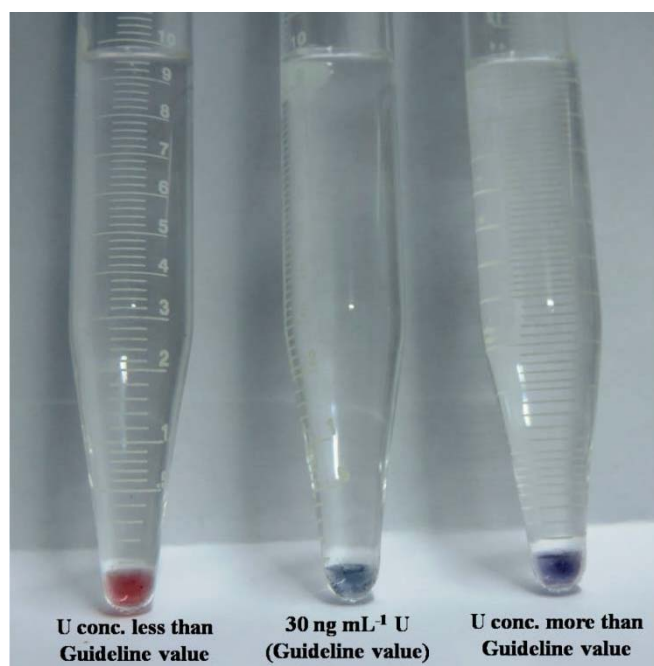


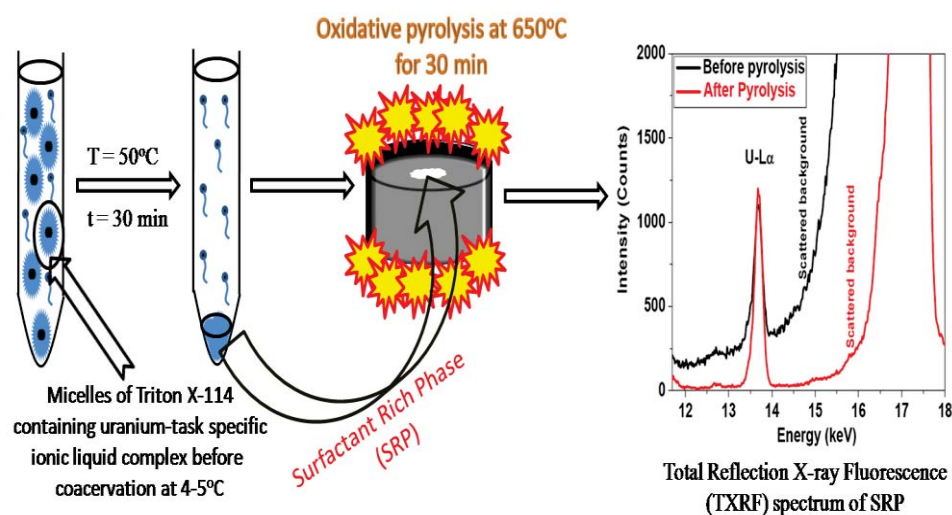
Figure 4.36. Reference colour change in U detection kit at, below and above the WHO and USEPA guideline limit of 30 ng mL⁻¹ U in drinking water.

4.2.12. Conclusion

The synthesis of a new compound viz., 3-mercaptopropionylamidoxime (3-MPD) resulted in developing a novel U(VI)-specific nanosensor. The coupling of AuNP assisted U detection procedure with CPE method made possible the visual detection of ultratrace level U. The visual detection kit for U will be very helpful for on-site testing of drinking water samples in the vicinity of U mining areas, nuclear facilities or nuclear accident/explosion sites.

Chapter 5

Application of task specific ionic liquid (TSIL) in cloud point extraction (CPE) of uranium (U) in aqueous samples



This page is kept blank intentionally

5.1. Introduction

Ionic liquids (ILs) are salts that are generally composed of an asymmetric and bulky organic cation and anions like bromide (Br^-), iodide (I^-), tetrafluoroborate (BF_4^-), hexafluorophosphate (PF_6^-) and bis(trifluoromethylsulfonyl)imide (NTf_2^-) [208-210] etc. The ILs which remain liquid at room temperature are called room temperature ionic liquids (RTILs). The cationic part is generally composed of alkylammonium, alkylphosphonium, N,N'-dialkylimidazolium, N-alkylpyridinium ions etc [167-169]. In the last two decades, compared to the conventional volatile organic solvents, RTILs have emerged as more eco-friendly alternative in the fields of organic synthesis, catalysis, electrochemistry, metal ion extraction etc [167-171]. Stability in air and water, wide liquidus range, low volatility, ability to dissolve both organic and inorganic materials and favorable viscosity and density characteristics of these RTILs encourage their uses as above discussed [168,172,173]. Additionally, RTILs have been reported as promising solvents in actinide and lanthanide extraction and separation due to their stability under α and γ irradiations [174-176]. However, lack of coordinating groups in RTILs limits their use in metal ion partitioning [177]. Currently many scientific groups around the world are engaged in developing tailored RTILs which contain metal ion coordinating groups in their structures. Such RTILs are generally called as task specific ionic liquids (TSILs). Improvements in the partition coefficient values of metal ions were reported in the literature using these TSILs [178-180].

In literature, ILs have been reported to mediate the CPE of several organic dyes, amino acids, parabens etc [181-183]. On the otherhand, there are a few reports on application of ILs in the CPE of metal ions [91,184]. In these reports, ILs have been

mainly used as micellar phase modifier to enhance the extraction efficiency (EE) of metal-ligand complexes [91,184]. Gao et. al. [91], demonstrated the improvement in the extraction efficiency (EE) from 45% to 80% of U(VI) by trioctylphosphine oxide (TOPO) by the use of NTf_2^- containing hydrophobic ILs. The increase in EE was explained in terms of involvement of NTf_2^- in the complexation with U(VI)-TOPO complex which also resulted in selective extraction of U(VI) in presence of equimolar lanthanum [91]. The concentration of the common interfering ions in any natural matrix is always much higher than that of the analyte of interest. Since TSILs were reported to improve partition coefficient values of metal ions, by the same analogy they can also improve the EE of metal ions in CPE. Till date no literature reports are available on the CPE of any metal ion employing TSIL.

Hence, there is a lot of scope in developing TSIL mediated CPE methodology for achieving better EE for U in presence of higher concentrations of foreign metal ions. With this in view, a phosphoramidate (phamd) group bearing TSIL was synthesized and characterized in the present work and was used for the CPE of U(VI) in aqueous samples. Total reflection X-ray fluorescence (TXRF) spectrometry was utilized for the first time to quantify uranium directly in the surfactant rich phase (SRP) of CPE procedure. The advantage of using TXRF spectrometry as an offline detection technique following CPE has been discussed in the later section of this chapter. Optimization of various CPE parameters resulted in efficient CPE of U even in presence of higher amounts of various interfering ions, especially lanthanides. In order to explain the selectivity of the developed CPE methodology, the complexation between U(VI) and TSIL was studied by isothermal calorimetry, liquid-liquid extraction, ^{31}P NMR, IR spectroscopy and electrospray ionization mass spectrometry

(ESI-MS). The proposed analytical methodology for preconcentration and quantification of U was validated by analyzing a certified reference material (CRM) viz., NIST SRM 1640a natural water and then used to analyze three real water samples from various sources of India.

5.2. Synthesis and characterization of TSIL

The schematic representation of the synthesis of TSIL bearing phosphoramidate group viz., N-propyl(diphenylphosphoramidate)trimethylammonium bis(trifluoromethanesulfonyl)imide, [phamdNMe₃][NTf₂] is given in **Figure 5.1**. The three step synthesis procedure involves amination of diphenylchlorophosphate by 3-dimethylamino-1-propylamine in the first step followed by its methylation to form N-propyl(diphenylphosphoramidate)trimethylammonium iodide, [phamdNMe₃][I]. In the last step metathesis between [phamdNMe₃][I] and lithiumbis(trifluoromethanesulfonyl)imide, LiNTf₂ resulted in the formation of [phamdNMe₃][NTf₂]. The complete experimental procedure of preparing [phamdNMe₃][NTf₂] is given in section 2.3.3 of chapter 2.

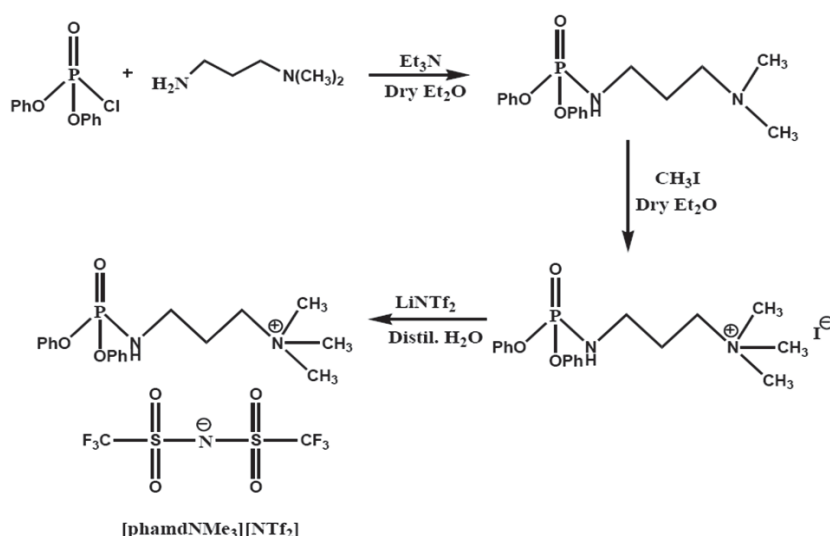


Figure 5.1. Schematic representation of the complete synthesis route of TSIL.

The characterization of synthesized TSIL viz., [phamdNMe₃][NTf₂] was carried out by ¹H NMR, ¹³C NMR, ³¹P NMR and IR spectroscopy, CHNS elemental analysis and ESI-MS measurement. The ¹H NMR spectrum of [phamdNMe₃][NTf₂] was recorded in CD₃COCD₃ solvent with 500 MHz spectrometer and is given in **Figure 5.2**. The ¹H chemical shifts in ppm (δ scale) were measured relative to CH₃COCH₃ (3.22 ppm) as internal standard: 2.063 (m, 3H, NHCH₂CH₂CH₂), 3.125 (s, 9H N⁺(CH₃)₃), 3.254 (m, 2H, NHCH₂), 3.490 (m, 2H, NHCH₂CH₂CH₂), 7.237 (t, 2H, *para* H's of Ph), 7.335 (d, 4H, *ortho* H's of Ph) and 7.420 (t, 4H, *meta* H's of Ph). The ¹³C NMR spectroscopic data of [phamdNMe₃][NTf₂] was recorded in CD₃COCD₃ solvent with 125 MHz spectrometer and is given in **Figure 5.3**. The ¹³C chemical shifts in ppm (δ scale) were measured relative to CD₃COCD₃ (205.75 ppm) as internal standard: 24.755 (d, NHCH₂CH₂CH₂), 38.361 (d, NHCH₂CH₂CH₂), 52.809 (s, N⁺(CH₃)₃), 64.464 (s, NHCH₂CH₂CH₂), 118.840 (q, J = 319.6, N⁻(SO₂CF₃)₂), 120.471 (d, *ortho* C's of Ph), 125.204 (d, *para* C's of Ph), 129.865 (d, *meta* C's of Ph) and 151.104 (d, substituted C's of Ph). The ³¹P NMR spectroscopic data was recorded in CD₃SOCD₃ solvent with 400 MHz spectrometer and the chemical shift was measured relative to external standard 85% H₃PO₄. The ³¹P NMR spectrum of [phamdNMe₃][NTf₂] is given in **Figure 5.4**, which shows a single peak at -11.887 ppm corresponding to the single P-atom in the molecule. The IR spectrum of the TSIL is represented in **Figure 5.5** showing the P=O and P-O-C stretching frequencies at 1230 and 1053 cm⁻¹ respectively. Elemental (CHNS) analysis of the TSIL results in (38.2±0.2)% of C, (4.08±0.03)% of H, (6.70±0.04)% of N and (10.1±0.1)% of S. These experimentally observed values are in good agreement with the expected concentrations of C (38.16%), H (4.16%), N (6.67%) and S (10.19%).

The ESI-MS spectrum of the TSIL is shown in **Figure 5.6**. The base peak at m/z 349.2816 corresponds to the $[\text{phamdNMe}_3]^+$ ion (exact mass, 349.1676 amu) of the TSIL. The other mass peaks at m/z 350.3376 and 290.2435 are due to $([\text{phamdNMe}_3]^+ + \text{H}\bullet)$ radical ion and one of the fragments of $[\text{phamdNMe}_3]^+$ ion, as shown in **Figure 5.6**.

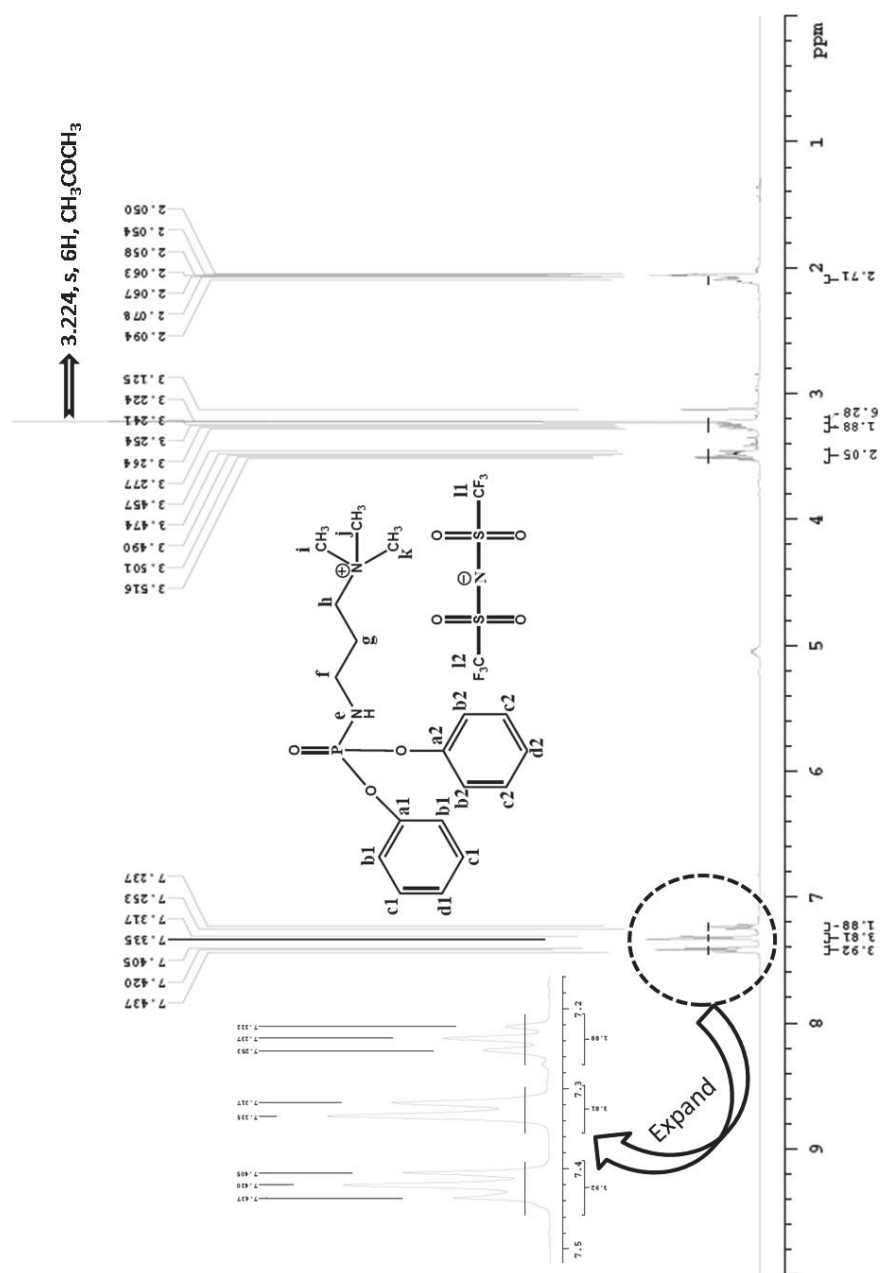


Figure 5.2. ^1H NMR spectrum of synthesized TSIL.

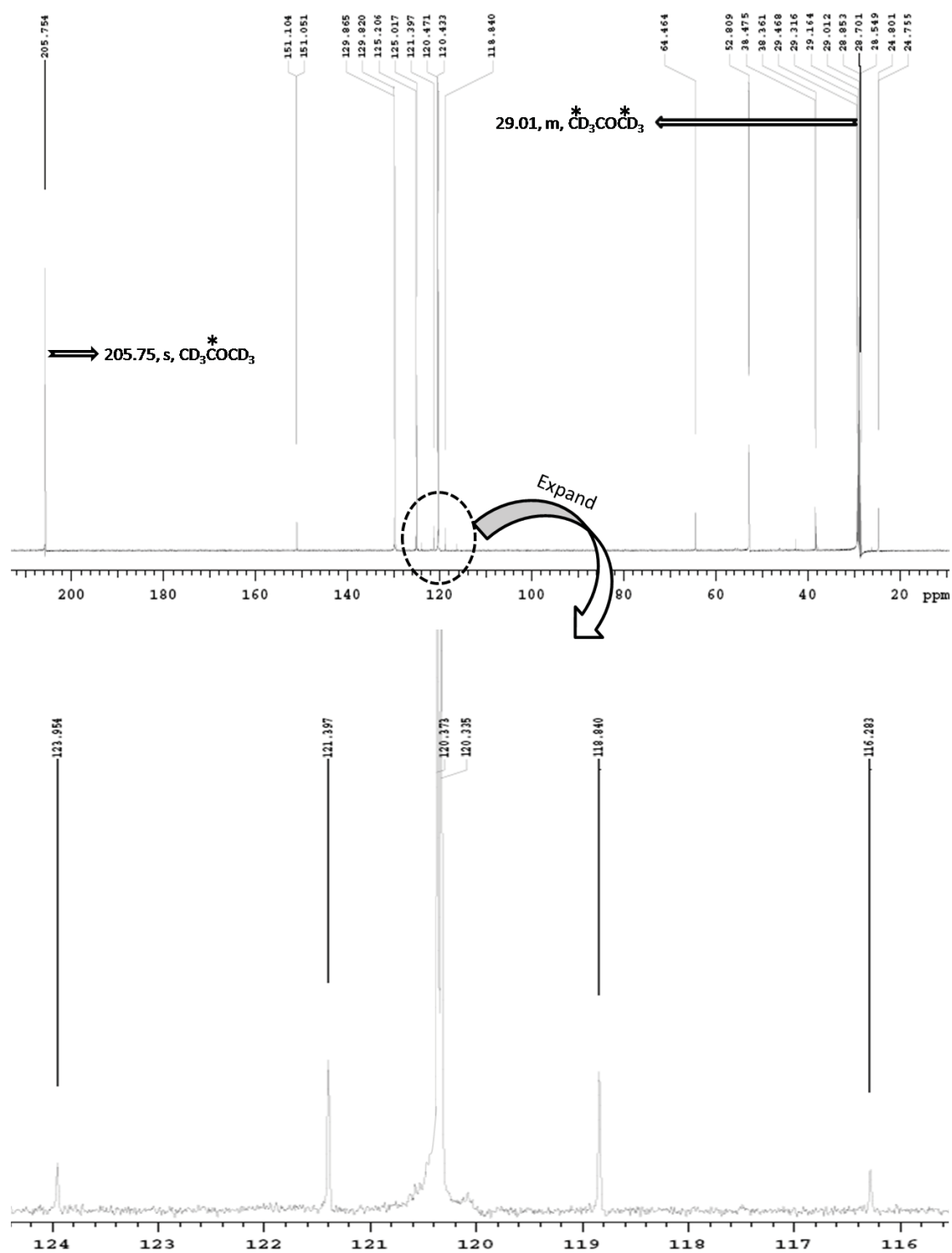


Figure 5.3. ^{13}C NMR spectrum of synthesized TSIL.

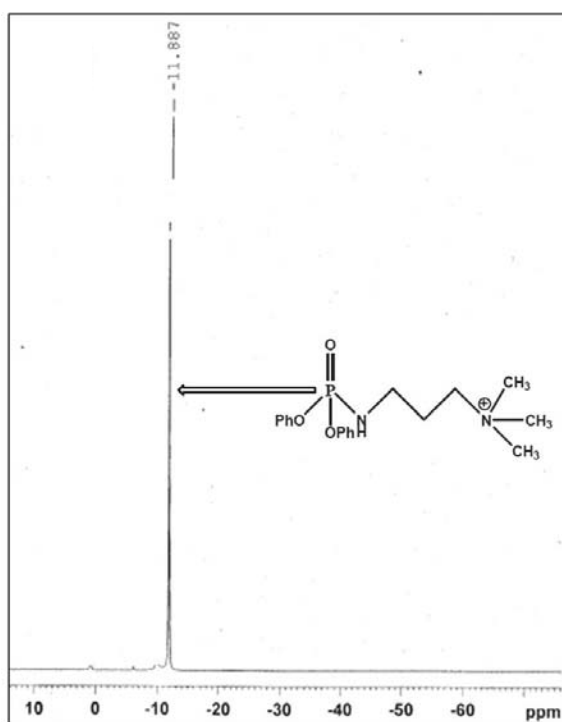


Figure 5.4. ^{31}P NMR spectrum of synthesized TSIL.

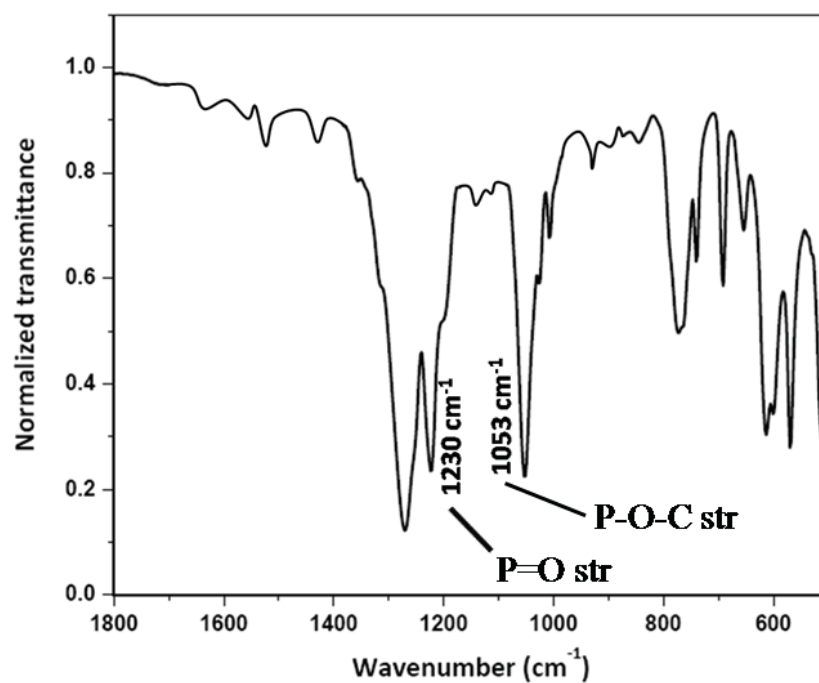


Figure 5.5. IR spectrum of synthesized TSIL.

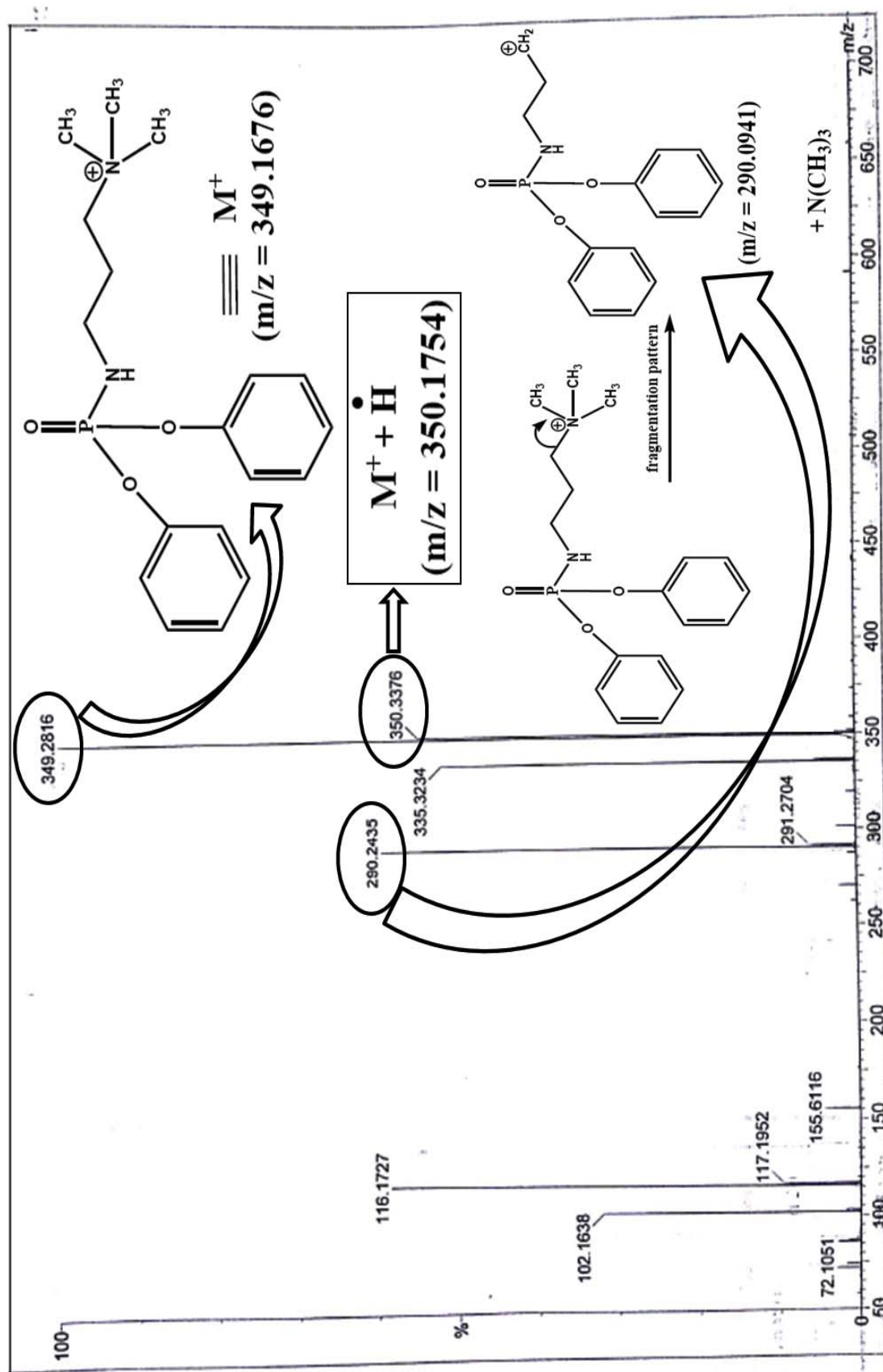


Figure 5.6. *ESI-MS spectrum of synthesized TSIL.*

5.3. CPE procedure

The water sample was initially filtered through Whatman™ filter paper 541 and then passed through a 0.2 µm PTFE membrane fitted syringe filter to get a clear solution. Subsequently, a 7.5 mL aliquot of it was transferred to a graduated glass centrifuge tube. A 0.5 mL solution of 2.0 mol L⁻¹ KNO₃ was then added to it. The pH of the solution was maintained at 6 by adding dilute HNO₃ and/or NaOH followed by adding 0.5 mL solution of pH 6 phosphate buffer. Afterwards, 0.4 mL of 125 mmol L⁻¹ TTX-114 solution containing 10 mmol L⁻¹ of TSIL and 0.12 mL of 10 mmol L⁻¹ of SDS solution were added to the sample solution. The volume was then made up to 10 mL and the solution mixture was kept in an ice bath at 4-5 °C for 30 min with constant stirring. Subsequently, the centrifuge tube was placed in a water bath at 50 °C for 30 min. The phase separation occurs due to high viscosity of the SRP which settles down at the bottom. Complete phase separation was achieved by centrifuging the biphasic mixture at 4000 rpm for 5 min. The 0.1 mL SRP was isolated by pipetting out the supernatant.

5.4. TXRF spectrometric analysis

The extraction of metal ion from the bulk aqueous medium to the small volume of SRP is the biggest advantage of CPE procedure to achieve high PF value. However, analysis of the analyte in the SRP by analytical techniques like inductively coupled plasma mass spectrometry (ICP-MS), ICP-atomic emission spectroscopy (ICP-AES), flame atomic absorption spectroscopy (FAAS), UV-Visible spectroscopy etc., needs dilution [32,185-190]. Hence, for all practical purposes the PF value gets diminished at the time of measurement which can affect the detection limit. In contrast, TXRF spectrometry can be used for direct analysis of SRP as this technique requires very

small amount of sample (as low as 5-10 μL) [191,192]. The concentration of the analyte was determined by using the equation:

$$c_A = (I_A/S_{iA}) \times c_i \quad (6)$$

Here c_A is the concentration of analyte A, I_A is the analyte peak area, S_{iA} is sensitivity of the analyte with respect to internal standard and c_i is the concentration of the internal standard [193]. In this work gallium (Ga) was used as an internal standard. Direct analysis of the SRP would result in improving the detection limit (DL) of the proposed methodology [192]. The DL was calculated using the equation:

$$\text{DL} = 3 \times (\sqrt{I_B/I_A}) \times c_A \quad (7)$$

Here I_B denotes the background area below the peak. I_A and c_A have been defined in equation (6). Exactly 50 μL of SRP phase along with 10 μL of 10 $\mu\text{g mL}^{-1}$ Ga solution was deposited on the quartz support and dried on a hot plate at 100 $^{\circ}\text{C}$. Then the quartz sample support was placed in a Muffle furnace at 650 $^{\circ}\text{C}$ for 30 min. After 30 min of oxidative pyrolysis the quartz sample support was taken out, cooled and placed in the TXRF instrument for measurement.

5.5. Complexation study between U(VI) and TSIL

Prior knowledge to the interaction mechanism between U(VI) and the TSIL will be helpful in understanding the effects of various parameters on CPE of U(VI), thereby facilitating the designing of a selective CPE procedure for U(VI). The liquid-liquid extraction studies of U(VI) at different HNO_3 concentrations by TSIL in butyltrimethylammonium bis(trifluoromethylsulfonyl)imide, $[\text{Me}_3\text{NBu}][\text{NTf}_2]$ were carried out to see the effect of acid concentration on extraction mechanism. A log-log plot of distribution ratio of U(VI) (D_U) vs. HNO_3 concentration is shown in **Figure**

5.7. This figure reveals two different straight lines fits with positive and negative slopes at higher and lower acidity respectively.

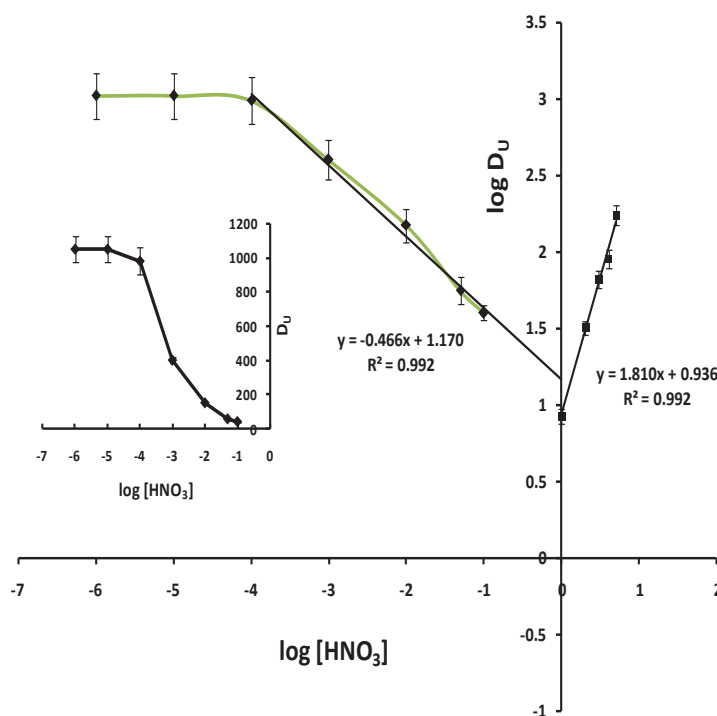


Figure 5.7. Log-log plot between the distribution ratio of U(VI) (D_U) and the concentration of the HNO_3 in the aqueous phase when extracted by TSIL in $[Me_3NBu][NTf_2]$.

This indicates solvation or ion-pair extraction mechanism at high acidity (1.0 – 5.0 mol L^{-1}) and a cation exchange mechanism at lower acidity (0.1 – $1 \times 10^{-6} \text{ mol L}^{-1}$) [143,144]. In addition, at lower acidity a plateau was observed below $1 \times 10^{-4} \text{ mol L}^{-1}$ HNO_3 concentration, which is a typical behavior of cation exchange extraction mechanism. As evident from **Figure 5.7**, the higher D_U values at lower acidity (approximate pH range 3–6) compared to the higher acidity indicates that this TSIL should be applicable at pH values typical for use in CPE systems. Hence, we have focused on determining the exact U(VI)-TSIL complex structure in low acidic medium which will help in designing a selective CPE technique for U.

Isothermal calorimetric titrations (ICT) were carried out between TSIL and U(VI) in 1:1 water/acetonitrile mixture at lower (0.01 mol L^{-1}) and higher (2.0 mol L^{-1}) HNO_3 concentrations. The analysis of the calorimetric data was similar to that described in Rawat et al [105]. The variations of heat flow in terms of power vs. time for both the experiments are shown in **Figure 5.8**. Using the data from these graphs, a plot of heat of reaction per mole of U(VI) ion (h_{vi}) vs. number of TSIL bound per U(VI) ion (n_{avg}) was generated and is represented in **Figure 5.9**. A linear relationship between h_{vi} and n_{avg} was observed for both the experiment up to n_{avg} equals to 2. Thus, under both these experimental conditions the TSIL forms only 1:2 U(VI)-TSIL complex. Beyond n_{avg} expected value of 2 no increase in h_{vi} value was observed and the plot becomes parallel to the X-axis, which confirms that maximum two TSIL molecule can bind to each U(VI) ion. However, the complexation mechanism was found to be exothermic in nature at lower as well as higher acidity, with much higher energy released (**Figure 5.9**) at lower acidity ($-75.7 \pm 0.3 \text{ kJ mole}^{-1}$) compared to higher acidic medium ($-38.7 \pm 0.2 \text{ kJ mole}^{-1}$). The release of this excess heat energy explains higher D_U values of U, particularly at lower acidity.

The above information along with ^{31}P NMR spectroscopy, IR spectroscopy and ESI-MS analysis of the U(VI)-TSIL complex (obtained by reacting 1:2 moles of U(VI) and TSIL in 1:1 0.02 mol L^{-1} HNO_3 /acetonitrile mixture followed by evaporating the solvent at reduced pressure) demonstrate the bonding patterns in that complex as discussed below. The ^{31}P NMR spectrum of U(VI)-TSIL complex shown in **Figure 5.10** shows that the singlet at -11.887 ppm of pure TSIL (**Figure 5.4**) undergoes a downfield shift to 0.761 ppm after complexing with U(VI) ion. The downfield shift is

a reflection of delocalization of electrons over the P=O group of the TSIL which is bonded to U(VI) via O-atom of P=O group.

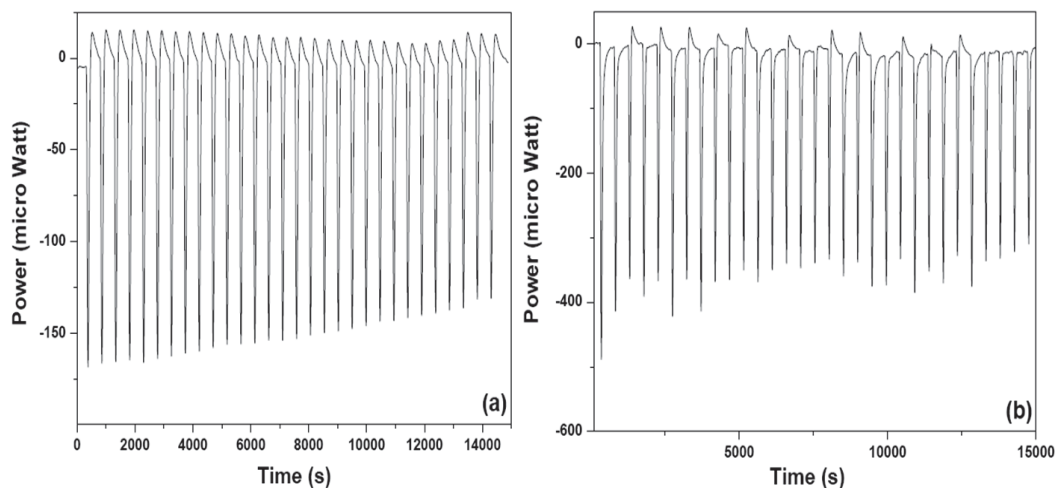


Figure 5.8. The peaks of power (micro watt) vs. time (s) graph for ICT experiment: (a) titration of U(VI) in 1:1 mixture of 4.0 mol L⁻¹ HNO₃ and acetonitrile and (b) titration of U(VI) in 1:1 mixture of 0.02 mol L⁻¹ HNO₃ and acetonitrile with TSIL in 1:1 water/acetonitrile mixture.

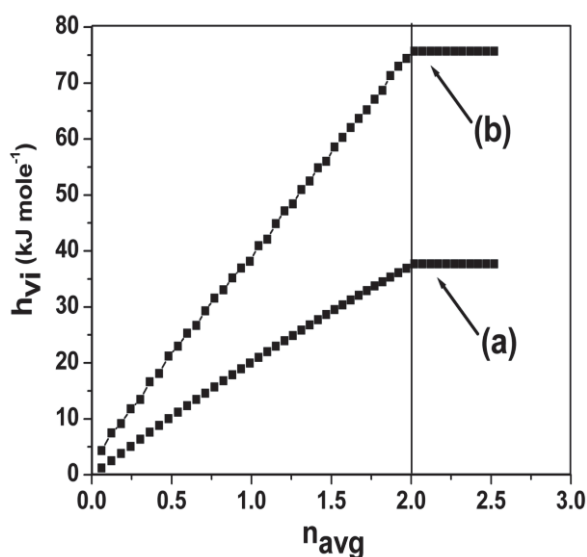


Figure 5.9. Plot of heat of reaction per mole of U(VI) ion (h_{vj}) vs. number of TSIL bound per U(VI) ion (n_{avg}) of the same reactions described in Figure 5.8.

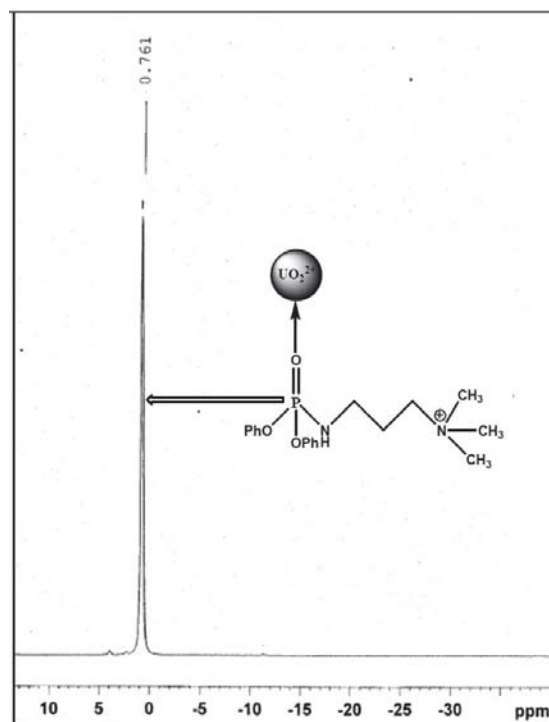


Figure 5.10. ^{31}P NMR spectrum of U(VI) -TSIL complex.

The IR spectrum of the complex, shown in **Figure 5.11** also proves this fact as $\text{P}=\text{O}$ stretching vibration of pure TSIL (**Figure 5.5**) shifts from 1230 cm^{-1} to 1132 cm^{-1} upon coordination to U(VI) ion [194]. The strong peak at 927 cm^{-1} corresponds to the $\text{U}=\text{O}$ stretching frequency of UO_2^{2+} ion and the $\text{P}-\text{O}-\text{C}$ vibration at 1053 cm^{-1} does not change even after coordination. The broad peak at 3420 cm^{-1} (**Figure 5.11**) indicates the presence of coordinated H_2O molecules in the UO_2^{2+} -TSIL complex. The ion exchange extraction mechanism of UO_2^{2+} by TSIL from low HNO_3 medium indicates no involvement of NO_3^- ion in the inner-sphere complexation and hence the remaining four coordination sites of UO_2^{2+} (maximum coordination number is six) would be occupied by four H_2O molecules. This corroborates the interaction of NTf_2^- ion of the TSIL with the hydrated UO_2^{2+} ions through H-bonding. It was previously reported in the literature that NTf_2^- ion cannot interact directly with the UO_2^{2+} ion in the inner coordination sphere while it interacts with hydrated UO_2^{2+} through H-bonding

forming an outer-sphere complex [91]. This statement is supported by the ICT experimental results. According to the literature, each H-bonding in water releases about $9.80 \text{ kJ mole}^{-1}$ of heat [195]. Therefore, if we consider four H-bonds in each UO_2^{2+} -TSIL complex, the excess heat released at low acidity would be (4×9.80) or $39.2 \text{ kJ mole}^{-1}$ and this value is in approximation with the excess heat observed in ICT experiments. Based on all these findings, the complex between UO_2^{2+} and TSIL in low acidic medium was proposed as $[(\text{UO}_2)(\text{OH}_2)_4(\text{phamdNMe}_3)_2(\text{NTf}_2)_2]^{2+}$. The proposed structure of the complex between UO_2^{2+} and TSIL is shown in **Figure 5.12**.

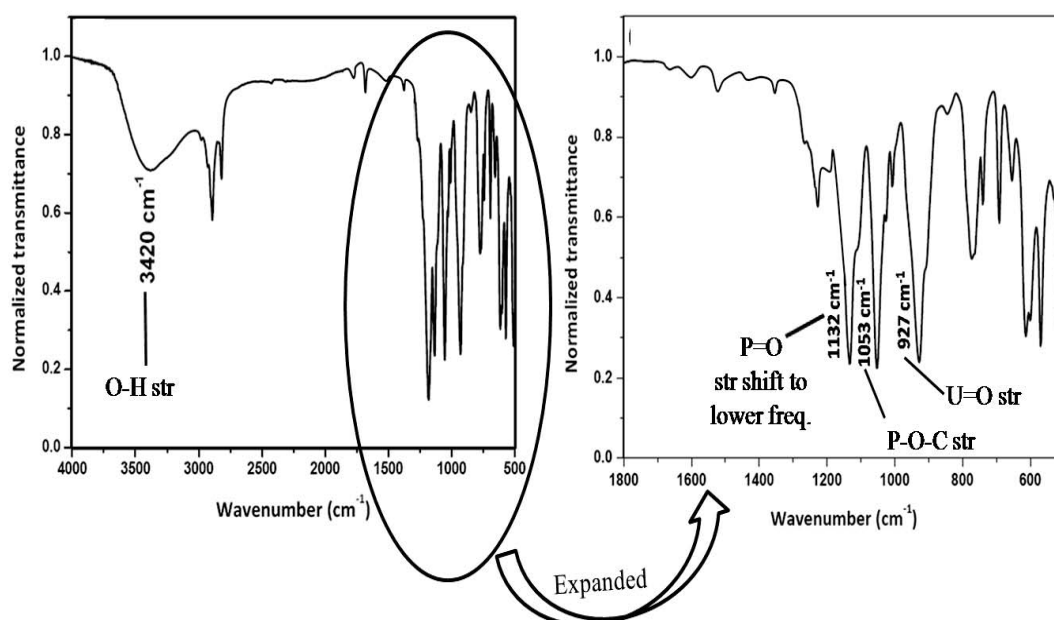


Figure 5.11. IR spectrum of U(VI)-TSIL complex.

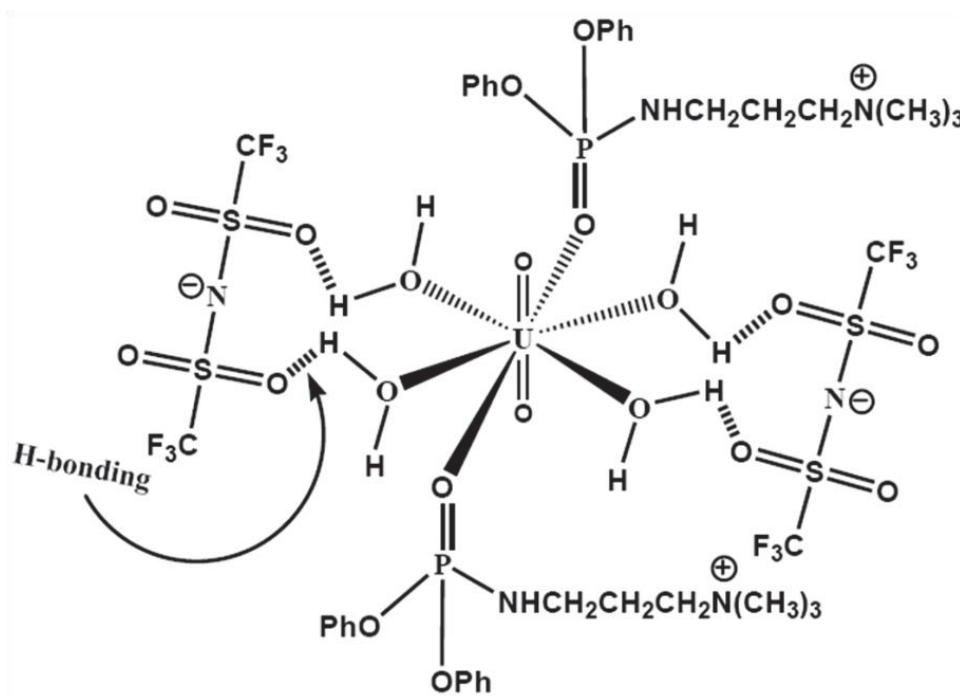


Figure 5.12. Proposed structure of the complex between U(VI) and TSIL.

The ESI-MS spectrum of the UO_2^{2+} -TSIL complex was recorded in acetonitrile medium and is shown in **Figure 5.13**. The spectrum reveals mass peak at m/z 800.2289 corresponding to the $[(\text{UO}_2)(\text{OH}_2)_4(\text{phamDNMe}_3)_2(\text{NTf}_2)_2]^{2+}$ (exact mass 1600.2526 amu) complex. The base peak at m/z 260.2200 and another mass peak at m/z 440.2245 are the $[(\text{UO}_2)(\text{OH}_2)_4(\text{phamDNMe}_3)_2]^{4+}$ and $[(\text{UO}_2)(\text{OH}_2)_4(\text{phamDNMe}_3)_2(\text{NTf}_2)]^{3+}$ fragments respectively of the UO_2^{2+} -TSIL complex.

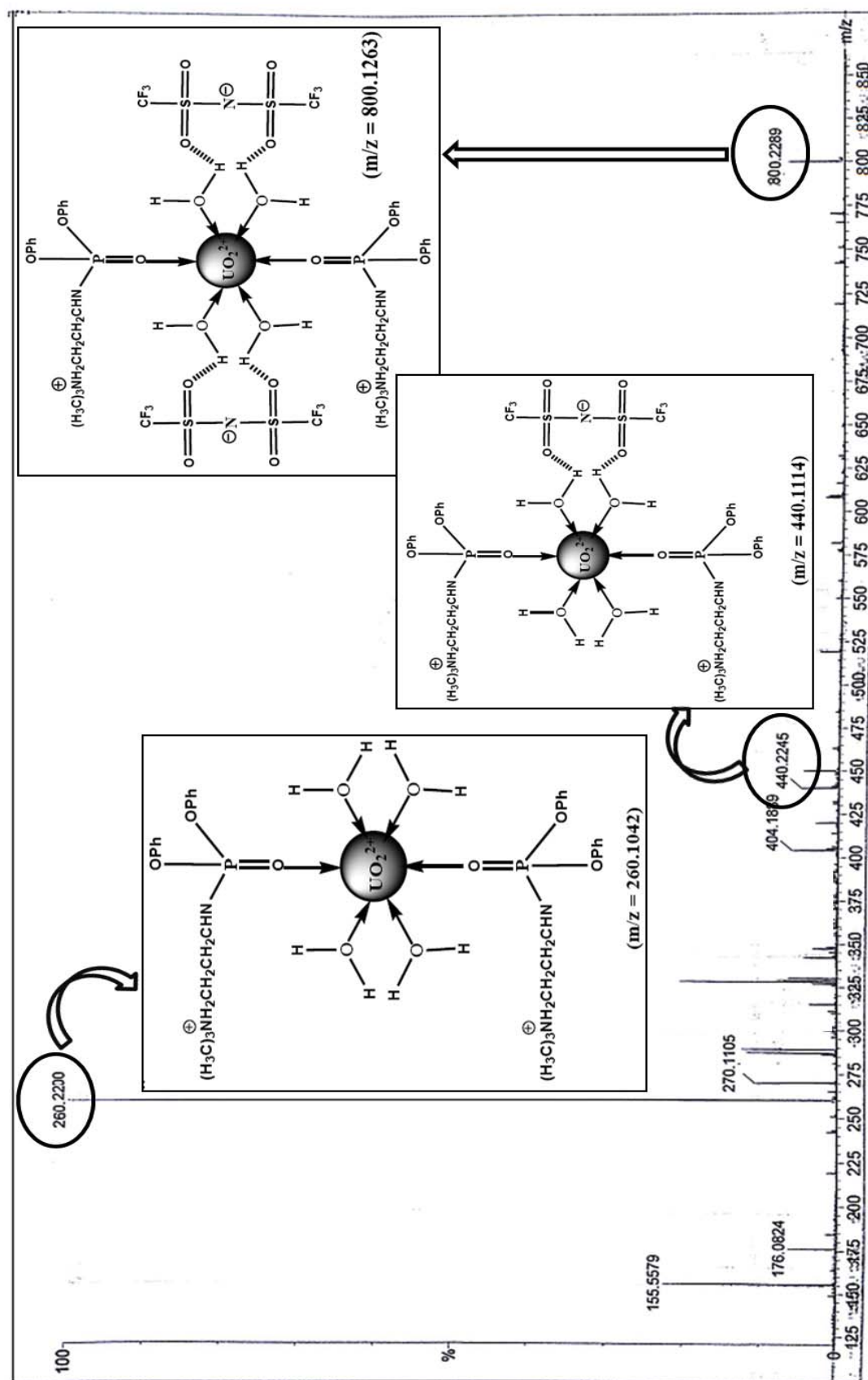


Figure 5.13. ESI-MS spectrum of UO_2^{2+} -TSIL complex in acetonitrile.

5.6. Optimization of CPE conditions

As discussed in the **chapter 3 (section 3.5)**, the similar cross-optimization method was adopted here to optimize various CPE conditions in order to get maximum percentage EE, percentage recovery and preconcentration factor (PF) of U. All experiments were carried out by taking 10 ng mL⁻¹ of U in the aqueous phase. The optimized CPE conditions of the aqueous phase before coacervation of micelles are presented in **Table 5.1**.

Table 5.1. *Optimized conditions of CPE procedure for total 10 mL aqueous phase before coacervation*

| Parameters | Optimized conditions | Units |
|-------------------------------|----------------------|----------------------|
| Sample volume | 7.5 | mL |
| pH | 6.0 | --- |
| [TTX-114] | 5.0 | mmol L ⁻¹ |
| [SDS] | 0.12 | mmol L ⁻¹ |
| [TSIL] | 0.4 | mmol L ⁻¹ |
| [KNO ₃] | 0.1 | mol L ⁻¹ |
| T _{extraction} | 4-5 | °C |
| t _{extraction} | 30 | min |
| T _{phase separation} | 50 | °C |
| t _{phase separation} | 30 | min |
| Centrifugation | 4000 | rpm |

5.6.1. Effect of pH

Initially, the recovery of U by CPE was studied in the pH range of 1-10. The variations in the recovery as a result of pH change are represented in **Figure 5.14**. The recovery was found to be as low as $\leq 10\%$ in the pH range of 1-2, but increased gradually with increase in pH and the maximum values were obtained in the pH region of 5.5-7.5. With further increase in pH, the recoveries were found to deteriorate due to the formation of non-extractable hydroxide, carbonate and/or

bicarbonate complexes of U in aerobic conditions at these pH values. Hence pH 6 was fixed for maximum analyte recovery. The pH dependent variation of U recovery is explained as follows.

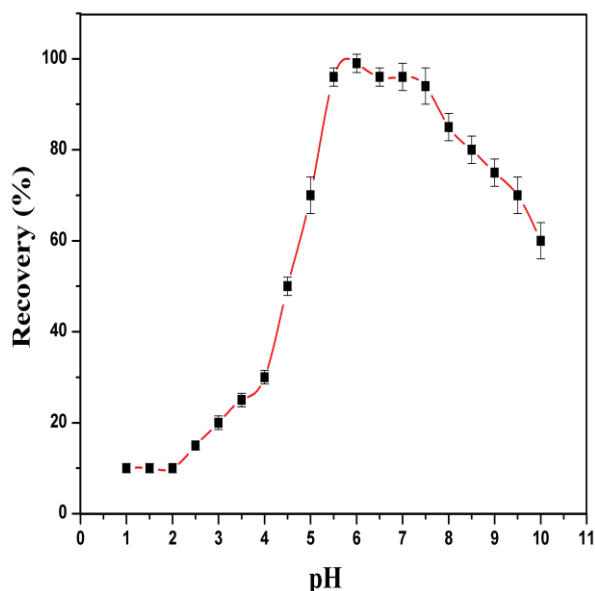


Figure 5.14. Effect of pH on the recoveries of 10 ng mL^{-1} of U. Other parameters were kept constant as presented in Table 5.1.

Previously it was reported in the literature that pH affects the CMC and size of the micelles of non-ionic surfactant [145]. The CMC was reported to increase with decreasing pH of the solution. Therefore, higher concentration of surfactant will be needed to accommodate maximum amount of metal-ligand complexes for optimum recovery at lower pH compared to higher pH region. On the other hand, the hydrated volume of the micelle is known to increase with lowering the pH due to increase in H-bonds between water molecules and etheral 'O' atoms of non-ionic surfactant in the micellar corona [145]. Hence, it can be expected that the S=O group of NTf_2^- and the P=O group of the TSIL are largely involved in H-bonding with those water molecules at low pH conditions. In addition to these two factors, the competition between H^+ and UO_2^{2+} to get extracted by cation exchange mechanism resulted in very low

recovery of U in the pH region of 1-2. With increase in pH the CMC, hydrated volume of micelles and competition between H^+ and UO_2^{2+} to get extracted were decrease, which resulted in higher recovery of U beyond pH 2.

5.6.2. Effect of non-ionic surfactant concentration

Non-ionic surfactant being the building block of CPE process, its concentration is a vital parameter towards metal ion recovery. The low theoretical CPT of TTX-114 solution (CPT: 23-25 °C) above its CMC (0.2-0.35 mmol L⁻¹) makes its widespread use as the non-ionic surfactant in CPE procedure of many metal ion [88]. The concentration of the non-ionic surfactant should be sufficient to trap maximum UO_2^{2+} -TSIL complex and at the same time it should result in minimum SRP volume to achieve higher PF value. The concentration of TTX-114 was varied from 2-10 mmol L⁻¹ as shown in **Figure 5.15** and maximum recovery was found beyond 4 mmol L⁻¹. Therefore, 5 mmol L⁻¹ of TTX-114 was chosen as the optimum value for further experiments.

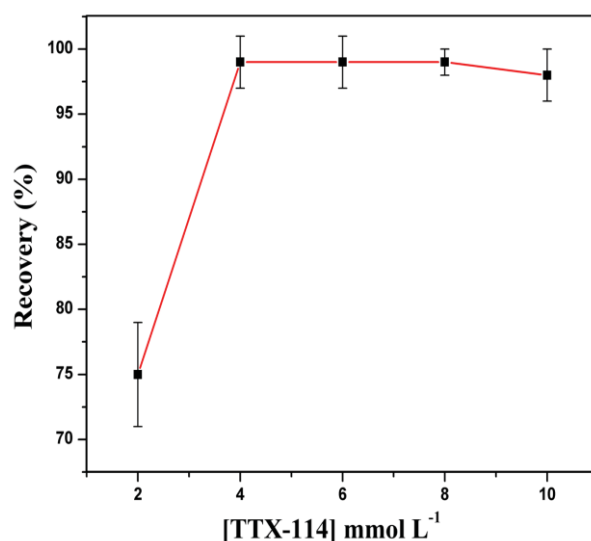


Figure 5.15. Effect of TTX-114 concentration on the recoveries of 10 ng mL⁻¹ of U. Other parameters were kept constant as presented in Table 5.1.

5.6.3. Effect of TSIL concentration

In the present work, phosphoamidate group bearing TSIL was employed as the reagent to develop new CPE methodology for U. The effect of TSIL concentration on the recovery of U was studied from 0.05 to 0.5 mmol L⁻¹. The recovery values are plotted against TSIL concentration in **Figure 5.16** which reveals that optimized recovery of $\geq 98\%$ was obtained at and above 0.3 mmol L⁻¹ of TSIL. Therefore, 0.4 mmol L⁻¹ concentration of TSIL was fixed for further experiments.

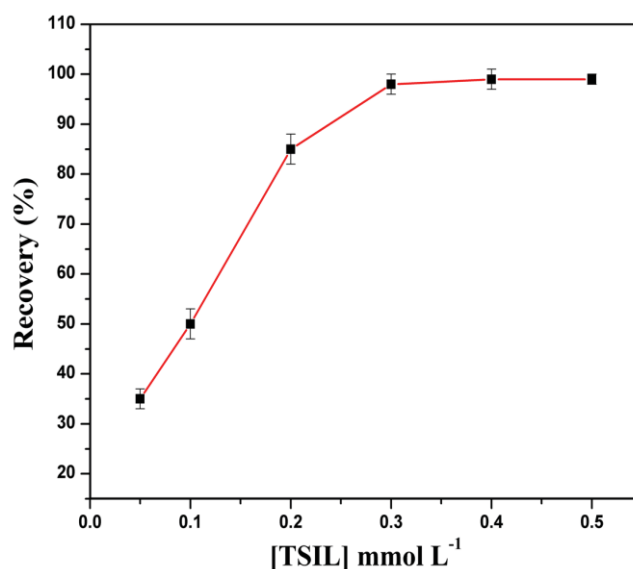


Figure 5.16. Effect of TSIL concentration on the recoveries of 10 ng mL⁻¹ of U. Other parameters were kept constant as presented in Table 5.1.

The non-requirement of any counter ion for inner sphere complexation between the UO₂²⁺ and TSIL in low acidic medium is the greatest advantage of using TSIL in CPE of U. On the other hand the complexation involves anionic part of the TSIL viz., NTf₂⁻ in the outer sphere coordination. Since the polar groups of the ligands protrude towards the hydrophilic part of the surfactants [85], it can be demonstrated that the interaction between the UO₂²⁺ ions and the P=O groups of TSIL takes place in the

micellar corona, as shown in **Figure 5.17**. Thus NTf_2^- must be present in the micelle corona for effective extraction of U. It was reported that by increasing the hydrophobicity of the cationic part of IL, a part of the cation will penetrate into the micelle attracting more NTf_2^- to penetrate into the micelle [91]. The zeta potential (ζ) measurement of the aggregates formed by 5 mmol L^{-1} TTX-114 in absence and presence of the TSIL (0.4 mmol L^{-1}) was found to be $-2 \pm 1 \text{ mV}$ and $-42 \pm 4 \text{ mV}$ respectively at 10°C . These results confirm the penetration of the NTf_2^- in the micelles and their distribution in the micellar corona.

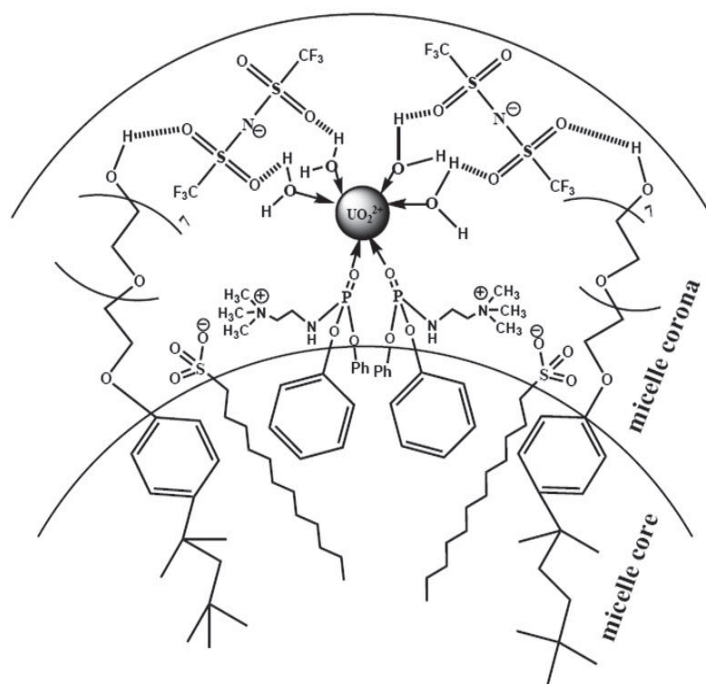


Figure 5.17. Proposed mechanism of selected CPE of UO_2^{2+} by TSIL.

5.6.4. Effect of ionic surfactant concentration

The effect of SDS concentration on the recovery of U was studied in the range of 0 to 0.3 mmol L^{-1} . The variations on the recovery of U with increasing SDS concentration are represented in **Figure 5.18**. It was observed that in absence of SDS the maximum recovery of U was as low as $\sim 10\%$. The cation exchange mechanism which is the

mode of metal ion extraction at pH conditions gets hampered by the high hydrophobicity of the TSIL. The addition of small quantity of SDS was found to drastically increase the recovery of U (**Figure 5.18**) by allowing the cation exchange mechanism through its hydrophilic Na^+ ion counterpart. In addition, the electrostatic attraction between the anionic part of SDS and the cationic UO_2^{2+} -TSIL complex (**Figure 5.17**) allows the extraction of the metal complex into the hydrophobic micellar core as a neutral moiety. Maximum recovery of $\geq 98\%$ was obtained in the range $0.1\text{--}0.2\text{ mmol L}^{-1}$ of SDS. Beyond 0.2 mmol L^{-1} SDS concentration, the recovery of U was further found to decrease drastically (**Figure 5.18**). At higher SDS concentration, the greater electrostatic repulsion between the same charge moieties increases the cloud point temperature (CPT) and this could be the reason for decrease in recovery values as previously suggested by Gu et al. [94]. Therefore, the concentration of SDS was fixed at 0.12 mmol L^{-1} .

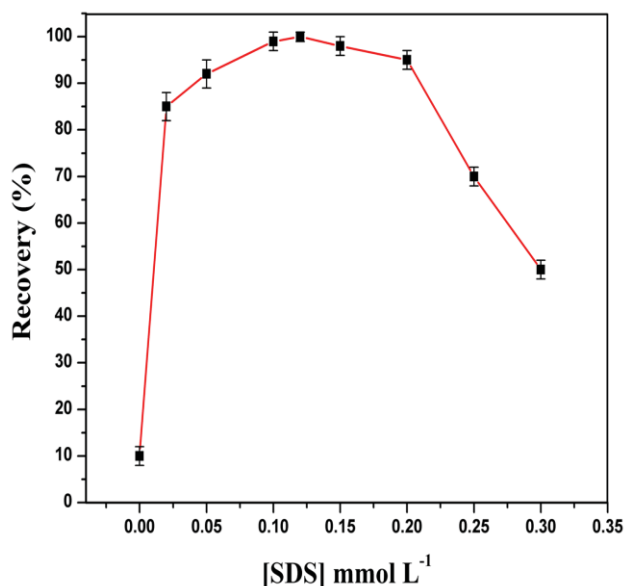


Figure 5.18. Effect of SDS concentration on the recoveries of 10 ng mL^{-1} of U. Other parameters were kept constant as presented in Table 5.1.

5.6.5. Effect of electrolyte concentration

Potassium nitrate (KNO_3) was added to the micelle solution in order to maintain its ionic strength, which has a direct impact on CPT of the system. The addition of TSIL and SDS to the micelle solution of TTX-114 is expected to increase the CPT of the system. In absence of KNO_3 the CPT of the system becomes 58 ± 2 °C. Such high CPT is difficult to handle, as it increases the possibility of resolubilization of the SRP during the centrifugation process which will directly affect the recovery values. In addition, the electrolyte also acts as a salting-out agent which forces the metal-ligand complex formation inside the micelles. The addition of minimum amount of 0.01 mol L^{-1} KNO_3 to the solution brings the CPT down to 35 ± 1 °C and resulted in 85% recovery of U. The amount of KNO_3 was then increased to obtain the maximum recovery of U and the results are shown in **Figure 5.19**. A 0.1 mol L^{-1} concentration of KNO_3 was found to be sufficient for maximum analyte recovery. At a concentration of 0.1 mol L^{-1} of KNO_3 solution, the CPT of the system was found to be 26 ± 1 °C which was obtained by visually observing the clear surfactant solution to get opaque above a particular temperature when we started heating the solution from 20 °C in step of 1 °C. When the temperature was decreased in a same manner, the solution was found to become clear just below that particular temperature.

5.6.6. Effect of temperature

Due to the exothermicity of UO_2^{2+} -TSIL complexation, the incubation temperature was primarily kept at 4-5 °C. The centrifuge tubes were kept at this temperature for 30 min to ensure maximum extraction of U. It was reported in the literature, that phase separation at temperatures higher than the CPT results in higher PF values by decreasing the SRP volume [99]. In order to have minimum SRP volume, the phase

separations were carried out at various temperatures ranging from its CPT to 60 °C for 30 min. This was followed by centrifugation at 4000 rpm for 5 min. Optimal recoveries of U were observed every time but the minimum SRP volume of 0.1 mL was obtained at and above 50 °C. Hence the extraction of metal ion was carried out at 4-5 °C with constant stirring, whereas the phase separation was carried out at 50 °C.

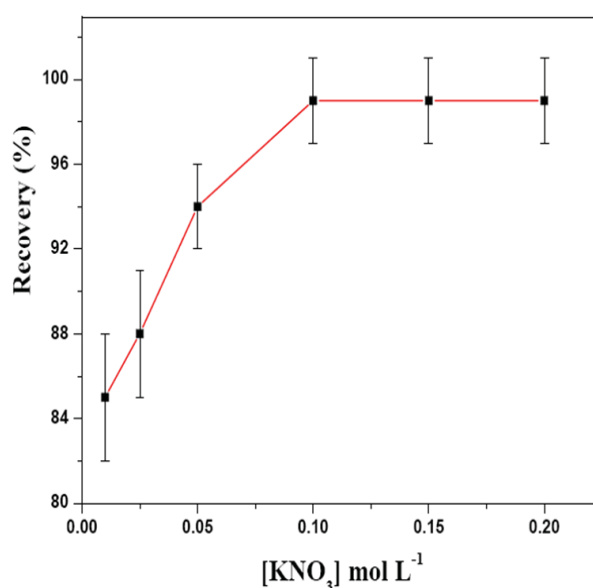


Figure 5.19. *Effect of KNO₃ concentration on the recoveries of 10 ng mL⁻¹ of U. Other parameters were kept constant as presented in Table 5.1.*

5.7. Optimization of TXRF spectrometric procedure

The recovery values of U were calculated using equation (6) after direct analysis of the SRP in TXRF spectrometer. Firstly, the SRP along with Ga (internal standard) solution was deposited on quartz sample support and dried at 100 °C to carry out the TXRF measurement. This resulted in the method detection limit (MDL) of U to be 1.0 ng mL⁻¹ using equation (7). The TXRF spectrum of the sample is shown in **Figure 5.20** (black line) which reveals that the scattered background is very large. This scattered background, which deteriorates the MDL of U appears due to the presence

of significant amount of low atomic number constituent elements of surfactants and TSIL. Minimization of the scattered background can improve the MDL value and can be done by removing the organic layer without affecting the metal ions. Therefore, oxidative pyrolysis of the SRP was carried out by keeping the quartz sample support into a Muffle furnace at 650 °C for 30 min. In this way all C and H atoms get oxidized to the CO₂ and water vapour leaving behind the metal ions on the quartz support. Analysis of this sample quartz support resulted in drastic reduction of the background in the TXRF spectrum, as shown by the red line in **Figure 5.20**. The MDL obtained after carrying out pyrolysis of the sample was 0.02 ng mL⁻¹.

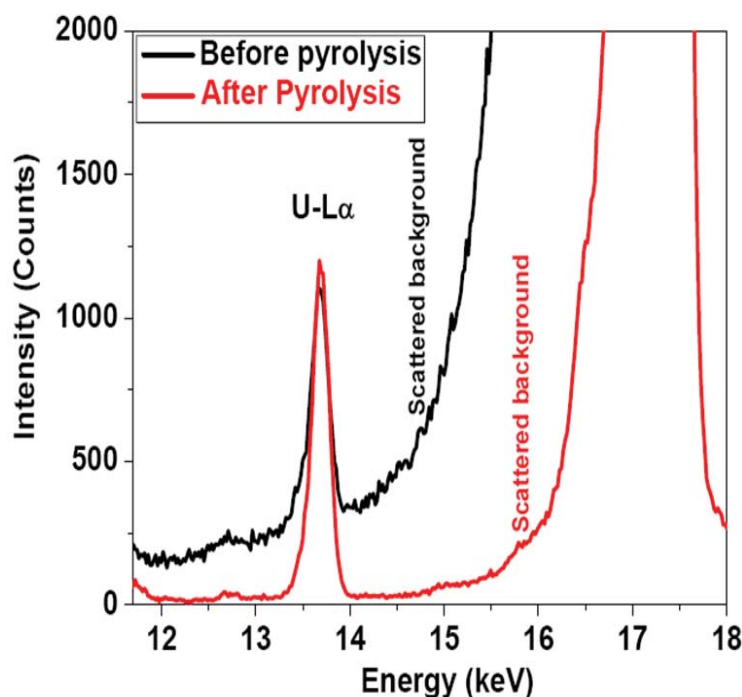


Figure 5.20. TXRF spectra of 50 µL SRP phase deposited on quartz sample support before the pyrolysis (black) and after the pyrolysis (red).

5.8. Impact of common interfering ions on CPE

The proposed CPE procedure was optimized for synthetic U(VI) solution, which did not resemble the actual samples. In reality the environmental samples are complex

matrices of various commonly available cations and anions at higher concentrations than the analyte of interest. Therefore, implementation of preconcentration methodology for any specific metal ion in environmental samples requires recovery studies in presence of common interfering ions. These interfering ions can affect the CPE procedure either by altering the CPE parameters or by competing with the specific metal ion in the extraction process. These ions were tested individually along with 10 ng mL^{-1} of U in the solution. The maximum tolerable concentration of each individual interfering ion was arrived at when the recovery of U was $\geq 95\%$ in its presence. The maximum tolerable limits of various common interfering ions which do not affect the recovery of U are represented in **Table 5.2**. Even though the alkali metals are not expected to be extracted by the TSIL due to their low oxidation state, it is necessary to carry out the recovery studies of U in their presence due to their high abundance in nature. It was observed that a maximum of $10000 \text{ } \mu\text{g mL}^{-1}$ of Li^+ , Na^+ or K^+ ions were found to have no adverse effect on the developed CPE methodology. The higher charge density of alkaline earth and transition metal ions enables them compete with UO_2^{2+} ion towards extraction by various ligands. However, an optimal recovery of U in their presence was obtained due to the unique complexation pattern of the TSIL with UO_2^{2+} (**Figure 5.17**) which provides a soft template of supramolecular recognition in the micelles [91]. The selectivity of the proposed methods towards U was found to remain unaffected in presence of $100 \text{ } \mu\text{g mL}^{-1}$ of La^{3+} , Ce^{4+} , Eu^{3+} or Tb^{3+} (**Table 5.2**). Due to their higher coordination numbers, lanthanides are expected to form bulky complexes which are not expected to form in the micelles due to steric hindrance. Due to the low concentrations of Zr^{4+} , Hf^{4+} and Th^{4+} in natural aquifers, their effect was studied upto 100 ng mL^{-1} . The results showed no effect of these elements on U recovery. High concentrations of some common

anions (**Table 5.2**) like, carbonate (CO_3^{2-}), phosphate (PO_4^{3-}), sulphate (SO_4^{2-}), chloride (Cl^-) and bromide (Br^-) were also observed to have no effects on the quantitative recovery of U. The CPE procedure was studied in presence of 100 $\mu\text{g mL}^{-1}$ humic acid (in the form of its sodium salt), the most abundant organic acid in nature, and the recovery of U was found unaffected.

Table 5.2. *Tolerance of the method to common interfering metal ions (experiments carried out with 10 ng mL⁻¹ of U)*

| Metal ion (M^{n+}) | Tolerance limit ($\mu\text{g mL}^{-1}$) |
|---|--|
| Li^+ , Na^+ , K^+ | 10000 |
| Mg^{2+} , Ca^{2+} , Sr^{2+} , Ba^{2+} | 1500 |
| Al^{3+} | 100 |
| Cr^{3+} , Fe^{3+} | 50 |
| Ni^{2+} , Mn^{2+} , Co^{2+} , Cu^{2+} | 200 |
| Hg^{2+} | 0.2 |
| Cd^{2+} , Pb^{2+} | 200 |
| La^{3+} , Ce^{4+} , Eu^{3+} , Tb^{3+} | 100 |
| Cl^- , Br^- | 10000 |
| CO_3^{2-} , PO_4^{3-} , SO_4^{2-} | 1500 |

Note: Cations were prepared using their chloride or nitrate salts. Anions were prepared using their sodium or potassium salts.

5.9. Analytical figures of merit

The values of certain important terms like percentage EE, PF, percentage recovery, MDL, dynamic linear concentration range (DLR) and relative standard deviation (RSD) etc., which are characteristic of the proposed CPE procedure, are represented in **Table 5.3**. Both the percentage EE and PF values were calculated by determining the U concentration in the supernatant using ICP-MS. The analytical figures of merit of the proposed methodology are compared with the previously reported CPE procedures of U in the same **Table 5.3**. Though a large number of studies on CPE of U are reported [32,56,89,90,95-100], only a few of them [32,89,98] have reported the

EE values in the CPE methods. The EE of any preconcentration procedure determines how efficiently the analyte of interest separates out from the bulk aqueous media to the extracting phase. In this work we had reported quantitative EE of $99.0 \pm 0.5\%$. The PF value of 99 of the proposed CPE methodology is not the highest reported one but surely is in the higher side of the reported CPE procedures for U. It can be seen from **Table 5.3** that offline pairing of CPE procedure with TXRF spectrometry provides much better MDL value of U compared to most of the other reported methodologies [56,89,90,95-100] except for one report where sophisticated and highly sensitive ICP-MS technique [32] was used. The wide dynamic linear concentration range (DLR) of $0.1\text{-}1000\text{ ng mL}^{-1}$ also makes this technique superior to most of the reported ones [56,89,90,95-100]. The minimum value of DLR was calculated from the equation of limit of quantification (LOQ) i.e., $10 \times (\sqrt{I_B/I_A}) \times c_A$. The developed CPE methodology showed good resilience to higher concentrations of common interfering ions and to the best of our knowledge, it is the first work to report such high tolerance limits for lanthanides.

Table 5.3. Comparison of the important CPE characteristics of the developed method for U with reported methodologies

| Ion(s) | Instruments | DLR (ng mL ⁻¹) | EE (%) | Recovery (%) | PF | RSD (%) | MDL (ng mL ⁻¹) | References |
|--------------------------------|-------------|-------------------------------|----------|-----------------|------|------------|-------------------------------|--------------|
| U(VI) | TXRF | 0.1-1000 | 99.0±0.5 | ≥ 98 | 99 | ≤ 4 | 0.02 | Present work |
| U(VI) | ICP-MS | 0.01-1000 | 99.5±0.5 | 99 | 92 | 4 | 0.003 | [32] |
| U(VI)-Th(IV)- Zr(IV)-Hf(IV) | ICP-OES | 2.5-1240 | N.P. | N.P. | 37 | <6.1 | 1.0 | [99] |
| U(VI) | UV-Vis | N.P. | N.P. | 98 | 100 | 5.1 | 1.1 | [95] |
| U(VI) | UV-Vis | 15-300 | N.P. | 98 | 62 | <3.7 | 11 | [96] |
| U(VI) | UV-Vis | N.P. | N.P. | 98-105 | 50.4 | N.P. | N.P. | [56] |
| U(VI) | UV-Vis | 0.18-10 | N.P. | N.P. | 14.3 | 3 | 0.06 | [90] |
| U(VI) | UV-Vis | 6-10 | N.P. | 105 | N.P. | 9 | 2 | [97] |
| U(VI) | LSC | N.P. | 55 | 55 | N.P. | 10 | 1.42x10 ⁵ | [98] |
| U(VI) | ICP-OES | N.P. | 99 | >98 | 122 | N.P. | N.P. | [89] |
| U(VI) | UV-Vis | 80-1600 | N.P. | N.P. | 14.3 | 74.6 | 3.6 | [100] |

N.P. = Not present

5.10. Analysis of certified reference material and real water sample

A CRM viz., NIST SRM 1640a natural water, was analyzed for its U concentration in order to validate the proposed analytical technique. The result is given in **Table 5.4**. The determined value is in agreement with the certified value at 95% confidence interval. Thereafter, the methodology was applied to determine U in three natural water samples employing standard addition. These studies are also shown in **Table 5.4**. The results reported in **Table 5.4** are the average values of three replicate CPE/TXRF measurements of every sample and the standard deviation reported with each value was determined by error propagation. It can be seen that the recovery of U in these samples is $\geq 96\%$.

Table 5.4. Analysis of a CRM and real samples viz., sea water from Mumbai coast, India; well water from West Bengal, India and Spring water from Sikkim, India ($n = 5$)

| Sample | Certified or added U conc. (ng mL ⁻¹) | Analyzed U conc. (ng mL ⁻¹) | Recovery (%) |
|----------------|--|--|--------------|
| NIST SRM 1640a | 25.35±0.27 ^a | 25.5±0.6 | 100±4.0 |
| Sea water | - | 2.7±0.1 | - |
| | 5.0 | 7.5±0.3 | 96±6 |
| | 50.0 | 53.0±1.0 | 101±2 |
| Well water | - | BDL | - |
| | 5.0 | 4.8±0.2 | 96±4 |
| | 50.0 | 49.4±0.5 | 99±1 |
| Spring water | - | BDL | - |
| | 5.0 | 4.9±0.2 | 98±4 |
| | 50.0 | 49.0±0.5 | 98±1 |

^aCertified value; BDL = Below detection limit

5.11. Conclusion

TSIL assisted CPE of U and its detection in the SRP by TXRF spectrometry has been reported for the first time. A novel approach of oxidative pyrolysis of the SRP before TXRF spectrometric analysis was found to improve the detection limit of the

methodology. The quantitative EE of $99.0 \pm 0.5\%$ and PF value of 99 for U indicate that the developed CPE technique could be successfully employed for remediation of U in contaminated waters as well as for its extraction from sources like sea water (on average contains 3 ng mL^{-1} of U). The high resilience of the method towards lanthanides in addition to common interfering ions provides higher selectivity towards U compared to the CPE methodologies reported so far.

Chapter 6

Summary and outlook

This page is kept blank intentionally

6.1. Complete work at a glance

The work presented in this thesis has been aimed at exploring simple organic molecules, functionalized nanoparticles (NPs) and task specific ionic liquids (TSIL) for developing novel cloud point extraction (CPE) procedures to detect ultratrace uranium (U) in environmental aqueous samples by using versatile and cost effective analytical instruments. In the very beginning, we had used a synergistic mixture of commonly known extractants viz., trioctylphosphine oxide (TOPO) and N,N,N',N'-tetraoctyldiglycolamide (TODGA) to simultaneously preconcentrate uranium (U) and thorium (Th) by the CPE procedure. The complexation chemistry of these extractants with metal ions reported in literature helped us in obtaining extraction efficiencies (EEs) of $98.0 \pm 0.5\%$ for U and $99.5 \pm 0.5\%$ for Th. Treatment of preconcentrated solution with arsenazo-III to detect U and Th simultaneously, by the combination of UV-Visible spectrophotometry and partial least square regression analysis resulted in dynamic linear concentration range (DLR) to be $15\text{--}1000 \text{ ng mL}^{-1}$ and $10\text{--}1000 \text{ ng mL}^{-1}$ for U and Th respectively. The preconcentration of analytes via synergistic extractant mixture and their spectrophotometric detection by arsenazo-III offered great tolerance to common interfering ions. To the best of our knowledge, this methodology offers the lanthanide (Ln^{n+} where $n = 3$ or 4) tolerance limit ($[\text{Ln}^{n+}]/[\text{UO}_2^{2+}]$ or $[\text{Ln}^{n+}]/[\text{Th}^{4+}]$) greater than 1 for the first time. The detection limits (DL) of 4.0 and 2.0 ng mL^{-1} for U and Th respectively, are well below the World Health Organization (WHO), United States Environmental Protection Agency (USEPA) and Atomic Energy Regulatory Board (AERB), India guideline values of these analytes when only the natural isotopic composition of these analytes is considered (WHO and USEPA: $[\text{U}] = 30 \text{ ng mL}^{-1}$ and $[\text{Th}]_{\text{calc}} = 68 \text{ ng mL}^{-1}$; AERB, India = 60 ng mL^{-1}) in drinking water.

The increased production of anthropogenic radioisotopes of U has enhanced the risk factors due to their high specific activity values. Thus improvement in the lower limit of quantification (LOQ) and detection limit (DL) values of analytical methodologies becomes important to calculate the actual risk factor. The high molar extinction coefficient, high quantum yield, large surface area and ease of surface functionalization have made nanoparticles (NPs) as better metal ion sensing materials compared to traditional dye sensors to achieve better LOQ and DL values by versatile and cost-effective spectroscopic techniques. Hence, after acquiring the experience on the CPE procedure from our previous work, we had decided to use functionalized NPs as both the extractant and chemosensor for CPE assisted detection of ultratrace U. In this regard, novel diglycolamide-capped CdS/ZnS core-shell QDs was synthesized for the first time. A micellar dispersion of this functionalized QD nanosensor was found to preconcentrate U in water by a factor of 100. A direct Föster Resonance Energy Transfer (FRET) interaction between the QD and UO_2^{2+} ion resulted in DLR and DL values of 1.0-100 and 0.03 ng mL⁻¹ respectively, for U employing fluorometry. The developed dual CPE procedure was found to offer tolerance to high concentrations of common interfering ions and $[\text{Ln}^{n+}]/[\text{UO}_2^{2+}]$ with ratio upto 100. With the availability of portable fluorometers, on-site and real-time environmental monitoring of U could be made feasible by the developed method.

A visual detection kit for U, prepared by maintaining its WHO and USEPA guideline limit (30 ng mL⁻¹) in drinking water is of importance in order to easily differentiate between drinkable and non-drinkable water. In this view, we have synthesized and characterized a novel U(VI)-specific nanosensor viz., 3-mercaptopropionylamidoxime (3-MPD) capped gold NPs (AuNPs). This newly synthesized AuNPs show a

bathochromic shift in its surface plasmon resonance (SPR) absorption spectrum via analyte-triggered aggregation mechanism. The CPE of 3-MPD capped AuNPs in the surfactant rich phase in absence and presence of U(VI) resulted its ultratrace level detection from 2 to 100 ng mL⁻¹ along with its DL value of 0.3 ng mL⁻¹. During this study, the most fascinating change was observed in the colour of surfactant rich phase which showed a bright red colour in absence of U and a blue colour beyond certain concentration of U. By studying the spectral shift parameter and optimizing the sample volume it was possible to develop a visual detection kit for U, which showed different surfactant rich phase (SRP) colours at U concentrations of 30 ng mL⁻¹, less than 30 ng mL⁻¹ and more than 30 ng mL⁻¹ in water sample.

In the final piece of work, the CPE of U by task specific ionic liquid (TSIL) was explored. In this work a new TSIL viz., N-propyl-(diphenylphosphoramidate)-trimethylammonium bis(trifluoromethane-sulfonyl)imide, [phamdNMe₃][NTf₂] was synthesized and characterized for the first time. At low HNO₃ medium, the higher exothermicity of U(VI)-TSIL complexation reaction without involving NO₃⁻ ion motivated us to use this TSIL in CPE of U. Unlike our previous chapter, here we aimed at the improvement of tolerance of the interfering ion concentrations without using any masking agent. This was easily achieved due to the unique complexation pattern between U and TSIL, which was also found to tolerate higher lanthanide concentrations than previous studies via the soft supramolecular recognition of U-TSIL complex in the micelles. Total reflection X-ray Fluorescence (TXRF) spectrometry was employed for the first time to detect the analyte concentration in surfactant rich phase (SRP) of CPE procedure. The small volume requirement of TXRF spectrometric analysis obviates the need for dilution of SRP phase and hence

resulted in DLR of 0.1-1000 ng mL⁻¹ for U. The DL was found to be as low as 0.02 ng mL⁻¹. The quantitative EE of 99.0±0.5% and preconcentration factor (PF) of 99 for U indicates that this CPE methodology can be successfully employed for the remediation of U in contaminated waters.

6.2. Future outlook

The production, use and storage of short lived actinides viz., ^{238,239,240,241,242}Pu, ^{241,243}Am, ²³⁹Np etc., has increased their chances of environmental contamination several times. Since these actinides are also radiotoxic to the living organisms at very low concentrations, their ultratrace level detection is very important. Hence, in near future it will be worthwhile to develop new CPE strategies to preconcentrate these actinide elements for their easy detection. In addition to the ultratrace level detection of toxic elements, their remediation from contaminated water samples is another major challenge due to the enhanced industrialization in recent decades. The adherence of CPE to the principles of 'Green Chemistry' made it as one of the most eco-friendly preconcentration procedures of recent times. Hence, implementation of the developed CPE methodologies for large scale removal of toxic elements from environmental water samples may be explored in our future studies.

References

This page is kept blank intentionally

-
- [1] N. Verma, M. Singh, *BioMetals* 18 (2005) 121–129.
- [2] S. Ge, X. He, J. Zhao, L. Duan, J. Gu, Q. Zhang, W. Geng, *Water Air Soil Pollut.* 228 (2017) 460.
- [3] M. Ahmad, K. Manzoor, S. Ikram, *Int. J. Biol. Macromol.* 105 (2017) 190–203.
- [4] F. R. Peligro, I. Pavlovic, R. Rojas, C. Barriga, *Chem. Eng. J.* 306(2016) 1035–1040.
- [5] F. Fu, Q. Wang, *J. Environ. Manage.* 92 (2011) 407–418.
- [6] G. Aragay, J. Pons, A. Merkoçi, *Chem. Rev.* 111 (2011) 3433–3458.
- [7] H.S. Peavy, D.R. Rowe, G. Tchobanoglous, *Environmental Engineering*, Singapore: McGraw Hill Inc. (1986).
- [8] C.D. Klaassen, Goodman and Gilman's The Pharmacological Basis of Therapeutics, P.B. Molinkoff and R.W. Ruddon, eds., (1996) 1649–1650.
- [9] A. Heidari, H. Younesi, Z. Mehraban, *Chem. Eng. J.* 153(2009) 70–79.
- [10] S. Wang, H. Li, L. Xu, *J. Colloid Interface Sci.* 295 (2006) 71–78.
- [11] V.P. Panov, I. V. Zykova, S. A. Chekrenev, *Fibre Chem.* 40 (2008) 241–245.
- [12] E. Schnug, B. G. Lottermoser, *Environ. Sci. Technol.* 47 (2013) 2433 –2434.
- [13] X. Zhao, N. Song, W. Zhou, Q. Jia, *Cent. Eur. J. Chem.* 10 (2012) 927–937.
- [14] K. Kiran, K. S. Kumar, B. Prasad, K. Suvardhan, L. R. Babu, K. Janardhanam, *J. Hazard. Mater.* 150 (2008) 582–586.
- [15] Y. Zhang, Y. Chen, H. Jiang, X. Wang, *J. Nanosci. Nanotechnol.* 16(2016) 12179–12186.
- [16] B. Wang, J. Hai, Z. Liu, Q. Wang, Z. Yang, S. Sun, *Angew. Chem. Int. Ed.* 49 (2010) 4576 –4579.
- [17] L.J. Mayne, S.D.R. Christie, M. Platt, *Nanoscale* 8 (2016) 19139–19147.
- [18] X. Liu, Y. Zhang, *J. Fluoresc.* 26 (2016) 2267–2270.

- [19] R.K. Sharma, A. Puri, A.Kumar, A. Adholeya, J. Environ. Sci. (China) 25 (2013) 1252–1261.
- [20] P.L. Malvankar, V. M. Shinde, Analyst 116 (1991) 1081–1084.
- [21] T. W Clarkson, Crit. Rev. Clin. Lab. Sci. 34 (1997) 369–403.
- [22] P. Miretzky, A. F. Cirelli, J. Hazard. Mater. 167 (2009) 10–23.
- [23] M. R. Sohrabi, Microchim. Acta 181 (2014) 435–444.
- [24] N. Johri, G. Jacquillet, R. Unwin, Biometals 23 (2010) 783–792.
- [25] S.B. Adeloju, Y. Zhang, Anal. Chem. 81(2009)4249–4255.
- [26] W. Chuachuad, J.F. Tyson, J. Anal. At. Spectrom. 20 (2005) 273–281.
- [27] Y.-L. Hung, T.-M. Hsiung, Y.-Y. Chen, C.-C. Huang, Talanta 82 (2010) 516–522.
- [28] I.-B. Kim, A. Dunkhorst, J. Gilbert, U.H. F. Bunz, Macromolecules 38 (2005) 4560–4562.
- [29] T. Lan, K. Furuya, Y. Lu, Chem. Commun. 46 (2010) 3896–3898.
- [30] C.-T. Yang, J. Han, M. Gu, J. Liu, Y. Li, Z. Huang, H.-Z. Yu, S. Hu, X. Wang, Chem. Commun. 51 (2015) 11769–11772.
- [31] R.H. Lin, L.J. Wu, C.H. Lee, S.Y. Lin-Shiau, Mutat. Res. 319 (1993) 197–203.
- [32] C. Labrecque, S. Potvin, L. Whitty-Léveillé, D. Larivière, Talanta 107 (2013) 284–291.
- [33] E. Ansoborlo, L. Lebaron-Jacobs, O. Prat, Environ. Int. 77 (2015) 1–4.
- [34] WHO: Guidelines for drinking-water quality, 4th ed., Geneva, Switzerland, (2011).
- [35] P. Steier, M. Bichler, L. Keith Fifield, R. Golser, W. Kutschera, A. Priller, F. Quinto, S. Richter, M. Srnecik, P. Terrasi, L. Wacker, A. Wallner, G. Wallner, K.M. Wilcken, E.M. Wild, Nucl. Instr. Meth. Phys. Res. B 266 (2008) 2246–2250.

- [36] M.J. Kristo, S.J. Tumey, Nucl. Instr. Meth. Phys. Res. B 294 (2013) 656-661.
- [37] Q.-H. Hu, J.-Q. Weng, J.-S. Wang, J. Environ. Radioact. 101 (2010) 426–437.
- [38] T. Mathews, K. Beaugelin-Seiller, J. Garnier-Laplace, R. Gilbin, C. Adam, C. Della-Vedova, Environ. Sci. Technol. 43 (2009) 6684–6690.
- [39] G.K. Schweitzer, L.L. Pesterfield, The Aqueous Chemistry of the Elements, Oxford University Press, New York (2010).
- [40] R.K. Dutta, A. Kumar, Anal. Chem. 88 (2016) 9071 –9078.
- [41] C.T. Garten, E.A. Bondietti, R.L. Walker, J. Environ. Qual. 10 (1981) 207–210.
- [42] D.P.S. Rathore, Talanta 77 (2008) 9 –20.
- [43] G. Mathews, N. Nagaiah, M. B. Karthik Kumar, M. R. Ambika, J. Radiol. Prot. 35 (2015) 447–455.
- [44] P. Kurttio, A. Auvinen, L. Salonen, H. Saha, J. Pekkanen, I. Mäkeläinen, S. B Väisänen, I.M. Penttilä, H. Komulainen, Environ. Health Perspect. 110 (2002) 337–342.
- [45] Toxicological profile for uranium, U.S. Department of Health and Human Services (2013).
- [46] N. Pavlakis, C.A. Pollock, G. McLean , R. Bartrop, Nephron. 72 (1996) 313-7.
- [47] L. Vicente-Vicente, Y. Quiros, F. Pérez-Barriocanal, J.M. López-Novoa, F.J. López-Hernández, A.I. Morales, Toxicol. Sci. 118 (2010) 324–347.
- [48] S. Lu, F.Y. Zhao, Health Phys. 58 (1990) 619-23.
- [49] M.J. Thun, D.B. Baker, K. Steenland , A.B. Smith , W. Halperin , T. Berl, Scand. J. Work Environ. Health 11 (1985) 83-90.
- [50] S. V. Gudkov, A. V. Chernikov, V. I. Bruskov, Russ. J. Gen. Chem. 86(2016) 1531-1538.

- [51] Common radionuclides found at superfund sites, EPA facts about uranium, Environmental Protection Agency, US (2002).
- [52] AERB, Drinking water specifications in India, Department of Atomic Energy, Govt. of India (2004).
- [53] J.B. Ghasemi, E. Zolfonoun, *Talanta* 80 (2010) 1191-1197.
- [54] A.M. Starvin, T. Prasada Rao, *Talanta* 63 (2004) 225–232.
- [55] A. Takahashi, Y. Ueki, S. Igarashi, *Anal. Chim. Acta* 387 (1999) 71–75.
- [56] H.S. Ferreira, M.D. Bezerra, S.L.C. Ferreira, *Microchim. Acta* 154 (2006) 163–167.
- [57] Ş. Tokalioğlu, Ş. Kartal, L. Elçi, *Anal. Chim. Acta* 413 (2000) 33-40.
- [58] T.P. Rao, P. Metilda, J.M. Gladis, *Talanta* 68 (2006) 1047-1064.
- [59] M. Ghaedi, M. Montazerozohori, M. Soylak *J. Hazard. Mater.* 142 (2007) 368-373.
- [60] M. Ghaedi, A. Shokrollahi, K. Niknam, E. Niknam, A. Najibi, M. Soylak, *J. Hazard. Mater.* 168 (2009) 1022-1027.
- [61] J. Hassan, S.M. Hosseini, S. Mozaffari, B. Jahanparast, M.H. Karbasi, *J. Braz. Chem. Soc.* 25 (2014) 1086-1090.
- [62] V. Hatzistavros, P. Koulouridakis, N. Kallithrakas-Kontos, *Anal. Sci.* 21 (2005) 823-826.
- [63] D. Schaumlöffel, P. Giusti, M.V. Zoriy, C. Pickhardt, J. Szpunar, R. Yobinski, J. S. Becker, *J. Anal. At. Spectrom.* 20 (2005) 17–21.
- [64] J.S. Becker, M. Burow, S.F. Boulyga, C. Pickhardt, R. Hille, P. Ostapczuk, *Atom. Spectrosc.* 23 (2002) 177-182.
- [65] J.S. Becker, *Trends Anal. Chem.* 24 (2005) 243-254.

- [66] S.A. Kumar, N.S. Shenoy, S. Pandey, S. Sounderajan, G. Venkateswaran, *Talanta* 77 (2008) 422–426,
- [67] E.C. Jung, H.-R. Cho, W. Cha, J.-H. Park, M.H. Baik, *Rev. Anal. Chem.* 33 (2014) 245–254.
- [68] D. Huang, F. Deng, J. He, T. Yu, *J. Radioanal. Nucl. Chem.* 307 (2016) 1359–1363.
- [69] L.H. Jones, R.A. Penneman, *J. Chem. Phys.* 21 (1953) 542–544.
- [70] M. Bühl, N. Sieffert, A. Chaumont, G. Wipff, *Inorg. Chem.* 50 (2011) 299–308.
- [71] S. Cotton, *Lanthanide and Actinide Chemistry*, John Wiley & Sons Ltd, Chichester, England (2006).
- [72] G. Choppin, J.-O. Liljenzin, J. Rydberg, *Behavior of radionuclides in the environment, Radiochemistry and Nuclear Chemistry*, Third edition. Butterworth-Heinemann, London (2002) 653–685.
- [73] S.J. Markich, *Sci. World J.* 15 (2002) 707–729.
- [74] D.R. Palleros, *J. Chem. Educ.* 72 (1995) 319–321.
- [75] C. Hanson, *Recent Advances in Liquid-Liquid Extraction*, Pergamon Press Ltd., Hungary (2013).
- [76] V.K. Jain, R.A. Pandya, S.G. Pillai, P.S. Shrivastav, *Talanta* 70 (2006) 257–266.
- [77] M. Shamsipur, A.R. Ghiasv, Y. Yamini, *Anal. Chem.* 71 (1999) 4892–4895.
- [78] F.A. Aydin, M. Soylak, *Talanta* 72 (2007) 187–192.
- [79] E.P. Horwitz, D.R. Mcallister, A.H. Bond, R.E. Barans, Jr. *solvent extr. Ion Exch.* 23 (2005) 319–344.
- [80] V.N. Epov, K. Benkhedda, R.J. Cornett, R.D. Evans, *J. Anal. At. Spectrom.* 20 (2005) 424–430.

- [81] M.d.A. Bezerra, M.A.Z. Arruda, S.L.C. Ferreira, *Appl. Spectrosc. Rev.* 40 (2005) 269–299.
- [82] W.L. Hinze, E. Pramauro, *Crit. Rev. Anal. Chem.* 24 (1993) 133–177.
- [83] F.H. Quina, W.L. Hinze, *Ind. Eng. Chem. Res.* 38 (1999) 4150–4168.
- [84] E.K. Paleologos, D.L. Giokas, M.I. Karayannis, *Trends Anal. Chem.* 24 (2005) 426–436.
- [85] C.B. Ojeda, F.S. Rojas, *Microchim. Acta* 177 (2012) 1–21.
- [86] J. Miura, H. Ishii, H. Watanabe, *Bunseki Kagaku* 25 (1976) 808.
- [87] Md. S. Noorashikin, N.M. Sohaimi, N. Suda, H.Z. Aziz, S.R.M. Zaini, S. Kandasamy, K. Suresh, *Journal of Sustainability Science and Management* 12 (2017) 79–95.
- [88] D.J. McClements, *Soft Matter* 8 (2012) 1719–1729.
- [89] A. Favre-Régouillon, D. Murat, G. Cote, M. Draya, *J. Chem. Technol. Biotechnol.* 81 (2006) 1872–1876.
- [90] T. Madrakian, A. Afkhami, A. Mousavi, *Talanta* 71 (2007) 610–614.
- [91] S. Gao, T. Sun, Q. Chen, X. J. Shen, *J. Hazard. Mater.* 263 (2013) 562–568.
- [92] L. Koshy, A.H. Saiyad, A.K. Rakshit, *Colloid. Polym. Sci.* 274 (1996) 582–587.
- [93] C. Labrecque, L. Whitty-Léveillé, D. Larivière, *Anal. Chem.* 85 (2013) 10549–10555.
- [94] T. Gu, P.A. Galera-Gómez, *Colloids Surf. A* 104 (1995) 307–312.
- [95] M.E.F. Laespada, J.L.P. Pavon, B.M. Cordero, *Analyst* 118 (1993) 209–212.
- [96] F. Shemirani, R.R. Kozani, M.R. Jamali, Y. Assadi, S.M.R. Milani, *Sep. Sci. Technol.* 40 (2005) 2527–2537.
- [97] J.B. Ghasemi, B. Hashemi, M. Shamsipur, *J. Iran. Chem. Soc.* 9 (2012) 257–262.
- [98] E. Constantinou, I. Pashadilis, *J. Radioanal. Nucl. Chem.* 286 (2010) 461–465.

- [99] S. Shariati, Y. Yamini, A.K. Zanjani, *J. Hazard. Mater.* 156 (2008) 583-590.
- [100] E. Bağda, E. Yabas, N. Karakus, *J. Radioanal. Nucl. Chem.* 299 (2014) 1813–1820.
- [101] R.A. Robinson, R. H. Stokes, *Electrolyte solutions*, 2nd ed., London, Butterworths (1968).
- [102] P.R. Nair, M. Xavier, S.K. Aggarwal, *Radiochim. Acta* 97 (2009) 419-422.
- [103] R.G. Ray, *Collected Papers on Methods of Analysis for Uranium and Thorium: Issues 1004-1006*, U.S. Government Printing Office (1954).
- [104] C.-S. Wu, M.K.K. Oo, X. Fan, *ACS NANO* 4 (2010) 5897-5904.
- [105] N. Rawat, R.S. Sharma, B.S. Tomar, V.K. Manchanda, *Thermochim. Acta* 501 (2010) 13-18.
- [106] A.L. de Souza, M.E.B. Cotrim, M.A.F. Pires, *Microchim. J.* 106 (2013) 194-201.
- [107] EPA facts about thorium, Environmental Protection Agency, US (2002).
- [108] A.S. Amin, M.A. Kassem, T.Y. Mohammad, *RSC Adv.* 5 (2015) 52095-52100.
- [109] B. Gupta, P. Malik, A. Deep, *J. Radioanal. Nucl. Chem.* 251 (2002) 451–456.
- [110] S. Panja, P.K. Mohapatra, S.C. Tripathi, V.K. Manchanda, *J. Membr. Sci.* 337 (2009) 274–281.
- [111] M. Chen, Z. Li, Y. Geng, H. Zhao, S. He, Q. Li, L. Zhang, *Talanta* 181 (2018) 311-317.
- [112] J. Chen, J.C. Wang, *Prog. Chem.* 23 (2011) 1366-1371.
- [113] D. Sandro, F. Mario, M. Anna, B. Livio, *Bull. Chem. Soc. Jpn.* 56 (1983) 904-908.
- [114] S.A. Ansari, P.N. Pathak, V.K. Manchanda, M. Husain, A. K. Prasad, V. S. Parmar, *Solvent Extr. Ion Exch.* 23 (2005) 463-479.

- [115] A. Safavi, H. Abdollahi, M.R.H. Nezhad, R. Kamali, *Spectrochim. Acta A60* (2004) 2897-2901.
- [116] A. Safavi, H. Abdollahi, M.R.H. Nezhad, R. Kamali, *Spectrochim. Acta A60* (2004) 2897-2901.
- [117] M.H. Khan, P. Warwick, N. Evans, *Chemosphere* 63 (2006) 1165-1169.
- [118] M. Khan, A. Ali, N. Khan, *J. Radioanal. Nucl. Chem.* 250 (2001) 353-357.
- [119] J. Uhrovčik, J. Lesný, *HEJ: ENV-120131-A*, 1-7.
- [120] J.A. Perez-Bustamante, F. Palomares Delgado, *Analyst* 96 (1971) 407-422.
- [121] C.-Y. George, X. Mao Chan, I. Choi, A. Sarkar, O.P. Lam, D.K. Shuh, R.E. Russo, *Spectrochim. Acta B* 89 (2013) 40-49.
- [122] A. Sarkar, X. Mao, G.C.Y. Chan, R.E. Russo, *Spectrochim. Acta B* 88 (2013) 46-53.
- [123] E. Constantinou, I. Pashadilis, *J. Radioanal. Nucl. Chem.* 287 (2011) 261-265.
- [124] B.S. Bajwa, S. Kumar, S. Singh, S.K. Sahoo, R.M. Tripathi, *J. Radiat. Res. Appl. Sci.* 10 (2017) 13-19.
- [125] N. Pourreza, T. Naghdi, *Talanta* 128 (2014) 164-169.
- [126] S. Dadfarnia, F. Shakerian, A.M.H. Shabani, *Talanta* 106 (2013) 150-154.
- [127] I. Lopez-García, Y. Vicente-Martínez, M. Hernandez-Cordoba, *Anal. Methods* 7 (2015) 3786-3792.
- [128] I. Lopez-García, Y. Vicente-Martínez, M. Hernandez-Cordoba, *J. Anal. At. Spectrom.* 30 (2015) 375-380.
- [129] Z.-q. Tan, J.-f. Liu, R. Liu, Y.-g. Yin, G.-b. Jiang, *Chem. Commun.* (2009) 7030-7032.
- [130] J.-f. Liu, R. Liu, Y.-g. Yin, G.-b. Jiang, *Chem. Commun.* (2009) 1514-1516.

- [131] J. Liu, A.K. Brown, X. Meng, D.M. Cropek, J.D. Istok, J.D. Watson, Y. Lu, PNAS 104 (2007) 2056-2061.
- [132] C.-S. Wu, J.M. Cupps, X. Fan, Nanotechnology 20 (2009) 305502.
- [133] M. Han, X. Gao, J.Z. Su, S. Nie, Nat. Biotechnol. 19 (2001) 631-635.
- [134] D.M. Willard, A. Van Orden, Nat. Mater. 2 (2003) 575-576.
- [135] S. Hohng, T. Ha, ChemPhysChem. 6 (2005) 956-960.
- [136] K. Swaminathan, H.M.N.H. Irving, J. Inorg. Nucl. Chem. 26(1964) 1291-1294.
- [137] H. Arslan, N. Külçü, U. Flörke, Transition Met. Chem. 28 (2003) 816-819.
- [138] A. Yamaguchi, R. B. Penland, S. Mizushima, T. J. Lane, Columba Curran, J. V. Quagliano, J. Am. Chem. Soc. 80 (1958) 527–529.
- [139] S.A. Abbasi, Int. J. Environ. Anal. Chem. 36 (1989) 163-172.
- [140] C.D. Wagner, W.M. Riggs, L.E. Davis, J.F. Moulder, G.E. Muilenberg, Handbook of X-ray photoelectron spectroscopy – A reference book of standard data for use in X-ray photoelectron spectroscopy, Perkin-Elmer Corporation, USA (1979).
- [141] S. Kannan, M.A. Moody, C.L. Barnes, P.V. Duval, Inorg. Chem. 47 (2008) 4691-4695.
- [142] E.A. Mowafy, H.F. Aly, Solvent Extr. Ion Exch. 25 (2007) 205-224.
- [143] P.K. Mohapatra, Chem. Prod. Process Model 10 (2015) 135–145.
- [144] Y. Shen, X. Tan, L. Wang, W. Wu, Sep. Purif. Technol. 78 (2011) 298-302.
- [145] J.R. Bloor, J.C. Morrison, C.T. Rhodes, J. Pharm. Sci. 59 (1970) 387-391.
- [146] A.H. Orabi, Journal of Radiation Research and Applied Sciences 6 (2013) 1-10.
- [147] C.S.K. Raju, M.S. Subramanian, Microchim. Acta 150 (2005) 297–304.
- [148] C. Ruan, W. Luo, W. Wang, B. Gu, Anal. Chim. Acta 605 (2007) 80–86.
- [149] V. Amendola, R. Pilot, M. Frasconi, O.M. Maragò, M.A. Iatì, J. Phys. Condens. Matter 29 (2017) 203002.

- [150] C. Pezzato, S. Maiti, J. L.-Y. Chen, A. Cazzolaro, C. Gobbo, L. J. Prins, *Chem. Commun.* 51 (2015) 9922-9931.
- [151] D.A. Giljohann, D.S. Seferos, W.L. Daniel, M.D. Massich, P.C. Patel, C.A. Mirkin, *Angew. Chem., Int. Ed.* 49 (2010) 3280–3294.
- [152] R. Gwak, H. Kim, S.M. Yoo, S.Y. Lee, G.-J. Lee, M.-K. Lee, C.-K. Rhee, T. Kang, B. Kim, *Sci. Rep.* 6 (2016) 1-7.
- [153] D. Zhang, Z. Chen, H. Omar, L. Deng, N.M. Khashab, *ACS Appl. Mater. Interfaces* 7 (2015) 4589–4594.
- [154] F. Xiao, Y. Sun, W. Du, W. Shi, Y. Wu, S. Liao, Z. Wu, R. Yu, *Adv. Funct. Mater.* 27 (2017) 1702147.
- [155] D.N. Castillo-López, U. Pal, *J. Nanopart. Res.* 16 (2014) 2571.
- [156] X. Liu, M. Atwater, J. Wang, Q. Huo, *Colloids Surf. B* 58 (2007) 3-7.
- [157] A. Zhang, T. Asakura, G. Uchiyama, *React. Funct. Polym.* 57 (2003) 67–76.
- [158] J. Kim, C. Tsouris, Y. Oyola, C.J. Janke, R.T. Mayes, S. Dai, G. Gill, L.-J. Kuo, J. Wood, K.-Y. Choe, E. Schneider, H. Lindner, *Ind. Eng. Chem. Res.* 53 (2014) 6076–6083.
- [159] P.A. Kavakli, N. Seko, M. Tamada, O. Güven, *Adsorption* 10 (2004) 309–315.
- [160] L. Chen, Z. Bai, L. Zhu, L. Zhang, Y. Cai, Y. Li, W. Liu, Y. Wang, L. Chen, J. Diwu, J. Wang, Z. Chai, S. Wang, *ACS Appl. Mater. Interfaces* 9 (2017) 32446–32451.
- [161] N. Mehio, M.A. Lashely, J.W. Nugent, L. Tucker, B. Correia, C.-L. Do-Thanh, S. Dai, R.D. Hancock, V.S. Bryantsev, *J. Phys. Chem. B* 119 (2015) 3567–3576.
- [162] I. Ugur, A. Marion, S. Parant, J.H. Jensen, G. Monard, *J. Chem. Inf. Model* 54 (2014) 2200–2213.

- [163] S. Aryal, R. Bahadur K.C., N. Bhattarai, C.K. Kim, H.Y. Kim, J. Colloid Interface Sci. 299 (2006) 191–197.
- [164] Y.J. Kim, R.C. Johnson, J.T. Hupp, Nano Lett. 1 (2001) 165–167.
- [165] P.K. Khanna, R. Gokhale, V.V.V.S. Subbarao, A. Kasi Vishwanath, B.K. Das, C.V.V. Satyanarayana, Mater. Chem. Phys. 92 (2005) 229–233.
- [166] A. Goel, N. Rani, Open Journal of Inorganic Chemistry 2 (2012) 67–73.
- [167] K.N. Marsh, J.A. Boxall, R. Lichtenthaler, Fluid Phase Equilib. 219 (2004) 93–98.
- [168] T. Welton, Chem. Rev. 99 (1999) 2071–2083.
- [169] J.G. Huddleston, H.D. Willauer, R.P. Swatloski, A.E. Visser, R.D. Rogers, Chem. Commun. (1998) 1765–1766.
- [170] P. Wasserscheid, T. Welton, Ionic Liquids in Synthesis, Wiley-VCH, Weinheim (2003).
- [171] A. Ouadi, O. Klimchuk, C. Gaillard, I. Billard, Green Chem. 9(2007) 1060–1062.
- [172] J. S. Wilkes, M. J. Zaworotko, J. Chem. Soc., Chem. Commun. (1992) 965.
- [173] J. Fuller, R. T. Carlin, H. C. De Long, D. Haworth, J. Chem. Soc., Chem. Commun. (1994) 299.
- [174] D. Allen, G. Baston, A. E. Bradley, T. Gorman, A. Haile, I. Hamblett, J. E. Hatter, M. J. F. Healey, B. Hodgson, R. Lewin, K. V. Lovell, B. Newton, W. R. Pitner, D. W. Rooney, D. Sanders, K. R. Seddon, H. E. Sims, R. C. Thied, Green Chem. 4 (2002) 152–158.
- [175] L. Berthon, S. I. Nikitenko, I. Bisel, C. Berthon, M. Faucon, B. Saucerotte, N. Zorz and P. Moisy, Dalton Trans. 21 (2006) 2526–2534.

- [176] C. D. Harmon, W. H. Smith, D. A. Costa, *Radiat. Phys. Chem.* 60 (2001) 157–159.
- [177] A.E. Visser, J.D. Holbrey, R.D. Rogers, *Chem. Commun.* 23 (2001) 2484-2485.
- [178] S.-G. Lee, *Chem. Commun.* 10 (2006) 1049-1063.
- [179] L.C. Branco, J.N. Rosa, J.J.M. Ramos, C.A.M. Afonso, *Chem. Eur. J.* 8 (2002) 3671-3677.
- [180] Y. Ko, J.M. Chen, J.X. Peng, W. Huang, J. Li, M. Zhai, *Nat. Sci. Rep.* 7 (2017) 44100.
- [181] D.R. Bhatt, K.C. Maheria, J.K. Parikh, *Indian Journal of Chemistry* 54A (2015) 1409-1413.
- [182] Md S. Noorashikin, M. Raoov, S. Mohamad, Mhd R. Abas, *Int. J. Mol. Sci.* 14 (2013) 24531-24548.
- [183] S. Pavagadhi, C. Basheer, R. Balasubramanian, *Anal. Chim. Acta* 686 (2011) 87–92.
- [184] S.A. Arain, T.G. Kazi, H.I. Afridi, M.S. Arain, A.H. Panhwar, N. Khan, J.A. Baig, F. Shah, *Ecotoxicol. Environ. Saf.* 126 (2016) 186–192.
- [185] S. Procházková, Radoslav Halko, *Anal. Lett.* 49 (2016) 1656-1668.
- [186] T. Li, J. Yang, *J. Iran Chem. Soc.* 12 (2015) 367–370.
- [187] S. Garcia, F. Gerondi, T.R.L.C. Paixão, M.A.Z. Arrudab, I. Gaubeur, *J. Braz. Chem. Soc.* 26 (2015) 490-497.
- [188] L.F.D. Silva, G.S. Lopes, W.O. Matos, *Anal. Methods* 7 (2015) 9844-9849.
- [189] X.P. Yang, Z.H. Jia, X.C. Yang, N. Luo, X.J. Liao, *Applied Ecology And Environmental Research* 15(2017) 537-548.
- [190] N. Altunay, R. Gürkan, U. Kır, *Food Addit. Contam. Part A Chem. Anal. Control. Expo. Risk Assess.* 33 (2016) 259-270.

- [191] K. Sanyal, A. Khooha, G. Das, M.K. Tiwari, N.L. Misra, *Anal. Chem.* 89 (2017) 871 – 876.
- [192] K. Sanyal, B. Kanrar, N.L. Misra, M. Czyzycki, A. Miliori, A.G. Karydas, *X-ray Spectrom.* 46 (2017) 164-170.
- [193] R. Klockenkämper, *Total Reflection X-ray Fluorescence Analysis, Chemical Analysis*, John Wiley & Sons, New York 140 (1996).
- [194] J. Stas, A. Dahdouh, H. Shelwit, *Period. Polytech. Chem.* 49 (2005) 3-18.
- [195] N. Muller, *J. Solution Chem.* 17 (1988) 661-672.
- [242] J.R. Bloor, J.C. Morrison, C.T. Rhodes, *J. Pharm. Sci.* 59 (1970) 387-391.
- [243] D.J. McClements, *Soft Matter* 8 (2012) 1719-1729.
- [244] C.B. Ojeda, F.S. Rojas, *Microchim. Acta* 177 (2012) 1–21.
- [245] T. Gu, P.A. Galera-Gómez, *Colloids Surf. A* 104 (1995) 307-312.
- [246] S. Shariati, Y. Yamini, A.K. Zanjani, *J. Hazard. Mater.* 156 (2008) 583-590.
- [247] M.E.F. Laespada, J.L.P. Pavon, B.M. Cordero, *Analyst* 118 (1993) 209-212.
- [248] F. Shemirani, R.R. Kozani, M.R. Jamali, Y. Assadi, S.M.R. Milani, *Sep. Sci. Technol.* 40 (2005) 2527-2537.
- [249] H.S. Ferreira, M.D. Bezerra, S.L.C. Ferreira, *Microchim. Acta* 154 (2006) 163-167.
- [250] T. Madrakian, A. Afkhami, A. Mousavi, *Talanta* 71 (2007) 610-614.
- [251] J.B. Ghasemi, B. Hashemi, M. Shamsipur, *J. Iran. Chem. Soc.* 9 (2012) 257-262.
- [252] E. Constantinou, I.J. Pashadilis, *Radioanal. Nucl. Chem.* 286 (2010) 461-465.
- [253] A. Favre-Régouillon, D. Murat, G. Cote, M. Draya, *J. Chem. Technol. Biotechnol.* 81 (2006) 1872-1876.

- [254] E. Bağda, E. Yabas, N. Karakus, J. Radioanal. Nucl. Chem. 299 (2014) 1813–1820.